

Matti Pajari

Shear-torsion interaction tests on single hollow core slabs

Shear-torsion interaction tests on single hollow core slabs

Matti Pajari

VTT Building and Transport



ISBN 951-38-6519-3 (URL: <http://www.vtt.fi/inf/pdf/>)
ISSN 1455-0865 (URL: <http://www.vtt.fi/inf/pdf/>)

Copyright © VTT 2004

JULKAISIJA – UTGIVARE – PUBLISHER

VTT, Vuorimiehentie 5, PL 2000, 02044 VTT
puh. vaihde (09) 4561, faksi (09) 456 4374

VTT, Bergsmansvägen 5, PB 2000, 02044 VTT
tel. växel (09) 4561, fax (09) 456 4374

VTT Technical Research Centre of Finland, Vuorimiehentie 5, P.O.Box 2000, FIN-02044 VTT, Finland
phone internat. + 358 9 4561, fax + 358 9 456 4374

VTT Rakennus- ja yhdyskuntatekniikka, Kemistintie 3, PL 1805, 02044 VTT
puh. vaihde 020 722 111, faksi 020 722 7007

VTT Bygg och transport, Kemistvägen 3, PB 1805, 02044 VTT
tel. växel 020 722 111, fax 020 722 7007

VTT Building and Transport, Kemistintie 3, P.O.Box 1805, FIN-02044 VTT, Finland
phone internat. +358 20 722 111, fax +358 20 722 7007

Pajari, Matti. Shear-torsion interaction tests on single hollow core slabs. Espoo 2004. VTT Tiedotteita – Research Notes 2275. 76 p. + app. 122 p.

Keywords shear tests, torsion tests, hollow core slabs, testing, test specimens, load testing, failure loads, concrete, precast, prestressed, structure

Abstract

To clarify the interaction of shear and torsion in prestressed hollow core slabs, 15 load tests on single prestressed hollow core units were carried out. The slabs were 1.2 m in width, 7 m in length and either 200 or 400 mm in depth. The ends of the slabs were simply supported. In 13 tests the loads comprised one or two point loads close to support. In two tests there was a uniform transverse line load close to one support while the slab unit was twisted by eccentric loads at the ends.

In ten tests the slabs were placed on neoprene strips with no end grouting. In these tests the transverse bending made the slab fail longitudinally first, which in most cases resulted in a lower resistance than that predicted using traditional design methods.

In five tests the conditions were more realistic, i.e. the slab ends were grouted and stiffened by supporting beams or spreader beams above the slab ends. In these tests the observed resistances were of the same order or higher than those predicted using the conventional calculation methods. However, some observed stiffnesses and resistances deviated so much from the predicted results that the conventional calculation methods have to be evaluated by comparison with numerical methods.

Preface

In 2002–2004, a European research project named HOLCOTORS was carried out. It aimed at providing numerical methods for analysis and simplified methods for design of prestressed hollow core floors subjected to shear and torsion. The calculation models were developed by Chalmers University of Technology, Sweden. The tests used for verification of the models were carried out and documented by VTT, Finland. The researchers in the involved research institutes were

Helen Broo	Chalmers
Björn Engström	Chalmers
Karin Lundgren	Chalmers
Matti Pajari	VTT
Mario Plos	Chalmers.

In addition to the researchers, the following representatives of the industrial partners participated in the work as members of the steering group and by participating in the workshops organised on the day before the steering group meetings:

Olli Korander	Consolis Technology, Finland, Chairman
Arnold van Acker	Belgium
Willem Bekker	Echo, Belgium
David Fernandez-Ordonez	Castelo, Spain
Ronald Klein-Holte	BVSH (VBI) The Netherlands
Gösta Lindström	Strängbetong, Sweden
Aad van Paassen	BVSH (VBI), The Netherlands
Nordy Robbens	Echo, Belgium
Bart Thijs	Echo, Belgium
Jan de Wit	IPHA (Dycore), The Netherlands
Javier Zubia	Castelo, Spain.

Gösta Lindström also worked in close co-operation with the researchers, participated in extra workshops between the steering group meetings and made proposals for the future design practice.

The experimental part of the research project, a part of which is documented in this report, was financed by the Fifth Framework Programme of European Commission (Competitive and Sustainable Growth, Contract N° G6RD-CT-2001-00641); International Prestressed Hollow Core Association, Bundesverband Spannbeton-Hohlplatten, Castelo, Consolis, Echo, Strängbetong, and VTT. The test specimens were provided by Parma Betonila, Finland.

Contents

Abstract.....	3
Preface	4
1. Introduction.....	7
2. Test arrangements	8
2.1 Characteristics of hollow core slabs	8
2.2 Shear tension tests on slabs supported on neoprene.....	10
2.3 Shear tension tests on slabs with grouted ends on mortar bearing.....	15
2.4 Shear tension tests on slabs with grouted ends on soft bearing.....	21
2.5 Shear flexure test	26
3. Material data given by the manufacturer of slabs.....	28
4. Results of load tests	29
4.1 About loading	29
4.2 Notation and some basic formulae	29
4.3 Shear tension tests on 200 mm slabs	31
4.3.1 Rate of loading and observations during tests.....	31
4.3.2 Deflections	33
4.3.3 Shear resistance and torsional stiffness.....	36
4.3.4 Horizontal displacements	38
4.4 Shear tension tests on 400 mm slabs with parallel supports	42
4.4.1 About initial cracks	42
4.4.2 Rate of loading and observations during tests.....	43
4.4.3 Deflections	44
4.4.4 Shear resistance and torsional stiffness.....	46
4.5 Tests ST400G	48
4.5.1 About initial cracks	48
4.5.2 About loading.....	48
4.6 Shear flexure test on 400 mm slab	52
4.7 Data about concrete	53
4.8 Notes on results	59

5. Analysis of shear tension tests	61
6. Discussion	74
References	76

Appendices

A	Photographs, 200 mm slabs
B	Photographs, 400 mm slabs
C	Measured geometry of slabs
D	200 mm slabs, measured displacements in shear torsion tests
E	400 mm slabs, measured displacements in shear torsion tests
F	Measured displacements in shear flexure test SF400C
G	Determining torque from measured results
H	Design of supporting beams in tests ST200E1M, ST200E2M and ST400E1M
I	Elasticity of neoprene strips

1. Introduction

The tests documented in this report were planned to clarify the effect of combined shear and torsion on the resistance of an isolated, prestressed hollow core unit. Tests without torsion were also carried out for reference. Pure bending failure modes were eliminated by placing the load close to the support.

2. Test arrangements

In all figures of this report the measures are given in millimetres unless otherwise specified. Photographs about test arrangements are shown in Appendices A and B. Names of type STabcXYZ, STSabcXYZ or SFabcX are used for different tests and test specimens. The symbols in the names have the following meaning:

ST	Shear Tension, extruded slab
STS	Shear Tension, slipformed slab
SF	Shear Flexure, extruded slab
200 or 400	Thickness of slab in millimetres
C	Centric load
E	Eccentric load
M	Mortar bearing with grouted ends
G	Grouted ends supported on wood fibre strips.

Other characters are used to make difference between different tests when the characters above are not enough for unique identification.

2.1 Characteristics of hollow core slabs

Some characteristics of the test specimens are given in Table 1. The nominal cross-section of the slab units is given in Figs 1–3 and the measured geometry in Appendix C. For the shape of the hollow cores see also Figs 79–81.

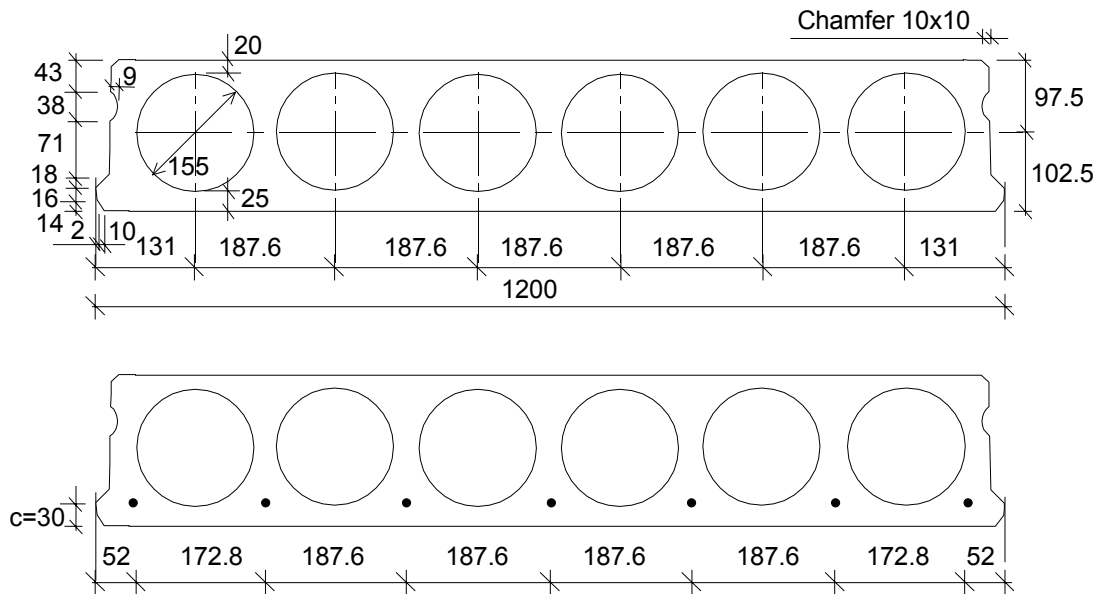


Fig. 1. Nominal cross-section and location of strands in test specimens ST200. *c* refers to concrete cover below the strand.

Table 1. Characteristics of test specimens.

Test specimen	Thickness mm	Number & diameter of strands mm	Initial prestress MPa	Length mm	Cast	Loaded
ST200C	200	7 d 12.5	900	7060	25.6.02	20.8.02
ST200E1a	200	7 d 12.5	900	7060	25.6.02	20.8.02
ST200E1b	200	7 d 12.5	900	7060	25.6.02	21.8.02
ST200E2	200	7 d 12.5	900	7060	25.6.02	21.8.02
ST200E1M	200	7 d 12.5	900	7060	25.6.02	5.6.03
ST200E2M	200	7 d 12.5	900	7060	10.10.03	2.12.03
STS200C	200	8 d 12.5	900	7060	16.7.02	22.8.02
		+ 6 d 6*	700			
STS200E1	200	8 d 12.5	900	7060	16.7.02	22.8.02
		+ 6 d 6*	700			
ST400C1	400	11 d 12.5	1000	7080	26.6.02	26.8.02
ST400C2	400	11 d 12.5	1000	7080	26.6.02	27.8.02
ST400E1	400	11 d 12.5	1000	7080	26.6.02	27.8.02
ST400E2	400	11 d 12.5	1000	7080	26.6.02	28.8.02
ST400E1M	400	11 d 12.5	1000	7080	26.6.02	18.10.02
ST400G1	400	11 d 12.5	1000	7080	26.6.02	19.8.03
ST400G2	400	11 d 12.5	1000	7080	26.6.02	19.8.03
SF400C	400	11 d 12.5	1000	7080	26.6.02	29.8.02

* Upper tendons, smooth prestressing wires

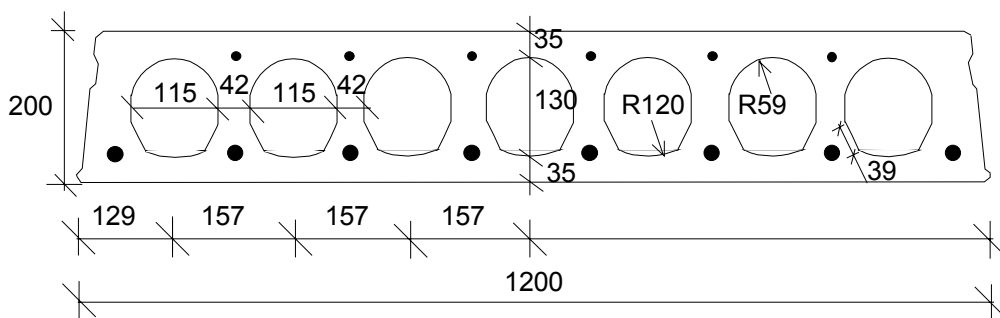


Fig. 2. Nominal cross-section and location of strands (lower tendons) and wires (upper tendons) in test specimens STS200. The vertical position of tendons was not specified in the drawings. The measured distance of lower and upper tendons from bottom and top fibre was 50 and 30 mm, respectively. For the hollow cores, see also Fig. 80.

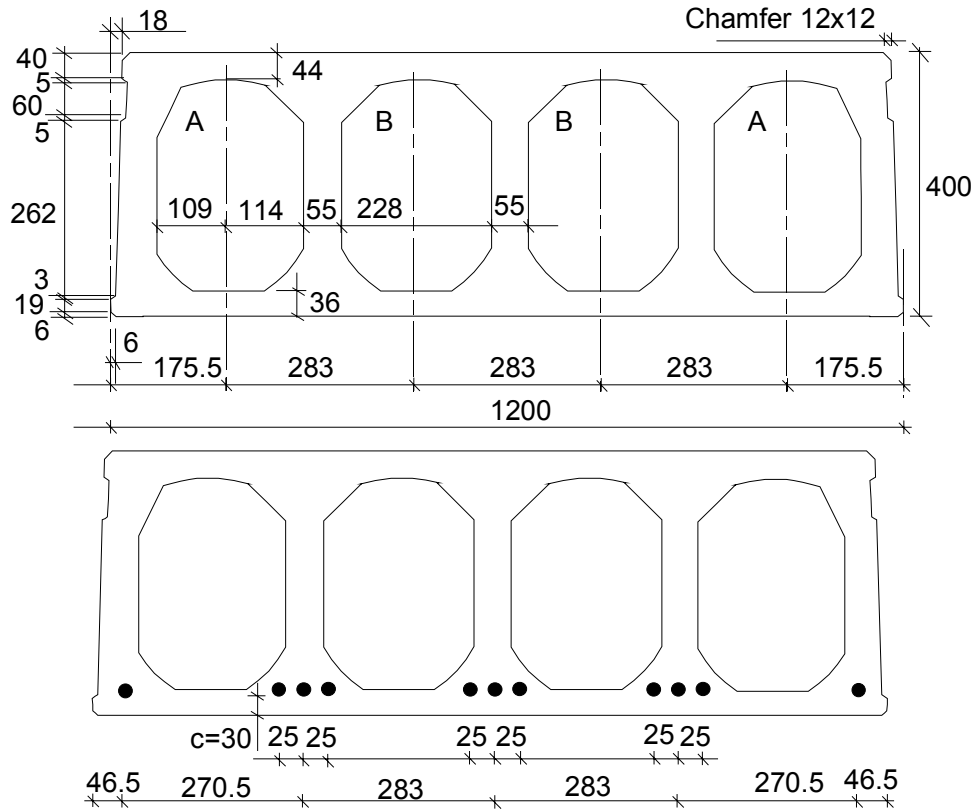


Fig. 3. Nominal cross-section and location of strands in test specimens ST400. c refers to concrete cover below the strand. For the hollow cores, see also Fig. 81.

2.2 Shear tension tests on slabs supported on neoprene

Ten tests of the type illustrated in Fig. 4 were carried out. There were one or two point loads on the webs of a slab unit. The loading was either centric or eccentric with respect to the longitudinal centroidal axis of the slab.

The support conditions and loading arrangements are presented in Figs 5–9. The loaded end of the slab is called active end, the opposite end is passive end.

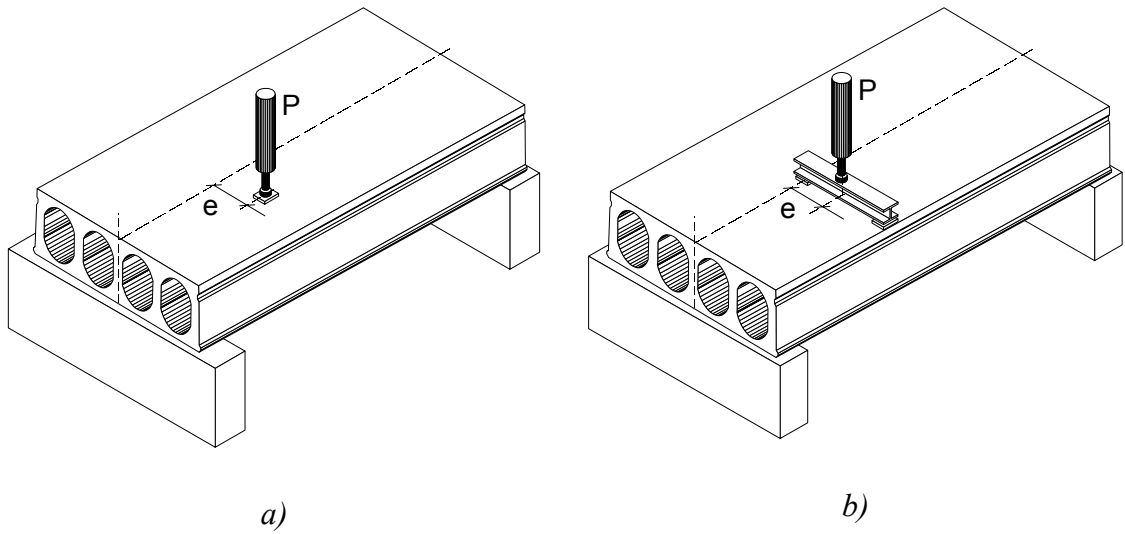


Fig. 4. General view on loading arrangements with eccentricity e . a) One point load on slab unit. b) Two point loads on slab unit.

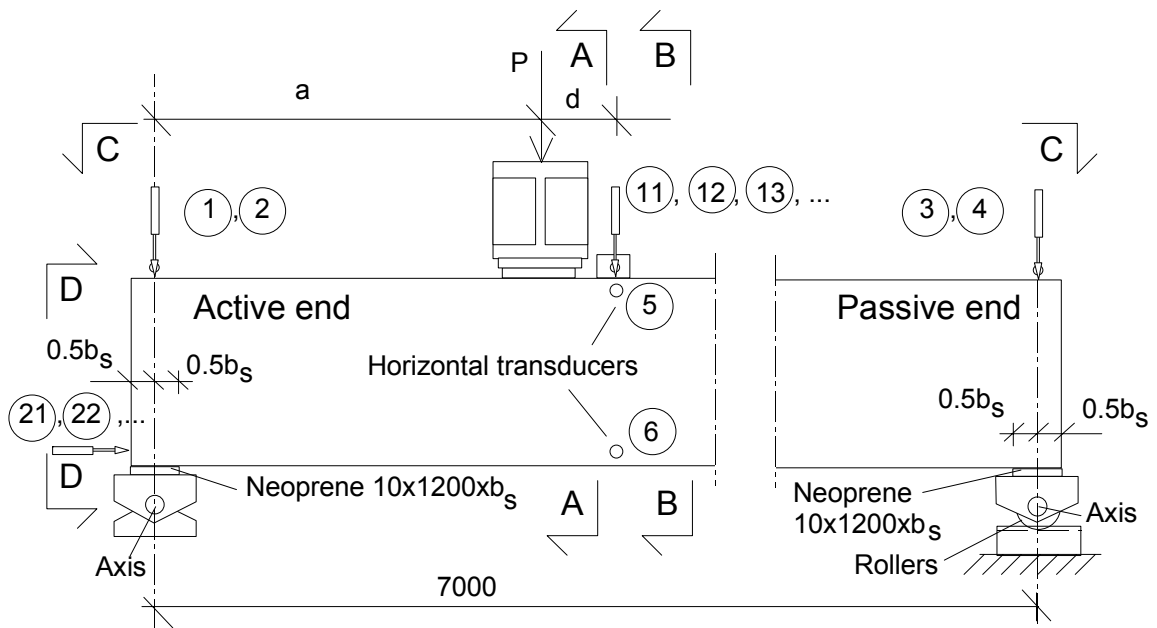


Fig. 5. Side view. Sections A–A, B–B, C–C and D–D are shown in Figs 6–10 and 12. $d = 100$ mm and 200 mm and $b_s = 60$ mm and 80 mm for 200 mm slabs and 400 mm slabs, respectively. For the properties of the neoprene, see App. I.

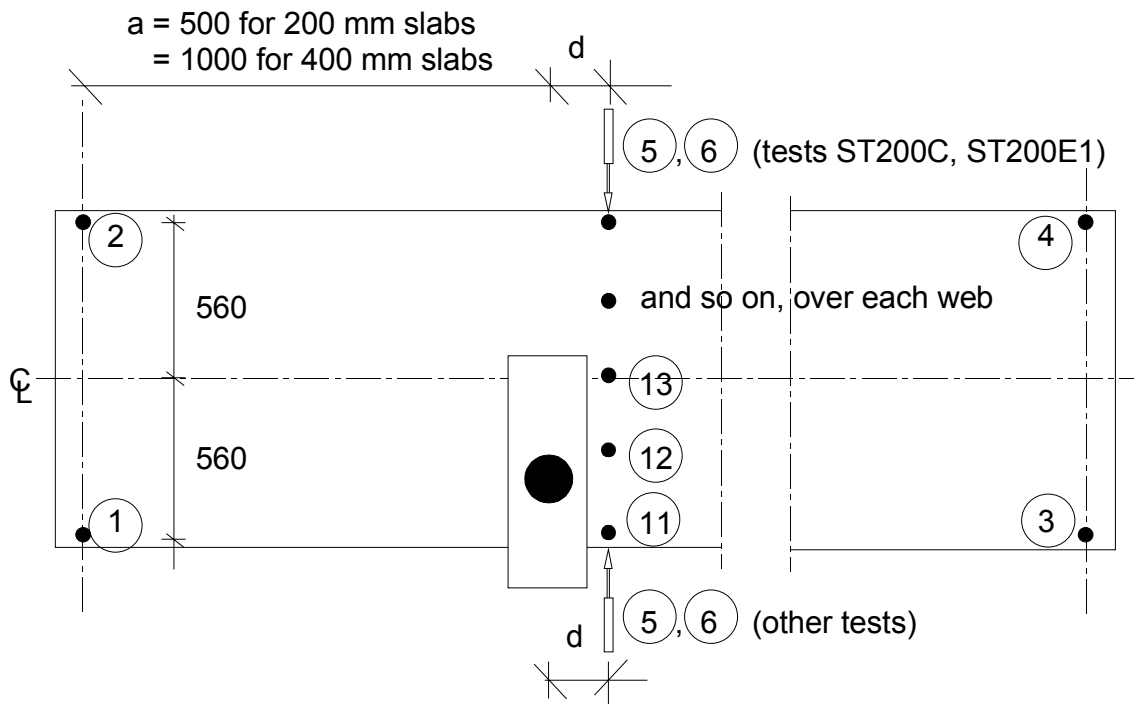


Fig. 6. Plan (section C–C in Fig. 5). $d = 100$ mm and 200 mm for 200 mm slabs and 400 mm slabs, respectively.

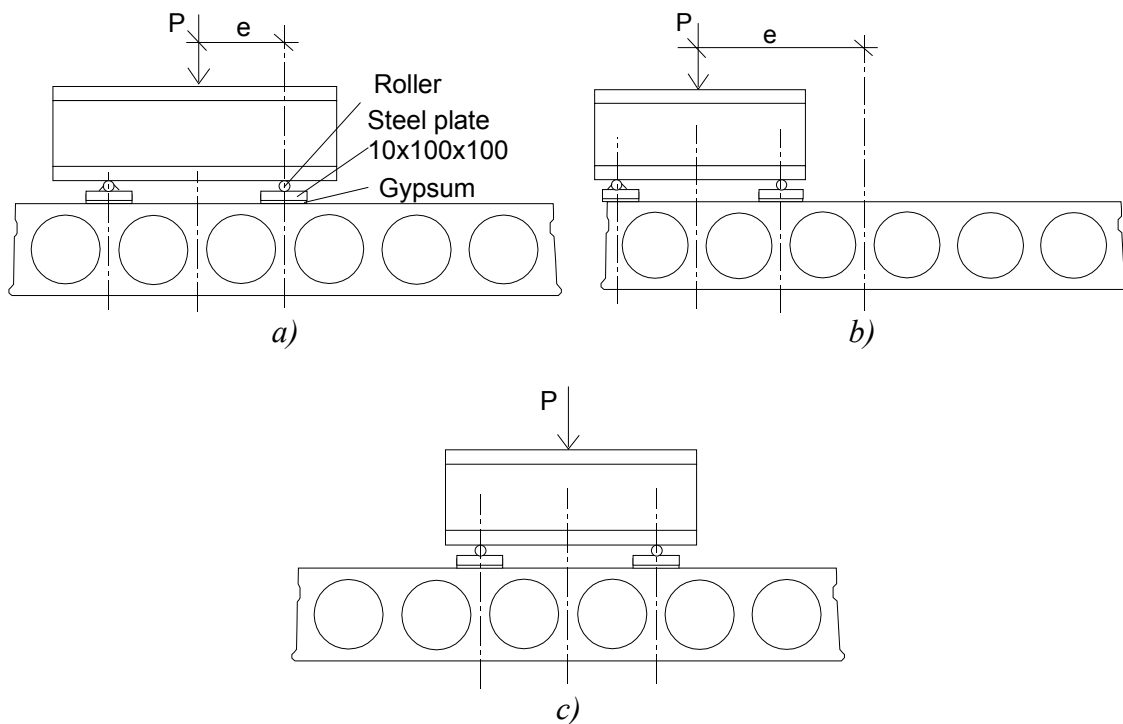


Fig. 7. Section A–A, see Fig. 5. a) Test ST200E1a and ST200E1b. b) Test ST200E2. c) Test ST200C. e is given in Table 3 in Section 4.3.1.

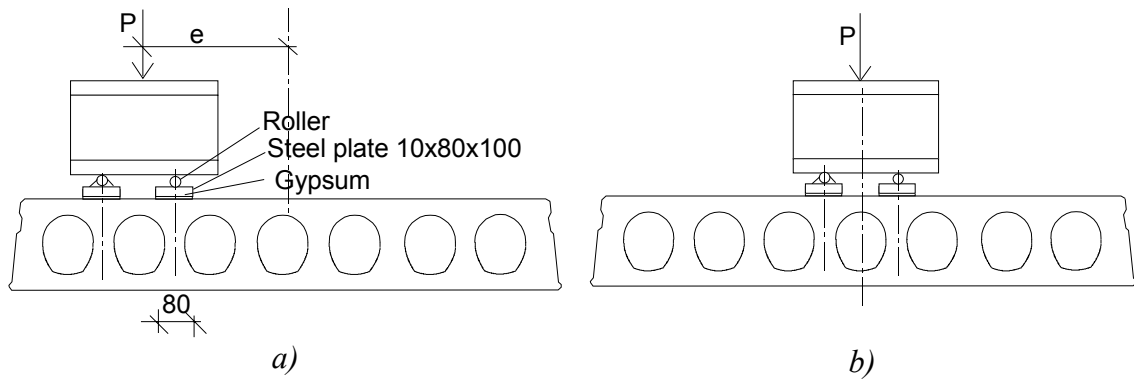


Fig. 8. Section A–A, see Fig. 5. a) Test STS200E1. b) Test STS200C. e is given in Table 3 in Section 4.3.1.

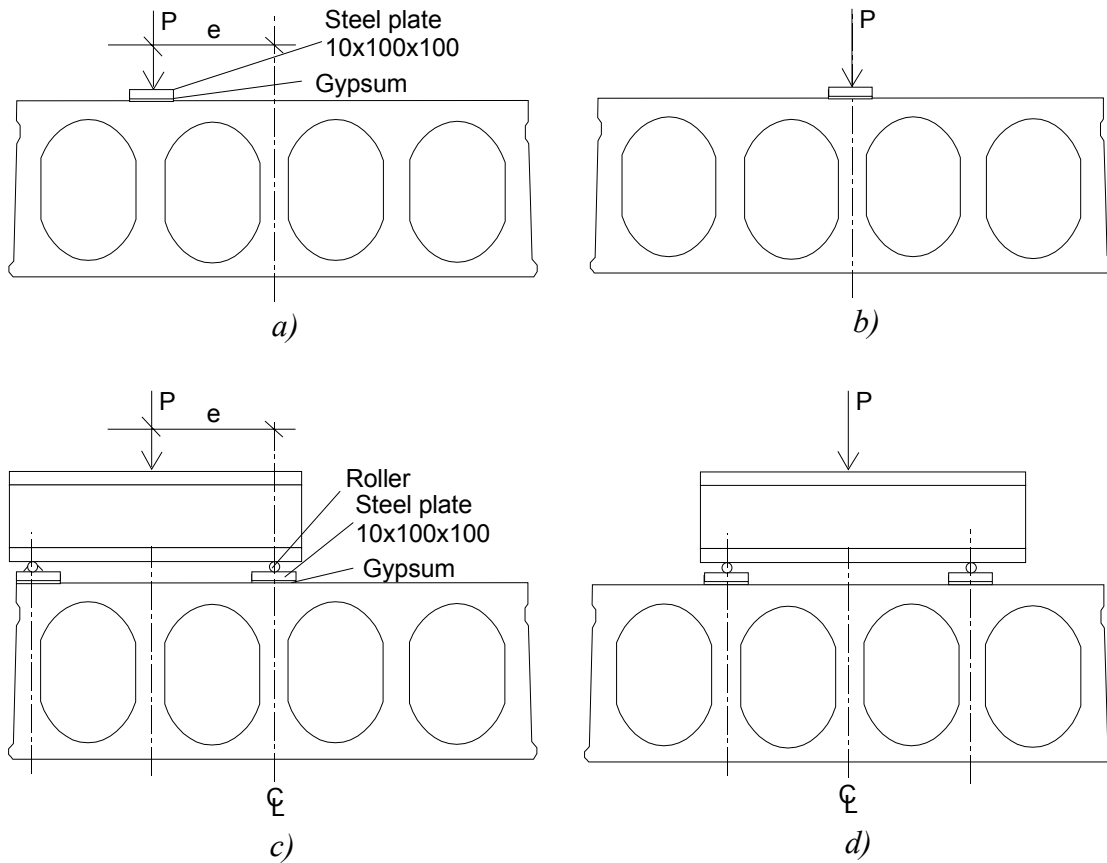


Fig. 9. Section A–A, see Fig. 5. a) Test ST400E1. b) Test ST400C1. c) Test ST4002E. d) Test ST400C2. e is given in Table 5 in Section 4.4.2.

Deflection was measured by inductive transducers placed vertically on the corners of the slab and on a transverse line above each web next to the load. See Fig. 10 for the location of the transducers.

Horizontal transducers 5 and 6 measured the possible transverse shear deformation in transverse direction close to the load. They were fixed to a steel bar, which was simply supported on an edge and centre line of the slab.

Slippage of strands relative to the concrete was measured at the active end by horizontal transducers as shown in Fig. 10. Since the transducers were fixed to the concrete at the active end, they gave unreliable or misleading results after cracking of the slab end.

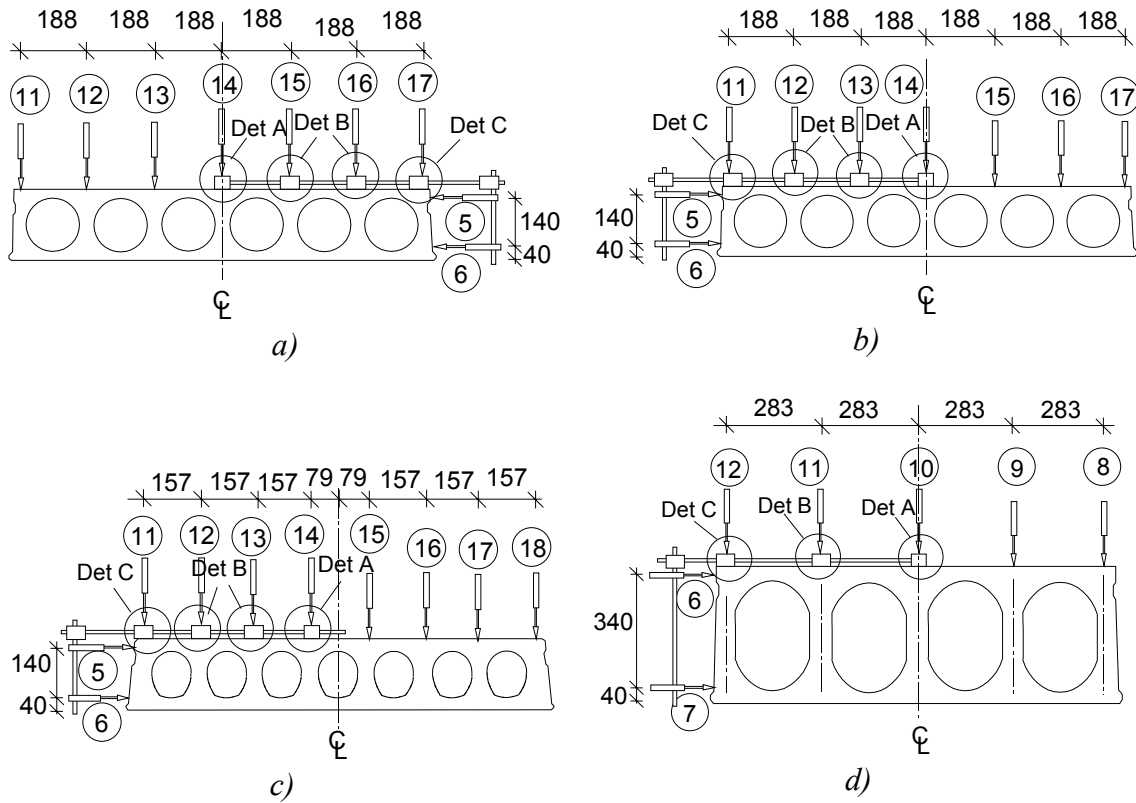


Fig. 10. Section B–B, see Fig. 5. a) Tests ST200C and ST200E1a. b) Tests ST200E1b and ST200E2. c) Tests STS200. d) Tests ST400. For Det A, B and C see Fig. 11.

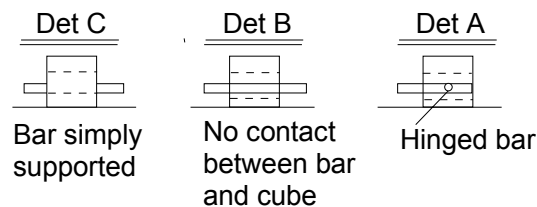


Fig. 11. Det A, Det B and Det C, see Fig. 10. The steel bar is in a hole in plastic cube.

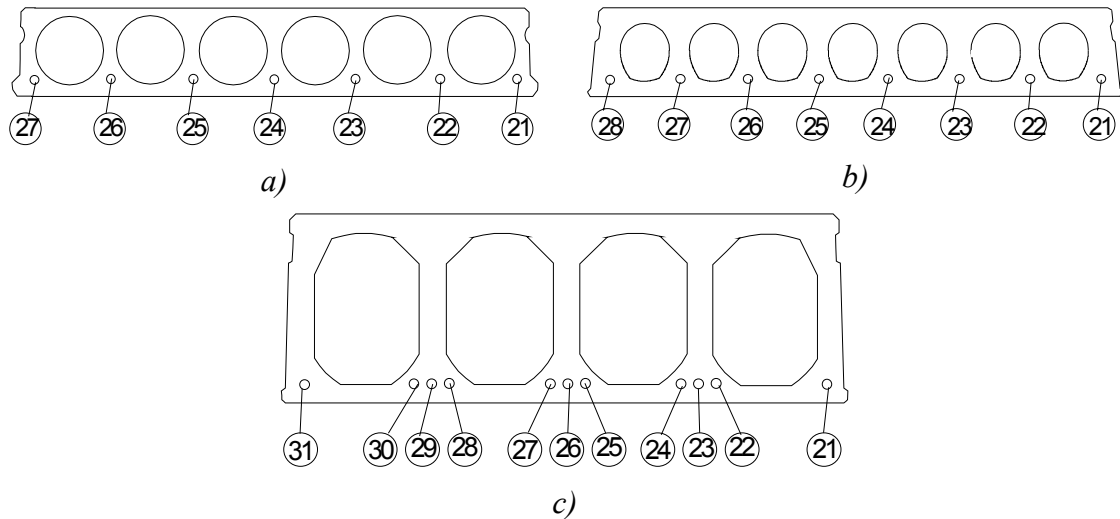


Fig. 12. Section D–D, see Fig. 5. Numbering of transducers for measuring bond slippage. a) Tests ST200. b) Tests STS200. c) Tests ST400.

At the active end the slab was placed on a support, free to rotate around an axis parallel to the slab, see Fig. 13. After this, the rotation (twisting of slab) was prevented by two wedges. In this way, a stress-free fitting of the test specimen with the supports was accomplished despite the possible spirality of the slab.

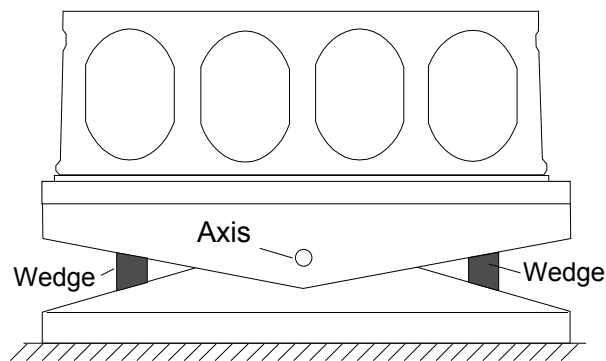


Fig. 13. Support at active end.

2.3 Shear tension tests on slabs with grouted ends on mortar bearing

After the pilot floor tests PF400 [6], a 400 mm slab, taken from the same casting bed as the slabs in test PF400, was placed on the concrete beams used in the floor test, reinforced and grouted in the same way as the slabs in the floor test. Tie beams, similar to those in the floor test, were reinforced and grouted. This means that the slabs were placed on small plywood pads and the space between the soffit of the slab end and the top surface of the beam was filled with grout. Thereafter a shear tension test ST400E1M similar to the test ST400E1 was carried out.

Later on a test ST200E1M with similar loading as in test ST200E1 was performed. Finally a test on a single slab, called ST200E2M, was carried out with similar support conditions as in floor tests FT200 and with similar loads as in floor test FT200:11. The arrangements for these tests are illustrated in Figs 14–20. In addition to different measurements and the greater eccentricity in test ST200E2M, the support conditions make the only essential difference in relation to tests ST400E1 and ST200E1. In all tests the supporting beams were placed on the concrete floor of the laboratory without any grout or mechanical fixing. A detailed description of their design is given in App. H.

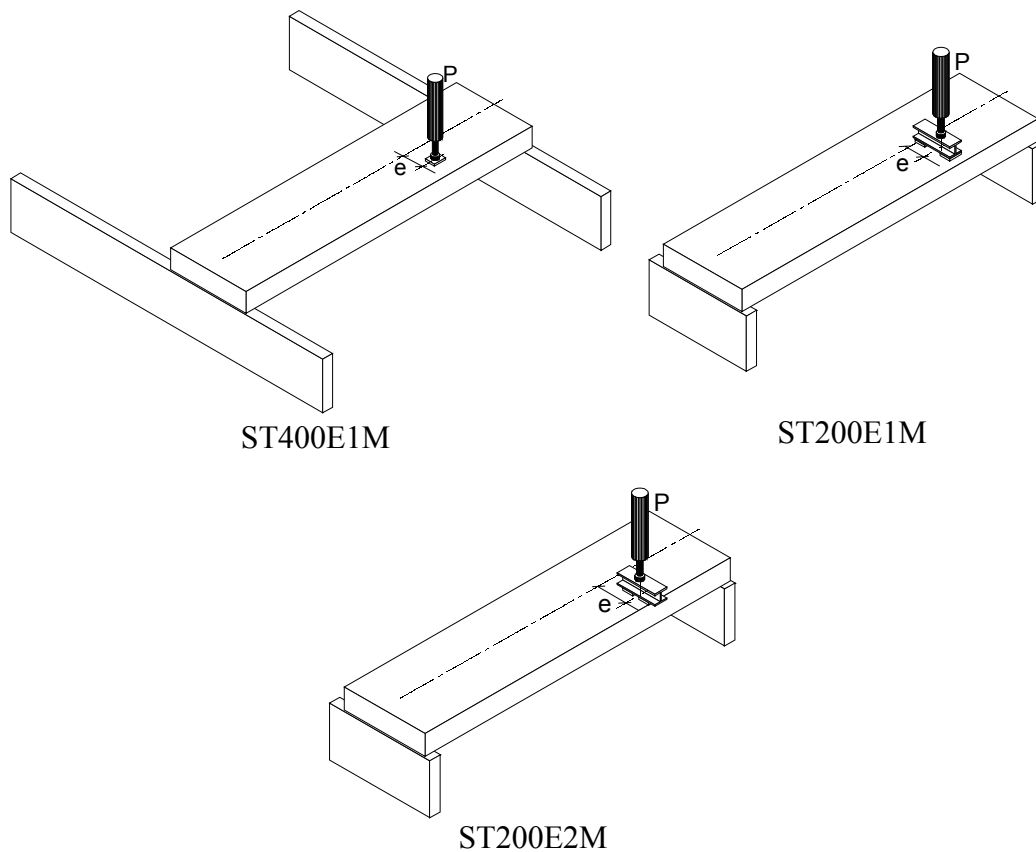


Fig. 14. Overview on arrangements.

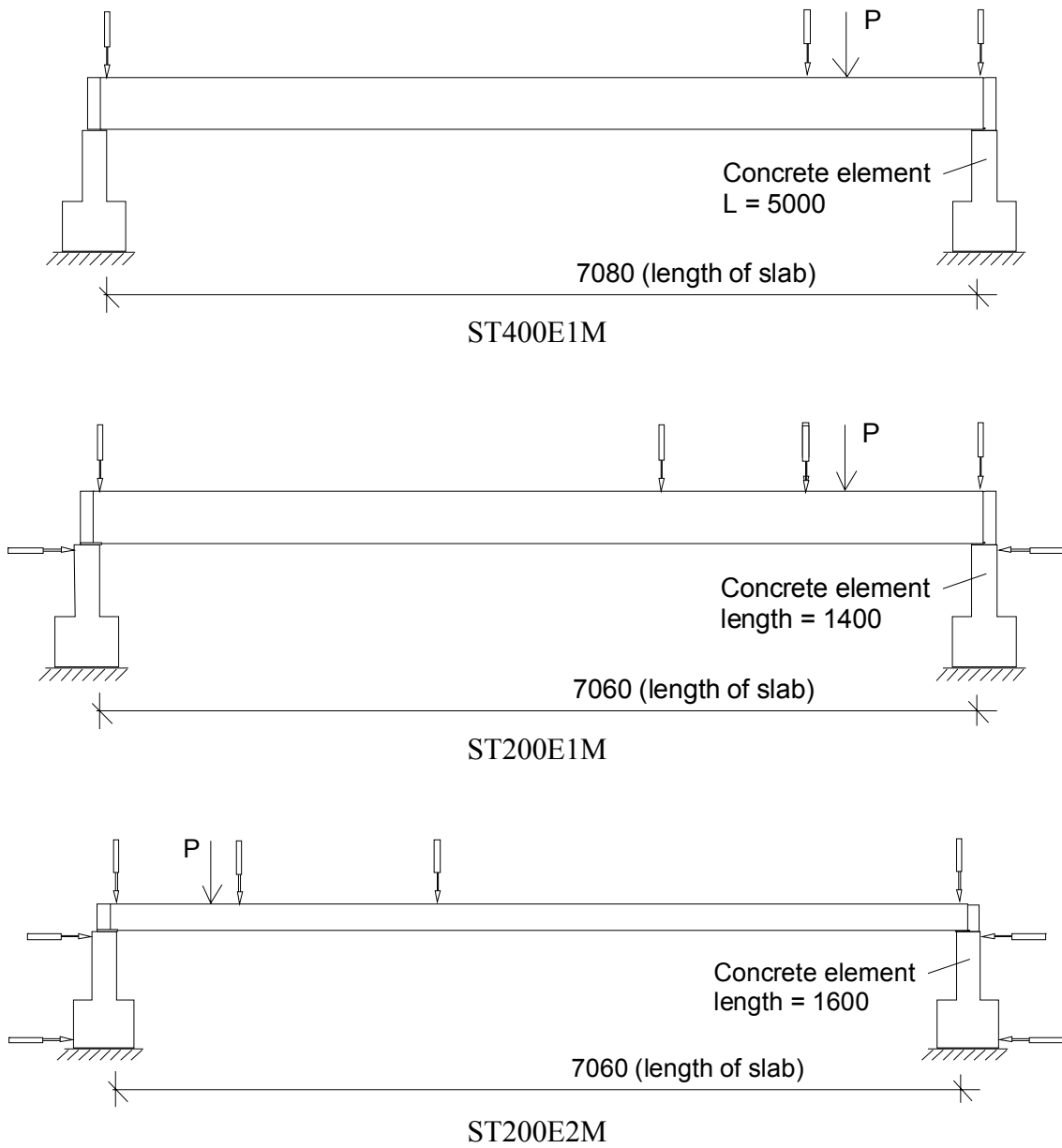


Fig. 15. Elevation.

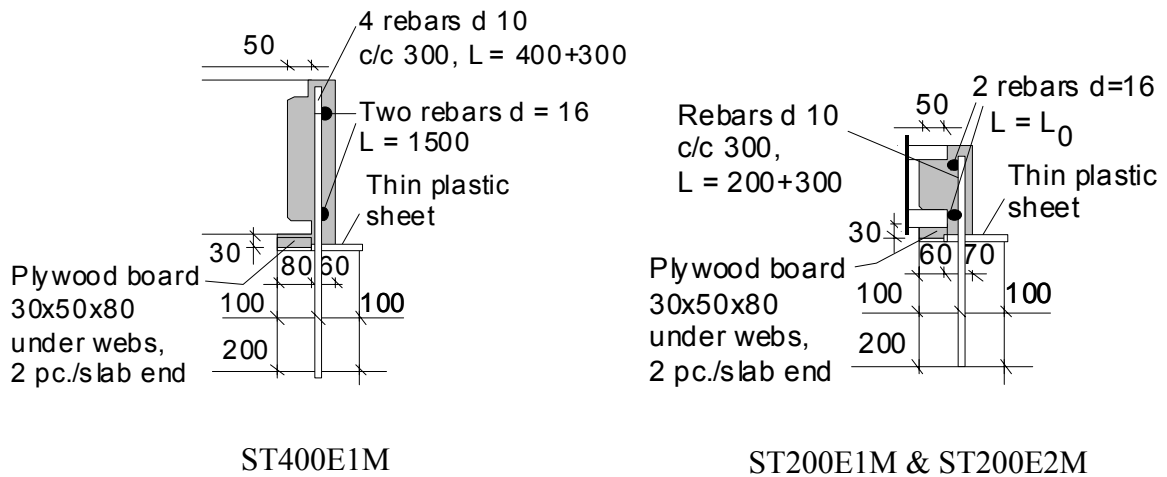


Fig. 16. Arrangements at support. The target grade of the grout was K30. The nominal yield strength of the reinforcing steel was 500 MPa. $L_0 = 1300$ and 1500 mm for ST200E1M and ST200E2M, respectively.

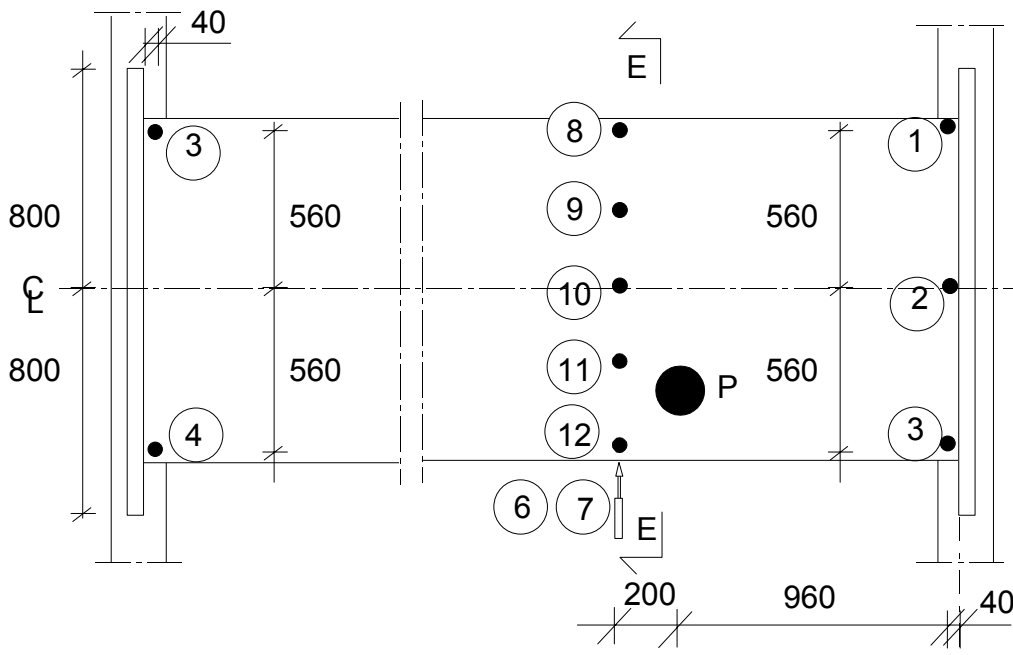


Fig. 17. ST400E1M, plan. Numbering and location of transducers. For section E-E see Fig. 18.

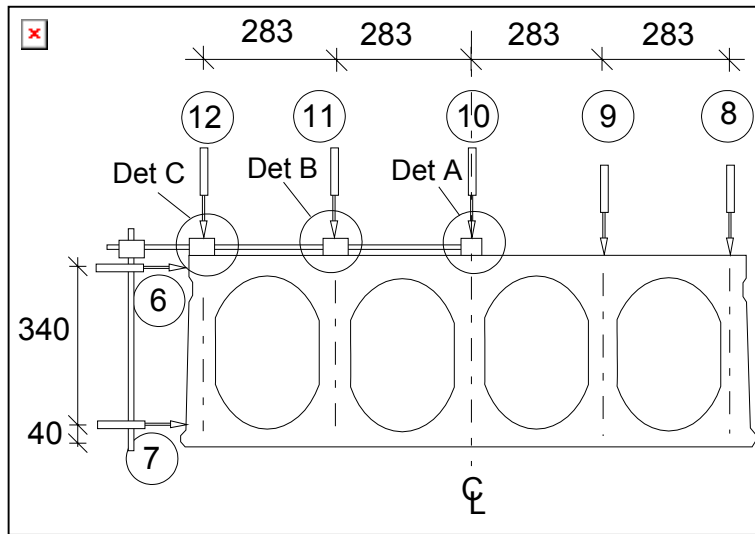


Fig. 18. ST400E1M. Section E-E, see Fig. 17. For Det A, DetB and Det C see Fig. 11.

The load in test ST400E1M was applied at one point as shown in Fig. 9.a.

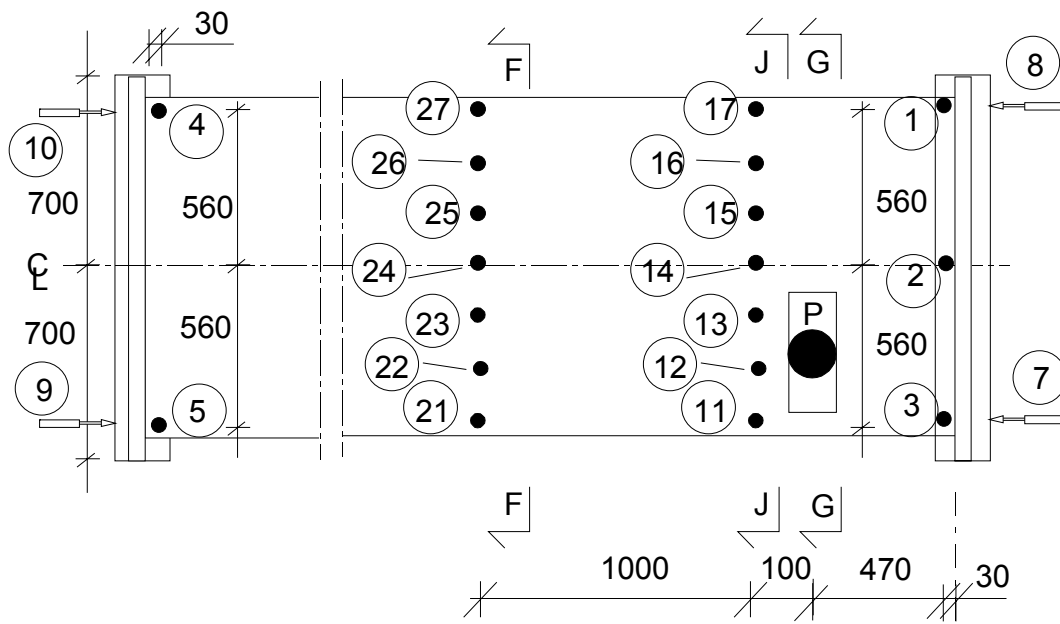


Fig. 19. ST200E1M, plan. Location and numbering of transducers. For sections J-J and F-F see Fig. 20. For section G-G see Fig. 7.c.

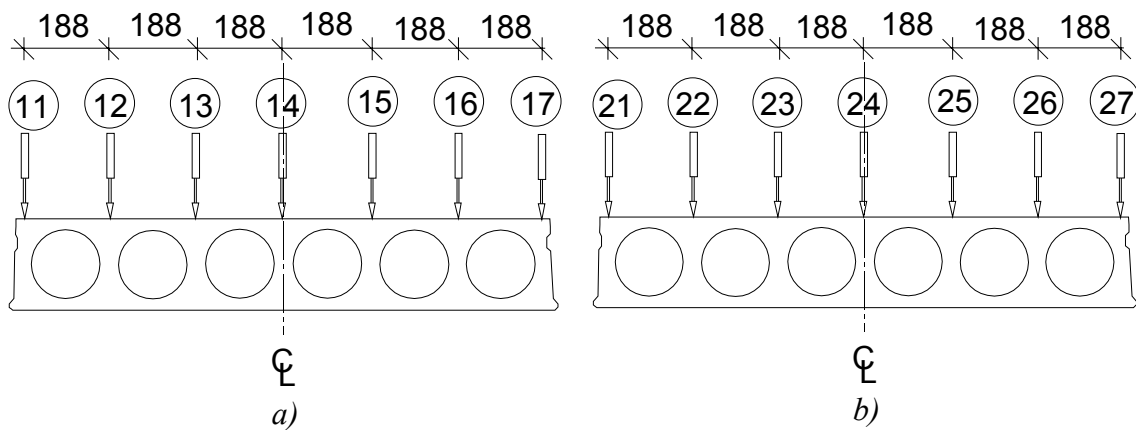


Fig. 20. ST200E1M. Sections of Fig. 19. a) J-J. b) F-F.

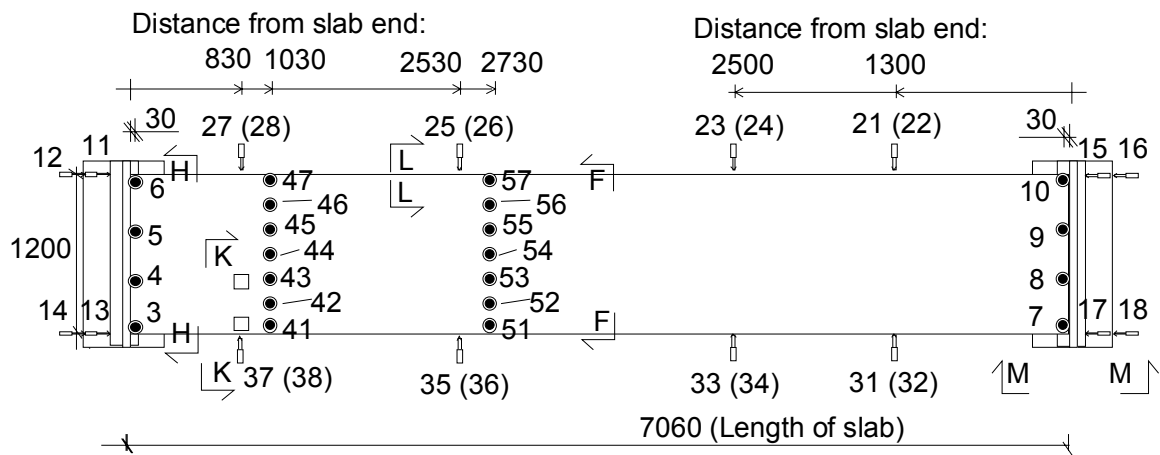


Fig 21. ST200E2M. Arrangements. Plan. For sections H-H, K-K, F-F, L-L and M-M see Figs. 22-24.

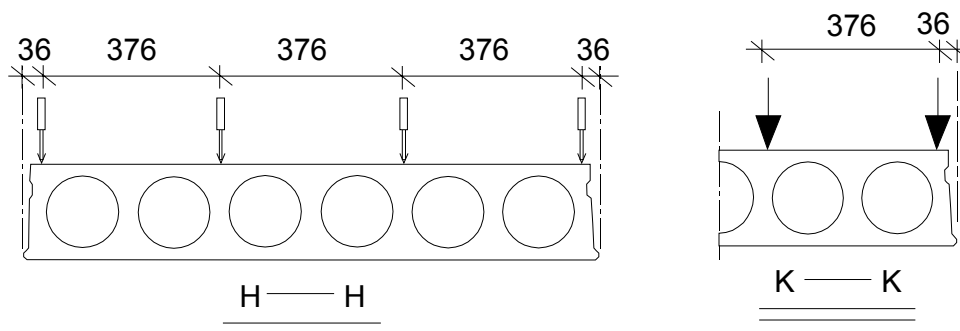


Fig. 22. ST200E2M. Sections H-H and K-K, see Fig. 21.

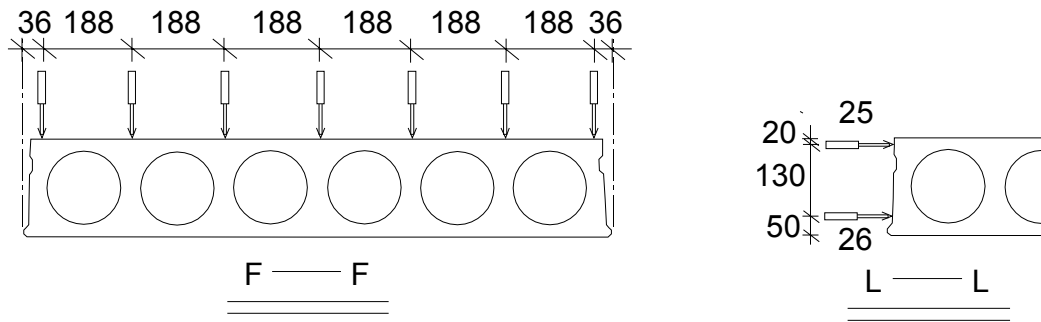


Fig. 23. ST200E2M. Sections F–F and L–L, see Fig. 21.

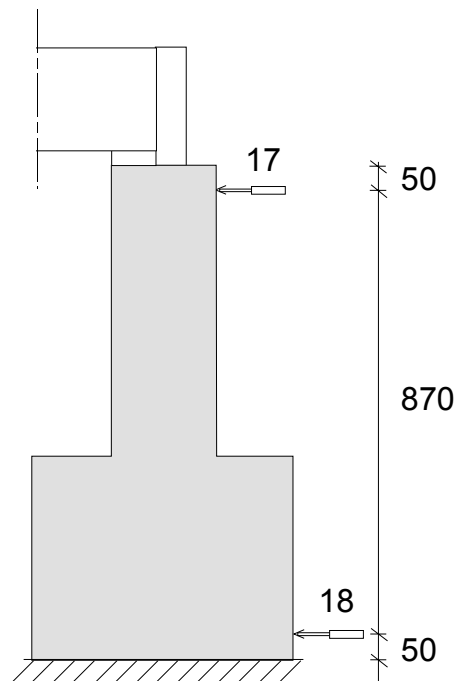


Fig. 24. ST200E2M, section M–M in Fig. 21. Vertical position of horizontal transducers measuring the displacements of the beams.

2.4 Shear tension tests on slabs with grouted ends on soft bearing

The slabs in these tests belonged to the same casting lot as those in previous tests ST400. The ends of the slab units were grouted with concrete K30 as shown in Fig. 1.

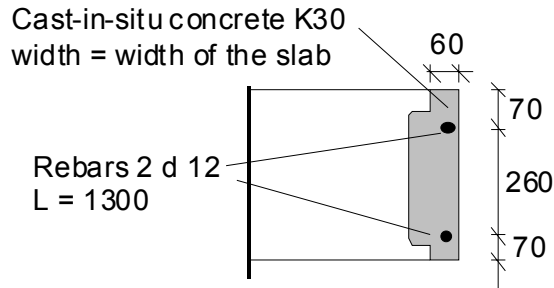


Fig. 25. ST400G. End grouting and reinforcement.

An overview on the loading arrangements is given in Fig. 2. The whole slab was subjected to a constant torque maintained by P_1 at the tilted end at which the twist of the slab end was free. Fig. 27 illustrates the possible failure modes. The eccentricity of P_1 at the tilted end, the span of the slab and the shear span of P_1 at the sheared end were chosen to eliminate failure modes other than the web failure. The balancing force P_2 was arranged by an auxiliary beam and by a force $= P_1$ as illustrated in App. B, Figs 46 and 47. With these arrangements P_2 was $\approx 1.14P_1 + 3.0$ kN. With the eccentricity of 0.15 m, P_2 was great enough to prevent the rigid body rotation of the slab due to torque $P_1 \times (0.2 \text{ m})$ at the tilted end.

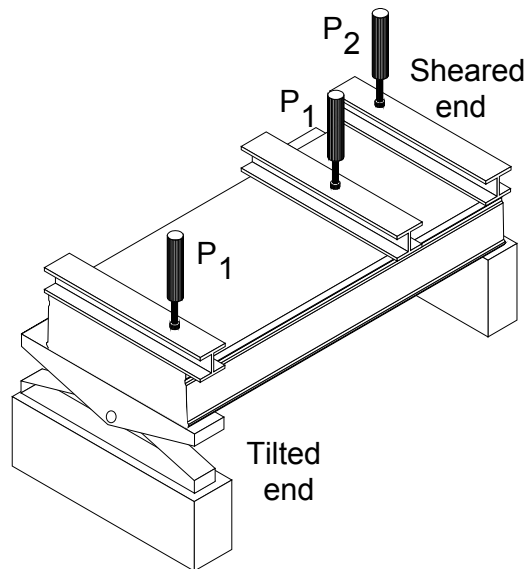


Fig. 26. ST400G. Overview on test arrangements.

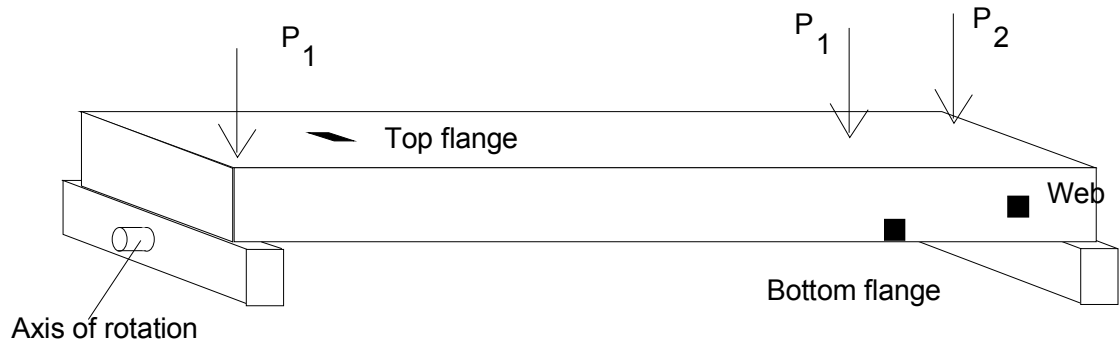


Fig. 27. ST400G. Possible failure modes.

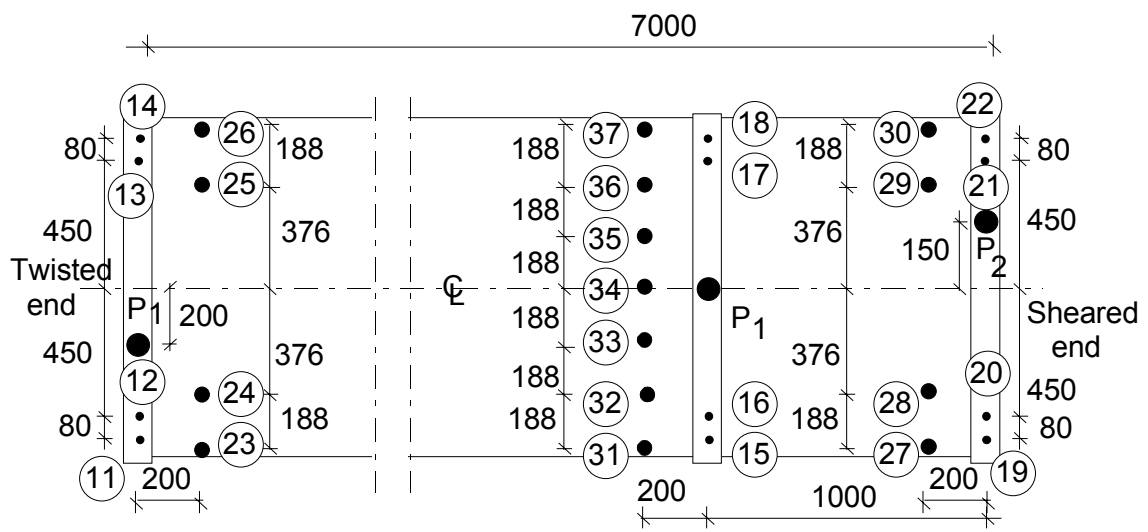


Fig. 28. ST400G, plan. Location of loads and vertical transducers 11–37.

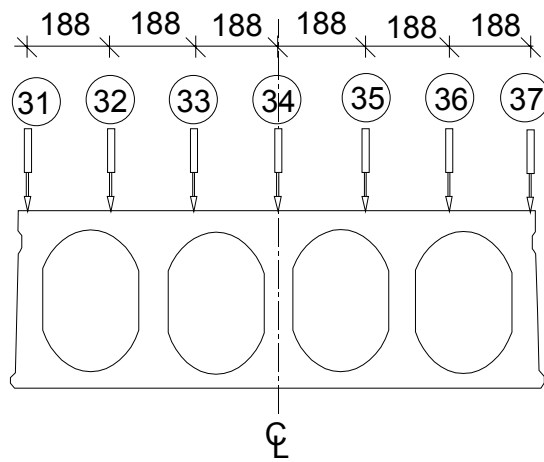


Fig. 29. ST400G. Location of transducers 11–37.

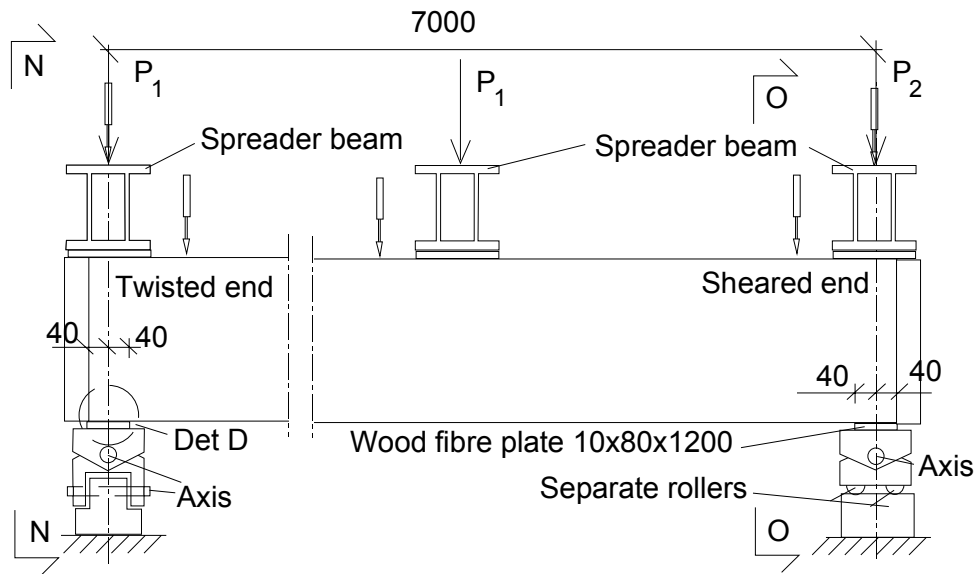


Fig. 30. ST400G. Arrangements at supports. For Det D and spreader beam see Figs 31–32 and 33, respectively.

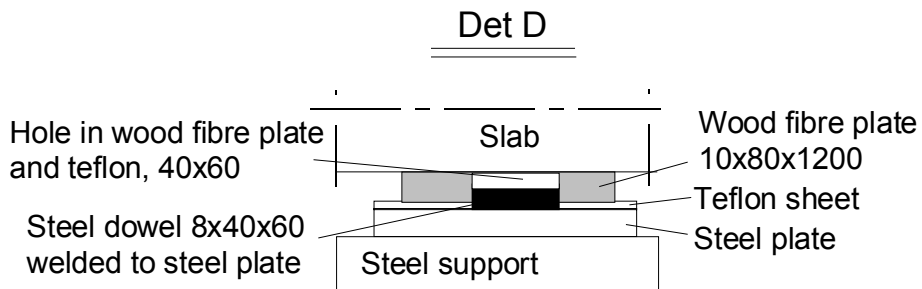


Fig. 31. ST400G. Detail of support, tilted end. See also Fig. 32.

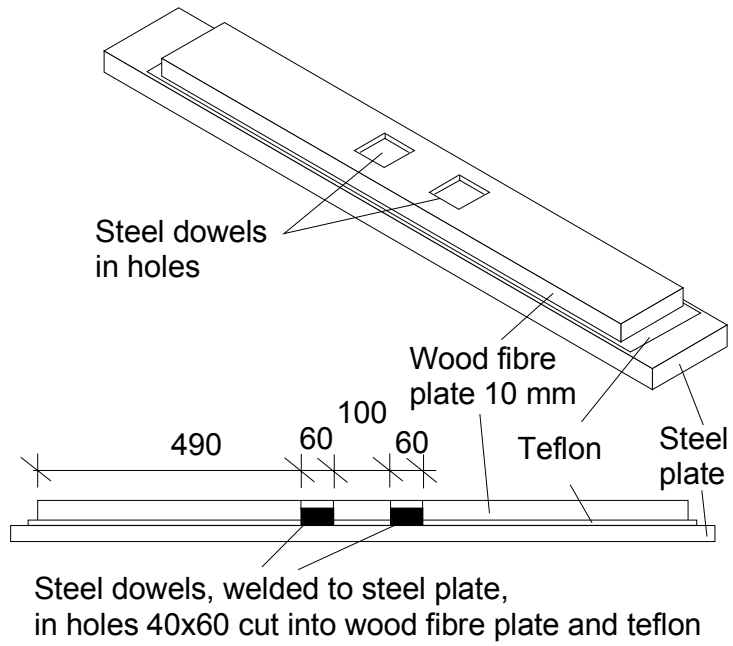


Fig. 32. ST400G. Illustration of bearing at tilted end.

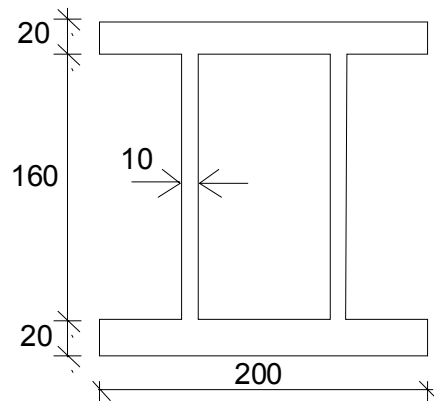


Fig. 33. ST400G. Spreader beam made of steel. Length = 1.2 m.

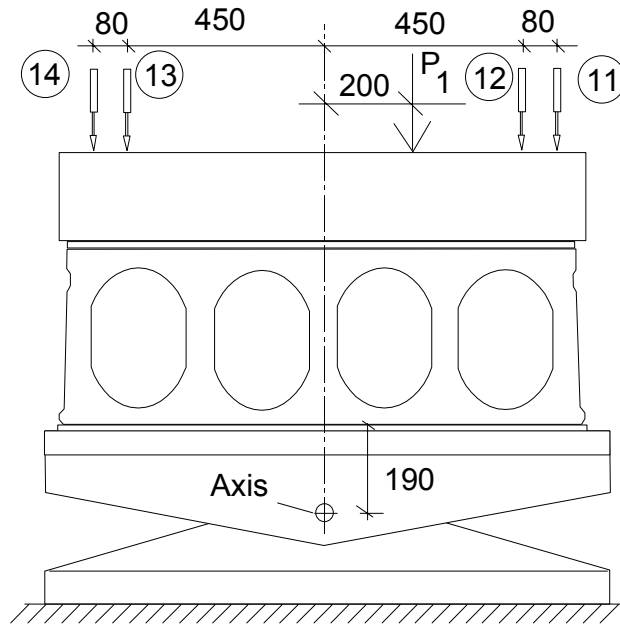


Fig. 34. ST400G. Section N-N.

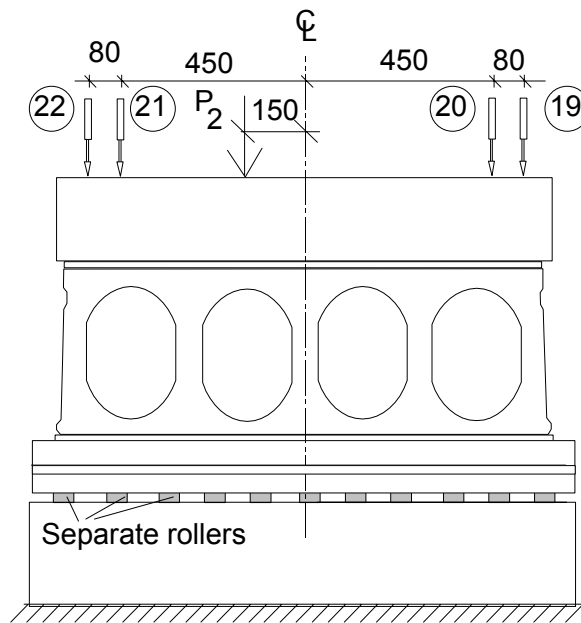


Fig. 35. ST400G. Section O-O.

2.5 Shear flexure test

In this test, the aim was to investigate flexural shear failure. However, the actual failure mode was shear tension failure. Therefore, the planned test with similar but eccentrically located loading was cancelled. Fig. 36 illustrates the test layout. More data

about test arrangements are given in Fig. 37 and in photographs 28–35, App. B. Fig. 9.a shows how the interface between the actuator and the slab surface was arranged. The support conditions were the same as those for test ST400C.

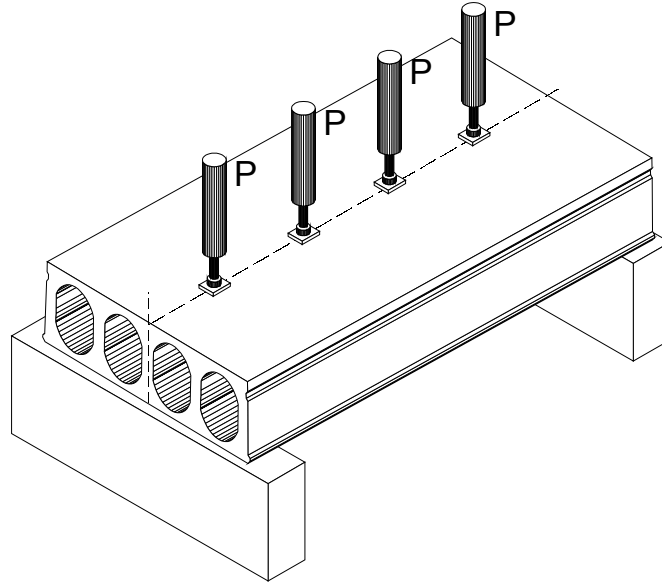


Fig. 36. Overview on test layout.

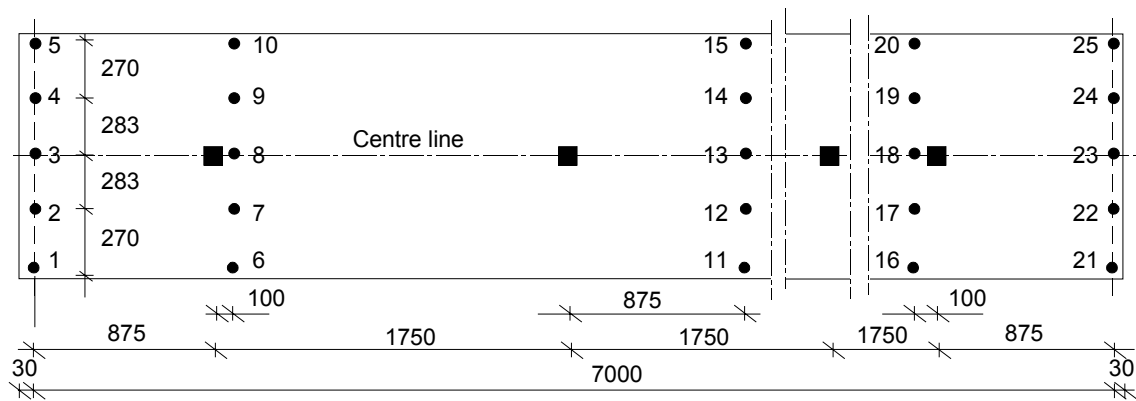


Fig. 37. Plan indicating the location of loads (black squares) and transducers for measuring deflections (black circles).

3. Material data given by the manufacturer of slabs

Table 2. Data given by the manufacturer.

	ST200E2M	ST200 (Except ST200E2M)	ST400 SF400	STS200
Concrete	K60	K60	K60	K55
Cement	CEM I 52,5 R	CEM I 52,5 R	CEM I 52,5 R	CEM I 52,5 R
Cement kg/m ³	245	240	270	310
Water l/m ³ +	120	130	145	141
Maximum aggregate size # [mm]	13	12	16	16
Number of aggregates	3	3	4	3
<u>Lower strands (smooth wires):</u>				
- strength [MPa]	1860	1860	1860	1770
- 0.2% yield strength [MPa]	1640	1640	1640	1570
- initial prestress [MPa]	900	900	1000	900
<u>Upper wires (smooth):</u>				
- strength	-	-	-	1770
- 0.2% yield strength [MPa]				1570
- initial prestress [MPa]				700

4. Results of load tests

4.1 About loading

The tests were carried out by controlling the elongation of one actuator. When more than one actuator was used, the actuator with the greatest expected elongation was chosen. Attempts were made to keep the rate of elongation piecewise as constant as possible.

4.2 Notation and some basic formulae

In tests ST400G1 and ST400G the torque over the whole slab is given by $(P_l + P_{eq})e = F_l e$ where P_{eq} is the eccentric load due to the loading equipment at the tilted end. In other tests with eccentric load the different rotation at different slab ends shall be taken into account. This can be done as follows.

Fig. 38 illustrates a beam simulating the slab in a shear-torsion test with almost non-rotating supports.

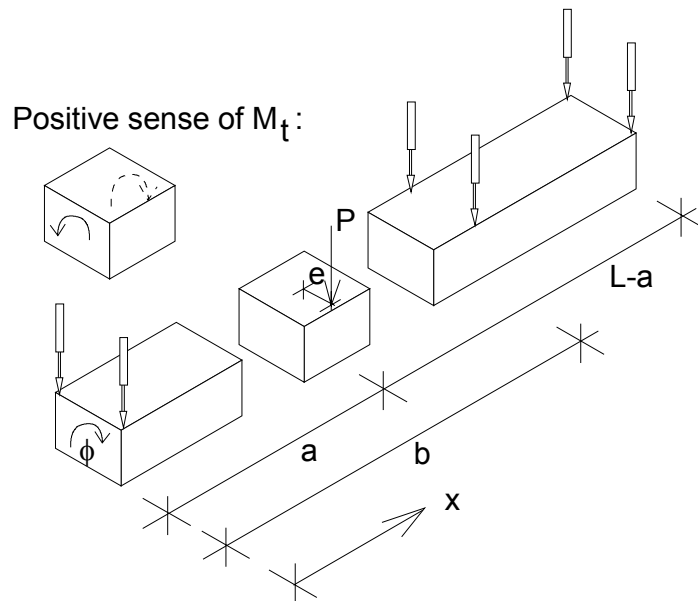


Fig. 38. Twisted member. Rotation ϕ is measured at $x = 0$, $x = b$ and $x = L$.

The interdependence of the torque M_t and relative angle of twist θ is generally given by

$$M_t = GI_t \theta \quad (1)$$

where $G = 0.5E/(1+\nu)$ and I_t denote the shear modulus and torsion modulus, respectively. E denotes the elasticity modulus and $\nu = 0.15$ Poisson's ratio. θ is defined by

$$\theta = \frac{d\phi}{dx} \quad (2)$$

where ϕ denotes the angle of twist, later also called rotation, and x is the coordinate measured along the axis of the twisted member.

Before cracking, θ and M_t can be considered constant between the load and a support, but they are discontinuous at the loaded cross-section $x = a$. Since a was shorter than L and the supports could not completely prevent twisting, $\phi(0)$ tended to be greater than $\phi(L)$. Therefore, the different rotations at the ends have to be taken into account when calculating the torque. How to do this is shown in App. G. The result is

$$M_{t,a+} \left(\frac{L-a}{\phi_L - \phi_a} - \frac{a}{\phi_a - \phi_0} \right) = Pe \frac{a}{\phi_a - \phi_0} \quad (3)$$

and

$$M_{t,a-} = M_{t,a+} + Pe \quad (4)$$

where $\phi_0 = \phi(0)$, $\phi_a = \phi(a)$ and $\phi_L = \phi(L)$. $M_{t,a-}$ and $M_{t,a+}$ denote the torque for $x < a$ and $x > a$, respectively. ϕ_a is obtained from

$$\phi_a = \phi_L + \frac{L-a}{L-b} (\phi_b - \phi_L) \quad (5)$$

where $\phi_b = \phi(b)$. ϕ_b is calculated from the displacements measured by the outermost transducers at cross-section $x = b$. If $\phi_0 = \phi_L$,

$$M_{t,a+} = -Pe \frac{a}{L} \quad (6)$$

and

$$M_{t,a-} = Pe \frac{L-a}{L} \quad (7)$$

are obtained. After cracking of the active end, $M_{t,a+}$ can be calculated from Eq. 1 if the part $x > b$ is still uncracked and (GI_t) is known. The relative angle of twist between $x = b$ and $x = L$ is then obtained from

$$\theta = \frac{\phi_L - \phi_b}{L-b} \quad (8)$$

In the following, P means actuator load, F the load on the slab due to the actuator load and the weight of the loading equipment used to spread P over the slab. In other words

$$F = P + P_{eq} \quad (9)$$

where P_{eq} is the weight of the loading equipment.

4.3 Shear tension tests on 200 mm slabs

4.3.1 Rate of loading and observations during tests

The rate of loading is given in Fig. 39. Load in all figures refers to actuator load P .

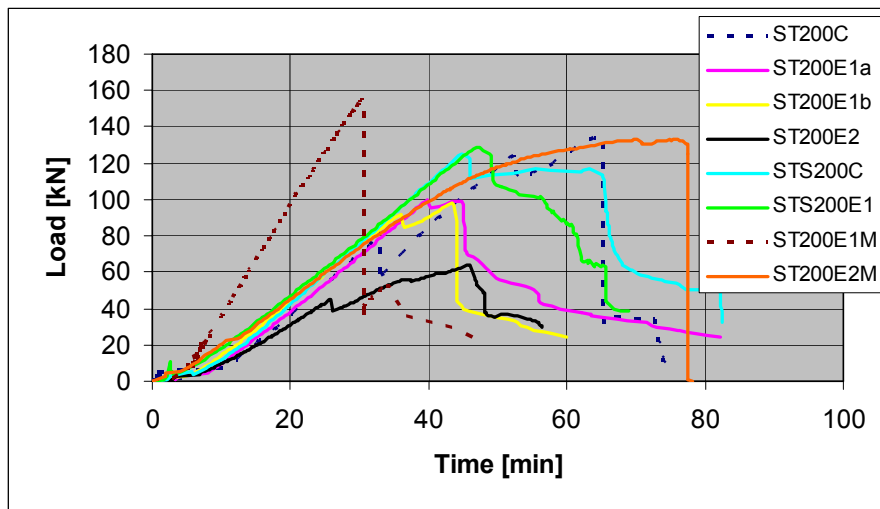


Fig. 39. Rate of loading for 200 mm slabs with horizontal supports.


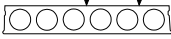
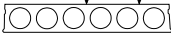



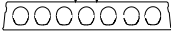

Photographs about the tests are shown in Appendix A. The measured loads and displacements are given graphically in Appendix D. The ultimate loads and observations made during the tests are summarized in Table 3.

When comparing the results of tests STS200C and STS200E1 it seems that with increasing eccentricity the resistance slightly increases. This may be due to the thick outer webs of the slab cross-section, one of which was more effectively mobilised in the eccentric test STS200E1 ($t = 65$ mm and 40 mm for the outermost and other webs, respectively).

In tests on other slab types the resistance clearly decreased with increasing eccentricity as expected.

In all tests except ST200E1M the observed resistance was considerably lower than that typical of tests with uniformly distributed transverse line load. This was the case not only with eccentric loads but also with centric loads.

Table 3. Failure load $F_{max} = P_{max} + P_{eq}$ (P_{eq} is the weight of loading equipment), its eccentricity e and description of response. The webs and voids are numbered starting from the right. The slabs are extruded unless otherwise specified. $P_{eq} = 0.5$ kN in test ST200E2M. In all other tests $P_{eq} = 0.4$ kN.

	F_{max} kN	e mm	Description
ST200C 	135.6	0	At $P = 124$ kN: a vertical crack above and below 2nd void. These cracks increased in width and length. P came down to 112 kN. When reloading, the tips of the longitudinal cracks had passed the loads at 115 kN. At 135 kN new longitudinal cracks appeared close to the existing cracks above and below the same void. At the same time webs 3–6 failed in shear tension. Webs 1, 2 and 7 remained intact. See App. A, Figs 1–9.
ST200E1a 	100.4	187	At 100 kN: a crack in the bottom corner on the right, load to 95 kN, then load increased a bit, at 96 kN: a diagonal crack in 1st web and 2 nd –4 th web failed in shear tension. See App. A, Figs 10–14.
ST200E1b 	98.4	187	At 90 kN: a longitudinal crack above the 1 st void, a diagonal crack in 1 st web, at 98 kN: a diagonal crack in the 2 nd , 3 rd and 4 th web (shear tension failure. See App. A, Figs 15–19.
ST200E2 	64.4	384	At 45 kN: diagonal shear crack in 1 st web, longitudinal crack above 1 st void, the right corner was cut off, at 58 kN: a longitudinal crack in 1 st web, at 64 kN: 2 nd web failed in shear tension, the element started to rotate around the 3 rd web. See App. A, Figs 20–24.
ST200E1M  Cast ends	156.3	187	At $P = 155.9$: a diagonal shear crack in 1 st –4 th web and a longitudinal crack above and below 4 th void. See App. A, Figs. 37–47.
ST200E2M  Grouted ends	133.5	384	At $P = 123$ kN: a flexural crack below the loads, at 127 kN: diagonal cracks on the top surface close to the support, at 133 kN: a punching failure accompanied by diagonal cracks both on the top and bottom surface in the shear span. See App. A, Figs 48–59.
STS200C Slip formed 	125.4	0	At 125 kN: a transverse flexural crack below the load, load reduced and increased until at 117 kN: crack along strand below 7 th web and 3 rd –7 th web failed in shear tension. See App. A, Figs 25–30.
STS200E1 Slip formed 	129.4	314	At 113 kN: a transverse flexural crack below the load, at 129 kN: shear cracks in 2nd and 3rd web, soffit cracked in transverse direction under these webs close to support, at 108 kN: shear crack in 1 st , 4 th and 5 th web, a longitudinal crack above 5 th void. See App. A, Figs 31–36.

4.3.2 Deflections

The measured deflection depicted in Figs 40–49 reflects the nonuniform load-sharing in transverse direction. The lowest (highest) load and smallest (greatest) deflection in Figs 40–49 correspond to uncracked (almost failed) slab.

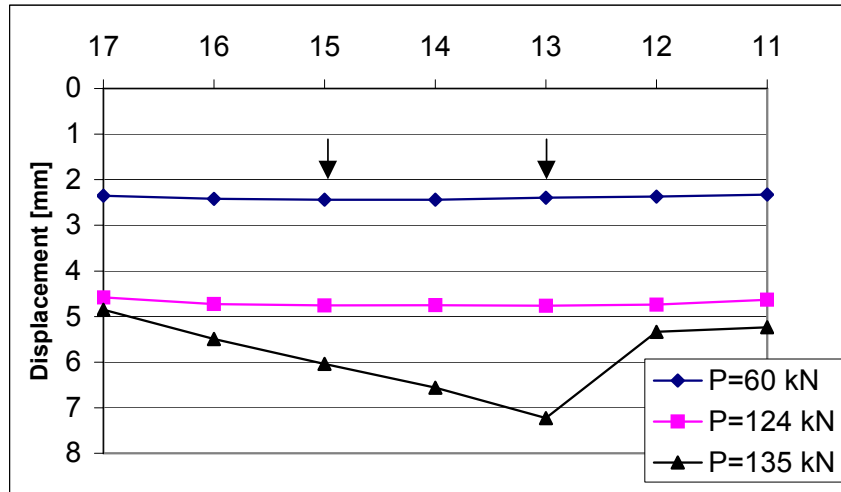


Fig. 40. ST200C. Deflection next to load, measured by transducers 11–17.

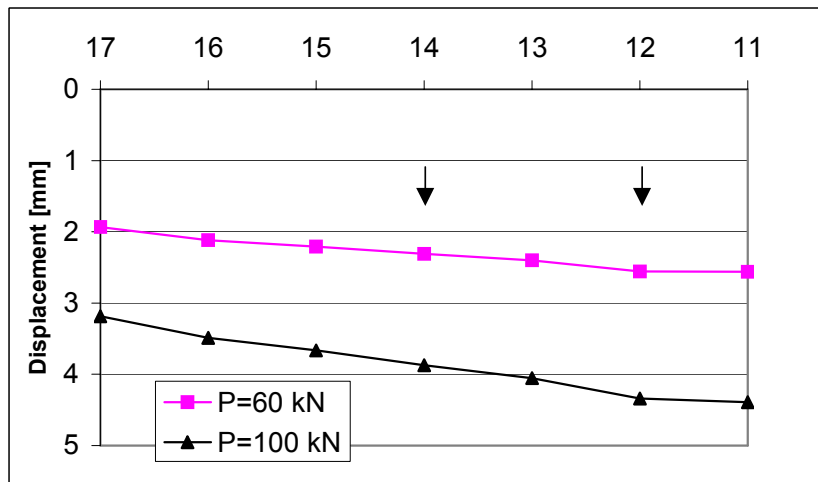


Fig. 41. ST200E1a. Deflection next to load, measured by transducers 11–17.

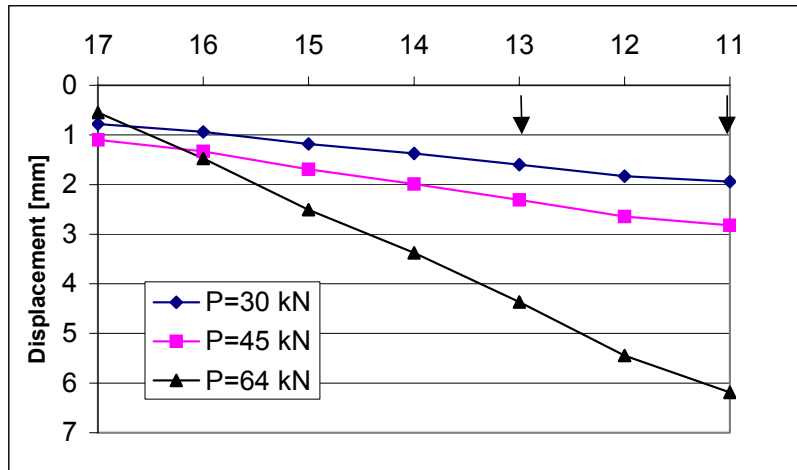


Fig. 42. ST200E2. Deflection next to load, measured by transducers 11–17.

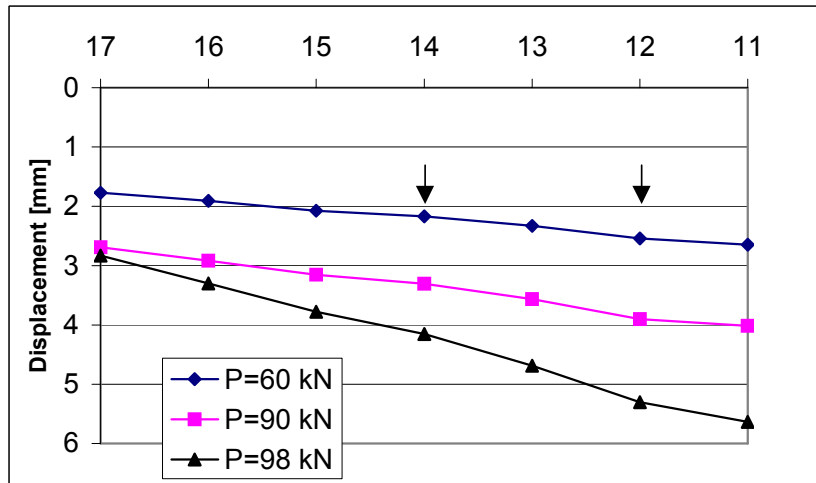


Fig. 43. ST200E1b. Deflection next to load, measured by transducers 11–17.

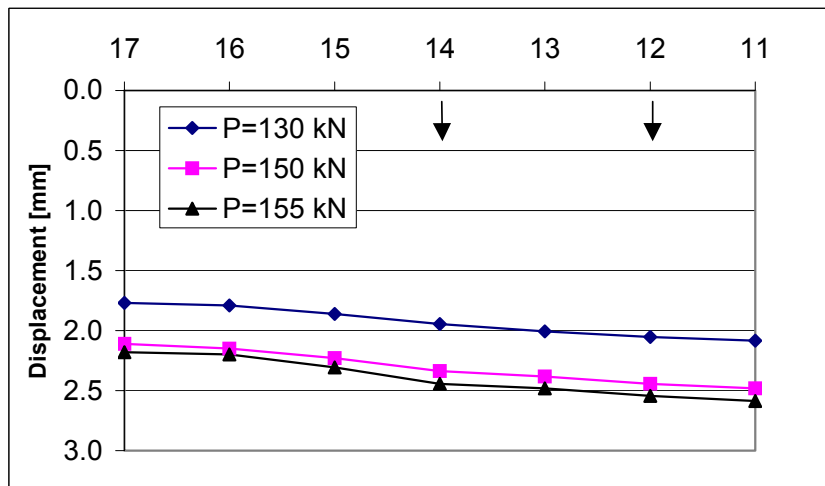


Fig. 44. ST200E1M. Deflection next to load, measured by transducers 11–17.

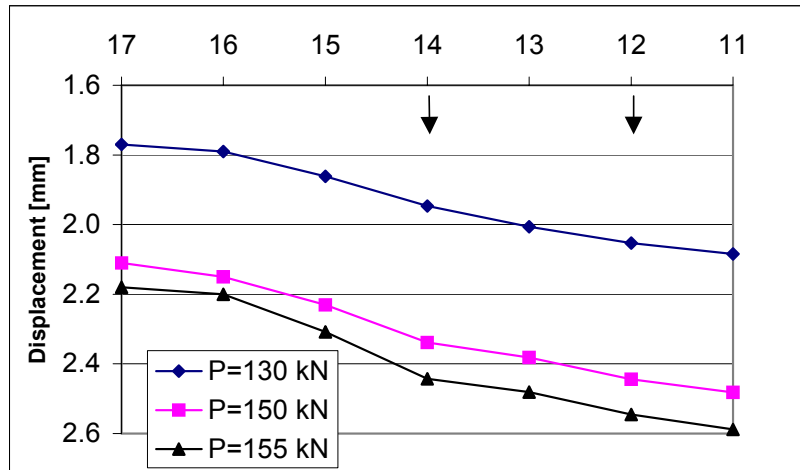


Fig. 45. ST200E1M. Deflection next to load, measured by transducers 11–17.

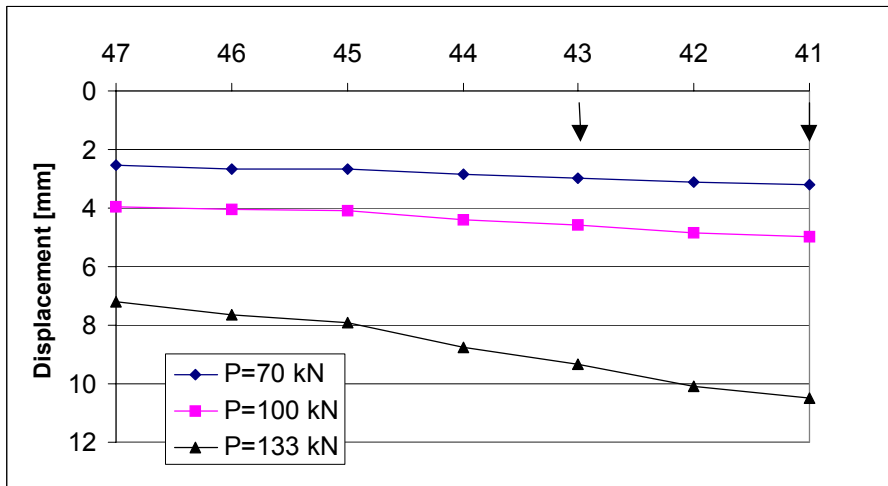


Fig. 46. ST200E2M. Deflection next to load, measured by transducers 41–47.

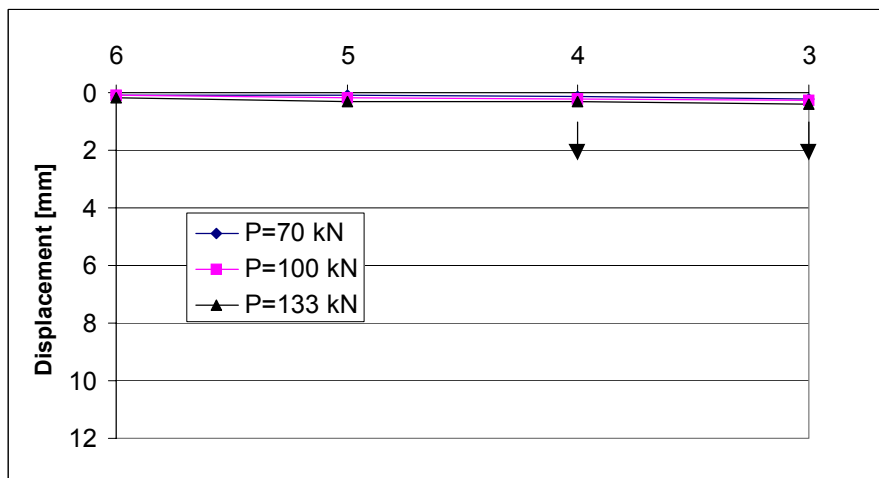


Fig. 47. ST200E2M. Settling of support at active end measured by transducers 41–47.

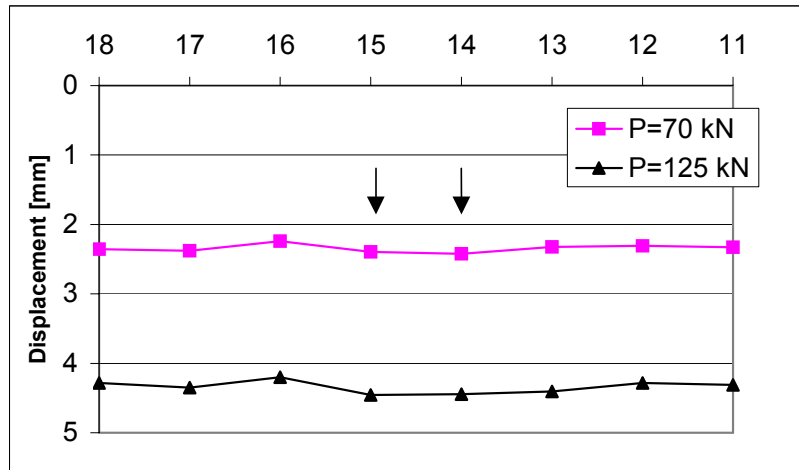


Fig. 48. STS200C. Deflection next to load, measured by transducers 11–18.

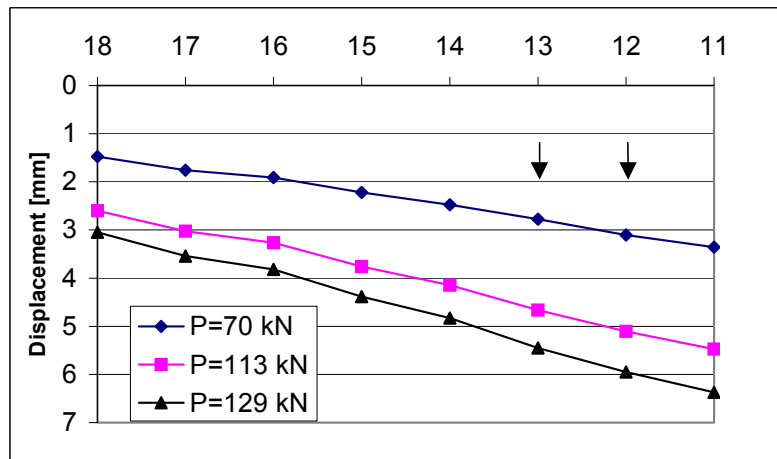


Fig. 49. STS200E1. Deflection next to load, measured by transducers 11–18.

4.3.3 Shear resistance and torsional stiffness

In Figs 50 and 51 the torsional response of the eccentrically loaded specimens is compared with the average response obtained from previous pure torsion tests [5] and denoted by PT200. The zone $b < x < L$, see Fig. 38, is considered from start until cracking of this zone. The torque in Figs 50 and 51 is calculated from Eqs 3–5 until cracking of the active end, and after cracking from Eqs 1 and 2 where GI_t equal to the secant torsional stiffness value obtained before cracking is used. The values of GI_t used in this stage as well as loads they correspond to are given in Table 4.

The curve for ST200E2 includes negative torque values and strong vibrations at the beginning. Arithmetically this is explained by the fact that rotation ϕ_0 was very close to ϕ_b and in some measurements even greater than ϕ_b . Physically this should not be

possible. On the other hand, the curve is later parallel to the other curves. No explanation for this behaviour could be detected. The vibrations in the curve for tests ST200E1M were pronounced. No explanation for the difference between identical tests ST200E1a and ST200E1b could be found, either.

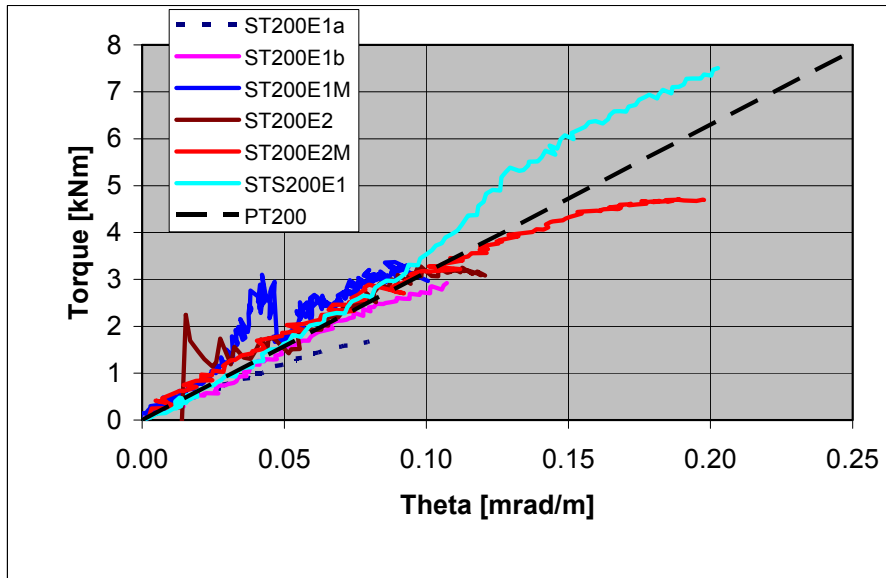


Fig. 50. Torque- θ relationship for excentrically loaded 200 mm slabs. Passive end.

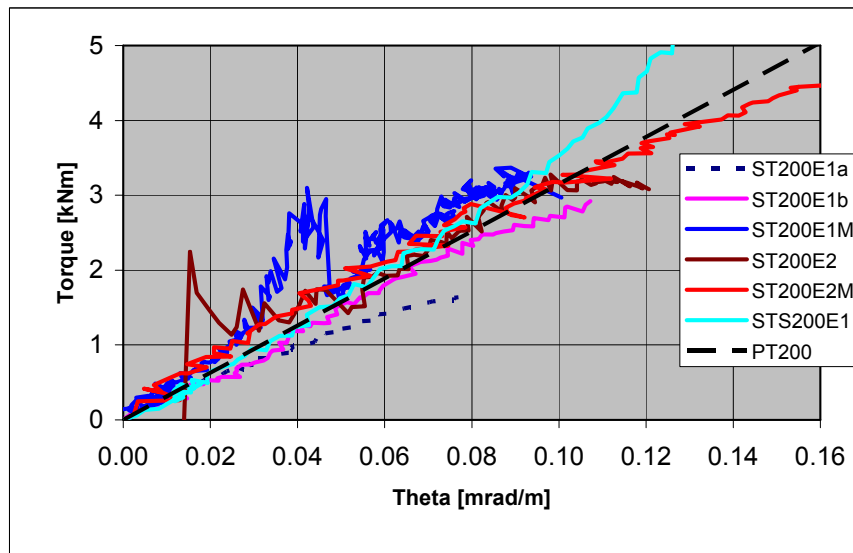


Fig. 51. Torque- θ relationship for excentrically loaded 200 mm slabs. Passive end.

In Fig. 52 the initial part of the real torque- θ curves for the pure torsion tests are compared with the curves for other tests. The slope of the pure torsion curves seems to be of the same order as in the other curves, but they do not behave logically at the origin.

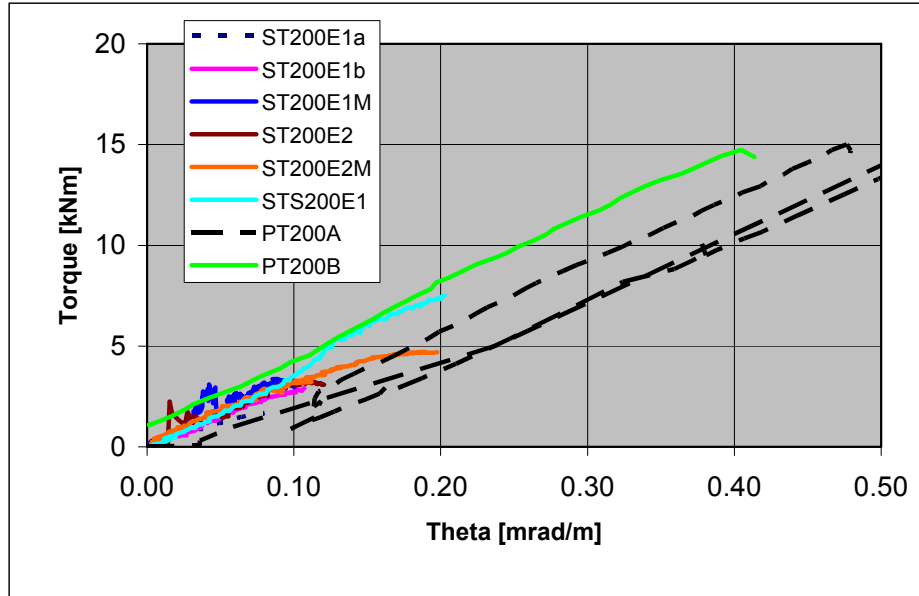


Fig. 52. Torque- θ relationship for eccentrically loaded 200 mm slabs (passive end) including initial part from pure torsion tests PT200A and PT200B.

Table 4. Load corresponding to first cracking F_{crack} , failure load F_{obs} , shear force (support reaction) at failure V_{obs} , F for calculating GI_t and GI_t for calculating M_t .

	F_{crack} kN	F_{obs} kN	V_{obs} kN	F for GI_t kN	GI_t MNm ²
ST200C	135.6	135.6	135.8	-	-
ST200E1a	100.4	100.4	103.0	-	-
ST200E1b	90.5	98.5	100.9	90.5	27.13
		92.5	95.7	90.5	27.13
ST200E1M	155.3	155.3	154.6	-	-
ST200E2	45.1	64.4	69.6	44.6	25.82
ST200E2M	126.5	133.5	128.0	123.5	25.39
STS200C	125.5	125.5	126.3	-	-
STS200E1	113.5	129.4	130.0	112.5	37.05

4.3.4 Horizontal displacements

Fig. 27 in App. D illustrates the measured horizontal displacements of the supporting beams in test ST200E1M. A positive displacement means that the beam is moving inwards (towards the inner edge of the beam), a negative displacement means that the beam is moving outwards. The displacements at the passive end are negative and those at the active end positive. As the absolute value of the negative displacement is greater than the positive one, the lower flange of the slab is getting longer as it should when the slab is subjected to vertical loading.

At first load steps there is no horizontal displacement at the active supports while the passive end moves outwards from the very beginning. At $P = 40$ kN the beam at the active support starts to move inwards. This may seem strange but can be explained, see report [6], 4.4.5. The horizontal parts in the curves might be attributable to sliding of beams along the floor, other parts could be attributable to tilting of the beams due to elongation of the bottom flange of the slab and support reaction of the slab.

Fig. 53 shows the elongation of the mutual distance of the supporting beams calculated from displacements measured by transducers 7–10. The curves look regular and show the same strain softening behaviour as the deflections shown in Figs 28 and 29 of App. D. Since the slab was uncracked in the early stage of the loading, the supporting beams must have provided an efficient horizontal restraint in this stage. In the later stage close to the failure the restraint played a minor role.

The horizontal displacements in test ST200E2M measured by transducers 11–18 are shown in App. D, Figs 32–33. They are also illustrated in Figs 54–57 at five load levels. All measurements show that the active support was tilted inwards and the passive support outwards. In addition, there was sliding at both ends, particularly at the passive end, but at the active end it only occurred at the non-loaded side and was much weaker than at the passive end. This is easily explained by the fact that the horizontal axial force in the slab was the same at both ends but due to the higher vertical force, the friction force at the active end was higher than that at the passive end.

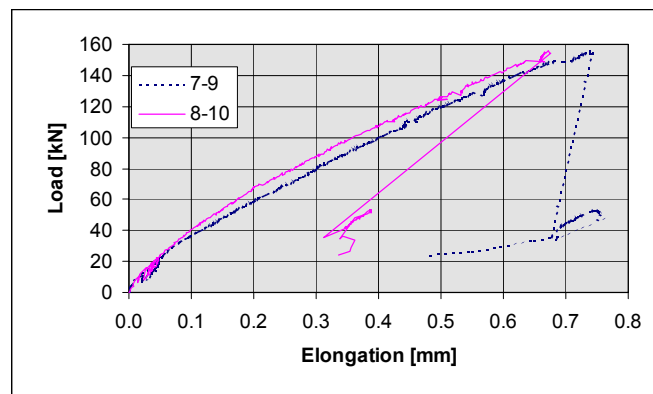


Fig. 53. ST200E1M. Elongation of mutual distance of beams measured by transducers 7–10.

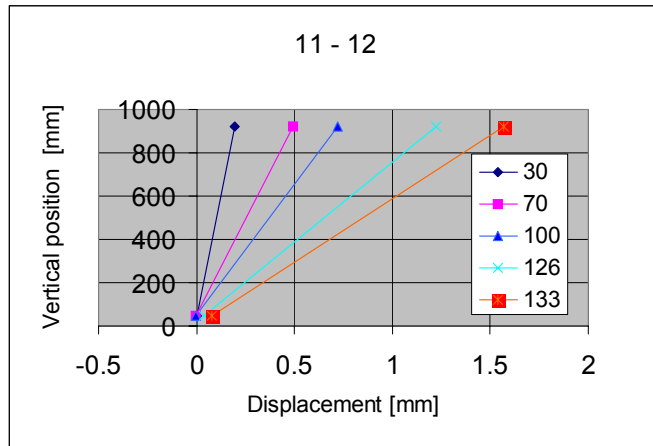


Fig. 54. ST200E2M. Horizontal displacement of beam at active end at loads $P_1 = 30\text{--}133$ kN. Transducers 11–12.

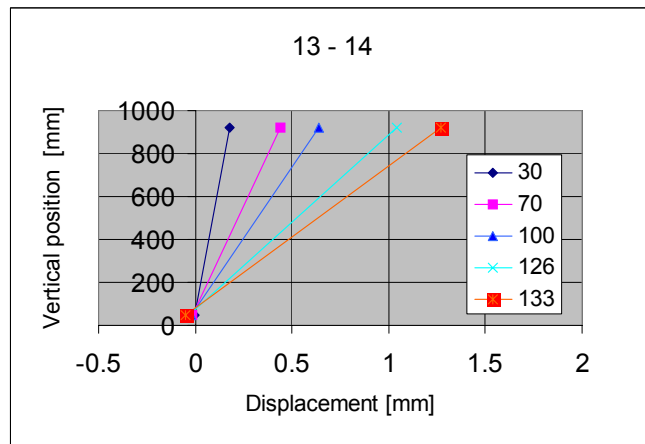


Fig. 55. ST200E2M. Horizontal displacement of beam at active end at loads $P_1 = 30\text{--}133$ kN. Transducers 13–14.

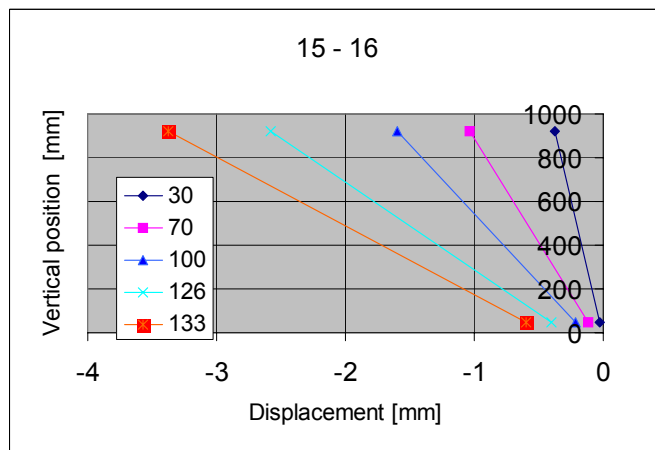


Fig. 56. ST200E2M. Horizontal displacement of beam at passive end at loads $P_1 = 30\text{--}133$ kN. Transducers 15–16.

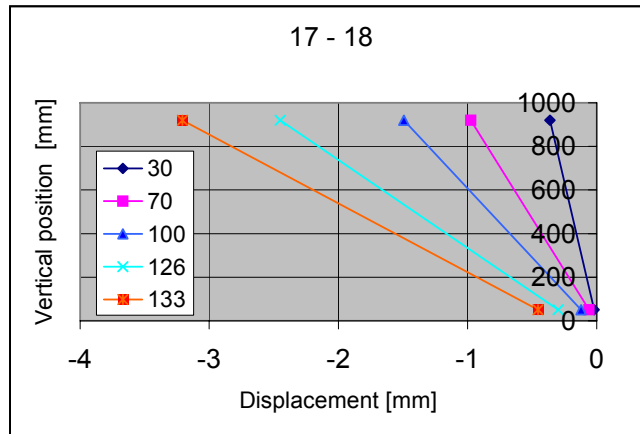


Fig. 57. ST200E2M. Horizontal displacement of beam at passive end at loads $P_1 = 30\text{--}133\text{ kN}$. Transducers 17–18.

Fig. 58 shows how the mutual distance of the supporting beam varied with load P_1 .

Fig. 59 illustrates the load-rotation relationship for all 200 mm slabs. Here the rotation means the difference $\phi_b - \phi_0$ (a) or $\phi_b - \phi_L$ (b). It should be noted that the shear span and the place where ϕ_b was measured were not the same in all tests. In the centrally loaded slab ST200C the rotation in Fig. 59.a is considerable when compared with the rotation observed in eccentrically loaded slabs. This is obviously attributable to some unsymmetry in the slabs which resulted in differences in settlement of the active support, see App. D, Fig.1.

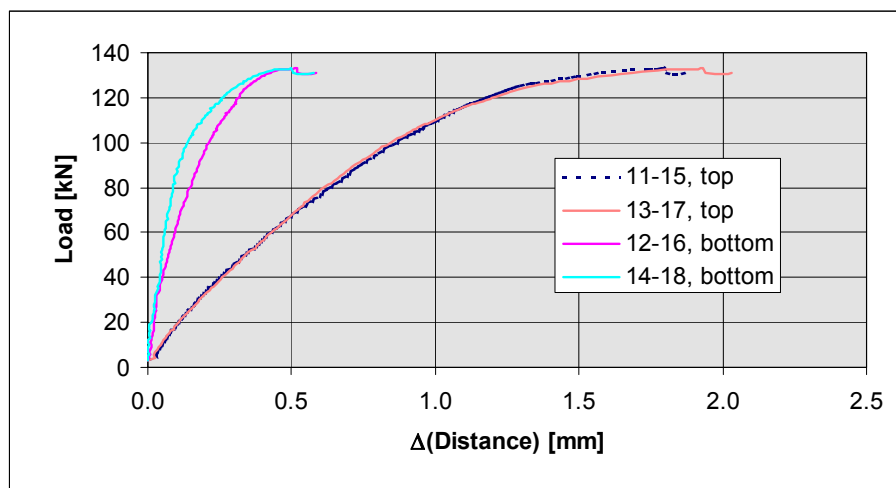
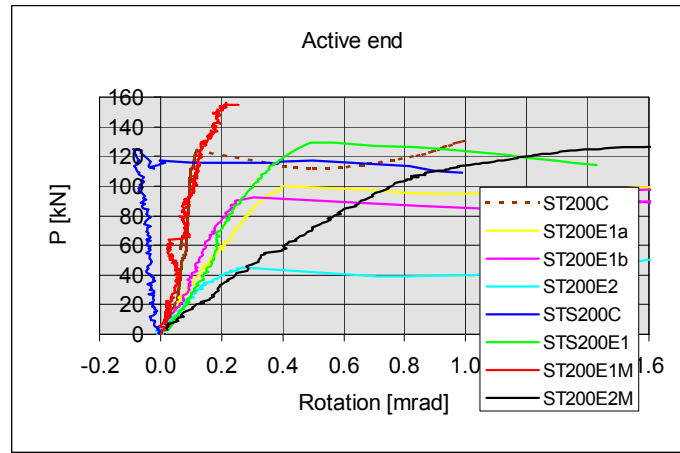
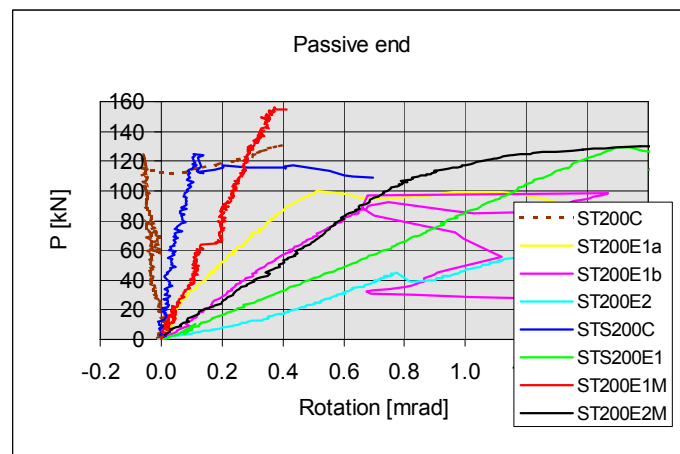


Fig. 58. ST200E2M. Elongation of mutual distance between supporting beams measured by transducers 11–18.



a)



b)

Fig. 59. Load-rotation relationship for all 200 mm tests. a) Rotation = $\phi_b - \phi_0$.
b) Rotation = $\phi_b - \phi_L$.

4.4 Shear tension tests on 400 mm slabs with parallel supports

4.4.1 About initial cracks

Before loading, a longitudinal crack in the concrete was observed above one of the outermost hollow cores at each end of each 400 mm slab unit. The reasons for such a cracking are discussed in report [5], Chapter 6. These initial cracks were typically 300–500 mm in length and 0,2 mm in thickness. They can be seen in App. B, Figs 5, 14, 20, and 43. In all tests on 400 mm slabs with eccentric load the load was placed on the opposite side of the initial crack. In these tests the initial crack remained unchanged and obviously had no effect on the failure load. For centric loads such an arrangement was not possible. Consequently, in tests ST400C1 and ST400C2 the initial crack grew in

length with increasing load, was part of the failure crack and may have reduced the observed resistance of the slab end.

4.4.2 Rate of loading and observations during tests

The rate of loading is given in Fig. 60. Photographs about tests are shown in App. B, Figs 1–27 and 36–43. The measured loads and displacements are given graphically in App. E. The ultimate loads and observations made during the tests are summarized in Table 5.

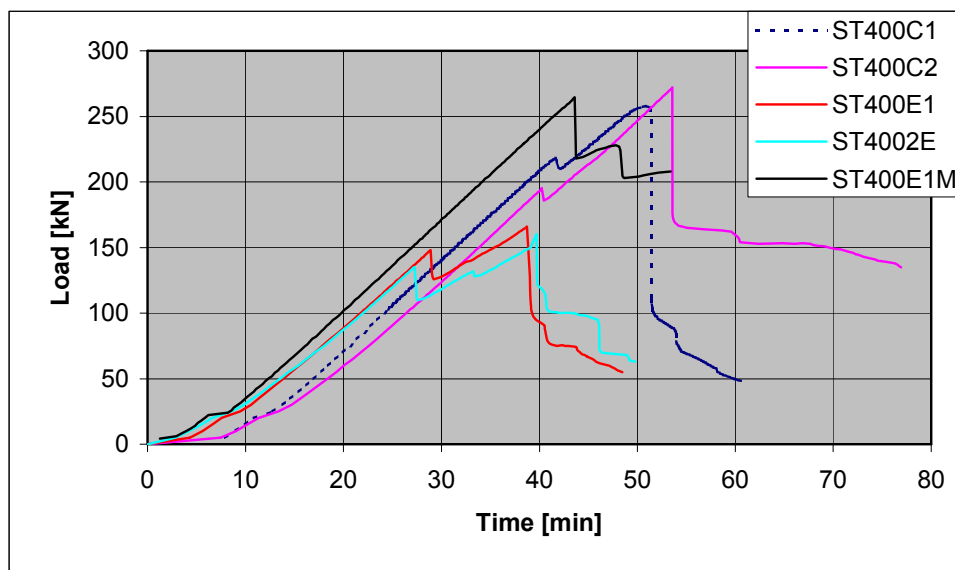



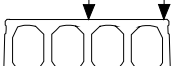



Fig. 60. Rate of loading for 400 mm slabs.

In all tests the observed resistance was considerably lower than that typical of tests with uniformly distributed transverse line load. This was the case not only with eccentric loads but also with centric concentrated loads.

Table 5. Failure load $F_{max} = P_{max} + P_{eq}$ (P_{eq} is the weight of loading equipment), its eccentricity e and description of response. The webs and voids are numbered starting from the right. $P_{eq} = 0.8$ kN for tests ST400C2 and ST4002E. For other tests $P_{eq} = 0.3$ kN.

	F_{max} kN	e mm	Description
ST400C1 	258.3	0	At $P = 218$ kN: a longitudinal crack below 1 st void and inclined shear crack in 1 st web, at 226 kN: a longitudinal crack above 1 st void, at 247 kN: a longitudinal crack along strand below 3 rd web, at 258 kN longitudinal crack above and below 3 rd void, inclined shear crack in 2 nd and 3 rd web. See App. B, Figs 1–6.
ST400C2 	272.8	0	At 195 kN: a longitudinal crack below 3 rd void and 4 th web, inclined shear crack in 5 th web, at 250 kN: a longitudinal crack above 4th void, at 272 kN: inclined shear cracks in 1 st –4 th web. See App. B, Figs 7–14.
ST400E1  Grouted ends	166.3	283	At 148 kN: longitudinal cracks above and below 1 st void and along a strand below 2 nd web, an inclined shear crack in 1 st web, at 166 kN: inclined shear cracks in 2 nd and 3 rd web, longitudinal cracks above 2 nd and 3 rd void, soffit cracked transversely below 1 st –3 rd web. See App. B, Figs 15–21.
ST4002E 	161.0	283	At 136 kN: a longitudinal crack above and below 1 st void, inclined shear crack in 1 st web, at 128 kN: an additional longitudinal crack above 1 st void, at 160 kN: inclined shear crack in 2 nd web and longitudinal crack above 2 nd void, later strong reduction in load and rotation of the slab end around 3 rd web. See App. B, Figs 22–27.
ST400E1M  Grouted ends	264.8	283	At 265 kN: a sudden shear failure in the webs and a longitudinal crack in the soffit below the load, a drop to 218 kN, an increase to 228 kN, followed by almost monotonous decrease of load and additional cracking. See App. B, Figs 36–43.

4.4.3 Deflections

The measured deflections depicted in Figs 61–65 reflect the nonuniform load-sharing in transverse direction. The lowest (highest) load and smallest (greatest) deflection in Figs 61–65 correspond to uncracked (almost failed) slab.

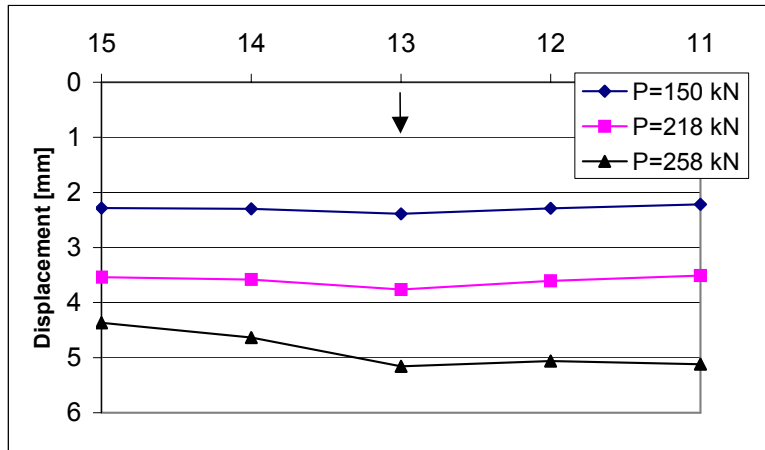


Fig. 61. ST400C1. Deflection next to load, measured by transducers 11–15.

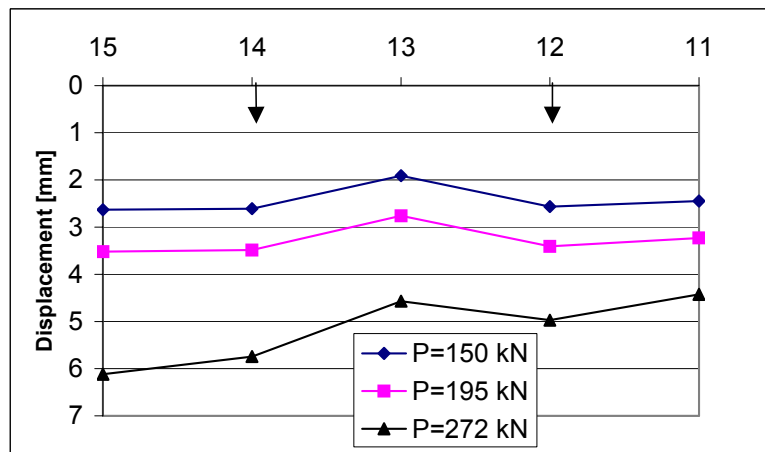


Fig. 62. ST400C2. Deflection next to load, measured by transducers 11–15.

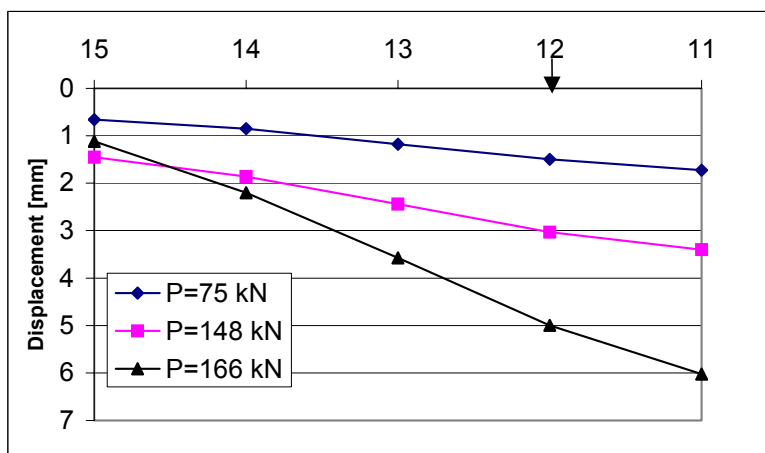


Fig. 63. ST400E1. Deflection next to load, measured by transducers 11–15.

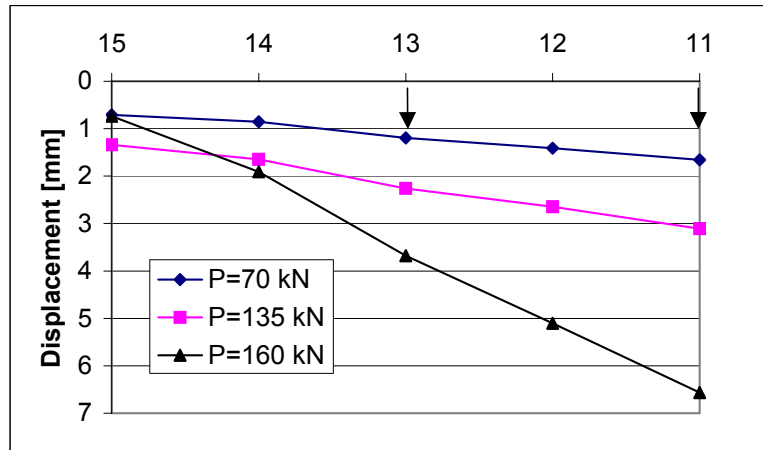


Fig. 64. ST4002E. Deflection next to load, measured by transducers 11–15.

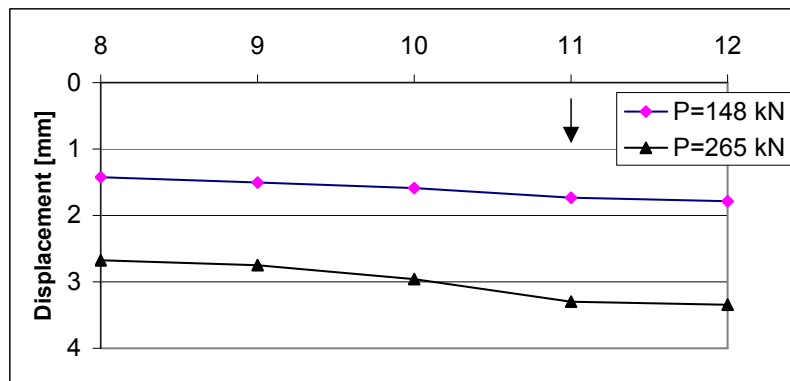


Fig. 65. ST400E1M. Deflection next to load, measured by transducers 8–12.

4.4.4 Shear resistance and torsional stiffness

In Fig. 66 the torsional response of the eccentrically loaded specimens is shown and in Fig. 72 and 73 compared with that obtained from previous pure torsion tests [5]. The zone $b < x < L$, see Fig. 38, is considered from start until cracking. The torque in Figs 66 and 72–73 is calculated from Eqs 3–5 until cracking of active end, and after cracking from Eqs 1 and 2 where GI_t equal to a typical secant torsional stiffness value obtained before cracking is used. The values of GI_t used in this stage, and loads they correspond to, are given in Table 6. The curves, especially that of test ST4002E show somewhat softer behaviour than the curve representing pure torsion tests.

Fig. 67 shows the load-rotation relationship for all 400 mm slabs with parallel supports. Here the rotation means the difference $\phi_b - \phi_0$, see Fig. 38. In centrally loaded slabs the rotation is small when compared with the rotation observed in eccentrically loaded slabs. Before cracking the differences in eccentrically loaded slabs are small.

Table 6. Load corresponding to first cracking F_{crack} , failure load F_{obs} , shear force at support at failure V_{obs} , F for calculating GI_t and GI_t for calculating $M_{t,obs}$.

	F_{crack} kN	F_{max} kN	V_{obs} kN	F for GI_t kN	GI_t MNm ²
ST400C1	218.5	258.3	407.2	-	-
ST400C2	196.1	272.8	402.2	-	-
ST400E1	147.5	166.3	257.2	147.5	114.9
ST4002E	136.0	161.0	254.7	70.9	100.2
ST400E1M	264.8	264.8	280.6	-	-

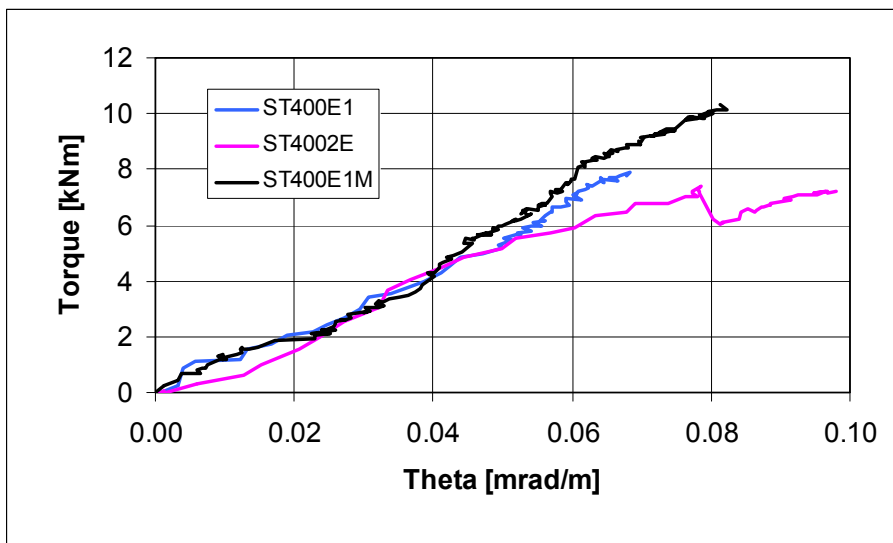


Fig. 66. Torque- θ relationship for eccentrically loaded 400 mm slabs.

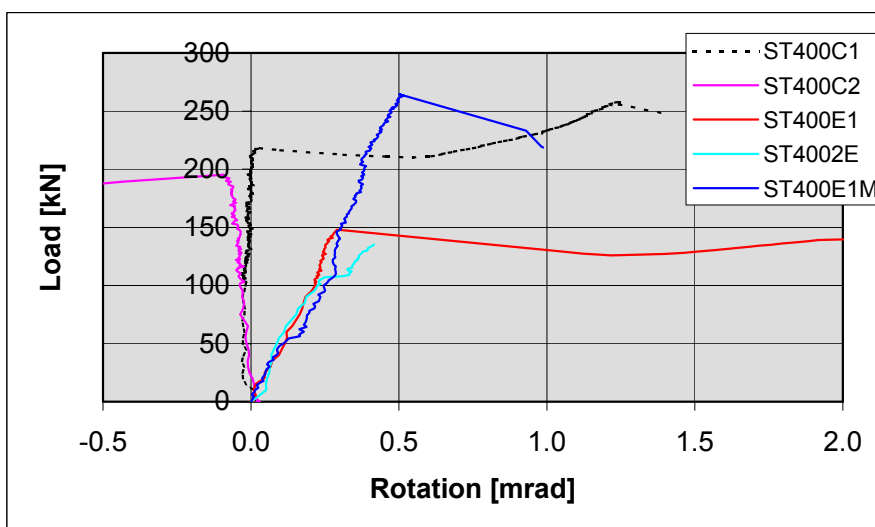


Fig. 67. Load-rotation relationship for 400 mm slabs.

4.5 Tests ST400G

4.5.1 About initial cracks

Before loading, a longitudinal crack in the concrete was observed above one of the outermost hollow cores at both ends of both 400 mm slab units. The reasons for such a cracking are discussed in [5]. These initial cracks were typically 300–500 mm in length and 0,2 mm in thickness. At the tilted end the load was placed on the opposite side of the initial crack. The length of the initial crack remained unchanged and obviously the crack had no effect on the failure load.

4.5.2 About loading

The rate of loading is given in Fig. 68. Photographs about tests are shown in App. B, Figs 44–63. The measured loads and displacements are given graphically in App. E. The ultimate loads and observation made during the tests are summarized in Table 7. In both tests the observed resistance was considerably lower than that typical of tests with a similar transverse line load but without torsion.

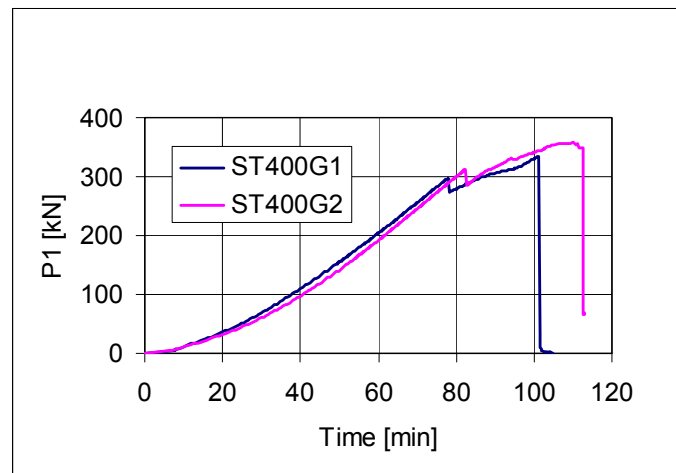


Fig. 68. Rate of loading in tests ST400G.

Table 7. Failure load $F_{max} = P_{max} + P_{eq}$ (P_{eq} is the weight of loading equipment), maximum shear force, maximum torque T_{max} and description of response. The webs and voids are numbered starting from the right. $P_{eq} = 1.18$ kN.

	F_{max} kN	V_{max} kN	T_{max} mm	Description
ST400G1	336.0	305.4	67.20	At $P_l = 297$ kN: an inclined flexural-torsional crack below the load, followed by reduction of load until 273 kN. At $P_l = 334,8$ kN a sudden shear-torsion failure in the webs. See App. B, Figs 49–55.
ST400G2	360.3	326.3	72.06	At $P_l = 313$ kN: an inclined flexural-torsional crack below the load, followed by reduction of load until 284 kN. At $P_l = 357,2$ kN a shear-torsion-anchorage failure close to the central load P_l . See App. B, Figs 56–63.

In test ST400G1 the failure was a clear shear-torsion failure in the webs. On the other hand, in test ST400G2 the failure mode is more difficult to classify. As in test ST400G1, the first crack appeared in the soffit below the line load. This helical crack increased in width until failure. At $P_l = 357,2$ kN a new inclined shear crack appeared in the web between the existing crack and the support on the South end of the slab. This crack was a consequence of the failure rather than a reason to it because on this edge the increasing torsion tended to prevent such a cracking.

The measured deflections at three different levels of load P_l , depicted in Figs 69–70, illustrate the nonuniform load-sharing in transverse direction. The lowest (highest) load and smallest (greatest) deflection correspond to uncracked (almost failed) slab.

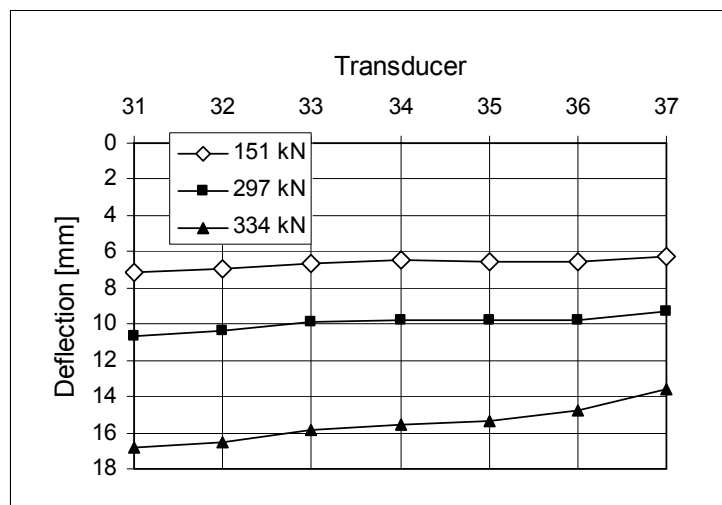


Fig. 69. ST200G1. Deflection next to load, measured by transducers 31–37.

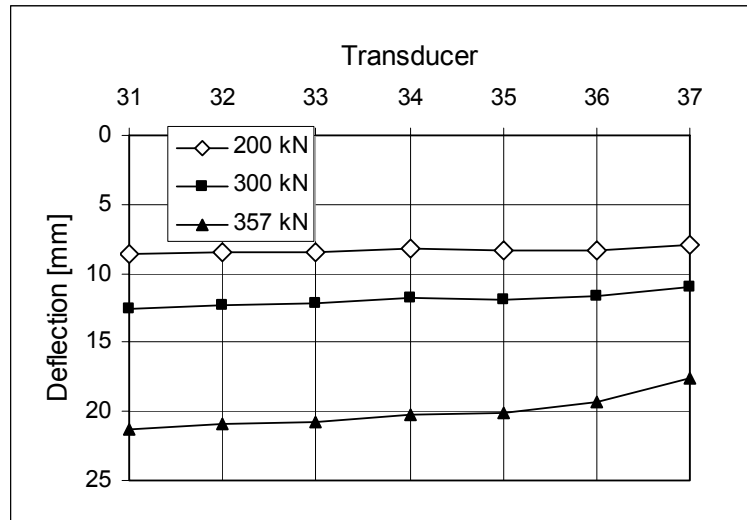


Fig. 70. ST200G2. Deflection next to load, measured by transducers 31–37.

Figs 71–73 illustrate the response of all twisted 400 mm slabs. The length of the span considered is of the order of 6 m. In pure torsion tests [5] this means the whole twisted span, in other tests the span between the shear load and the passive end (ST400E1, 2E, E1M) or tilted end (ST400G1, G2). Fig. 71 shows the torque- θ relationship for tests with one tilted support. The same curves are also shown in Fig. 72 but the curves for pure torsion tests include only the first monotonous part before the first unloading during the cyclic loading phase. Curves for tests with parallel supports are also incorporated. Fig. 73 shows the lower left corner of Fig. 72 in a larger scale.

The slabs in tests ST400G were roughly one year older than those in eccentric shear tests. Due to this, the concrete strength was higher in the former tests, but the moderate difference in the strength alone does not explain the major difference in the observed torsional stiffnesses. It is possible that in eccentrically loaded shear tests the transverse bending due to concentrated loads contributed to the measured displacements effectively and reduced the apparent torsional stiffness.

In the pure torsion tests PT400 the slab concrete was slightly weaker than that in tests ST400G. In the pure torsion tests the prestressing force was only 45% of that in tests ST400G. These two differences do not, however, explain why the torsional stiffness in the pure torsion tests was so much lower than that in tests PT400G, not only after cyclic loading stage in pure torsion tests but also before the first unloading, see Figs 72 and 73. A nonlinear FEM analysis on each test might give an answer to the observed differences.

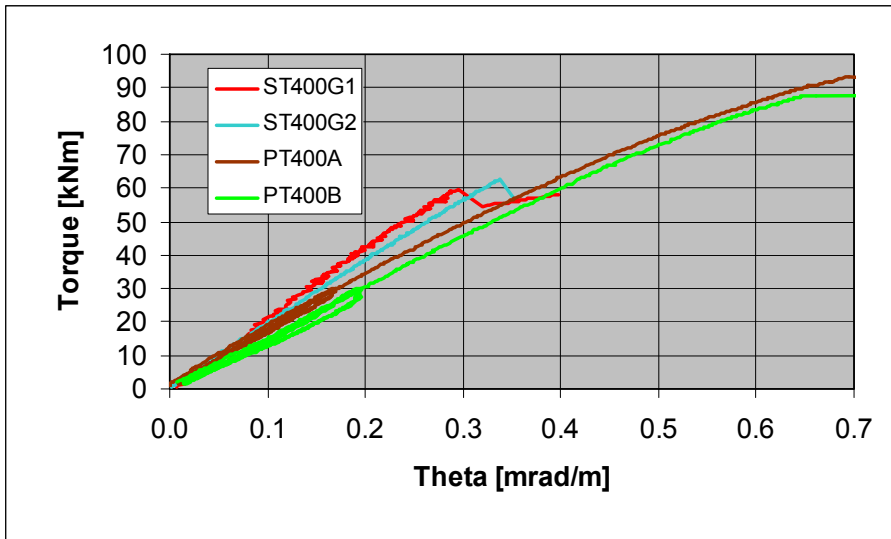


Fig. 71. Torque- θ relationship in tests ST400G and PT400.

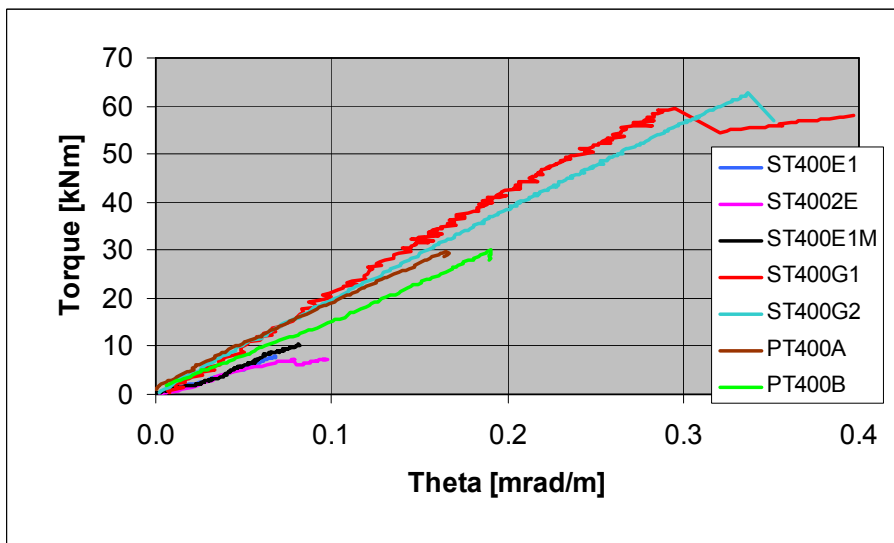


Fig. 72. Torque- θ relationship in tests on 400 mm slabs.

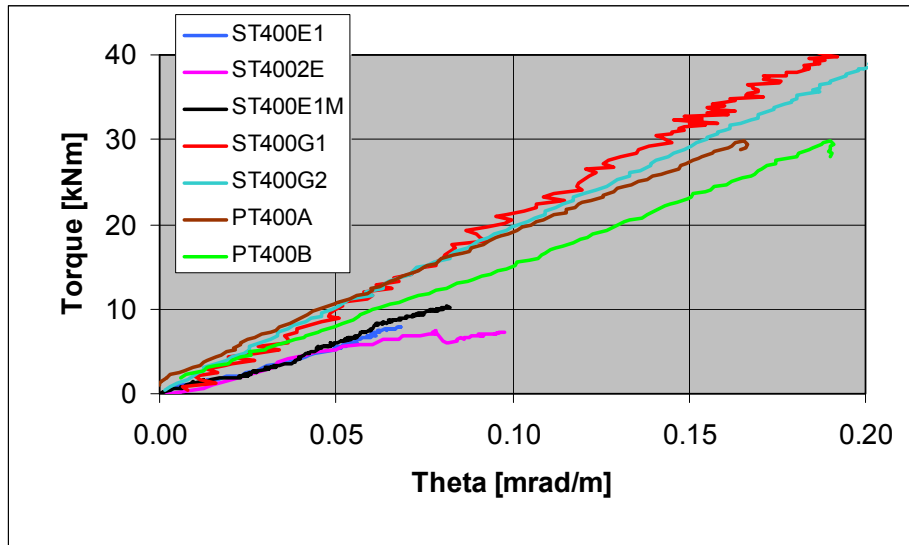


Fig. 73. Torque- θ relationship in tests on 400 mm slabs, lower left corner of previous figure.

4.6 Shear flexure test on 400 mm slab

The rate of loading is given in Fig. 74.

The first flexural cracks were observed at $P = 89.5$ kN. The load decreased temporarily until 86 kN. At $P = 90$ kN an inclined shear crack in the 5th web and a longitudinal crack below the 4th void were observed. The flexural cracks increased in number and width. Suddenly, at $P = 108.1$ kN, the Eastern end of the slab failed in shear. Instead of a flexural shear failure, a shear tension failure took place. Photographs are shown in App. B, Figs 28–35. The measured deflections are given graphically in App. F.

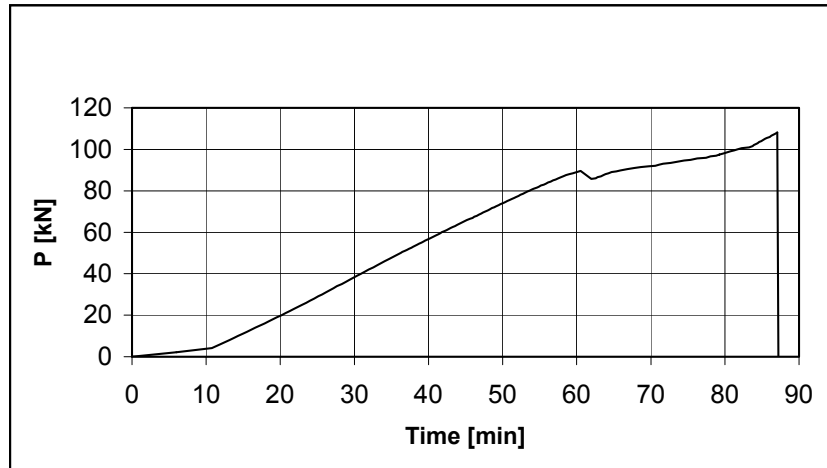


Fig. 74. Rate of loading.

The measured self weight of the slab was $g_{sl} = 4.99$ kN/m and the weight of the loading equipment $P_{eq} = 0.3$ kN per each point load P . From this data and from the measured loads the observed shear resistance (support reaction) and flexural resistance in the mid-span given in Table 8 are obtained. The predicted flexural resistance $M_{u,pre}$ is calculated using the nominal geometry of the cross-section and nominal 0.2% yield strength of the prestressing steel = 1630 MPa. It is obvious that the strands had not started to yield at failure.

Table 8. Point load at cracking ($F_{crack,obs}$) and at failure ($F_{u,obs}$), shear force at cracking ($V_{crack,obs}$) and at failure $V_{u,obs}$, bending moment at cracking ($M_{crack,obs}$) and at failure ($M_{u,obs}$), as well as predicted flexural resistance ($M_{u,pre}$).

$F_{crack,obs}$ kN	$F_{u,obs}$ kN	$V_{crack,obs}$ kN	$V_{u,obs}$ kN	$M_{crack,obs}$ kNm	$M_{u,obs}$ kNm	$M_{u,pre}$ kNm
89.8	108.4	197.1	234.3	421.3	486.4	566.0

Before loading similar initial cracks were observed in the slab as in shear tension tests, see Section 4.4. In this test the initial crack at the Eastern end (left end in Fig. 37) was part of the failure crack and may have reduced the observed resistance of the slab end.

4.7 Data about concrete

The strength of the concrete in slab elements was measured from drilled cores which were still wet due to the drilling and sawing when tested. The strength of the grouting concrete was measured from 150 mm cubes. For all specimens the measured strength, see Tables 9–19, was typical of normal production.

Table 9. Strength and density of 50 mm cores drilled from slab unit ST200E1b and tested on 26th of August 2002.

Specimen	Strength MPa	Density kg/m ³
B1	60.0	2440
B2	70.0	2440
B3	67.0	2400
B4	69.5	2420
B5	64.0	2400
B6	68.0	2420
Mean x	66.4	2420
Standard deviation s	3.8	18
Characteristic strength $f_{ck,C50} = x - 1.65s$	60.1	

Table 10. Strength and density of 50 mm cores drilled from slab unit STS200C and tested on 26th of August 2002.

Specimen	Strength MPa	Density kg/m ³
S1	70.0	2400
S2	81.0	2390
S3	72.5	2410
S4	82.5	2400
S5	78.0	2380
S6	74.0	2400
Mean x	76.3	2397
Standard deviation s	5.0	10
Characteristic strength $f_{ck,C50} = x - 1.65s$	68.2	

Table 11. Strength and density of 50 mm cores drilled from slab unit ST4002E and tested on 30th of August 2002.

Specimen	Strength MPa	Density kg/m ³
A1	61.0	2410
B2	60.0	2390
C3	56.5	2430
D4	66.5	2450
E5	57.0	2420
F6	68.5	2430
Mean x	61.6	2422
Standard deviation s	4.9	20
Characteristic strength $f_{ck,C50} = x - 1.65s$	53.4	

Table 12. Strength and density of 50 mm cores drilled from slab unit ST400E1M and tested on 21st of October 2002.

Specimen	Strength MPa	Density kg/m ³
M1	76.5	2460
M2	73.5	2350
M3	76.5	2450
M4	72.0	2480
M5	76.5	2480
M6	79.0	2450
Mean x	75.7	2462
Standard deviation s	2.5	15
Characteristic strength $f_{ck,C50} = x - 1.65s$	71.5	

Table 13. Strength and density of 150 mm cubes cast from the grouting concrete in test ST400E1M and tested on 18th of October 2002.

Specimen	Strength MPa	Density kg/m ³
HK1	34.5	2240
HK2	35.0	2270
HK3	35.5	2270
HK4	35.0	2260
HK5	35.5	2280
HK6	35.5	2270
Mean x	35.2	2265
Standard deviation s	0.4	14
Characteristic strength $f_{ck,C50} = x - 1.65s$	34.5	

Table 14. Strength and density of 50 mm cores drilled from slab unit ST200E1M and tested on 9th of June 2003.

Specimen	Strength MPa	Density kg/m ³
EM1	74.5	2370
EM2	69.5	2350
EM3	66.5	2320
EM4	68.5	2330
EM5	69.0	2340
EM6	58.5	2340
Mean x	67.8	2342
Standard deviation s	5.3	17
Characteristic strength $f_{ck,C50} = x - 1.65s$	59.1	

Table 15. Strength and density of 150 mm cubes cast from the grouting concrete in test ST200E1M and tested on 5th of June 2003.

Specimen	Strength MPa	Density kg/m ³
K2	34.0	2260
K3	34.5	2250
K4	36.5	2300
Mean x	35.0	2270

Table 16. Strength and density of 50 mm cores drilled from slab unit ST400G2 and tested on 21st of August 2003.

Specimen	Strength MPa	Density kg/m ³
G21	70.5	2300
G22	75.5	2300
G23	73.5	2320
G24	73.5	2330
G25	67.5	2320
G26	71.5	2340
Mean x	72.0	2318
Standard deviation s	2.8	16
Characteristic strength $f_{ck,C50} = x - 1.65s$	67.4	

Table 17. Strength and density of 150 mm cubes cast from the grouting concrete in tests ST400G on 8th of August and tested on 19th of August 2003.

Specimen	Strength MPa	Density kg/m ³
P1 8.8.03	31.0	2290
P2 8.8.03	31.0	2280
P3 8.8.03	28.5	2240
Mean x	30.2	2270

Table 18. Strength and density of 50 mm cores drilled from slab unit ST200E2M and tested on 4th of December 2003.

Specimen	Strength MPa	Density kg/m ³
F1	54.0	2400
F2	53.0	2410
F3	51.5	2380
F4	55.0	2410
F5	54.0	2410
F6	53.5	2410
Mean x	53.5	2403
Standard deviation s	1.2	12
Characteristic strength $f_{ck,C50} = x - 1.65s$	51.5	

Table 19. Strength and density of 150 mm cubes cast from the grouting concrete in test ST200E2M on 24th of November and tested on 2nd of December 2003.

Specimen	Strength MPa	Density kg/m ³
2	32.0	2240
3	30.0	2230
4	30.5	2210
5	30.0	2220
6	29.0	2230
Mean x	30.3	2226
Standard deviation s	1.10	11
Characteristic strength $f_{ck,C50} = x - 1.65s$	28.5	

Both slip-formed 200 mm slabs and all 400 mm slabs were sawn from the same casting bed and from the same casting lot. So were also all extruded 200 mm slabs except the slab in test ST200E2M. Most tests were carried out in August 2002 but ST400E1M in October 2002, ST200E1M in June 2003, ST400G1 and G2 in August 2003 and ST200E2M in December 2003.

The development of slab strength measured from drilled cores is illustrated in Figs 75 and 76. The concrete in extruded 200 mm slabs seems to have hardened only slightly in ten months, but the concrete in 400 mm slabs has gained more than 20% additional strength from August 2002 to October 2002. A similar conclusion can be drawn from the results of pilot floor test [6]. It is not typical that slabs from the age of two months to the age of three months and a half gain so much strength when rapidly hardening cement is used. It is possible that the cores taken in August from slab ST4002E have been drilled from a local weak zone.

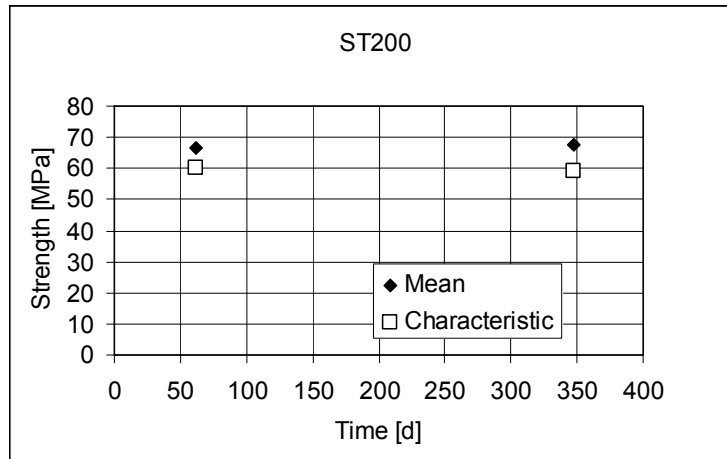


Fig. 75. Development of mean and characteristic core strength (50 x 50 mm cores) in extruded 200 mm slabs.

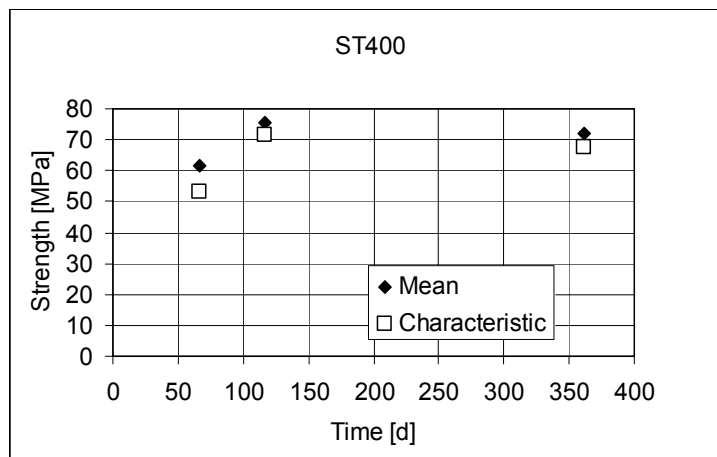


Fig. 76. Development of mean and characteristic core strength (50 x 50 mm cores) in 400 mm slabs.

4.8 Notes on results

The test specimens seemed to be typical of normal production, the strength of the concrete was high enough and the initial slippage of the strands was small in all elements. The loading and measuring equipment worked as intended with some insignificant exceptions.

No punching failure was observed in the tests except in test ST200E2M in which a mixed shear-torsion-punching failure took place, see Fig. 77.

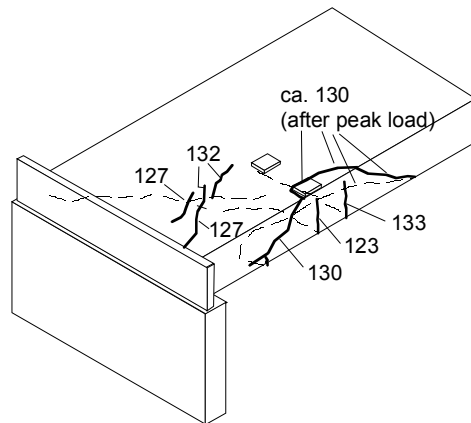


Fig. 77. Cracking pattern at failure in test ST200E2M. The dashed lines represent cracks on nonvisible surfaces.

In tests ST200E1M, ST200E2M and ST400E1M the slab elements were supported on mortar bed and their ends were grouted. In tests ST400G1 and ST400G2 the slabs were placed on soft wood fibre strips and their ends were grouted. In the rest of the tests the slabs were supported on neoprene strips 10 mm in thickness with no end grouting. The soft bearing and concentrated loads in the latter tests together with missing end grouting resulted in longitudinal cracking of slab ends in transverse bending. This explains why the failure load in tests ST200E1M, ST200E2M and ST400E1M with less deformable mortar bearing and end grouting was considerably higher than in other tests with point loads and with the same or no eccentricity.

In test STS200C a transverse flexural crack appeared below the load at ultimate load. This was followed by slippage of strands and a shear tension failure in a few webs at a lower load. In tests STS200E1 and SF400C transverse flexural cracks were observed in the soffit before ultimate load. Despite these cracks, the failure mode was web shear failure near support which was the failure mode in other tests, too.

When comparing the deflections of 200 mm and 400 mm slabs it looks like the point loads in 400 mm slabs were less uniformly shared in transverse direction than those in 200 mm slabs.

5. Analysis of shear tension tests

It is assumed that the strength measured from 50 mm drilled cores gives directly the cubic strength measured from 150 mm cubes and that the lower characteristic cylinder strength $f_{ck,C150}$ (150 mm x 300 mm cylinders) is equal to 85% of the cubic strength. In this way, $f_{ck,C150}$ given in Table 20 is obtained. From this, the mean tensile strength

$$f_{ctm} = 0.30 f_{ck,C150}^{2/3} \quad (10)$$

$f_{ck,C150} \leq 50$ MPa and the lower characteristic tensile strength

$$f_{ctm} = (2.12 \text{MPa}) \ln \left(1 + \frac{f_{ck,C150} + 8 \text{MPa}}{10 \text{MPa}} \right) \quad (11)$$

for $f_{ck,C150} > 50$ MPa are obtained according to Eurocode 2 [4] (EC2). The tensile strength calculated according to CEB Bulletin 228 [1] (CEB228) and given by

$$f_{ctm} = 0.3178 \text{MPa} \left(\frac{f_{ck,C150} + 8 \text{MPa}}{1 \text{MPa}} \right)^{0.6} \quad (12)$$

is also used to show how much the assumed tensile strength affects the results. However, when calculating according to Eurocode 2 in the following, Eq. 10 is also applied to strengths higher than 50 MPa to eliminate the discontinuity between expressions 10 and 11 at 50 MPa when the difference between the mean and characteristic strength is different from 8 MPa.

The elasticity modulus of concrete is calculated according to the Model Code [2] from

$$E_c = 0.85 \cdot (21.5 \text{GPa}) \cdot \left(\frac{f_{ck} + 8 \text{MPa}}{10 \text{MPa}} \right)^{1/3} \quad (13)$$

where the factor 0.85 takes into account the difference between initial and effective elasticity modulus. Poisson's ratio 0.15 is used for the concrete. Other material parameters for the concrete are given in Table 20. For the strands, elasticity modulus $E_p = 195$ GPa is used. The resulting strength and elasticity parameters are given in Table 20.

Table 20. Measured cylinder strength $f_{ck,C150}$, elasticity modulus E_c and mean tensile strength f_{ctm} .

	$f_{ck,C150}$ MPa	E_c GPa	Mean tensile strength MPa	
			EC2	CEB228
ST200 ¹⁾	51.1	33.0	4.13	3.67
ST200E1M	50.2	32.9	4.08	3.64
ST200E2M	43.8	32.0	3.73	3.39
STS200 ²⁾	58.0	34.3	4.49	3.92
ST400 ³⁾	45.4	31.9	3.82	3.46
ST400G	57.3	34.2	4.46	3.90
ST400E1M	60.8	34.8	4.64	4.02

1) All extruded 200 mm slabs except ST200E1M and ST200E2M

2) Both slipformed slabs

3) All 400 mm slabs except ST400E1M and ST400G

When analysing the effects of the torsion, the traditional simplification illustrated in Fig. 78 is applied.

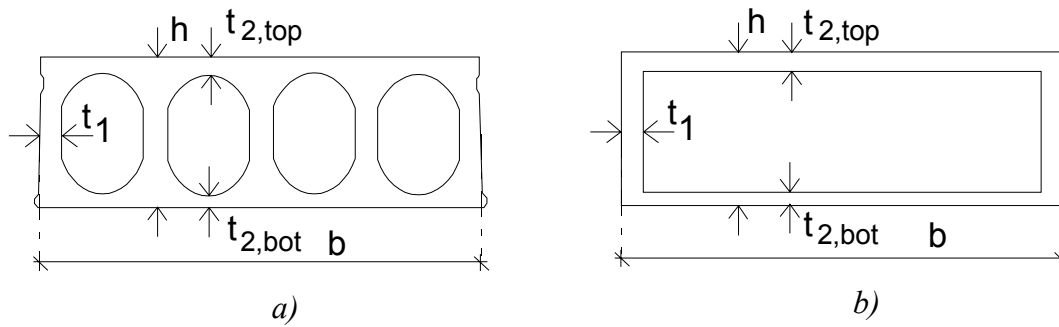


Fig. 78. Transforming a hollow core cross-section (a) into a tubular cross-section (b).

The maximum shear stress $\tau_{t,max}$ due to M_t can be evaluated using

$$\tau_{t,max} = \frac{M_t}{W_t} \quad (14)$$

where the section modulus in torsion for the web is calculated from

$$W_{t1} = 2t_1(h - t_{2,m})(b - t_1) \quad (15)$$

and that for the bottom flange from

$$W_{t2} = 2t_{2,bot}(h - t_{2,m})(b - t_1) \quad (16)$$

$t_{2,m}$ is the mean of $t_{2,top}$ and $t_{2,bot}$, see Fig. 78.

Table 21 gives both the geometry of the tubular slab cross-section without inner webs and the resulting geometric moduli. The width and depth of the cross-section are nominal values. The thickness of flanges and outer webs are means of measured values.

Table 22 gives the cross-sectional characteristics e , A , I and S of the slabs calculated using the nominal geometry shown in Figs 79–81. The measured average web width b_w and the average slab weight g_{sl} are also given. These characteristics are used for analysis of the effects of vertical shear force and bending moment.

For most parameters, the nominal geometry is used instead of measured geometry because

- when compared with other sources of error like transfer of prestressing force, tensile strength of concrete etc., the cross-sectional characteristics e , S/I , A and W (section modulus), and hence the calculated stresses are not sensitive to the measured small deviations from the nominal geometry
- the top surface of the slab is curved, see e.g. Fig. 4 in App. A, the real geometry does not correspond to any regular geometric figures and a significant improvement in the accuracy would require much more sophisticated measurements and numerical analyses of results than those within the scope of the present project.

The measured web width b_w and position of the strands are used in the analysis because the results are sensitive to them. The measured average weight of the slabs is also used because it is easy to measure. Other parameters of the slab cross-sections, see App. C, were measured to justify the use of nominal geometry in calculations.

The transfer length l_{pt} is calculated according to Eurocode 2 from

$$l_{pt} = \frac{\alpha_1 \alpha_2 \phi \cdot (\sigma_{p0} - \Delta \sigma_{p0})}{\eta_{p1} \cdot \eta_1 \cdot (0.30 f_{ck,C150}^{2/3} / \gamma_c)} \quad (17)$$

where the following parameters are applied here: $\alpha_1 = 1.25$, $\alpha_2 = 0.19$, $\sigma_{p0} - \Delta \sigma_{p0}$ is the tendon stress after the release = $\sigma_{p0} - 50 \text{ MPa}$, $\eta_{p1} = 3.2$, $\eta_1 = 0.7$ and $f_{ck,C150}$ is the characteristic strength at the release of the prestressing force. The strength at the release of the prestress, is assumed to be 70% of the cylinder strength at the age of 28 d. Including γ_c in expression 3 is confusing, because later in the code it is stated that "The design value of transmission length should be taken as the less favourable of two values, depending on the design situation: $l_{pt1} = 0.8l_{pt}$ or $l_{pt2} = 1.2l_{pt}$." This suggests that the characteristic value for l_{pt} is obtained using a nationally determined safety factor which cannot be tuned for the transfer length only. The transfer length is calculated here using $\gamma_c = 1.0$ and 1.5. In this way the transfer lengths given in Table 22 are obtained.

Table 21. Geometry and torsional characteristics of tubular cross-section. Width b and depth h of whole section, thickness of web t_1 , thickness of bottom flange $t_{2,bot}$ and that of top flange $t_{2,top}$, torsion modulus I_t as well as section moduli in torsion W_{t1} (web) and W_{t2} (bottom flange). Measured values are in italics. Slabs belonging to different casting lots are separated with continuous, horizontal lines.

	b mm	h mm	$t_{1,web}$ mm	$t_{2,bot}$ mm	$t_{2,top}$ mm	I_t mm ⁴	W_{t1} mm ³	W_{t2} mm ³
ST200C	1160	200	28.7	23.7	23.8	$1.48 \cdot 10^9$	$1.14 \cdot 10^7$	$9.48 \cdot 10^6$
ST200E1	1160	200	28.7	23.7	23.8	$1.48 \cdot 10^9$	$1.14 \cdot 10^7$	$9.48 \cdot 10^6$
ST200E1b	1160	200	28.7	23.7	23.8	$1.48 \cdot 10^9$	$1.14 \cdot 10^7$	$9.48 \cdot 10^6$
ST200E2	1160	200	28.7	23.7	23.8	$1.48 \cdot 10^9$	$1.14 \cdot 10^7$	$9.48 \cdot 10^6$
ST200E1M	1160	200	28.7	23.7	23.8	$1.48 \cdot 10^9$	$1.14 \cdot 10^7$	$9.48 \cdot 10^6$
ST200E2M	1160	200	40.0	28.8	31.0	$1.74 \cdot 10^9$	$1.52 \cdot 10^7$	$1.14 \cdot 10^7$
STS200C	1155	200	64.5	38.1	35.2	$1.97 \cdot 10^9$	$2.30 \cdot 10^7$	$1.31 \cdot 10^7$
STS200E1	1155	200	64.5	38.1	35.2	$1.97 \cdot 10^9$	$2.30 \cdot 10^7$	$1.31 \cdot 10^7$
ST400C1	1160	400	51.6	37.7	38.3	$8.94 \cdot 10^9$	$4.15 \cdot 10^7$	$3.06 \cdot 10^7$
ST400C2	1160	400	51.6	37.7	38.3	$8.94 \cdot 10^9$	$4.15 \cdot 10^7$	$3.06 \cdot 10^7$
ST400E1	1160	400	51.6	37.7	38.3	$8.94 \cdot 10^9$	$4.15 \cdot 10^7$	$3.06 \cdot 10^7$
ST400E2	1160	400	51.6	37.7	38.3	$8.94 \cdot 10^9$	$4.15 \cdot 10^7$	$3.06 \cdot 10^7$
ST400E1M	1160	400	51.6	37.7	38.3	$8.94 \cdot 10^9$	$4.15 \cdot 10^7$	$3.06 \cdot 10^7$
ST400G1	1160	400	51.0	37.4	38.1	$8.85 \cdot 10^9$	$4.108 \cdot 10^7$	$3.03 \cdot 10^7$
ST400G2	1160	400	51.0	37.4	38.1	$8.85 \cdot 10^9$	$4.108 \cdot 10^7$	$3.03 \cdot 10^7$

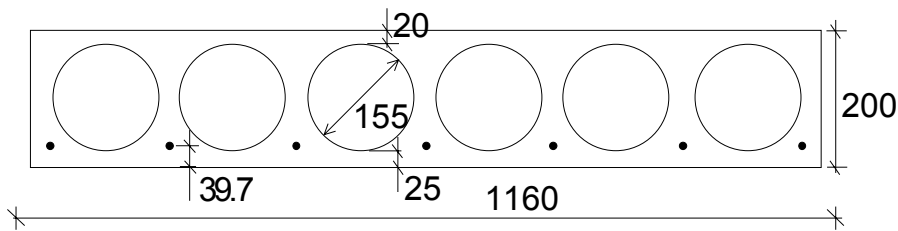


Fig. 79. Geometry of extruded 200 mm slabs used for calculation of cross-sectional characteristics.

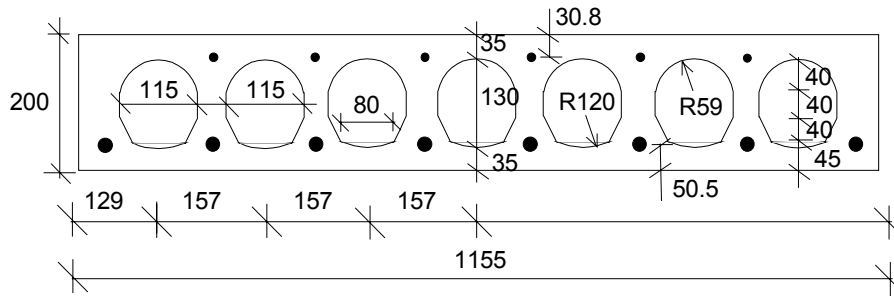


Fig. 80. Geometry of slipformed 200 mm slabs used for calculation of cross-sectional characteristics.

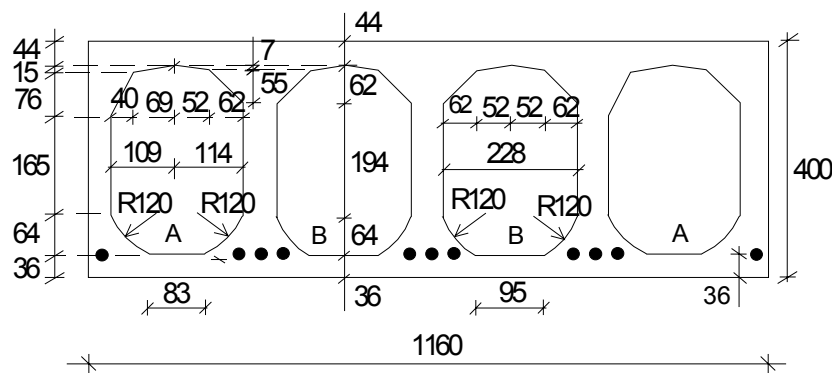


Figure 81. Geometry of 400 mm slabs used for calculation of cross-sectional characteristics. Note that there are two different types of hollow core.

Table 22. Self weight of slab g_{sl} , eccentricity of strands $e_{p,bot}$ and that of upper wires $e_{p,top}$, sum of web widths b_w , cross-sectional area A , distance from centroidal axis to bottom fibre e , second moment of area I , first moment of area S and transfer length l_{pt} . Measured values are in italics. $e_{p,bot}$ and $e_{p,top}$ are calculated from nominal e and measured average position of strands. Slabs belonging to different casting lots are separated with continuous, horizontal lines.

	g_{sl} kN/m	$e_{p,bot}$ mm	$e_{p,top}$ mm	b_w mm	A mm ²	e mm	I mm ⁴	S mm ³	l_{pt} mm
ST200C	<i>2.804</i>	56.4		228	$1.22 \cdot 10^5$	96.1	$6.12 \cdot 10^8$	$4.01 \cdot 10^{6(*)}$	385
ST200E1a	<i>2.804</i>	56.4		228	$1.22 \cdot 10^5$	96.1	$6.12 \cdot 10^8$	$4.01 \cdot 10^{6(*)}$	385
ST200E1b	<i>2.804</i>	56.4		228	$1.22 \cdot 10^5$	96.1	$6.12 \cdot 10^8$	$4.01 \cdot 10^{6(*)}$	385
ST200E2	<i>2.804</i>	56.4		228	$1.22 \cdot 10^5$	96.1	$6.12 \cdot 10^8$	$4.01 \cdot 10^{6(*)}$	385
ST200E1M	<i>2.784</i>	56.4		228	$1.22 \cdot 10^5$	96.1	$6.12 \cdot 10^8$	$4.01 \cdot 10^{6(*)}$	385
ST200E2M	<i>2.857</i>	54.9		278	$1.39 \cdot 10^5$	96.1	$6.60 \cdot 10^8$	$4.43 \cdot 10^{6(*)}$	427
STS200C	<i>3.342</i>	48.6	-69.3	367	$1.47 \cdot 10^5$	100.0	$6.83 \cdot 10^8$	$4.64 \cdot 10^6$	354 ^{**)}
STS200E1	<i>3.342</i>	48.6	-69.3	367	$1.47 \cdot 10^5$	100.0	$6.83 \cdot 10^8$	$4.64 \cdot 10^6$	354 ^{**)}
ST400C1	<i>5.010</i>	168.9		275	$2.13 \cdot 10^5$	204.9	$4.48 \cdot 10^9$	$1.43 \cdot 10^7$	466
ST400C2	<i>5.010</i>	168.9		275	$2.13 \cdot 10^5$	204.9	$4.48 \cdot 10^9$	$1.43 \cdot 10^7$	466
ST400E1	<i>5.010</i>	168.9		275	$2.13 \cdot 10^5$	204.9	$4.48 \cdot 10^9$	$1.43 \cdot 10^7$	466
ST400E2	<i>5.010</i>	168.9		275	$2.13 \cdot 10^5$	204.9	$4.48 \cdot 10^9$	$1.43 \cdot 10^7$	466
ST400E1M	<i>5.010</i>	168.9		275	$2.13 \cdot 10^5$	204.9	$4.48 \cdot 10^9$	$1.43 \cdot 10^7$	466
ST400G1	<i>4.930</i>	168.9		273	$2.13 \cdot 10^5$	204.9	$4.48 \cdot 10^9$	$1.43 \cdot 10^7$	466
ST400G2	<i>4.940</i>	168.9		273	$2.13 \cdot 10^5$	204.9	$4.48 \cdot 10^9$	$1.43 \cdot 10^7$	466

^{*)} First moment of area above the thinnest part of the web

^{**)} Lower strands, $l_{pt} = 203$ for upper wires

In Table 23 the predicted torsional stiffness is compared with the experimental values obtained from the present tests, see Tables 4 and 6 and previous pure torsion tests [5]. In the pure torsion tests the slab cross-sections were identical to the extruded cross-sections in the present tests with the exception that the number of strands in 400 mm slabs was five instead of eleven in the present tests.

The observed stiffness given in Table 23 is the secant stiffness determined before the first cracks appeared. In pure torsion tests the whole span, in the other tests the span between the shear load and the distant support is considered. The secant stiffness is solved from Eq. 1.

The torsional stiffness observed in pure torsion tests and in tests ST400G exceeded the stiffness observed in shear torsion tests on neoprene bearing and ST400E1M. In addition to the unavoidable scatter in all experimental results, the different test

arrangements may explain the difference. The way of measuring the angle of twist, see Section 4.2, is not accurate, because it is also affected by the transverse bending. In pure torsion tests and in tests ST400G the slabs were not subjected to transverse bending. Therefore, the observed stiffness for these tests is more reliable than that for the other tests in which the concentrated loads gave rise to transverse deformations which are not present in pure torsion. In other words, the slabs in the shear torsion tests behaved partly as slabs, those in pure torsion tests and tests ST400G mainly as beams. Consequently, the deflection of a hollow core slab cannot be accurately predicted by modelling it as a beam with longitudinal bending and torsional degrees of freedom only.

Table 23. Observed ($GI_{t,obs}$) and predicted ($GI_{t,pre}$) torsional stiffness as well as torsional stiffness $GI_{t,obs,PT}$ observed in previous pure torsion tests.

	$GI_{t,obs}$ MNm ²	$GI_{t,obs,PT}$ MNm ²	$GI_{t,pre}$ MNm ²	$\frac{GI_{t,pre}}{GI_{t,obs}}$
ST200E1a	20.9	31.5	21.1	1.01
ST200E1b	27.1		21.6	0.80
ST200E2	25.8		21.0	0.81
ST200E1M	35.0		21.6	0.62
ST200E2M	25.4 ¹⁾ 22.3 ²⁾		21.4	0.84 0.96
STS200E1	37.1		31.0	0.83
ST400E1	114.9	133.9	122.1	1.06
ST400E2	73.5		123.9	1.68
ST400E1M	124.8		131.3	1.05
ST400G1	203.1		137.9	0.68
ST400G2	186.0		136.5	0.73

1) Obtained from displacements measured by transducers 41, 47, 7 and 10, see Fig. 21

2) Obtained from displacements measured by transducers 51, 57, 7 and 10, see Fig. 21

In tests ST200E1M, ST200E2M and ST400E1M the cast-in-situ concrete stiffened the slab ends against transverse bending. The supporting beams provided the slab with a longitudinal, partial restraint which also reduced the deflections of the slab. In tests ST200E1M and ST400E1M these two restraints are reflected in the observed torsional stiffness which is higher than in the tests with neoprene bearing. Odd enough, no such stiffening was observed in test ST200E2M.

In Table 24 the observed torque at failure is given. It is calculated from test results either using Eqs 1, 4 & 8 and $GI_{t,obs}$ from Table 23 (active end cracked before failure), or applying Eqs 3, 4 & 5 directly to the measured loads and displacements (slab uncracked until failure).

Table 24. Observed torque $M_{t,obs}$ and shear resistance V_{obs} (shear force at support) at failure as well as equations used for calculating $M_{t,obs}$.

	$M_{t,obs}$ kNm	V_{obs} kN	Equations
ST200C	-	135.8	-
ST200E1a	17.03	103.0	3, 4 & 5
ST200E1b	14.23	95.7	1, 4 & 8
ST200E2	18.95	69.6	1, 4 & 8
ST200E1M	26.02	154.6	3, 4 & 5
ST200E2M	42.44	128.0	1, 4 & 8
STS200C	-	126.3	-
STS200E1	31.83	130.0	1, 4 & 8
ST400C1	-	238.9	-
ST400C2	-	251.4	-
ST400E1	34.92	160.1	1, 4 & 8
ST400E2	38.26	155.5	1, 4 & 8
ST400E1M	64.55	244.5	3, 4 & 5
ST400G1	67.20	305.4	1, 4 & 8
ST400G2	72.06	326.3	1, 4 & 8

The observed torque and shear resistance (shear force at support) are compared with the predicted values in Figs 82–88. The predicted values are calculated using two different tensile strengths, the mean tensile strength according to Eq. 10 (from Eurocode 2 [4]) or according to Eq. 11 (from CEB Bulletin 228 [1]). It is also assumed that

- the strength is that measured for ST200E1b (Fig. 82), ST200E1M (Fig. 83), ST200E2M (Fig. 84), STS200C (Fig. 85), ST400E2 (Fig. 86), ST400E1M (Fig. 87) and ST400G2 (Fig. 88)
- the losses of prestress are
 - = 150 MPa for tests ST200E1M and ST400G
 - = 100 MPa for other tests
- the prestress is transferred linearly
- for each slab type the cross-sectional characteristics given in Tables 21–22 are used.

The limit states considered in Figs 82–88 are cracking in the webs and cracking in the bottom flange below the load. Cracking of the webs is considered according to EN1168 [3] at a distance of $b_s+0.5h$ from slab end, where b_s is 60 mm and 80 mm for 200 mm and 400 mm slabs, respectively, and h is the slab thickness. For 400 mm slabs the cracking of webs is also considered according to Yang [8] at a distance of 183 mm from slab end and 100 mm from the soffit. The normal stresses in slab cross-section at a distance of x from the slab end are calculated assuming that the cross-section is loaded by a normal force equal to the prestressing force transferred within the distance x .

The curves or points referring to the cracking of bottom flange are indicated by *bot.fl.* Cracking in the bottom flange does not necessarily mean failure. The criterion for both considered limit states is the same: cracking takes place when the maximum tensile stress of the concrete becomes equal to the mean tensile strength f_{ctm} .

The rough assumptions for the losses of prestress mean that the prestressing force may be slightly under- or overestimated. This has a minor effect on the predicted shear failure curves in Figs 82–88. The curves representing flexural cracking are more sensitive to the prestressing. In any case, conclusions can be drawn from the figures because the error due to the uncertainty of the prestressing force is not significant when compared with other uncertainties.

The resistance of the bottom flange is not particularly sensitive to the tensile strength because the compression due to the prestressing force is the prevailing factor affecting the cracking resistance. This can be seen in Figs 82 and 84 in which one point of the flexural cracking curve, calculated according to EC2, is shown. It was not considered necessary to include further points.

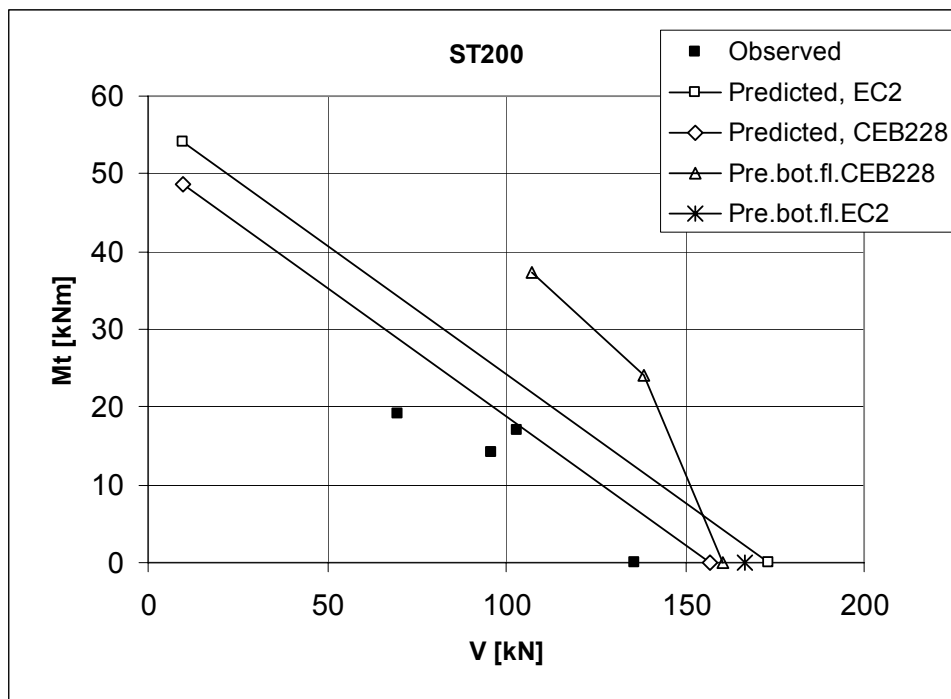


Fig. 82. Comparison of predicted and observed results for extruded 200 mm slabs on neoprene bearing.

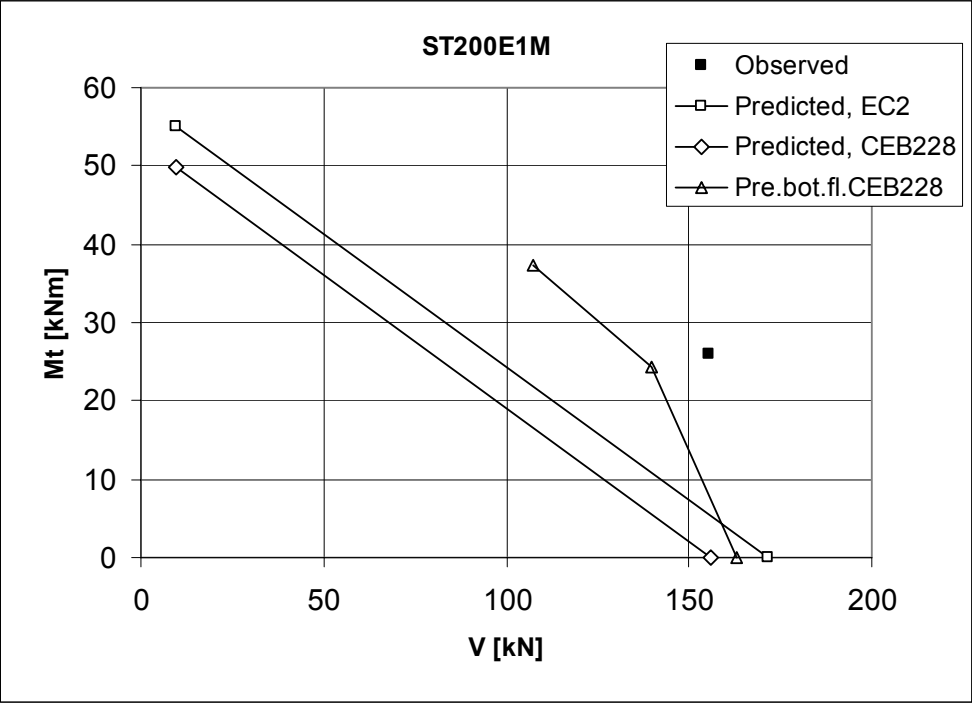


Fig. 83. Comparison of predicted and observed results for test ST200E1M.

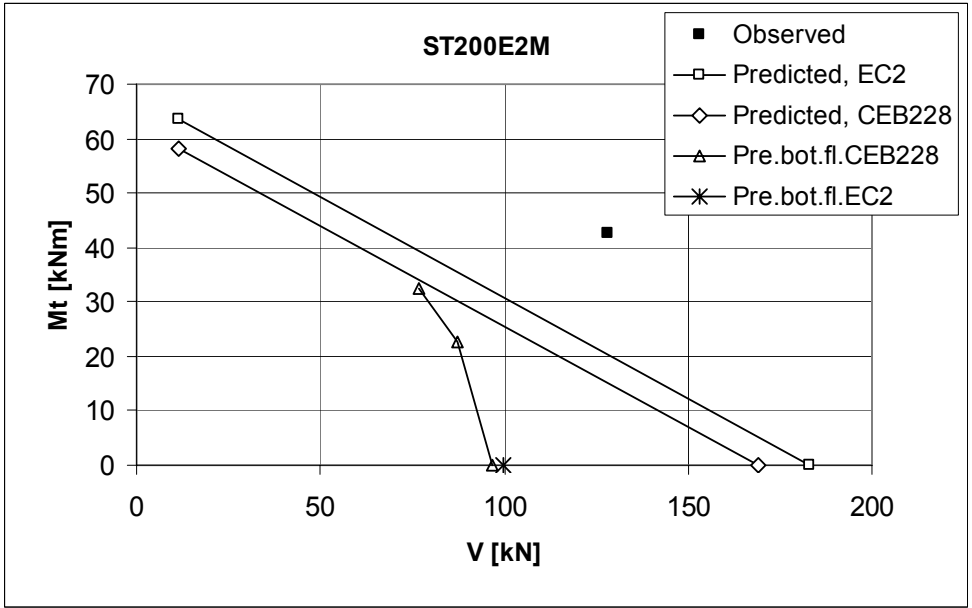


Fig. 84. Comparison of predicted and observed result for test ST200E2M.

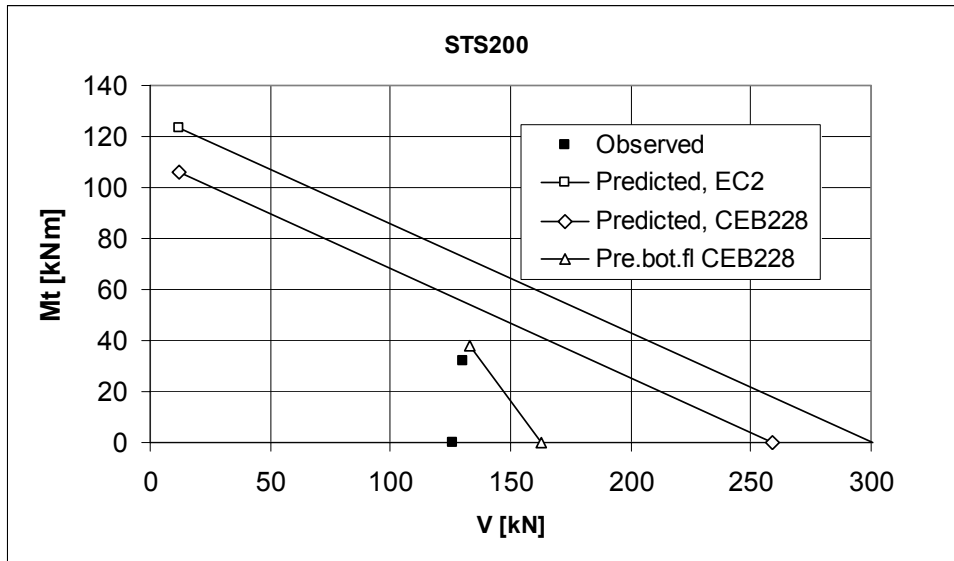


Fig. 85. Comparison of predicted and observed results for slip-formed 200 mm slabs.

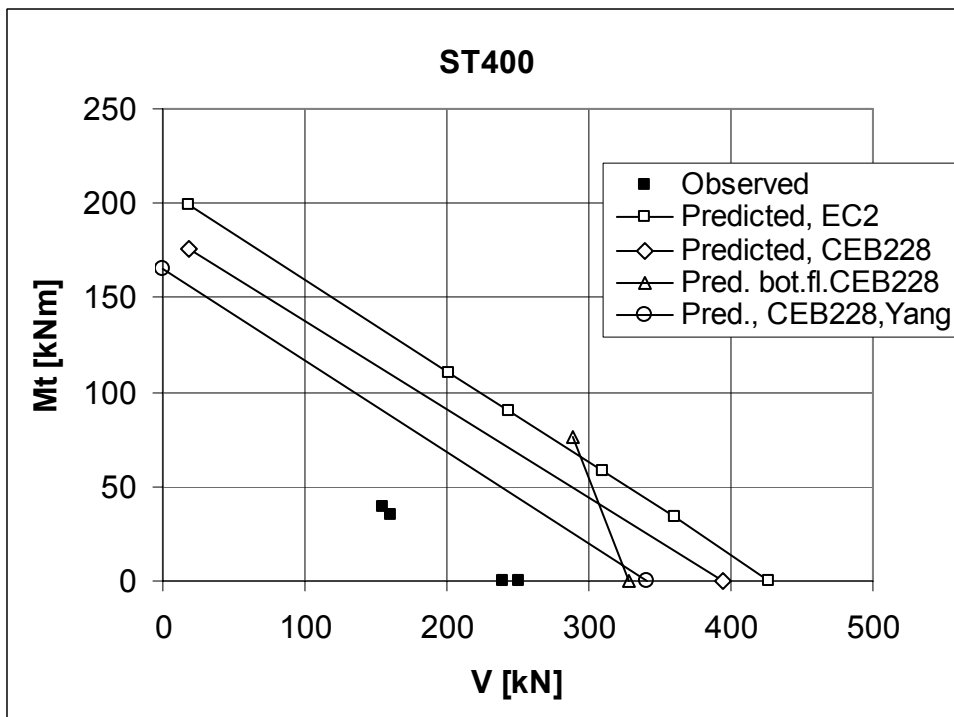


Fig. 86. Comparison of predicted and observed results for 400 mm slabs on neoprene bearing.

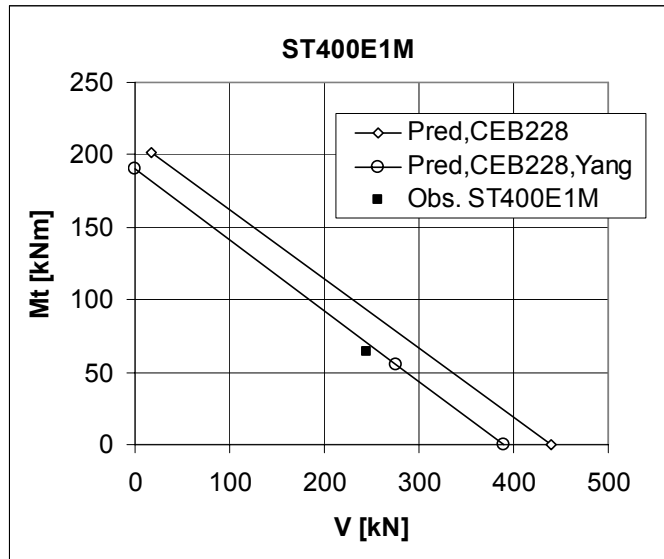


Fig. 87. Comparison of predicted and observed result for test ST400E1M.

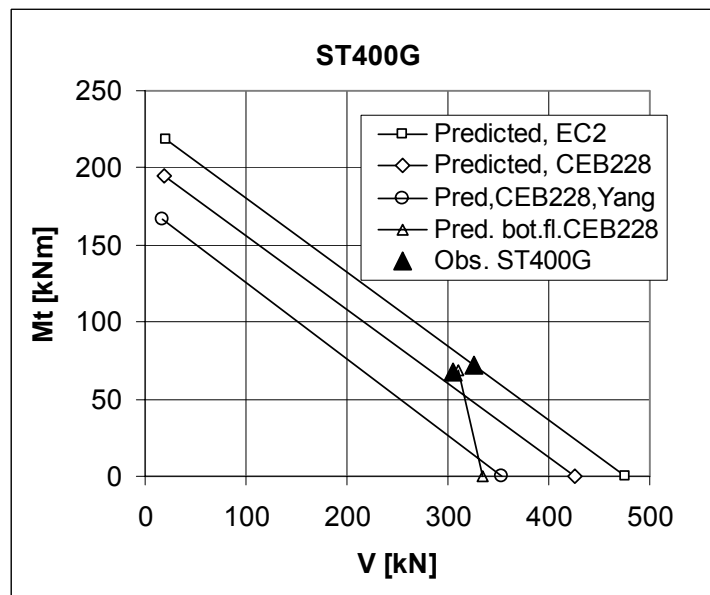


Fig. 88. Comparison of predicted and observed results for 400 mm slabs.

For extruded 200 mm slabs, see Fig. 82, one test result (ST200E1a) lies on the curve corresponding to the tensile strength of CEB228. The other test results lie on the unconservative side but not too far. It is likely that with more realistic support conditions, i.e. grouted slab ends and mortar bed below the slab, all points corresponding to the observed resistance would have been close to the predicted curves.

In test ST200E1M and particularly in test ST200E2M, see Figs 83 and 84, the observed test results lies far above the predicted curves for web failure. In the former test the failure mode was shear failure in web, in the latter test some kind of flexural-shear-torsion-punching failure. The failure modes are not easily explained by the predicted curves.

For the slip-formed 200 mm slabs, see Fig. 85, the cracking of the bottom flange seems to precede the failure theoretically. This was also the case in the tests. Whether this type of cracking corresponds to failure, depends on the anchorage. In test STS200C the cracking in flexure and the failure took place simultaneously; in test STS200E1 the load could be increased after the first flexural cracks had been observed. Both test results lie on the unconservative side of the predicted curves.

In tests STS200, see Fig. 85, the two concentrated loads were closer to each other than in tests ST200. This explains why, despite the stronger cross-section, the resistance in test STS200C was lower than in test ST200C: The outermost webs in the slipformed slabs were considerably thicker than the inner webs. This explains why the observed shear resistance in test STS200C was lower than that in test STS200E1. In addition, small eccentricity of the lower strands and existence of the upper prestressing wires facilitated the cracking in bottom flange.

For extruded 400 mm slabs on neoprene bearing, see Fig. 86, the results of tests are far from the predicted values and on the unconservative side. On the other hand, the test with a mortar bearing and grouted ends (ST400E1M, see Fig. 87) as well as those with wood fibre bearing and grouted ends (ST400G1 and ST400G2, see Fig. 88) gave results that are closer to the predicted results.

The difference in behaviour of 200 mm and 400 mm slabs can partly be explained by the fact that the conventional formula for calculating the shear stress in the web from

$$\tau = \frac{VS}{Ib_w} \quad (18)$$

does not take into account the shear stresses due to the stress gradient in the prestressing steel. Such a gradient has little or no effect in cross-sections like those in slabs ST200 or STS200, but for slabs of the type ST400 the gradient increases the maximum principal stress in the web by tens of percent depending on the prestressing force. When the stress gradient in the tendons is taken into account using Yang's method [8], see Figs 86–88, the predicted curve for web shear failure comes closer to the observed results but there is still a considerable gap in Fig. 86. As for 200 mm slabs, this gap can be explained with the neoprene bearing, at least partly. In tests ST400E1M and ST400G with cast in situ concrete at the ends of the slab, the test results are clearly on the safe side when compared with Yang's curve.

6. Discussion

The tests in which slabs were supported on a neoprene strip without any means to keep the slab ends undeformed, resulted in a considerably lower load-carrying capacity and apparent torsional stiffness than what was observed in tests in which the deformation of the slab ends was restricted by end grouting, stiff beams on the slab end, mortar bearing or a combination of these aids. The main reason for a premature slab failure on a neoprene bearing was the longitudinal cracking at slab end due to transverse bending at support. Longitudinal cracks were observed above or below hollow cores. Such cracks cut off one or two webs from the rest of the slab which is then too weak to resist the loading. The results of these tests are not informative for ordinary cases in which the slab ends are grouted and tied with reinforcement to the surrounding structures. The results can be used to calibrate computer models, but only in cases in which the calculation model can be made fine enough to simulate also the transverse bending. For this reason only the results of tests with grouted slab ends are considered in the following.

The tests on 400 mm slabs with grouted ends seem to give resistances which are on the unsafe side when compared with the present design practice specified in EN1168 [3], but on the safe side, if the method for shear stress calculation proposed by Yang is applied [8]. On the other hand, the torsional stiffness calculated from the test results varies a lot. For test ST400E1M the observed torsional stiffness was 5% lower, for test ST400G1 47% higher and for test ST400G2 37% higher than the predicted stiffness. Taking the inner webs into account when calculating the stiffness would have increased not only the predicted stiffness but also the predicted resistance.

In tests ST200E1M and ST200E2M, the only tests on 200 mm slabs with grouted ends, the observed resistance was higher, and in test ST200E2M considerably higher than the predicted resistance calculated according to EN1168. Particularly the resistance against the web failure was 40–90% higher than the predicted resistance of the web. The horizontal restraint at the slab ends must have had an effect on the observed resistance but it cannot be so great. Taking into account the contribution of the inner webs would have increased the predicted resistance and also reduced the gap between observed and predicted resistances. It would also have increased the predicted torsional stiffness which was lower than the observed one. The longitudinal restraint provided by the supporting beams may also have enhanced the observed resistance.

To conclude: the observed resistances in the tests on slabs with grouted ends gave formally safe resistances when compared with results calculated using elementary beam theory and common simplifications. However, a more thorough analysis showed inconsistencies in torsional stiffnesses and observed resistances which suggest that the

simpliest possible beam theory is too rough to properly model a single hollow core slab subjected to point loads very close to the support. Obviously the assumptions made when the elementary torsion theory has been developed are not in force in this case. It is suggested to analyse the most interesting test using FE method to explain the behaviour. In addition, it may be necessary to modify the traditional design method for 400 mm slabs as Yang [8] has proposed.

References

1. EN 1992-1-1. *Eurocode 2: Design of concrete structures – Part 1: General rules and rules for buildings*. 2004.
2. *CEB-FIP Model Code 1990*. Comité Euro-International du Béton. Thomas Telford, London 1993. ISBN: 0 7277 1696 4.
3. Pajari, M. *Shear-torsion tests on 400 mm hollow core floor*. VTT Research Notes 2274. Espoo 2004. 30 p. + app. 82 p.
<http://www.vtt.fi/inf/pdf/tiedotteet/2004/T2274.pdf>
4. Pajari, M. *Pure torsion tests on single hollow core slabs*. VTT Research Notes 2273. Espoo 2004. 29 p. + app. 28 p.
<http://www.vtt.fi/inf/pdf/tiedotteet/2004/T2273.pdf>
5. CEB Bulletin 228. *High Performance Concrete – Recommended Extensions to the Model Code 90 – Research Needs, 1995*. Comité Euro-International du Béton. ISBN: 2-88394-031-21995. 60 p.
6. Yang, L. *Design of Prestressed Hollow core Slabs with Reference to Web Shear Failure*. ASCE Journal of Structural Engineering, 1994. Vol. 120, No. 9, pp. 2675–2696.
7. EN 1168. *Precast concrete products – Hollow core slabs*. 2005.
8. Pajari, M. *Shear-torsion tests on 200 mm hollow core floor*. VTT Research Notes 2276. Espoo 2004. 55 p. + app. 116 p.
<http://www.vtt.fi/inf/pdf/tiedotteet/2004/T2276.pdf>

Appendix A: Photographs, 200 mm slabs

The numbers on the surface of the slabs refer to the actuator load. They tell the load at which the crack grew until the indicated position.



Fig. 1. ST200C. Arrangements at the loaded end.

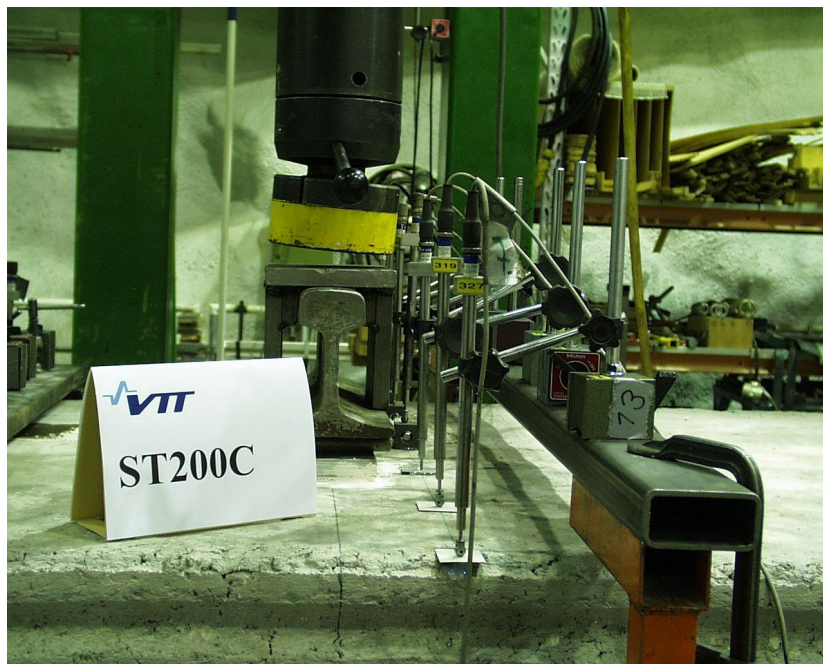


Fig. 2. ST200C. Transducers for measuring vertical displacement next to the load.



Fig. 3. ST200C. Horizontal transducers for measuring transverse shear deformation.

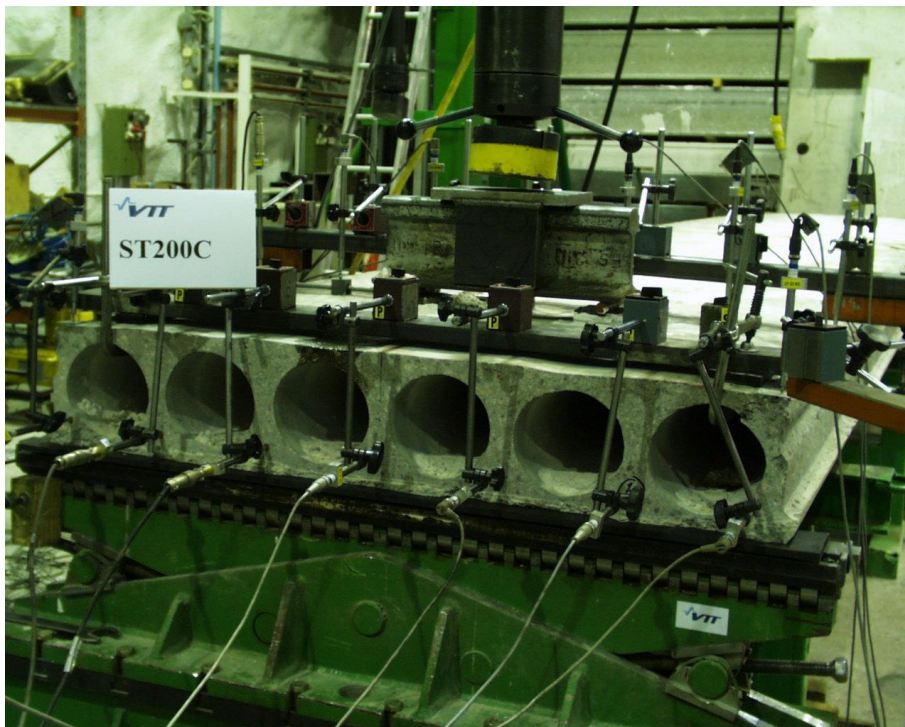


Fig. 4. ST200C. Transducers for measuring bond slip and settlement of supports.

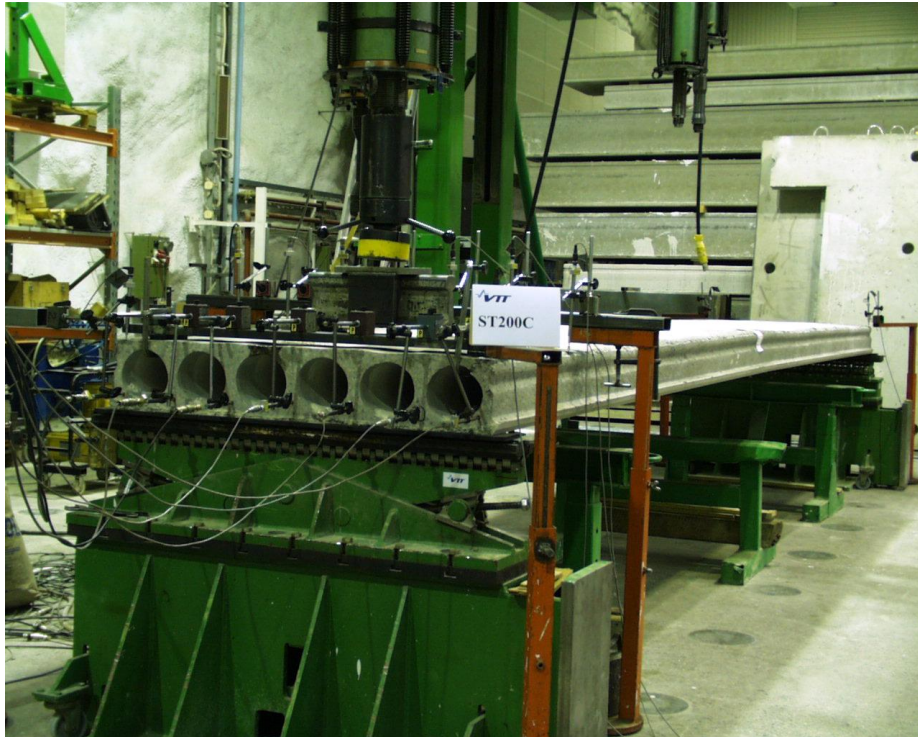


Fig. 5. ST200C. Longitudinal overview on test arrangements.



Fig. 6. ST200C. First cracks at load $P = 112.5$ kN.



Fig. 7. ST200C. Cracks in webs after failure.

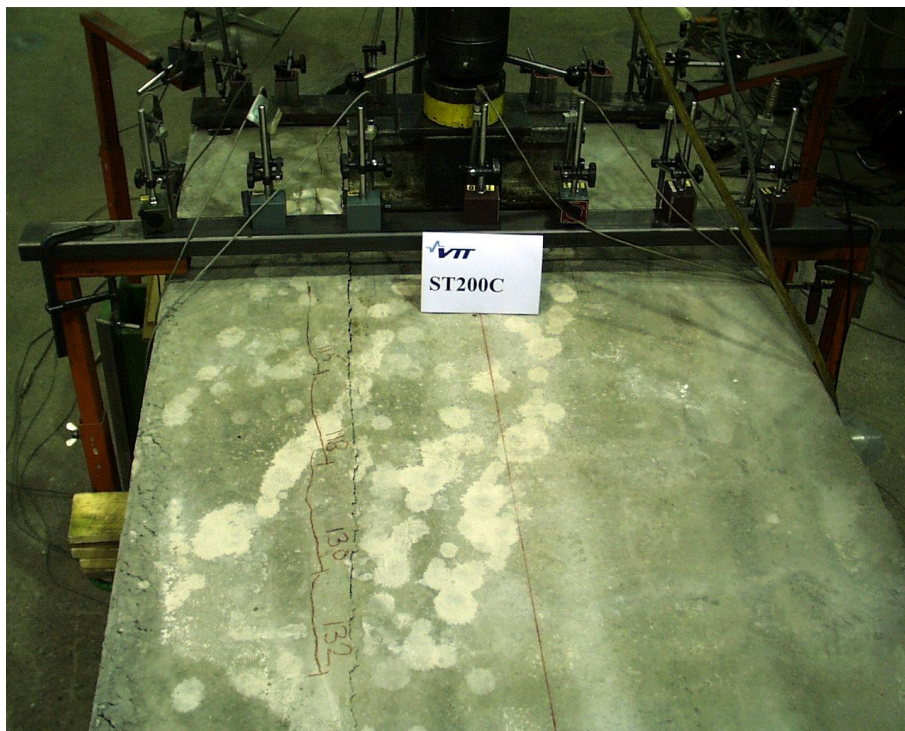


Fig. 8. ST200C. Top view. Longitudinal cracks after failure.



Fig. 9. ST200C. Cracking of soffit.



Fig. 10. ST200E1a. Arrangements.



Fig. 11. ST200E1a. Cracks after failure. North edge.

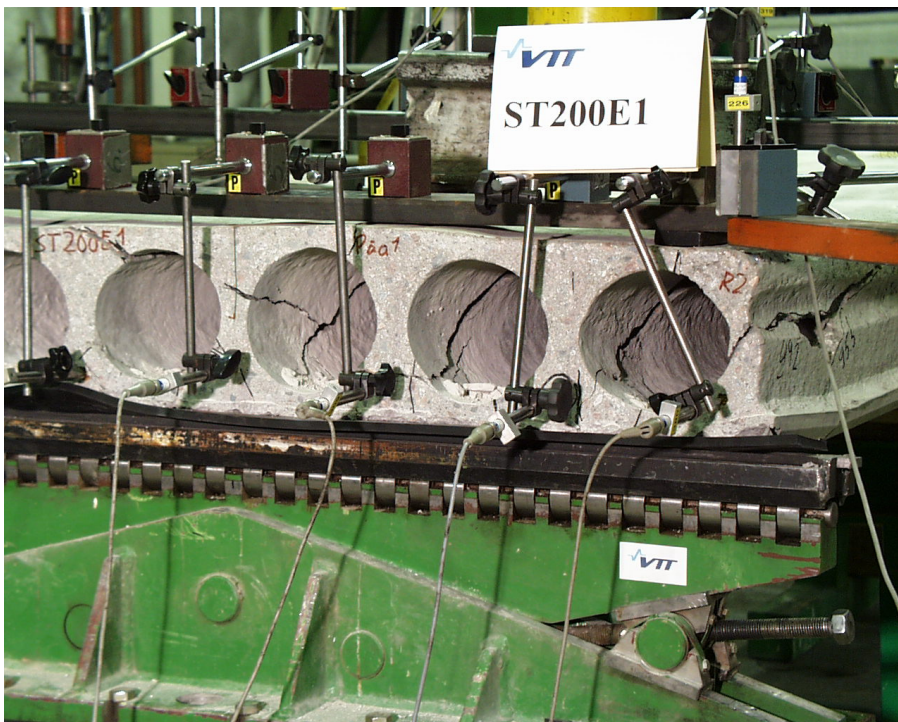


Fig. 12. ST200E1a. Cracks in webs after failure.

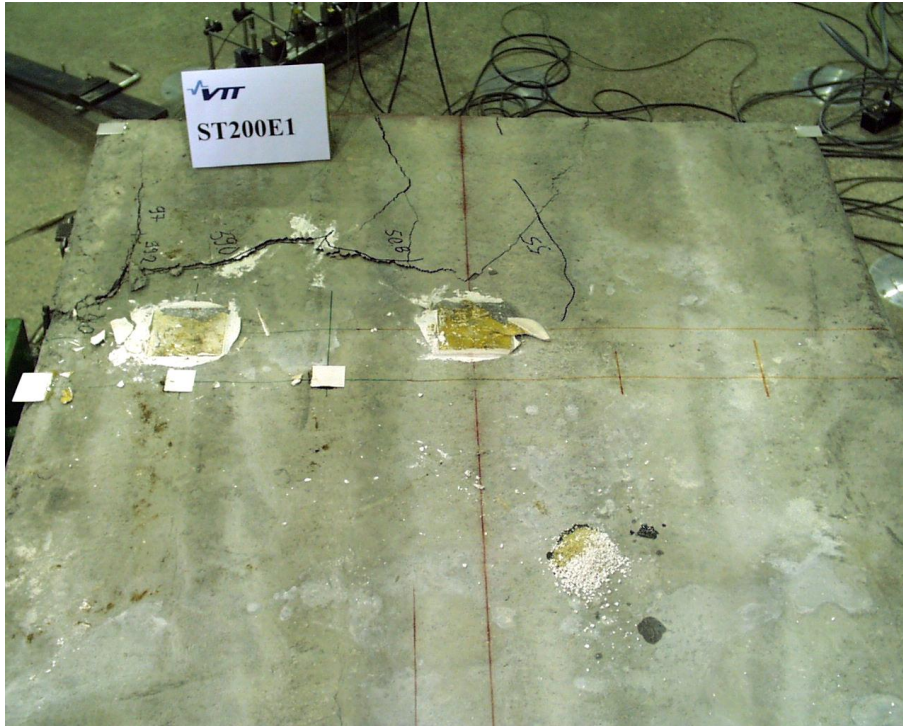


Fig. 13. ST200E1a. Cracks after failure. Top view.

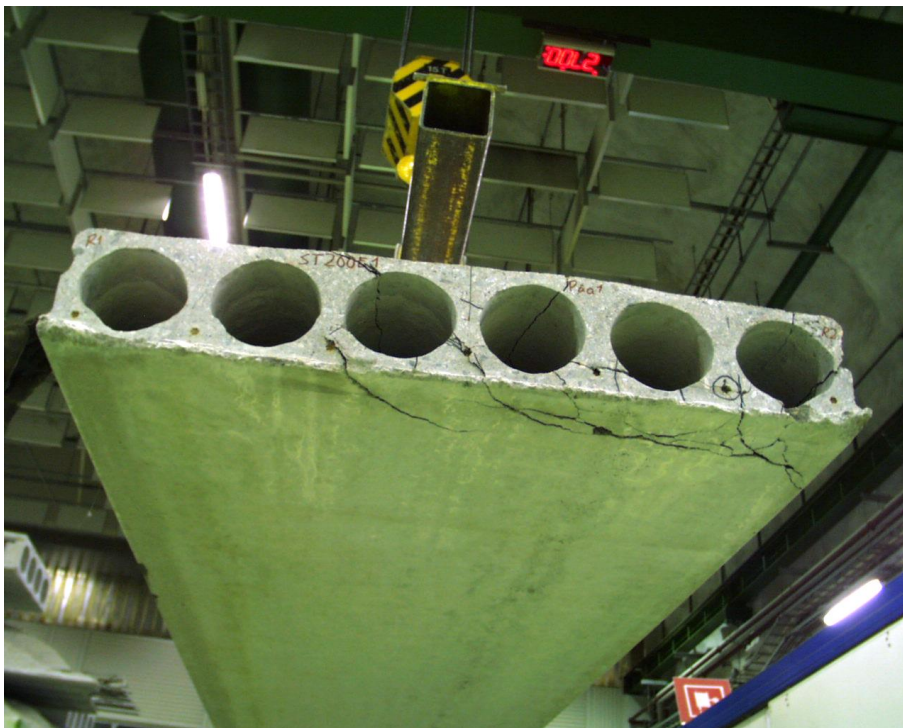


Fig. 14. ST200E1a. Soffit after failure.

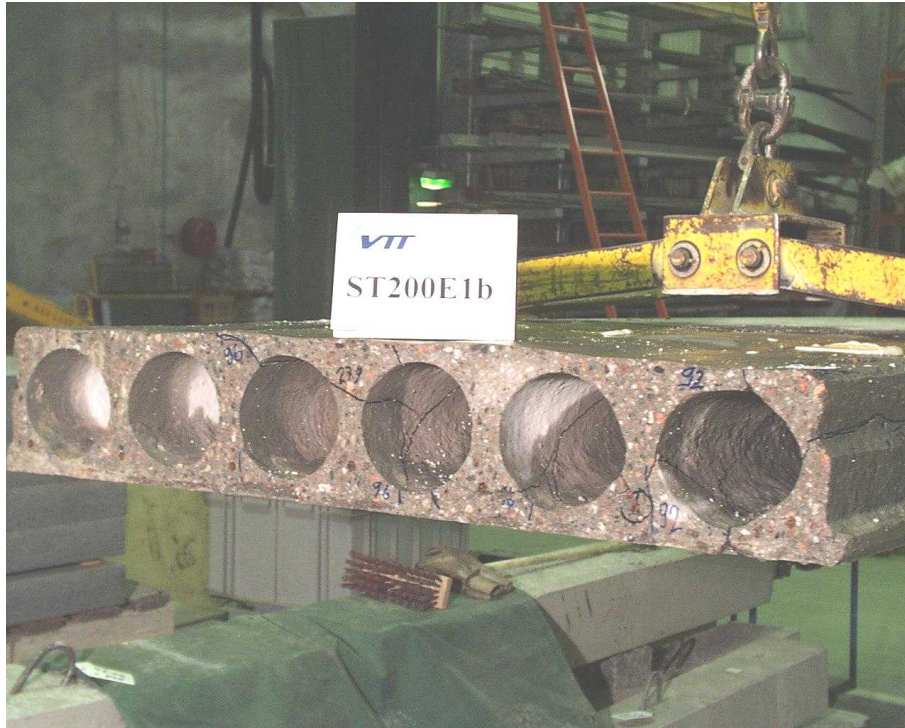


Fig. 15. ST200E1b. Cracking pattern in webs after failure.



Fig. 16. ST200E1b. Northern edge after failure.



Fig. 17. ST200E1b. Cracking pattern in soffit.

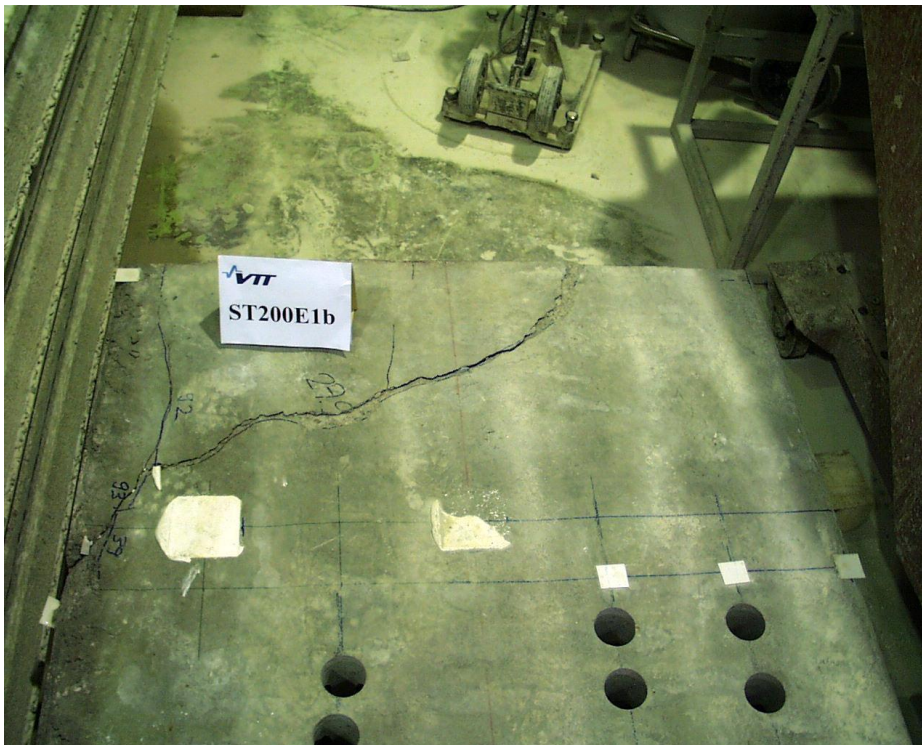


Fig. 18. ST200E1b. Cracking pattern in top flange.



Fig. 19. ST200E1b. Cracking pattern in webs.

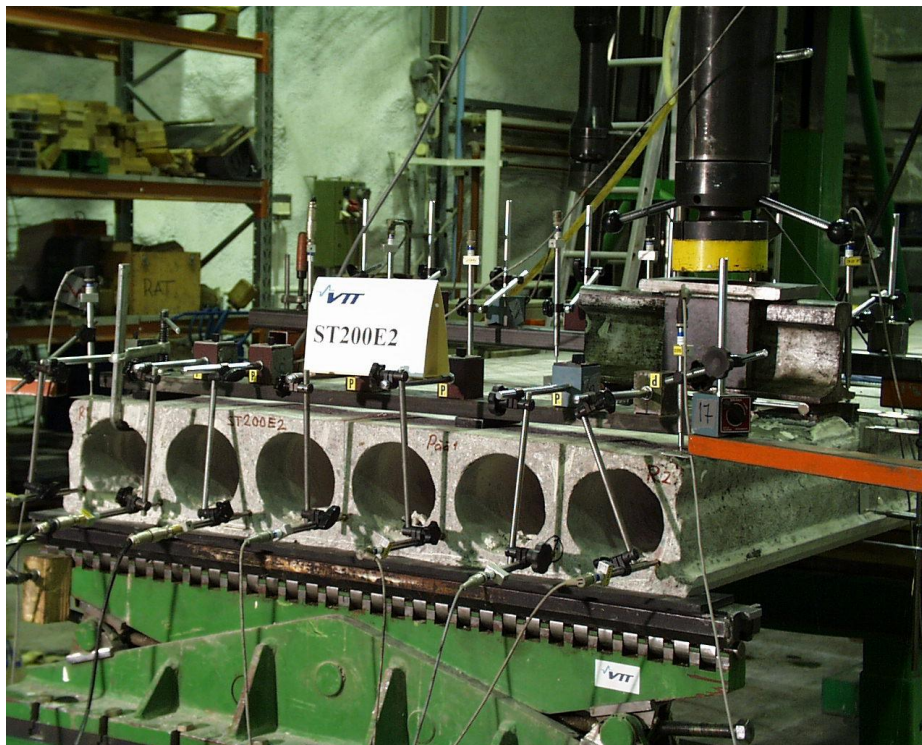


Fig. 20. ST200E2. Arrangements.



Fig. 21. ST200E2. First crack at Northern edge.



Fig. 22. ST200E2. Cracking pattern after failure. Northern edge.

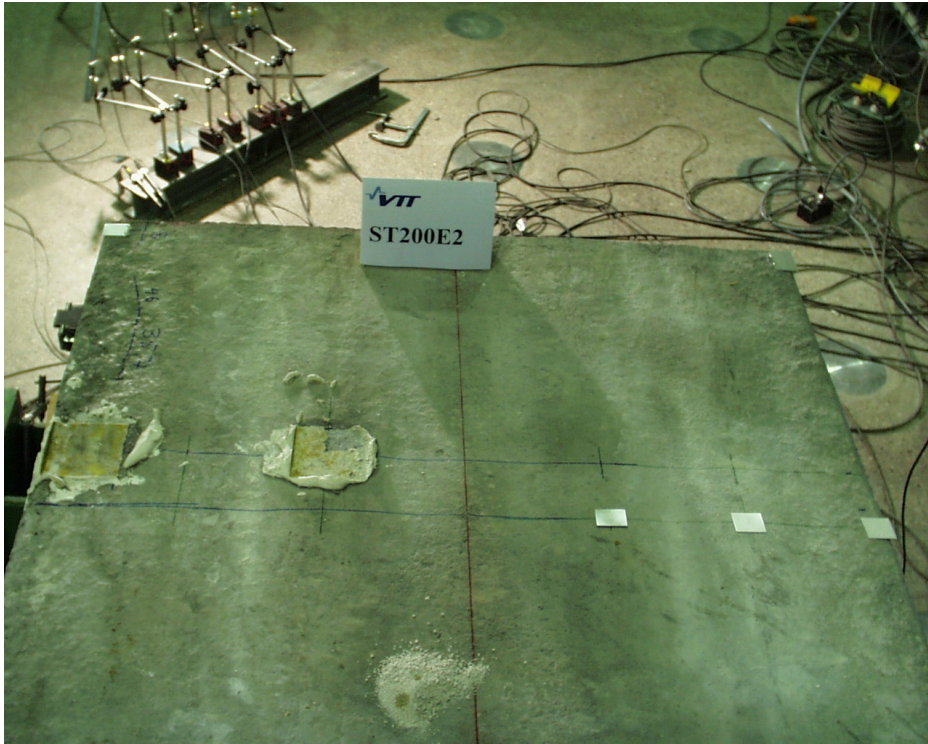


Fig. 23. ST200E2. Top view after failure.



Fig. 24. ST200E2. Soffit after failure.



Fig. 25. STS200C. Arrangements.



Fig. 26. STS200C. Cracking pattern after failure. Northern edge.



Fig. 27. STS200C. Cracking pattern in webs after failure.



Fig. 28. STS200C. Cracking pattern after failure. Southern edge.

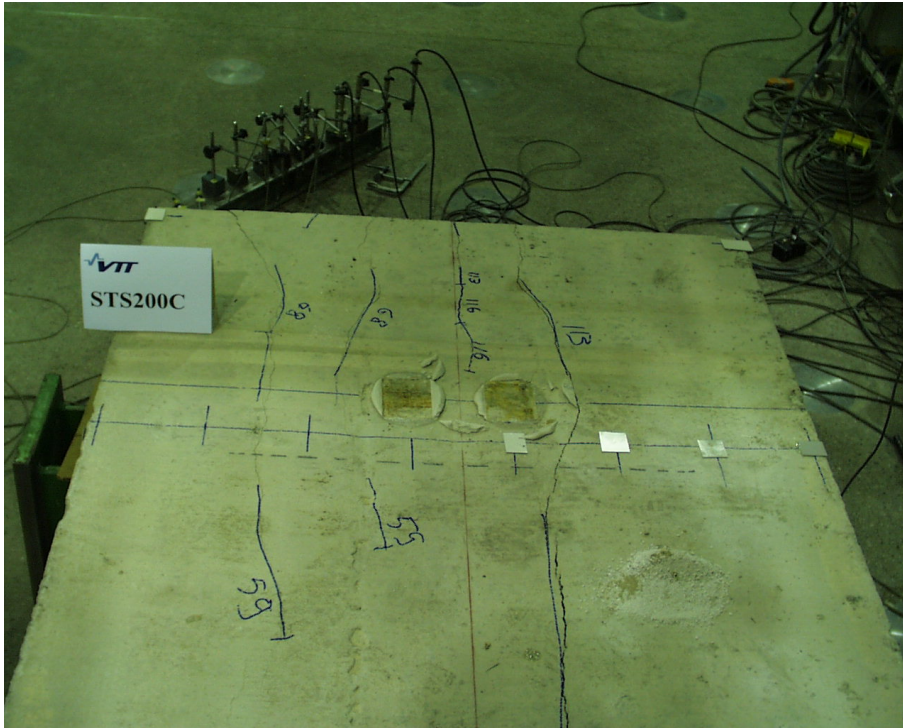


Fig. 29. STS200C. Cracking pattern after failure. Top view.



Fig. 30. STS200C. Soffit after failure.

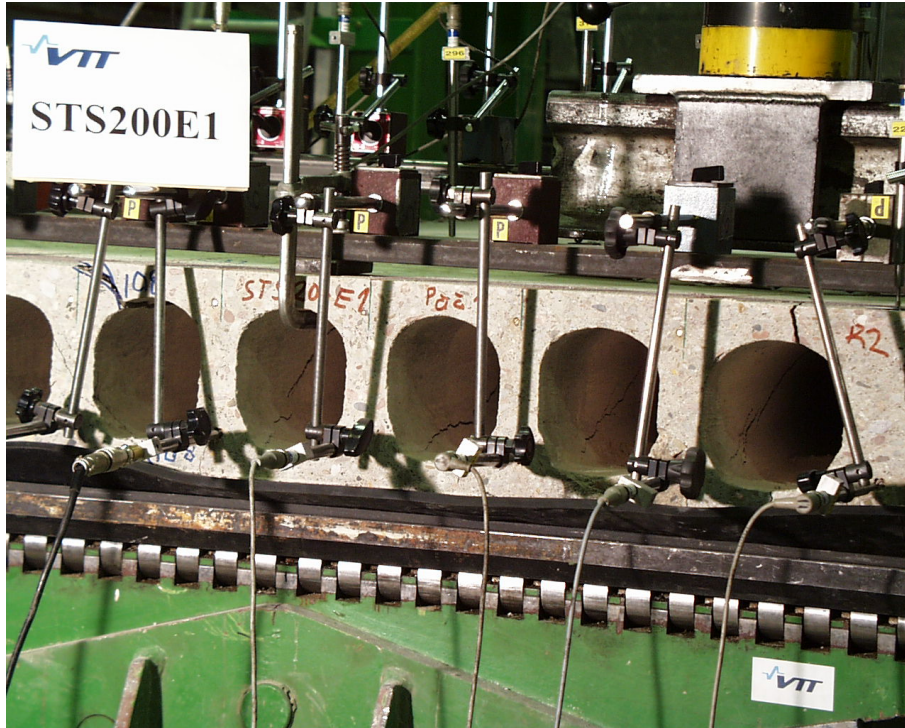


Fig. 31. STS200E1. Cracking pattern in webs after failure.



Fig. 32. STS200E1. Cracking pattern in webs after failure.



Fig. 33. STS200E1. Cracking after failure. Northern edge.

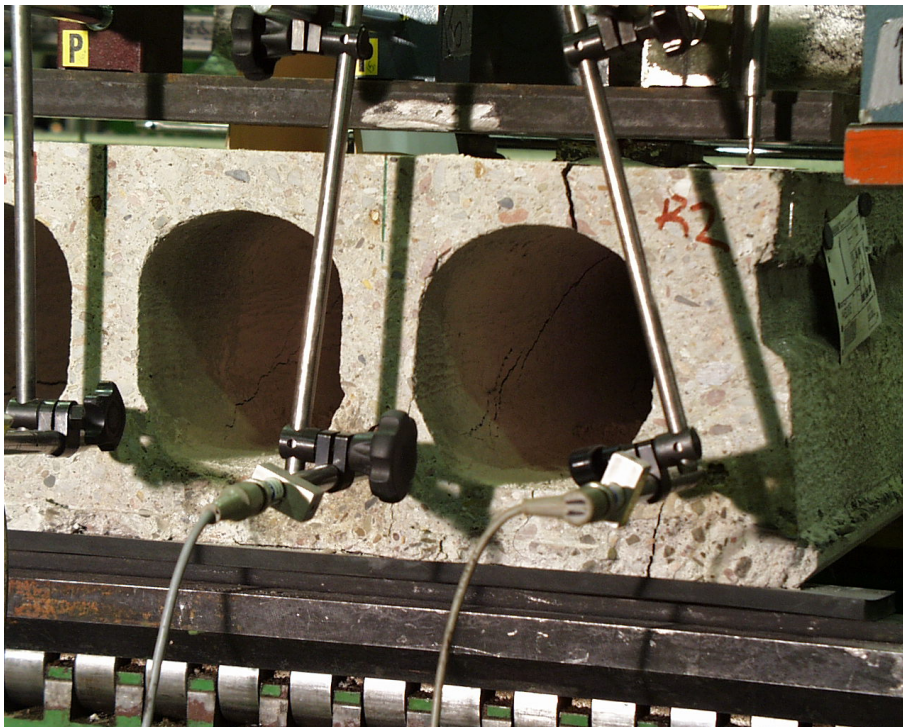


Fig. 34. STS200E1. Detail of cracking.

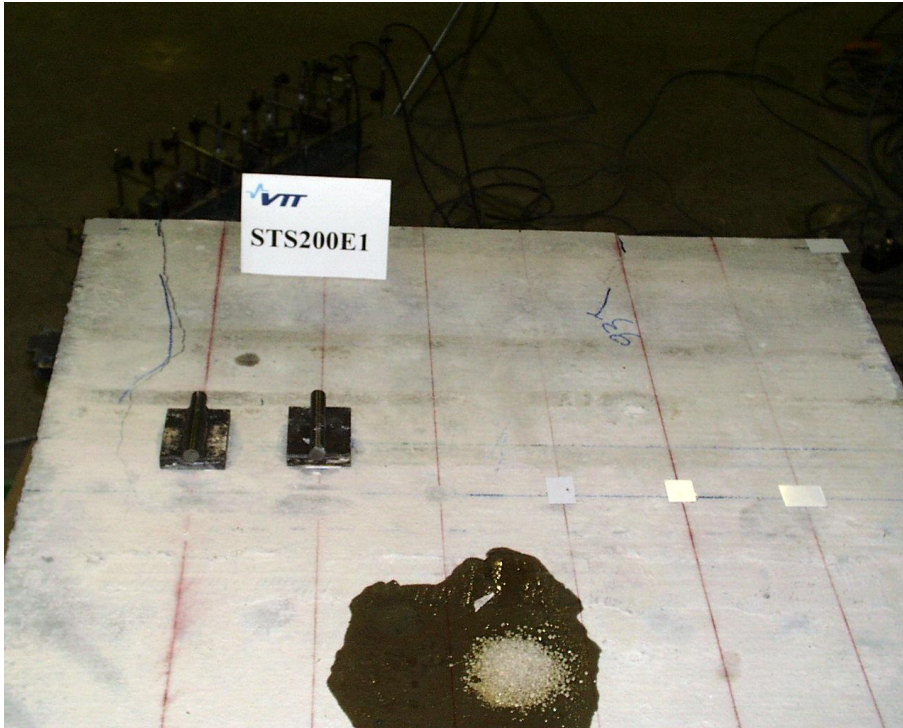


Fig. 35. STS200E1. Top surface after failure.



Fig. 36. STS200E1. Soffit after failure.

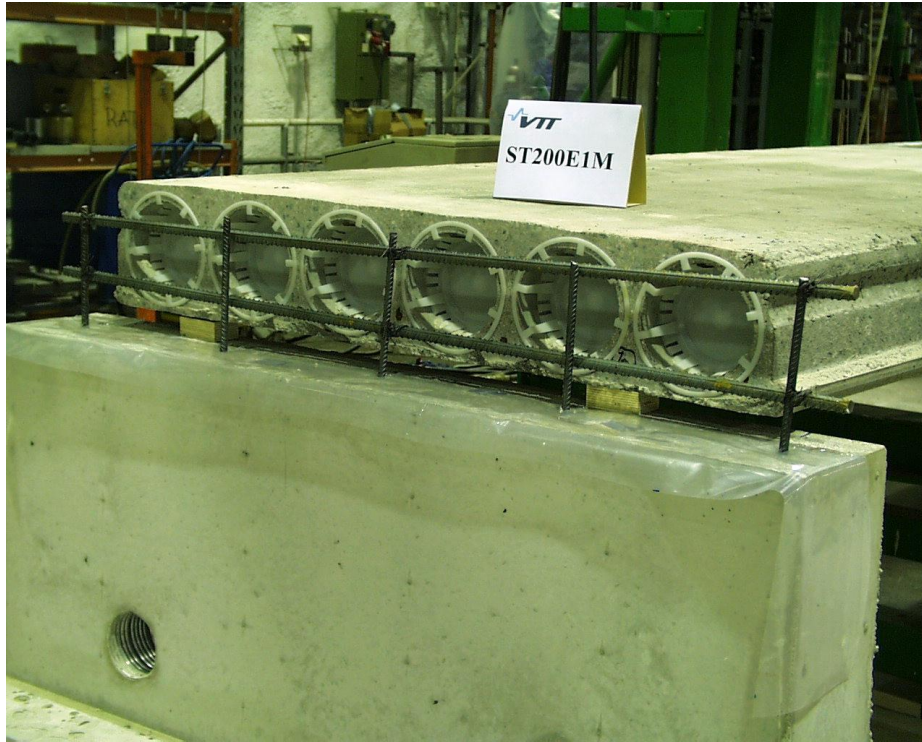


Fig. 37. ST200E1M. Arrangements at support before grouting.



Fig. 38. ST200E1M. Longitudinal view on arrangements.



Fig. 39. ST200E1M. Loading.



Fig. 40. ST200E1M. Measuring deflection. Note the curved top surface of the slab.



Fig. 41. ST200E1M. Cracking pattern after failure.

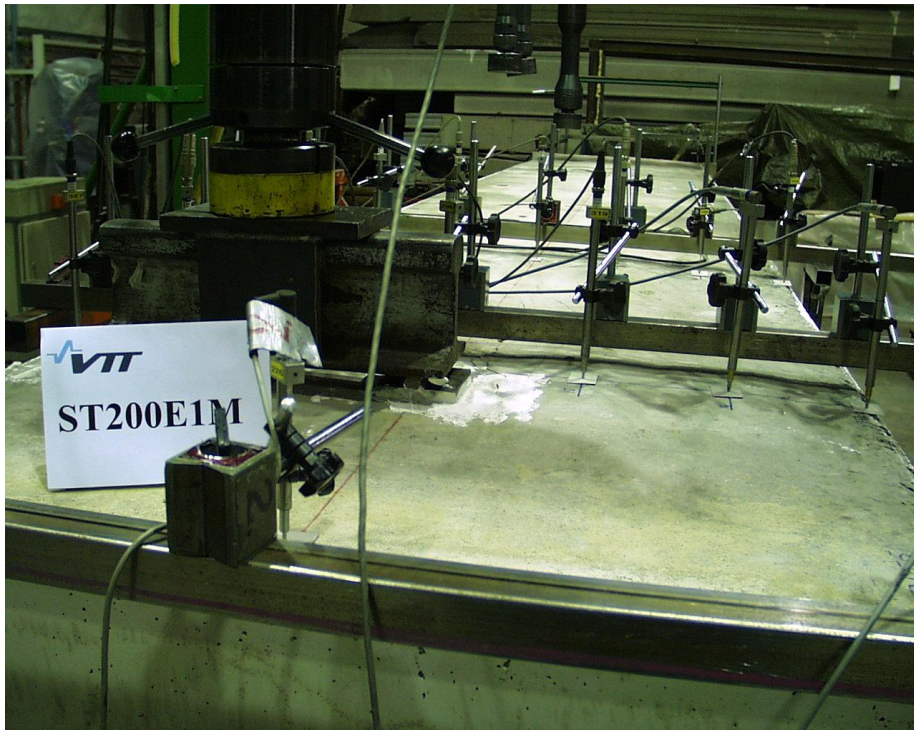


Fig. 42. ST200E1M. Longitudinal view after failure.



Fig. 43. ST200E1M. Cracking pattern between load and support.

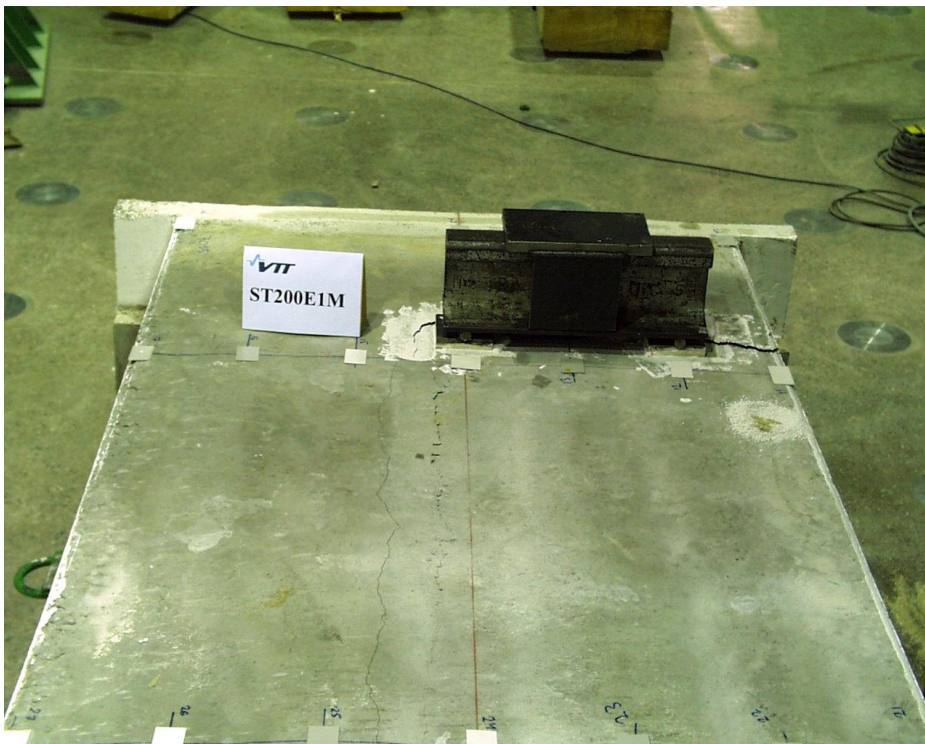


Fig. 44. ST200E1M. Top surface after removal of measuring devices.

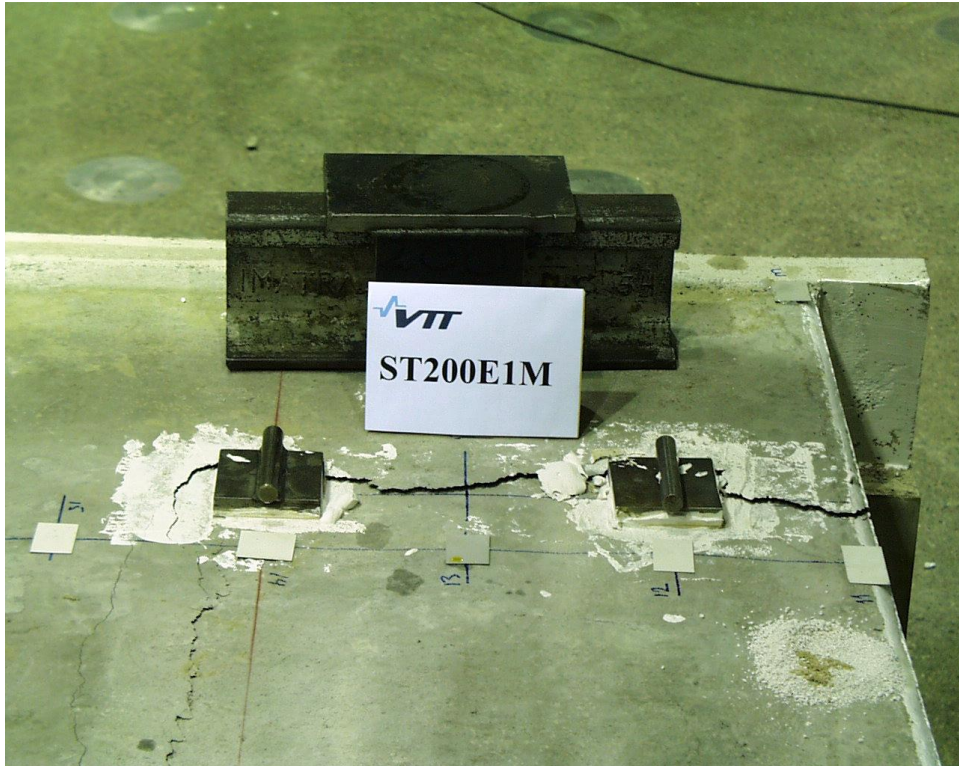


Fig. 45. ST200E1M. Loaded area after removal of spreader beam.



Fig. 46. ST200E1M. Soffit after failure.



Fig. 47. ST200E1M. Transverse cracking of soffit next to support.



Fig. 48. ST200E2M. Arrangements at support before grouting.



Fig. 49. ST200E2M. Overview on arrangements.



Fig. 50. ST200E2M. Arrangements to spread one actuator load to two point loads.

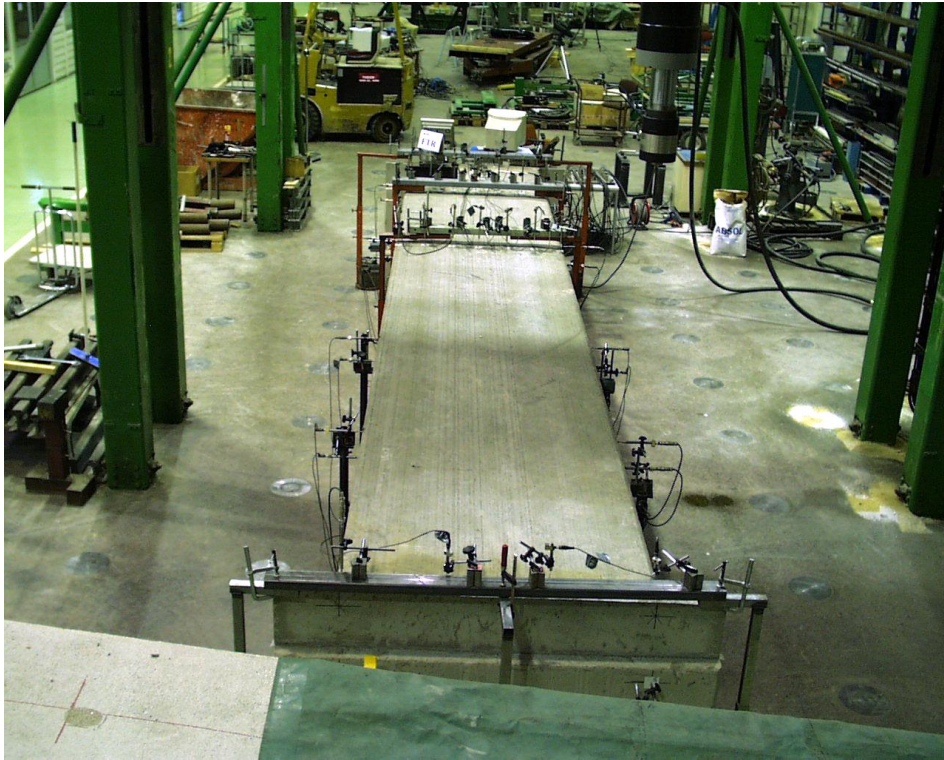


Fig. 51. ST200E2M. Overview on arrangements.

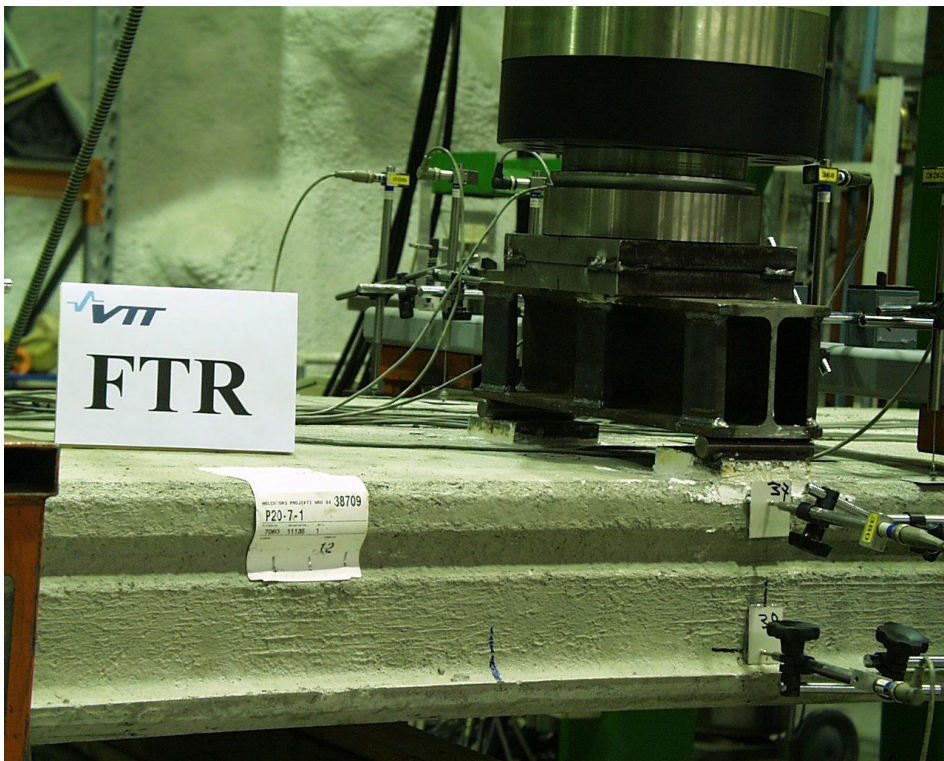


Fig. 52. ST200E2M. Loading arrangements.

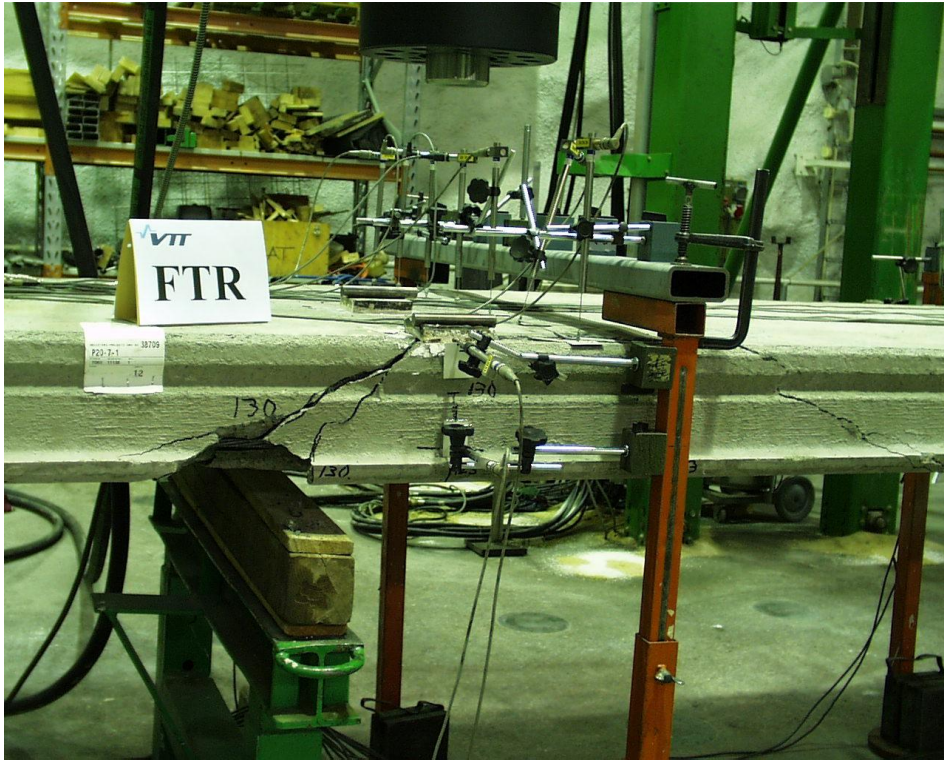


Fig. 53. ST200E2M. Cracking pattern after failure.



Fig. 54. ST200E2M. Cracking pattern after failure.

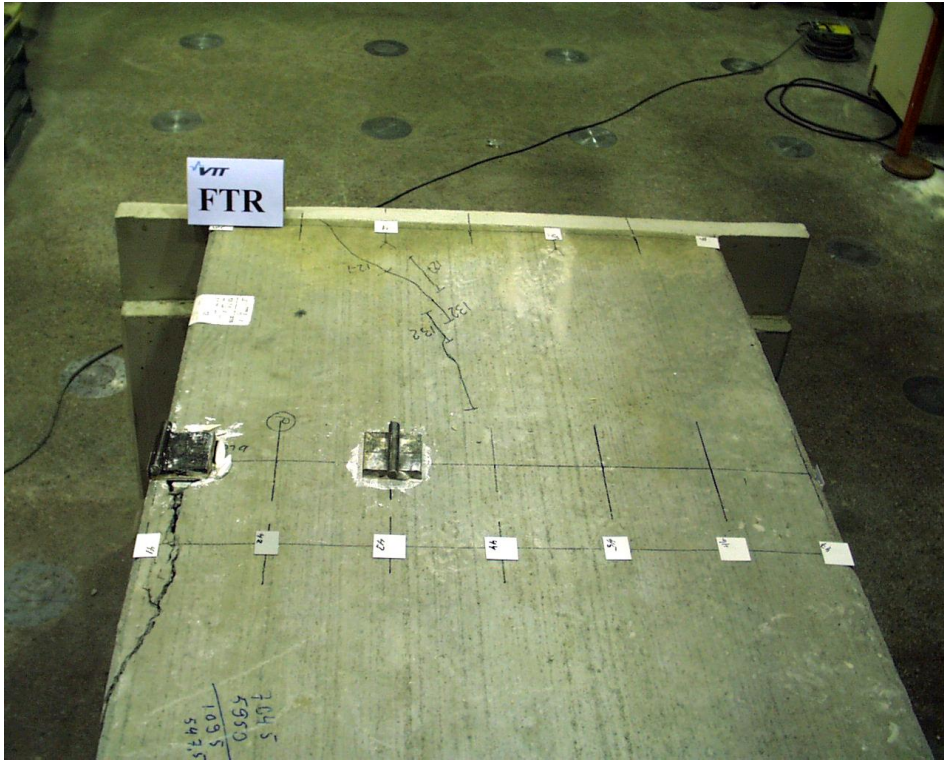


Fig. 55. ST200E2M. Cracking pattern after failure.

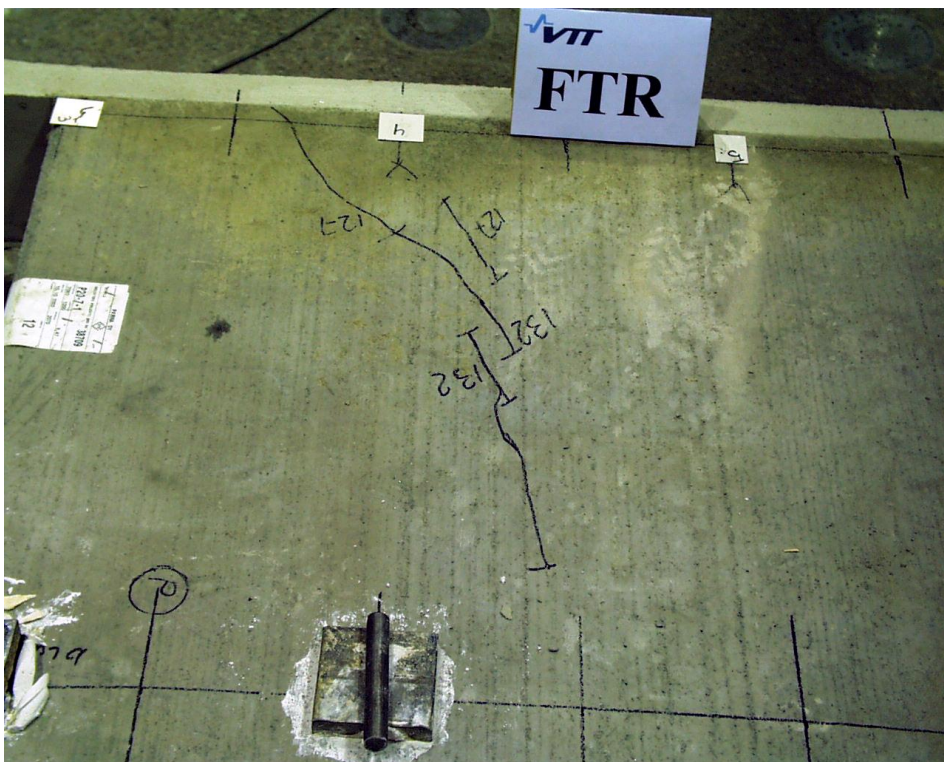


Fig. 56. ST200E2M. Cracking pattern after failure.

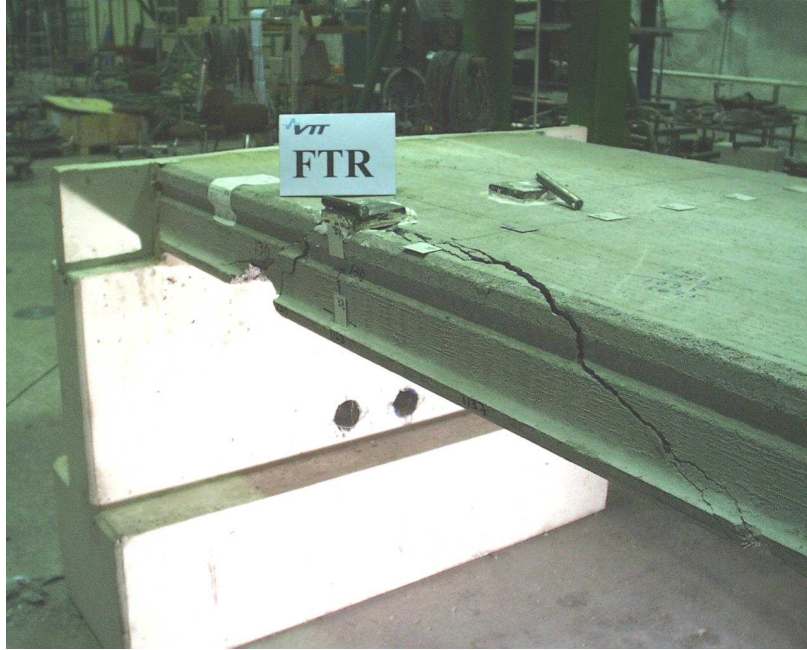


Fig. 57. ST200E2M. Cracking pattern after failure.

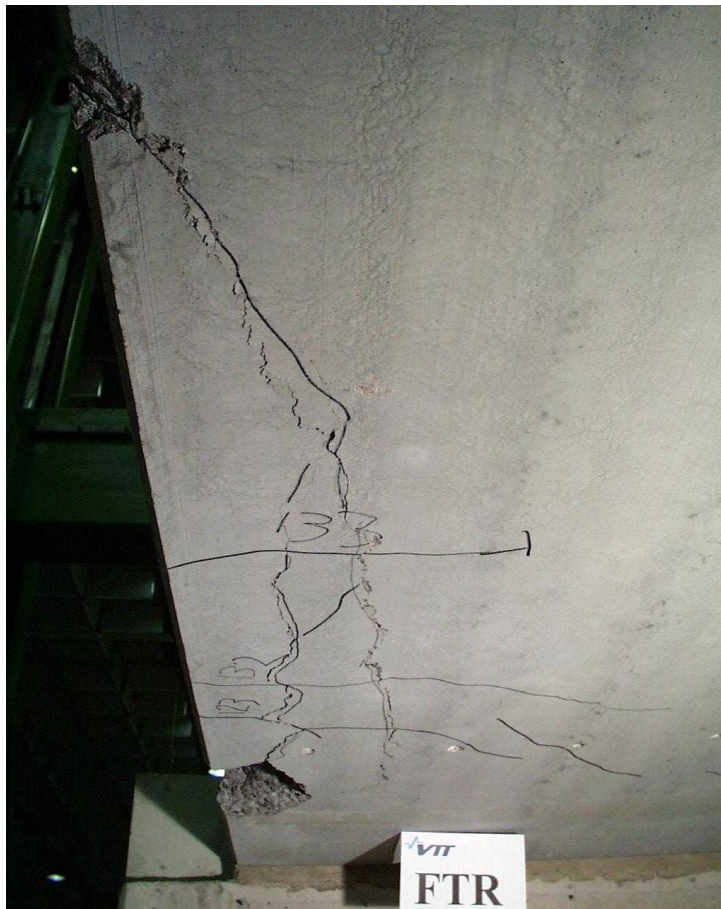


Fig. 58. ST200E2M. Cracking pattern after failure.



Fig. 59. ST200E2M. Cracking pattern after failure.

Appendix B: Photographs, 400 mm slabs

The numbers on the surface of the slabs refer to the actuator load. They tell the load at which the crack grew until the indicated position.



Fig. 1. ST400C1. Arrangements.

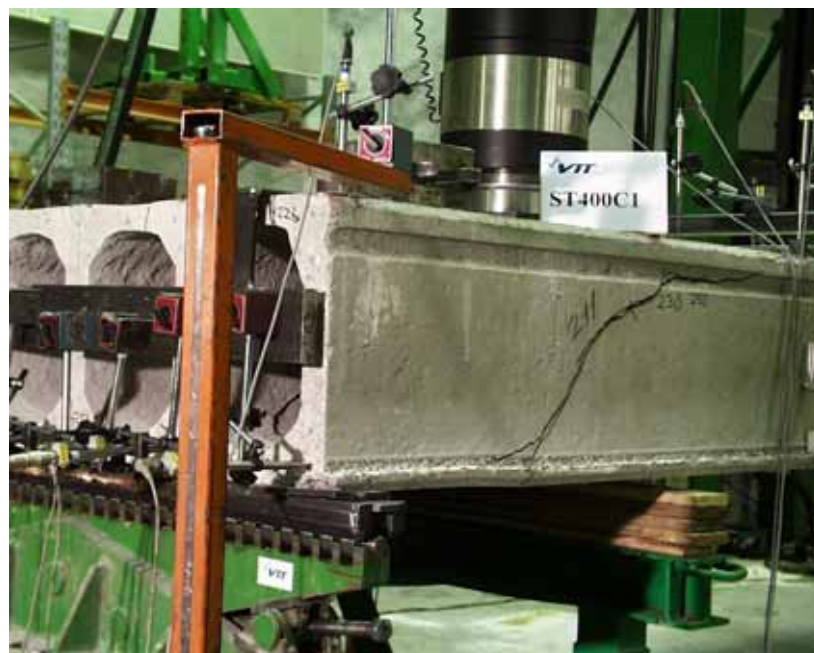


Fig. 2. ST400C1. Northern edge after failure.



Fig. 3. ST400C1. Cracks in webs after failure.



Fig. 4. ST400C1. Cracks in webs after failure.



Fig. 5. ST400C1. Top surface after failure. Note the letter A on the upper left corner of the figure. Before loading there was an initial crack from the slab end to letter A.



Fig. 6. ST400C1. Top surface and soffit seen from below.

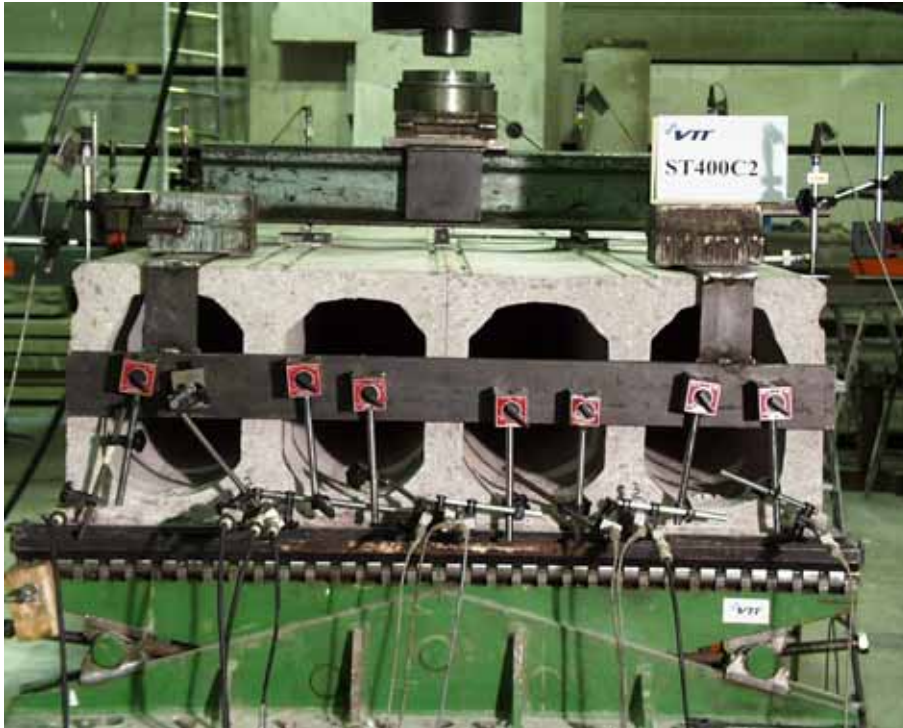


Fig. 7. ST400C2. Arrangements.



Fig. 8. ST400C2. Southern edge after failure.



Fig. 9. ST400C2. Soffit after failure seen from the North.



Fig. 10. ST400C2. Cracks in webs after failure.



Fig. 11. ST400C2. Cracks in webs after failure.



Fig. 12. ST400C2. Northern edge after failure.



Fig. 13. ST400C2. Soffit after failure. See also Fig. 45.



Fig. 14. ST400C2. Top surface after failure. A thin crack until letter A was observed before loading.



Fig. 15. ST400E1. Arrangements.



Fig. 16. ST400E1. Cracks at the end after failure.



Fig. 17. ST400E1. Northern edge after failure.



Fig. 18. ST400E1. Webs after failure.



Fig. 19. ST400E1. Webs after failure.

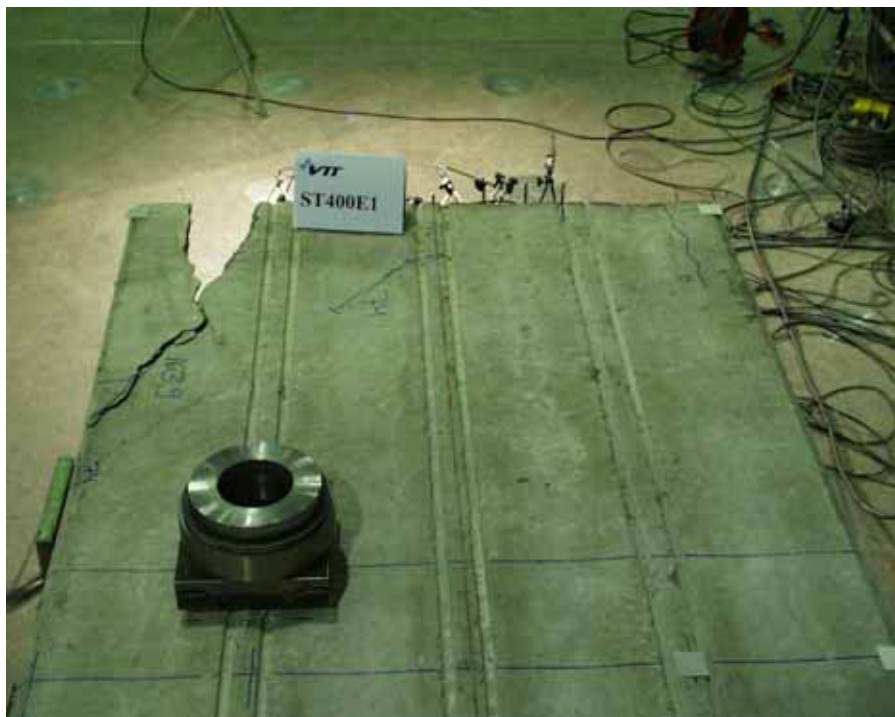


Fig. 20. ST400E1. Top surface after failure. Note the initial crack, marked with A on the upper right corner of the figure.



Fig. 21. ST400E1. Soffit after failure.



Fig. 22. ST4002E. Arrangements.



Fig. 23. ST4002E. Cracks in webs after failure.



Fig. 24. ST4002E. Cracks in webs after failure.

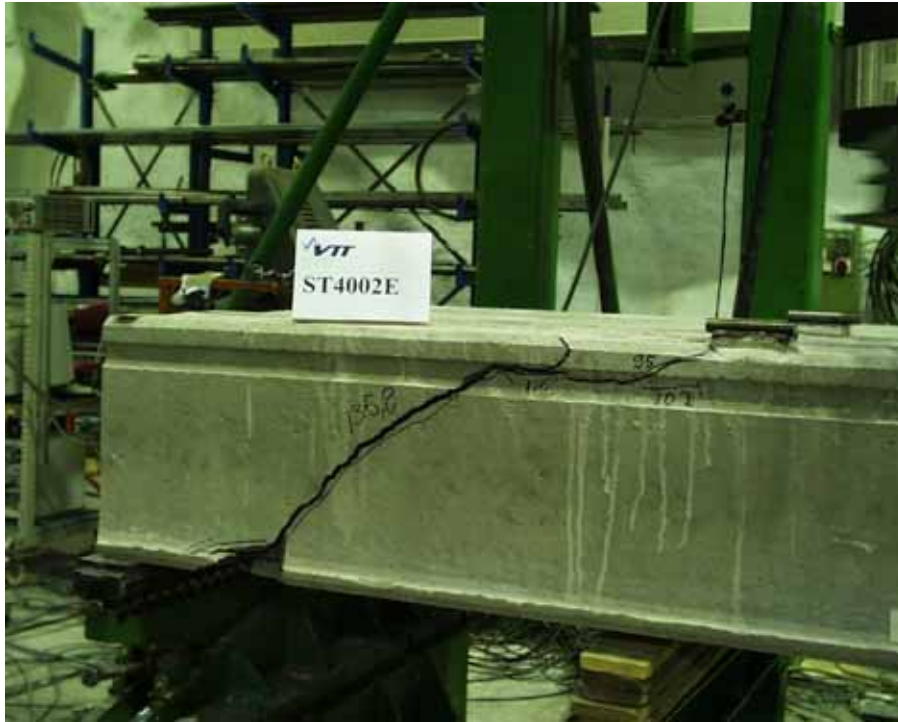


Fig. 25. ST4002E. Northern edge after failure.



Fig. 26. ST4002E. Top surface after failure. Note the thin crack at the upper right corner of the figure. This crack existed before loading.



Fig. 27. ST4002E. Soffit after failure.



Fig. 28. SF400C. Arrangements.



Fig. 29. SF400C. Failure mode.



Fig. 30. SF400C. Southern edge after failure. Before loading there was an initial crack above the first hollow core in the front. It extended ≈ 450 mm from slab end to the span.



Fig. 31. SF400C. Failure mode.



Fig. 32. SF400C. Flexural cracks in mid-span, Northern edge.

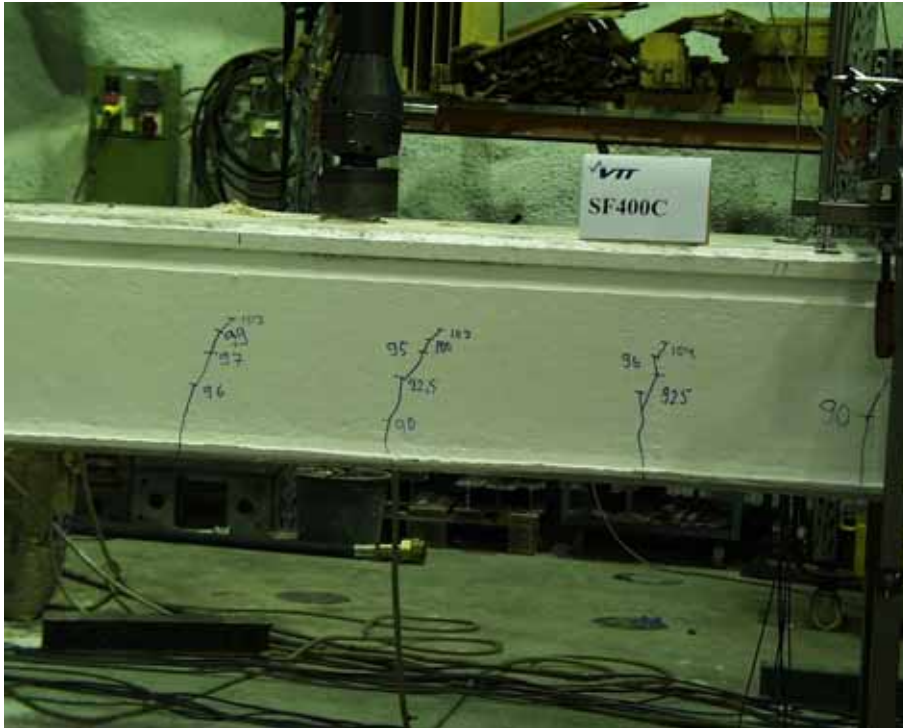


Fig. 33. SF400C. Flexural cracks in mid-span, detail of Fig. 68.

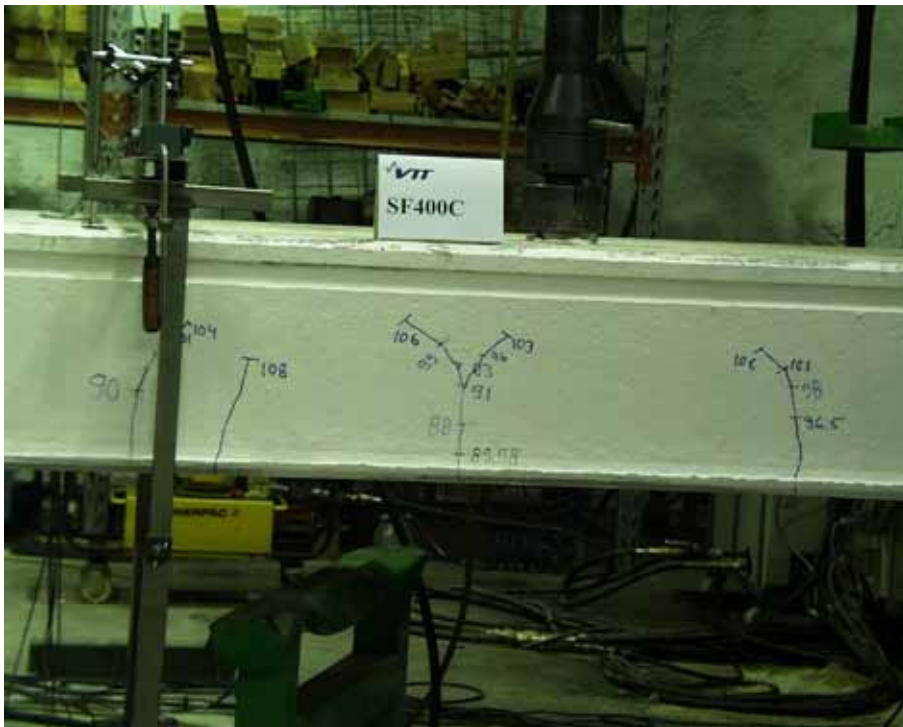


Fig. 34. SF400C. Flexural cracks in mid-span, detail of Fig. 68.



Fig. 35. SF400C. Flexural cracks in mid-span, Southern edge.

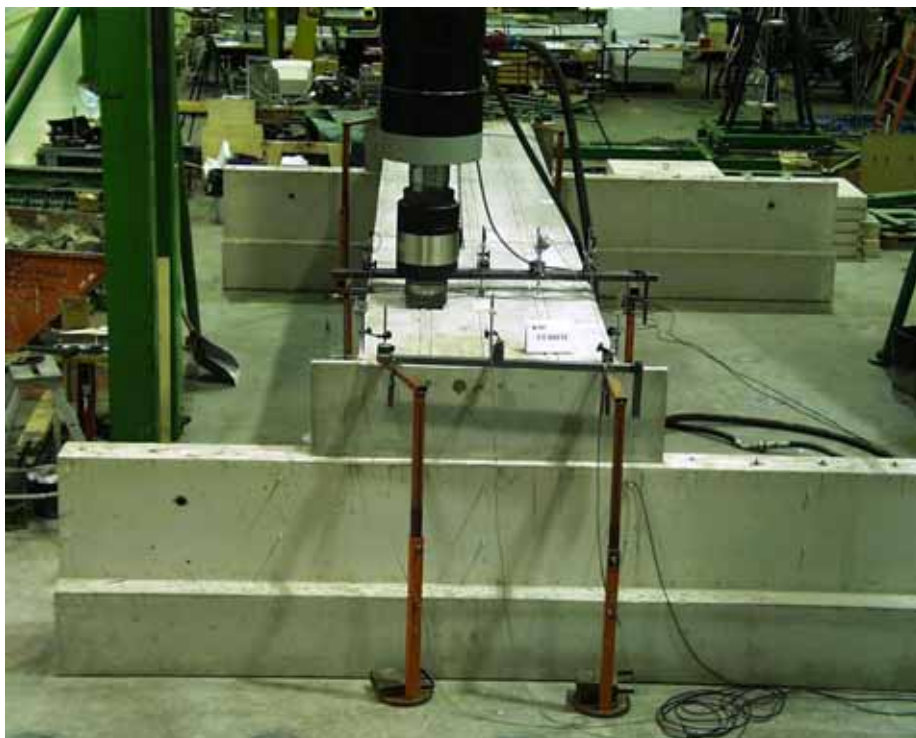


Fig. 36. ST400E1M. General view.



Fig. 37. ST400E1M. Well-compacted grout below the slab end.

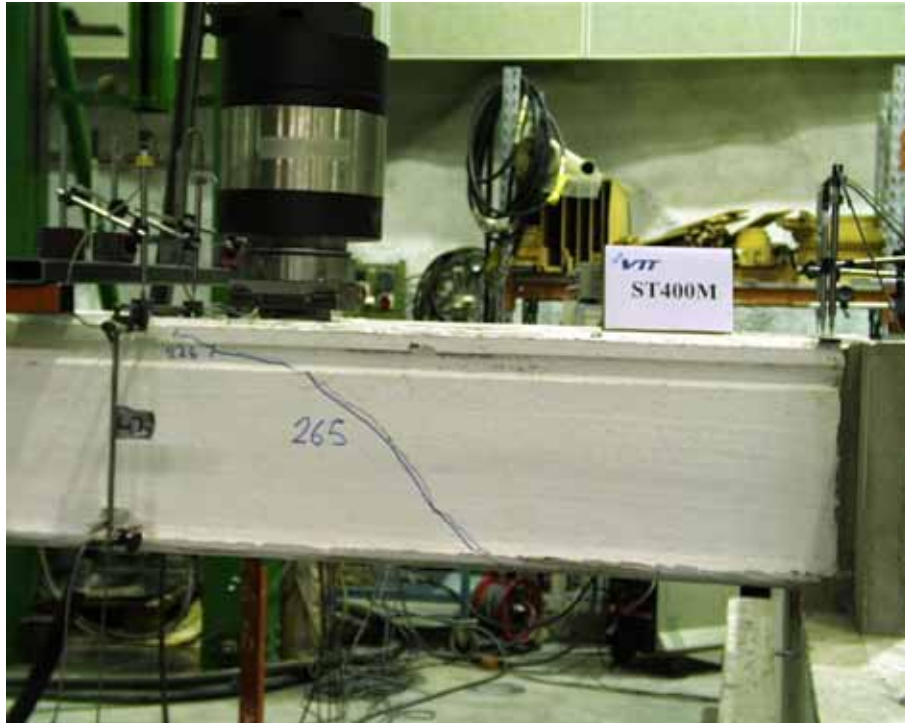


Fig. 38. ST400E1M. Shear crack after failure.



Fig. 39. ST400E1M. Shear crack after unloading.



Fig. 40. ST400E1M. Cracks on the top after unloading.



Fig. 41. ST400E1M. Cracking of soffit after unloading.



Fig. 42. ST400E1M. Cracking of soffit after unloading.

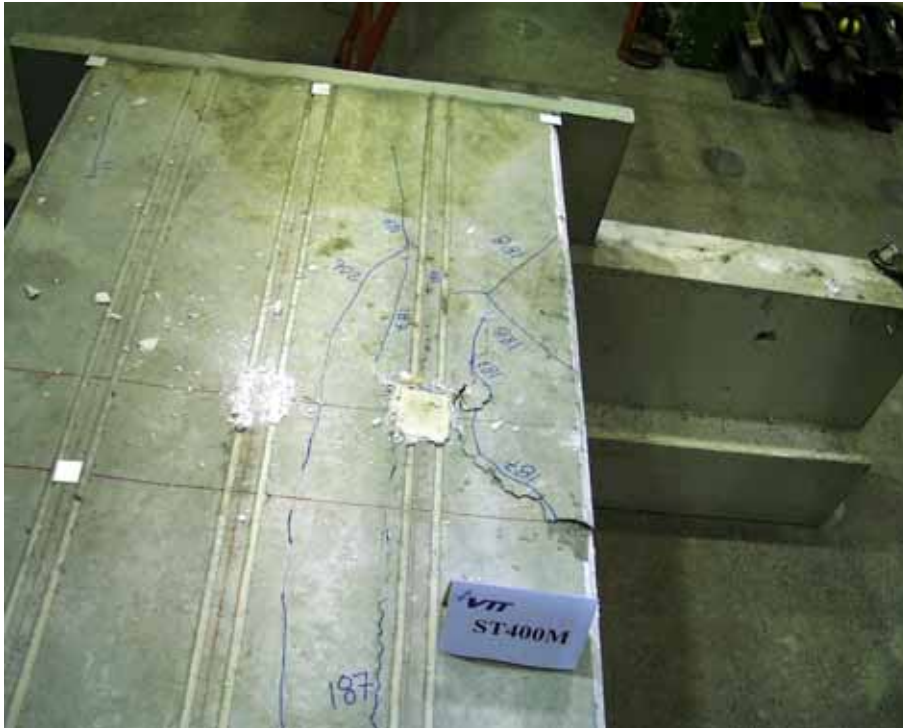


Fig. 43. ST400E1M. Cracking of the top surface after unloading. Note the letter A on the upper left corner of the figure. Before loading there was an initial crack from the slab end to letter A.

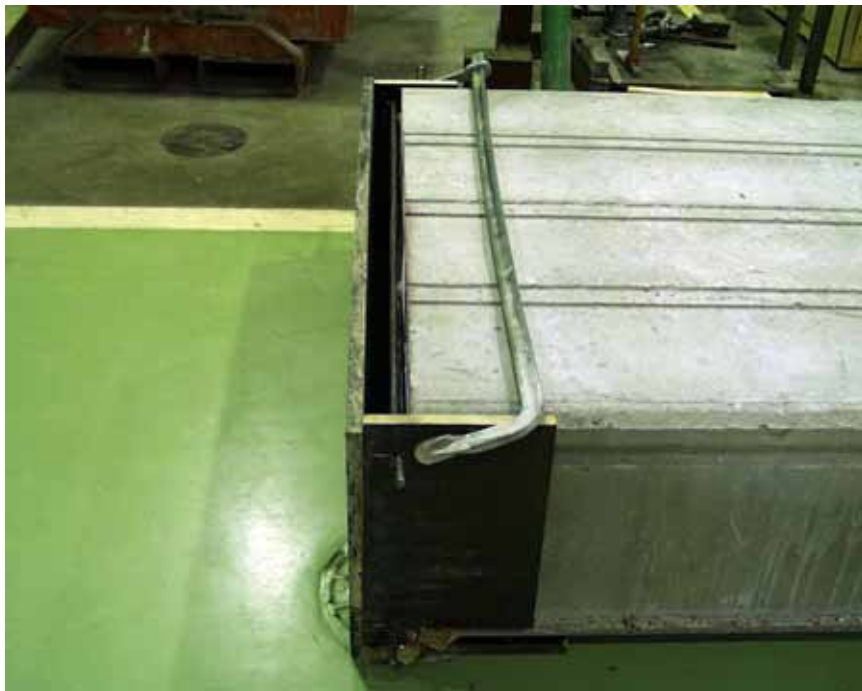


Fig. 44. ST400G. Arrangements before grouting.



Fig. 45. ST400G. Overview on arrangements.



Fig. 46. ST400G. Auxiliary beam for creating eccentric load at sheared end.

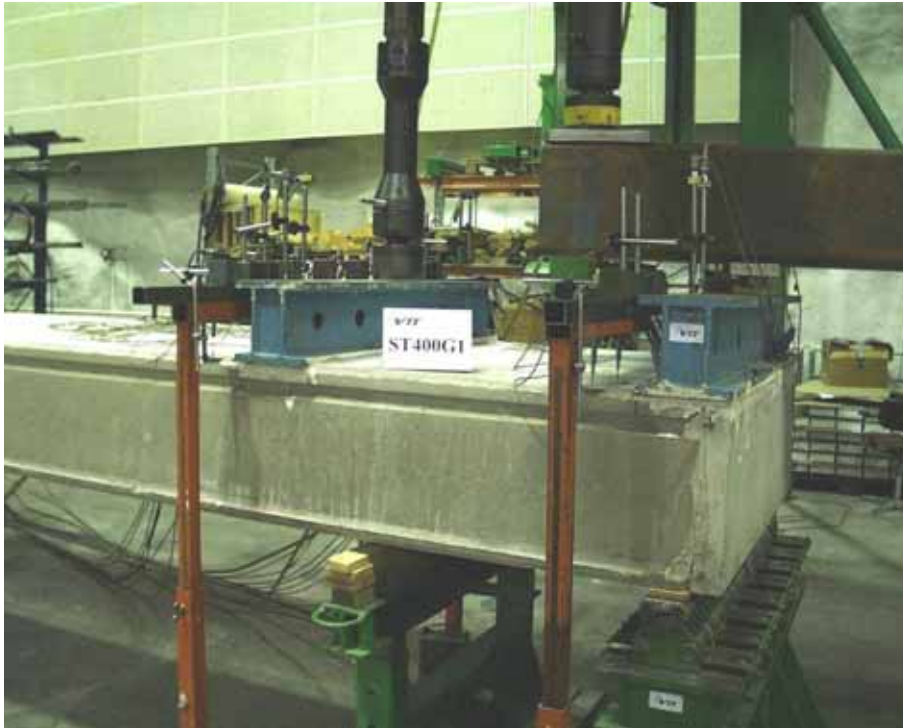


Fig. 47. ST400G. Arrangements at sheared end.



Fig. 48. ST400G. Arrangements at tilted end.



Fig. 49. ST400G1, South edge, first cracks.



Fig. 50. ST400G1, North edge, first cracks.



Fig. 51. ST400G1, North edge, cracks before failure.



Fig. 52. ST400G1, North edge, cracks after failure.

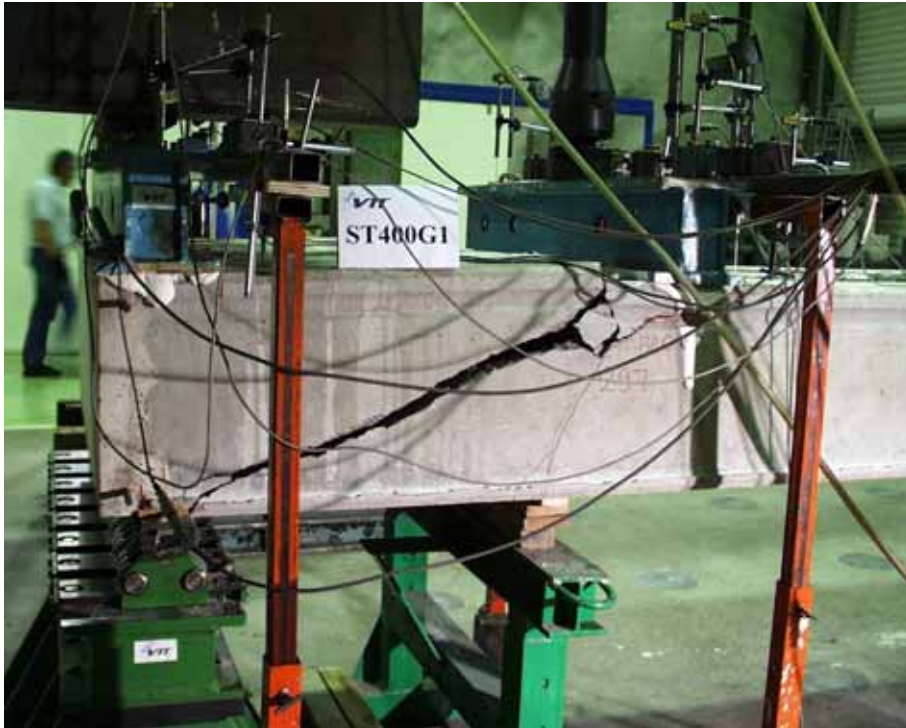


Fig. 53. ST400G1, South edge, cracks after failure.

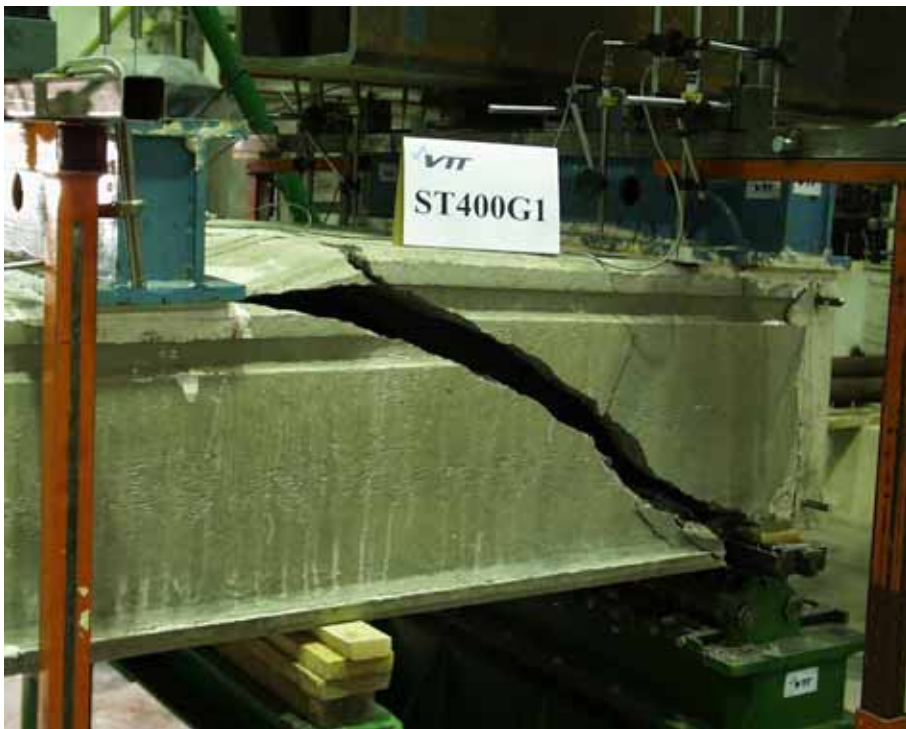


Fig. 54. ST400G1, North edge, failure cracks.



Fig. 55. ST400G1, active end, soffit after failure.

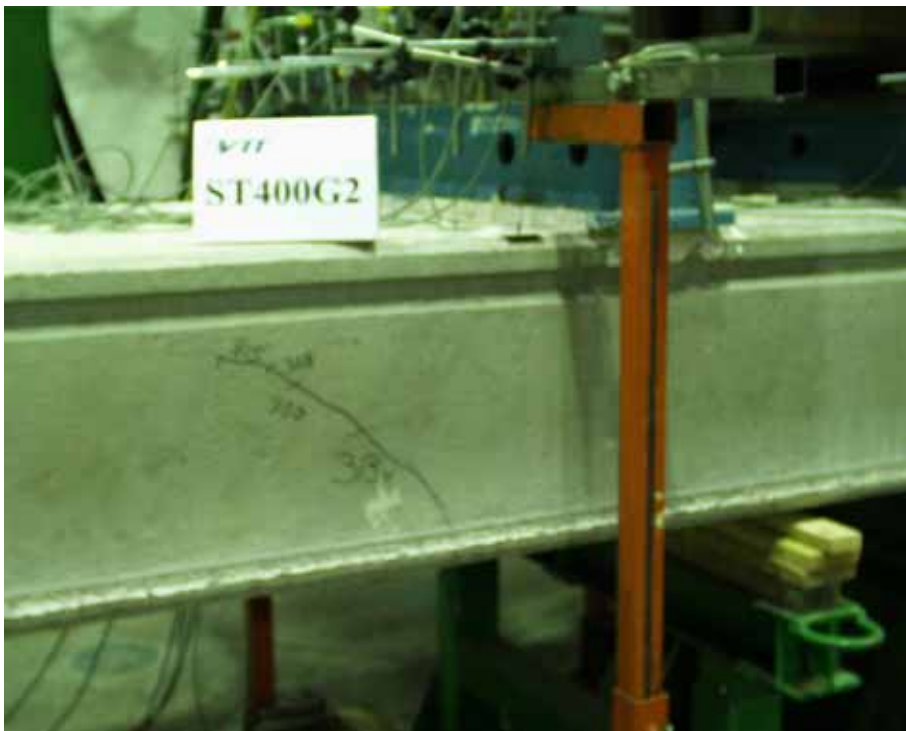


Fig. 56. ST400G2, North edge, cracks before failure.



Fig. 57. ST400G2, South edge, cracks before failure.



Fig. 58. ST400G2, North edge, cracks after failure.



Fig. 59. ST400G2, North edge, detail of failure cracks.



Fig. 60. ST400G2, South edge, cracks after failure.



Fig. 61. ST400G2, South edge, detail of failure cracks.



Fig. 62. ST400G2, top surface, cracks after failure.



Fig. 63. ST400G2, top surface, cracks after failure.

Appendix C: Measured geometry of slabs

In the following figures *prestress* refers to the nominal prestress in the strands after pretensioning (initial prestress). The underlined values refer to initial slippage of the strands. The strands are made of seven wires. The cross-sectional area of a strand is 93 mm².

End 1 was in all shear tests the active end and in test SF400C the Eastern end that failed. In tests STG400G1 and ST400G2 End 1 was the twisted end.

ST200C

Lower strands : 7 d 12.5, prestress = 900 MPa

Length : 7054 mm

Mass : 2000 kg

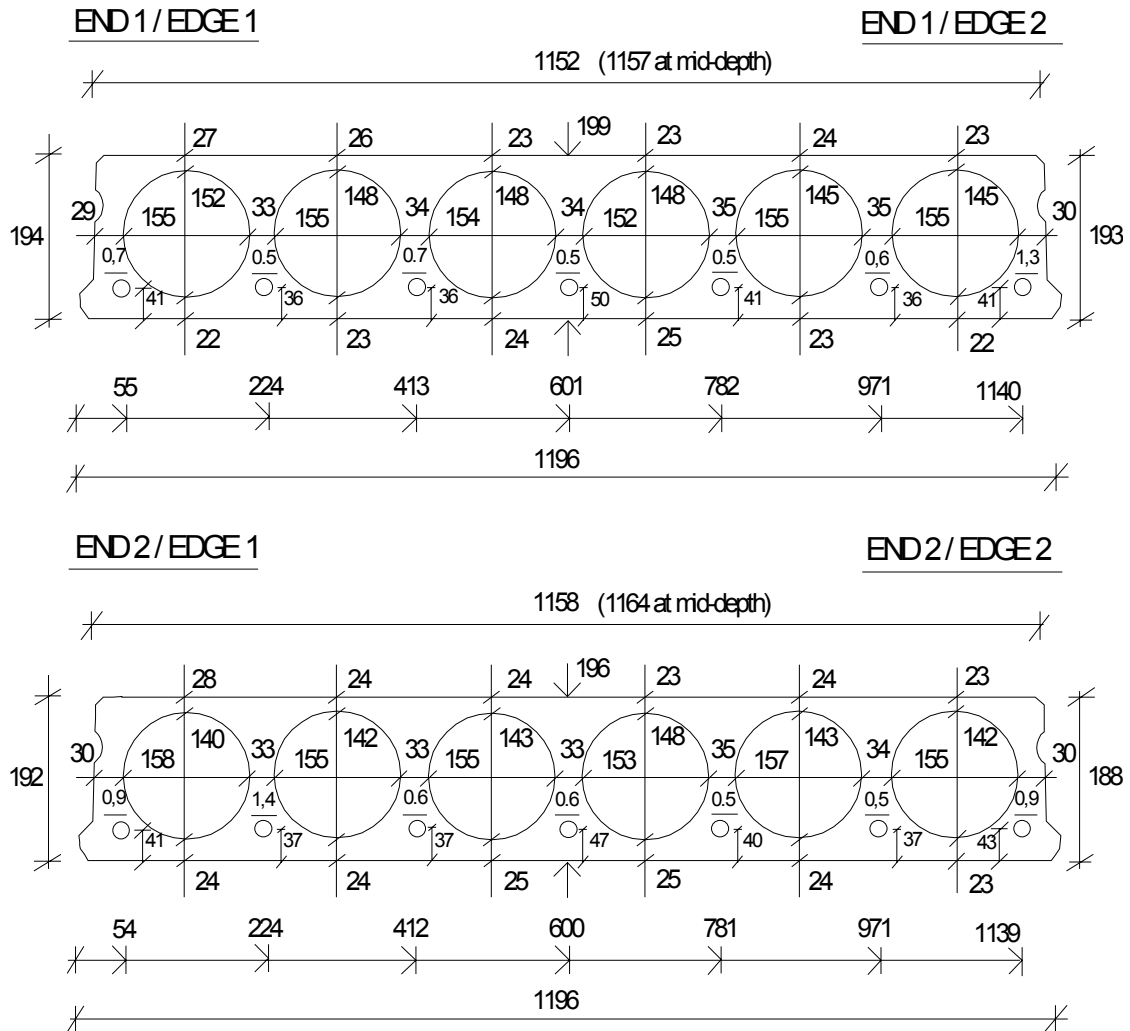


Fig. 1. ST200C.

ST200E1

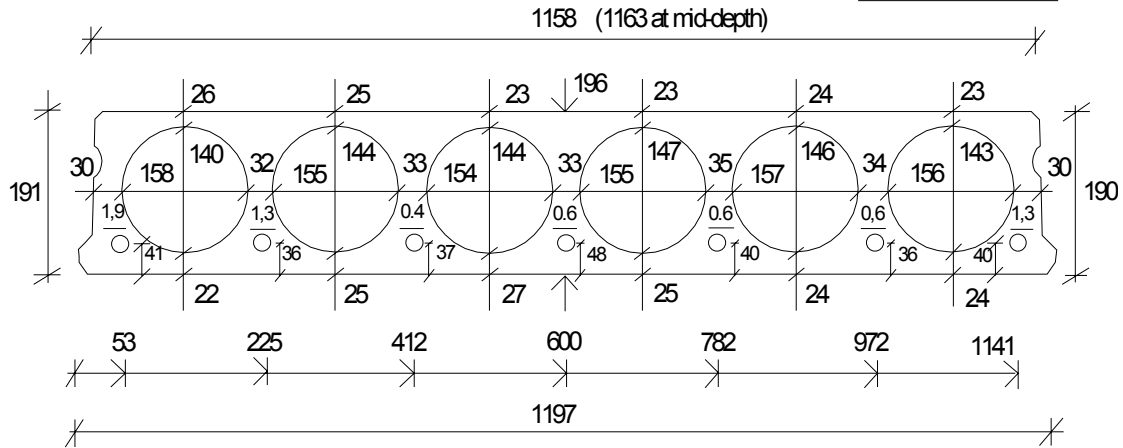
Lower strands : 7 d 12.5, prestress = 900 MPa

Length : 7050 mm

Mass : 2020 kg

END 1 / EDGE 1

END 1 / EDGE 2



END 2 / EDGE 1

END 2 / EDGE 2

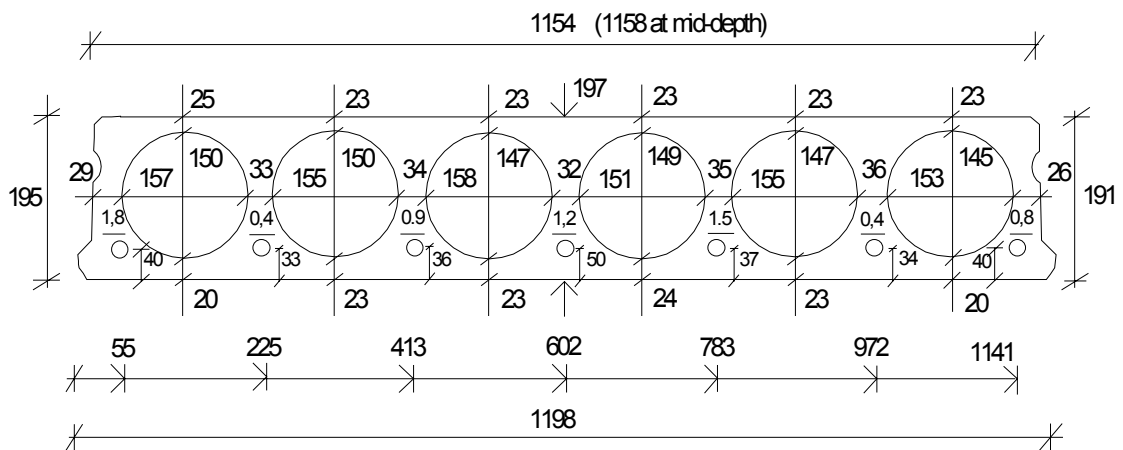


Fig. 2. ST200E1a.

ST200E1b

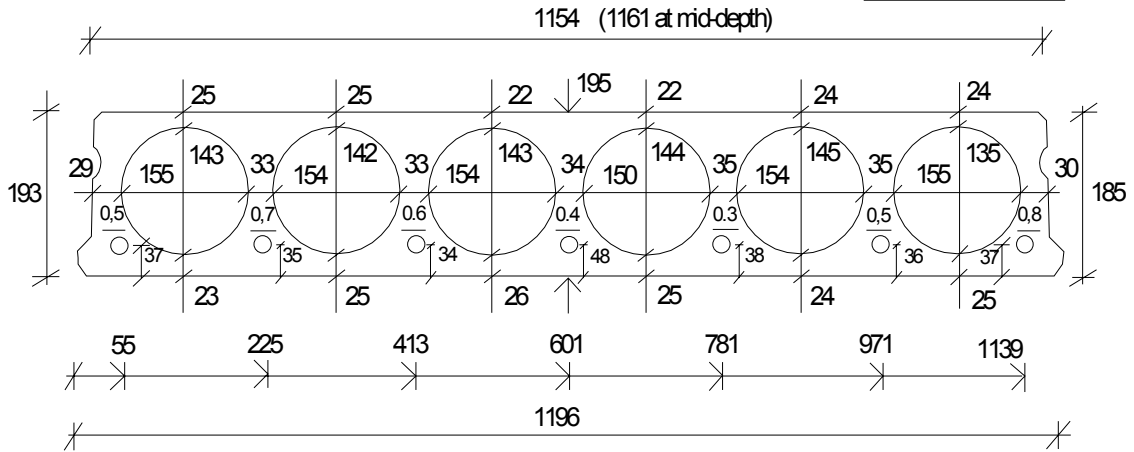
Lower strands : 7 d 12.5, prestress = 900 MPa

Length : 7056 mm

Mass : 2020 kg

END 1 / EDGE 1

END 1 / EDGE 2



END 2 / EDGE 1

END 2 / EDGE 2

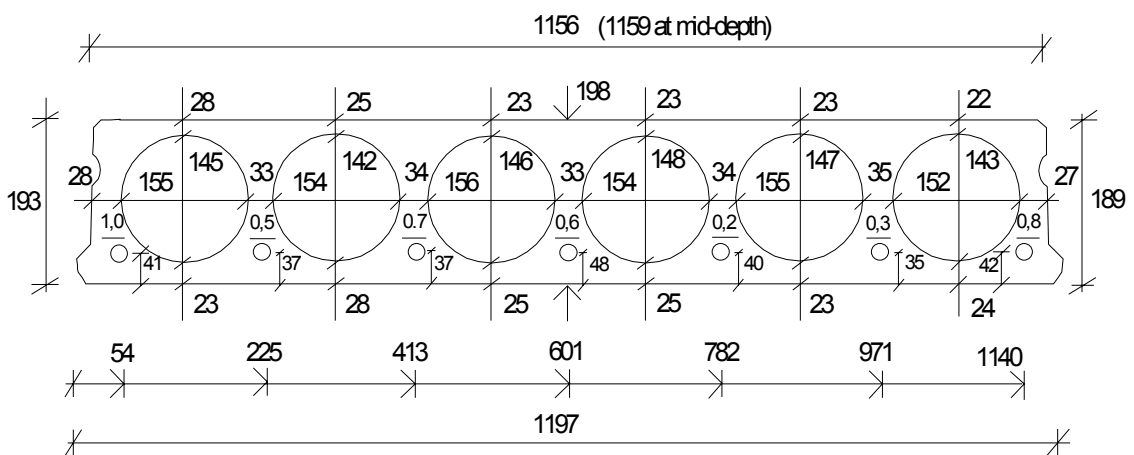


Fig. 3. ST200E1b.

ST200E2

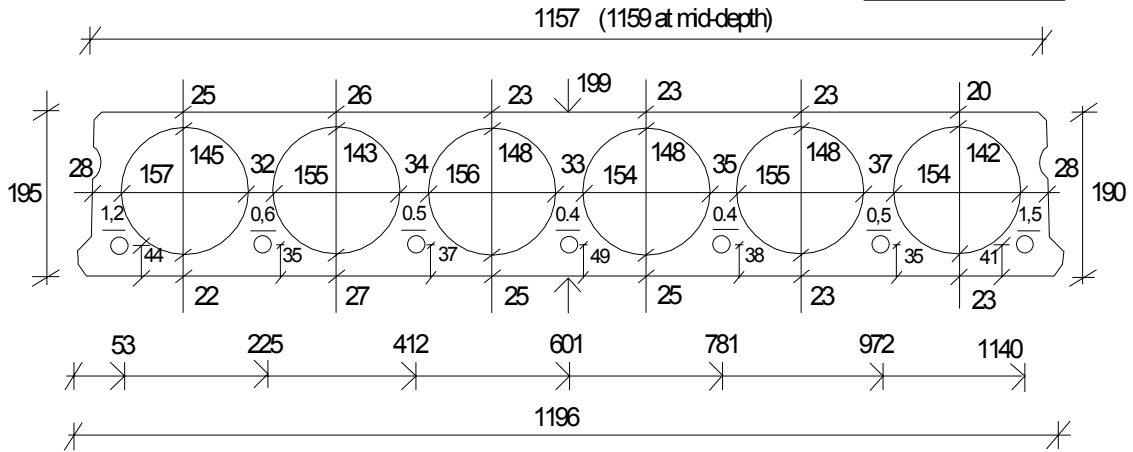
Lower strands : 7 d 12.5, prestress = 900 MPa

Length : 7063 mm

Mass : 2020 kg

END 1 / EDGE 1

END 1 / EDGE 2



END 2 / EDGE 1

END 2 / EDGE 2

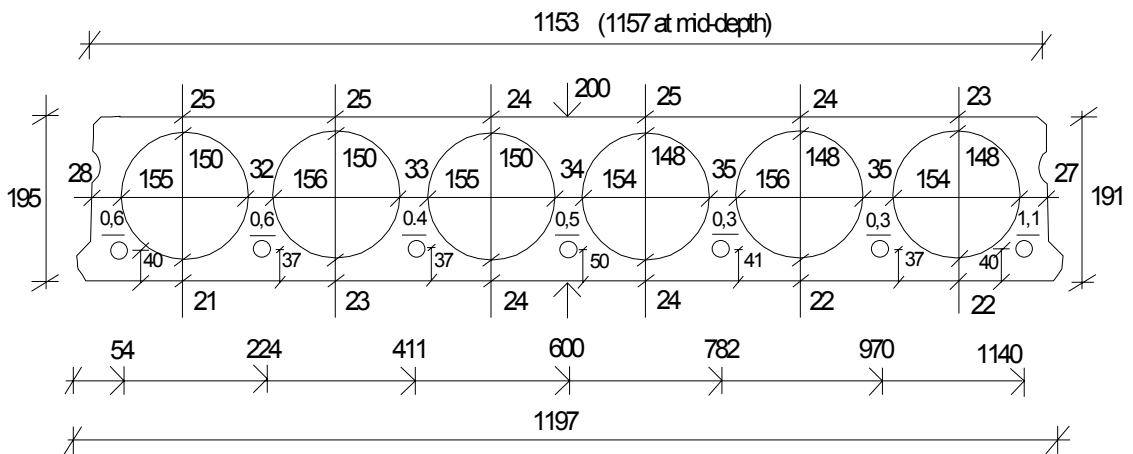


Fig. 4. ST200E2.

STS200C

Lower strands : 8 d 12.5, prestress = 900 MPa

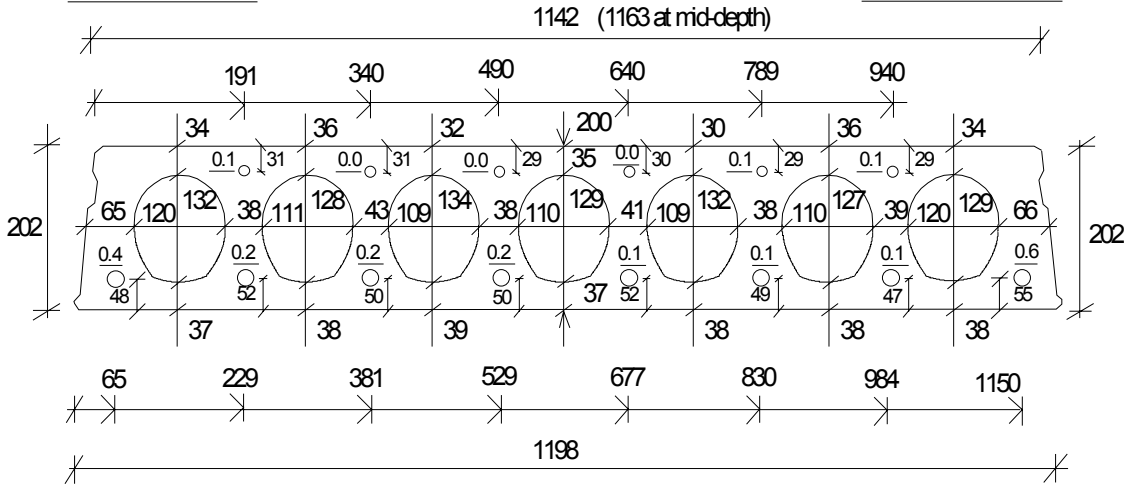
Length : 7028 mm

Upper wires : 6 d 6, prestress = 700 MPa

Mass : 2400 kg

END 1 / EDGE 1

END 1 / EDGE 2



END 2 / EDGE 1

END 2 / EDGE 2

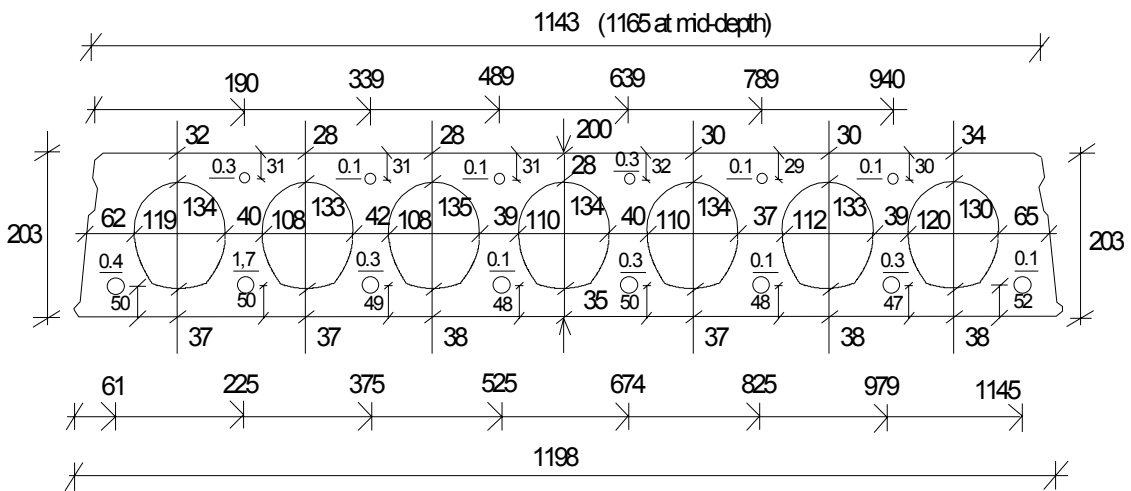


Fig. 5. STS200C.

STS200E1

Lower strands : 8 d 12.5, prestress = 900 MPa

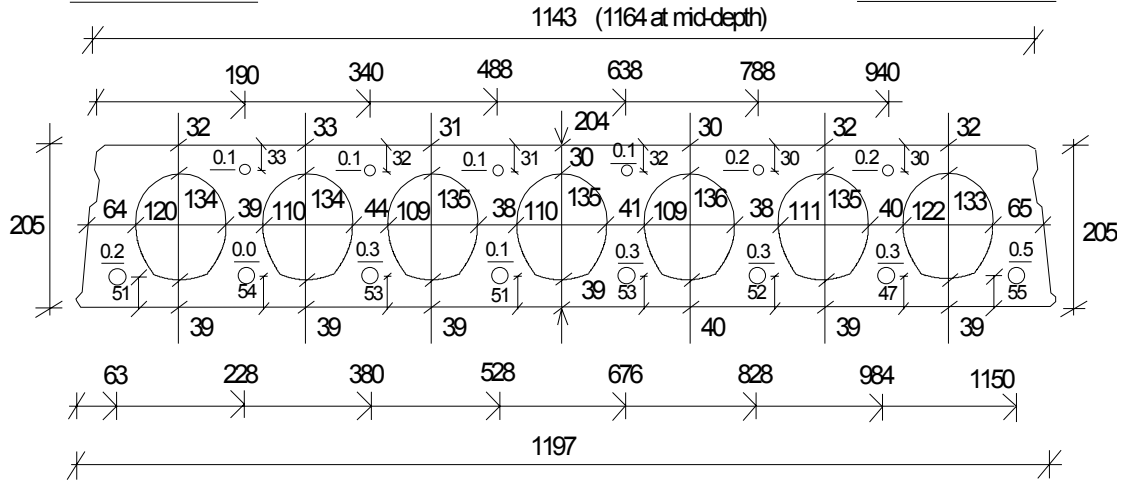
Length : 7046 mm

Upper wires : 6 d 6, prestress = 700 MPa

Mass : 2390 kg

END 1 / EDGE 1

END 1 / EDGE 2



END 2 / EDGE 1

END 2 / EDGE 2

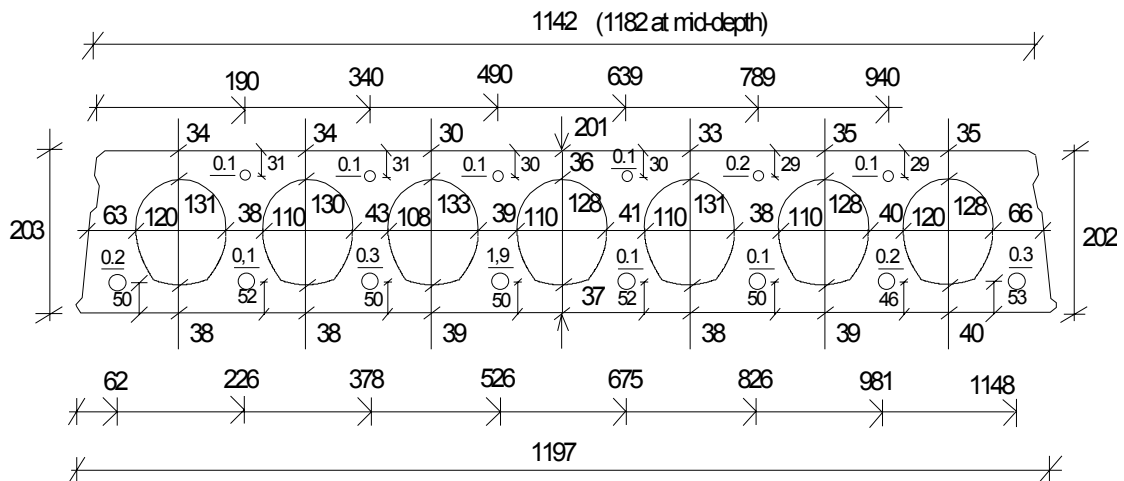


Fig. 6. STS200E1.

ST200E1M

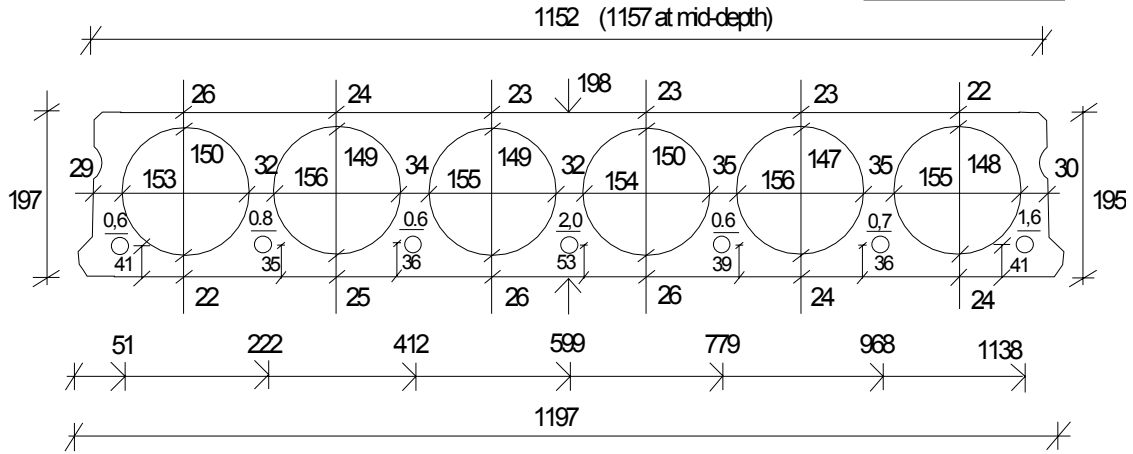
Lower strands : 7 d 12.5, prestress = 900 MPa

Length : 7055 mm

Mass : 2000 kg

END 1 / EDGE 1

END 1 / EDGE 2



END 2 / EDGE 1

END 2 / EDGE 2

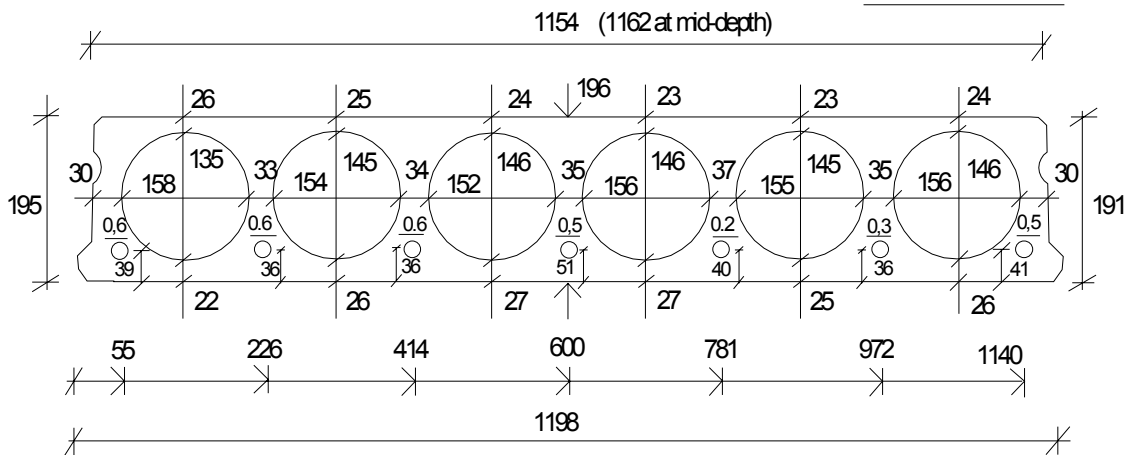


Fig. 7. ST200E1M.

ST200E2M

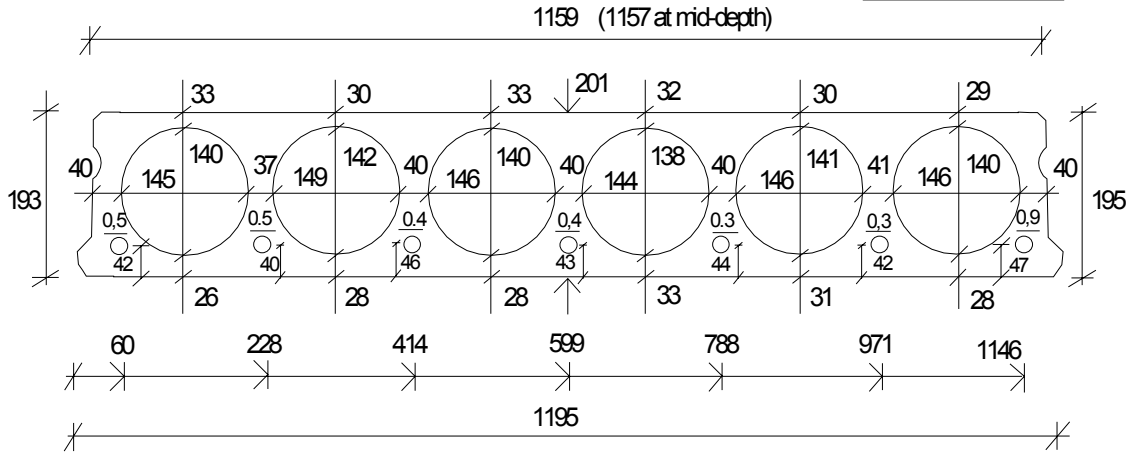
Lower strands : 7 d 12.5, prestress = 900 MPa

Length : 7045 mm

Mass : 2050 kg

END 1 / EDGE 1

END 1 / EDGE 2



END 2 / EDGE 1

END 2 / EDGE 2

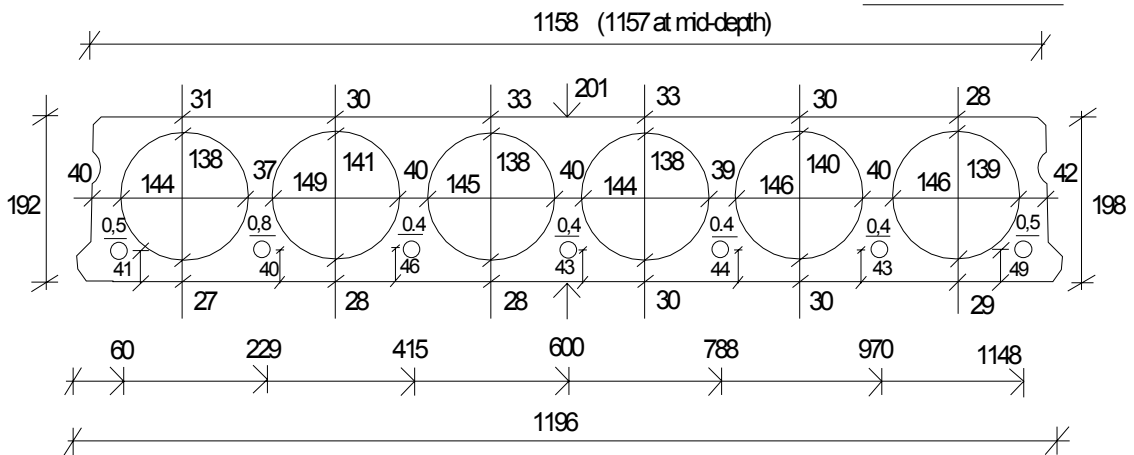


Fig. 8. ST200E2M.

ST400C1

Lower strands : 11 d 12.5, prestress = 1000 MPa

Length : 7083 mm

Mass : 3630 kg

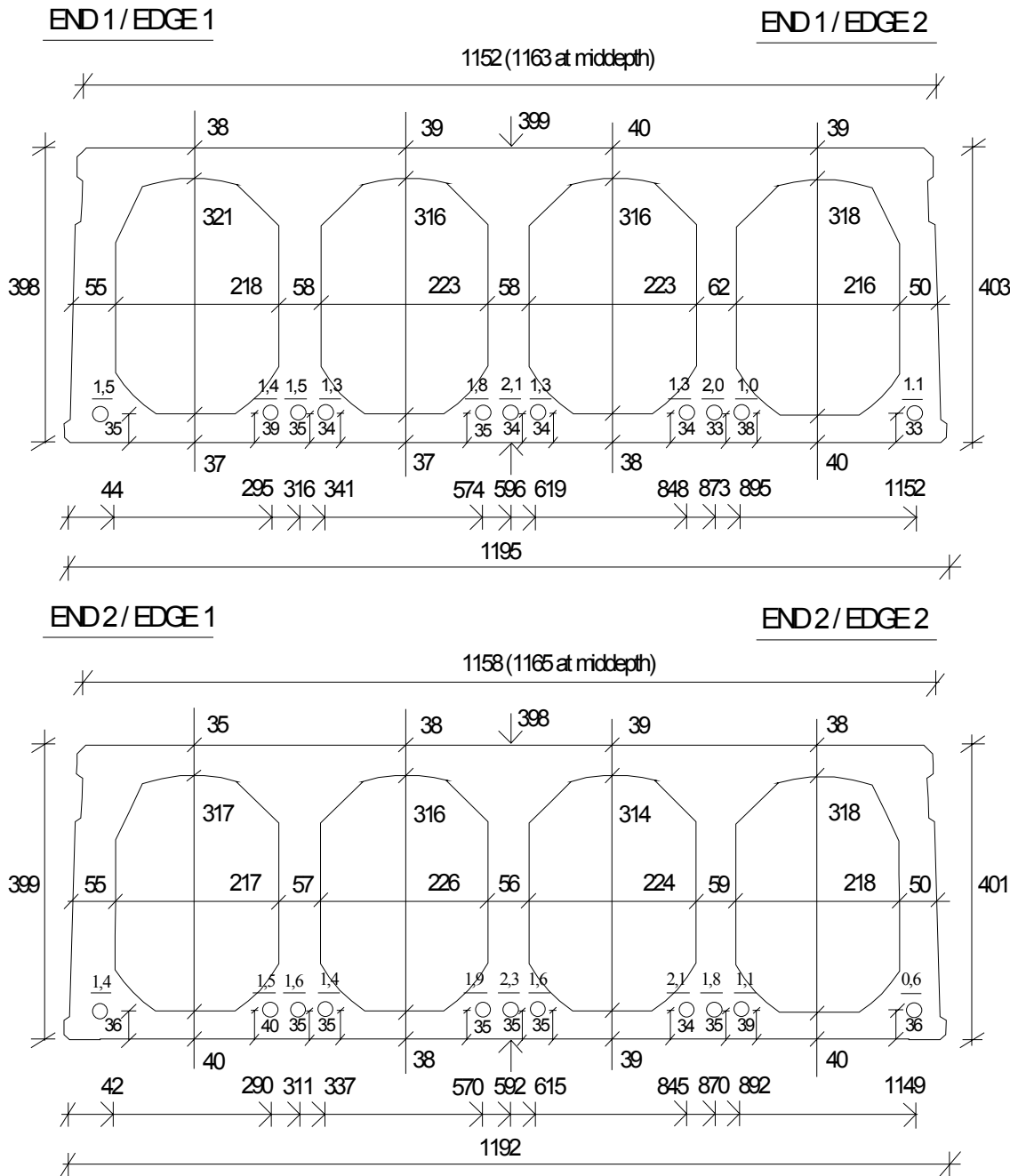


Fig. 9. ST400C1.

ST400C2

Lower strands : 11 d 125, prestress = 1000 MPa

Length : 7082 mm

Mass : 3610 kg

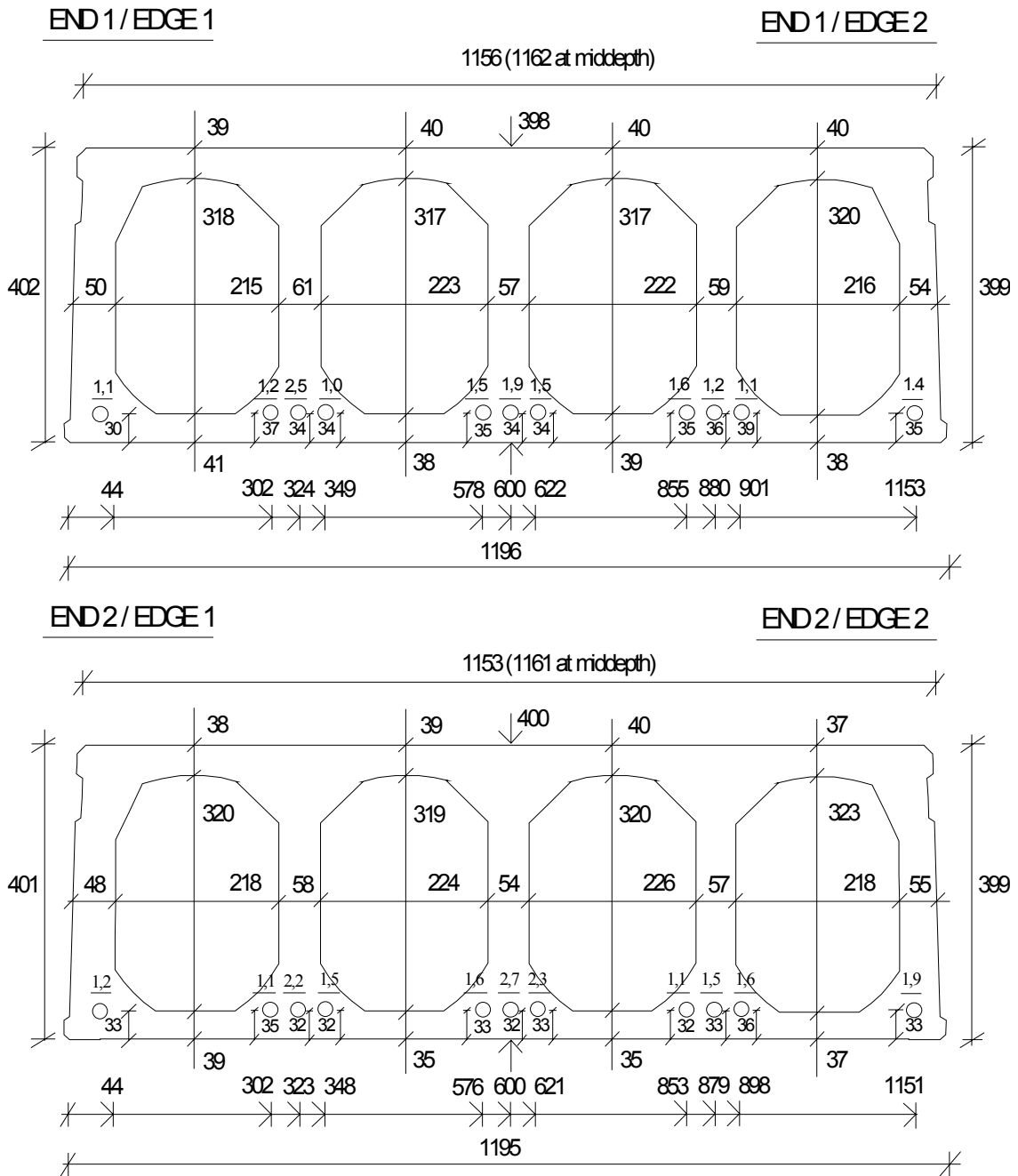


Fig. 10. ST400C2.

ST400E1

Lower strands : 11 d 125, prestress = 1000 MPa

Length : 7075 mm

Mass : 3600 kg

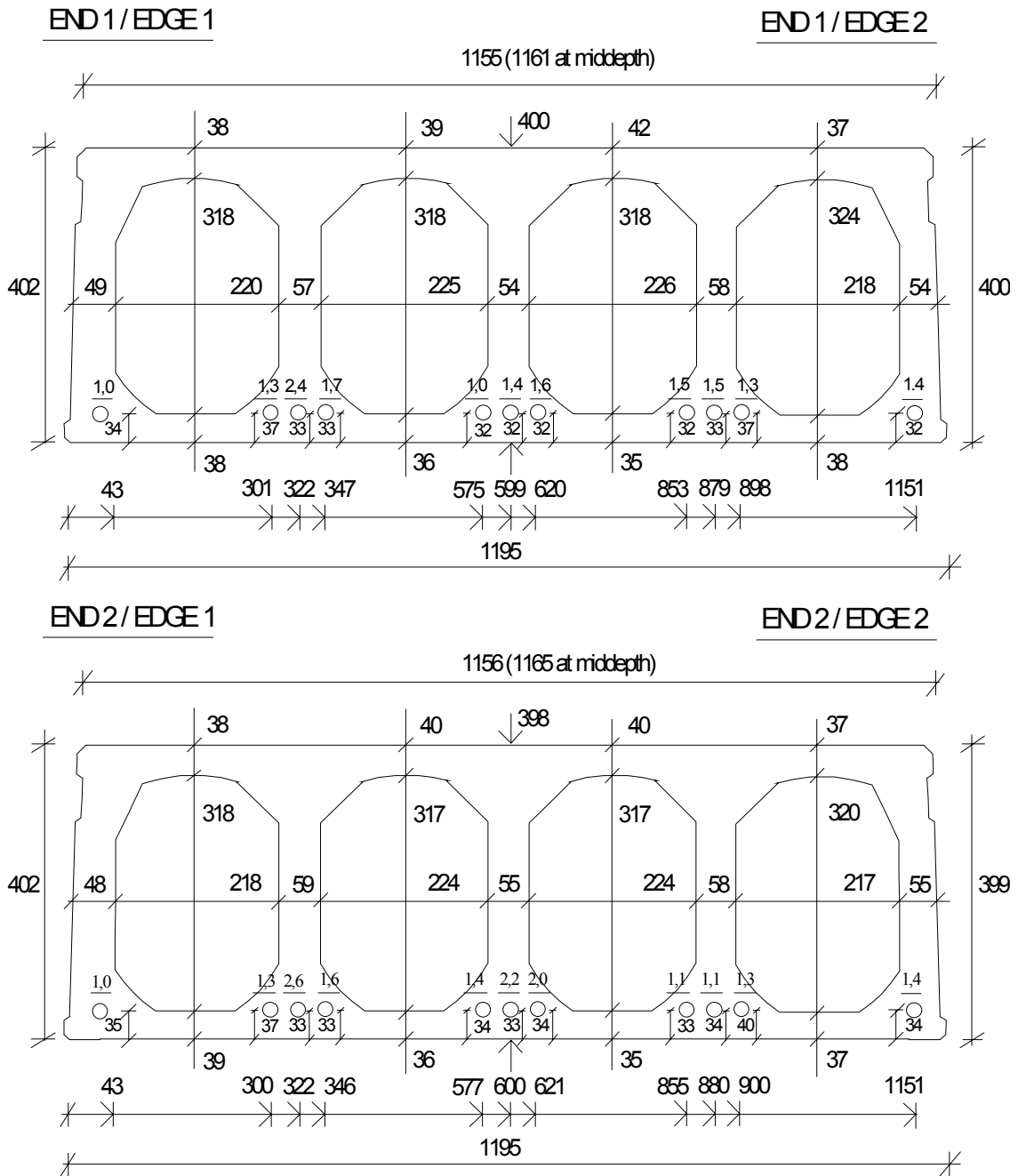


Fig. 11. ST400E1.

ST4002E

Lower strands : 11 d 125, prestress = 1000 MPa

Length : 7075 mm

Mass : 3620 kg

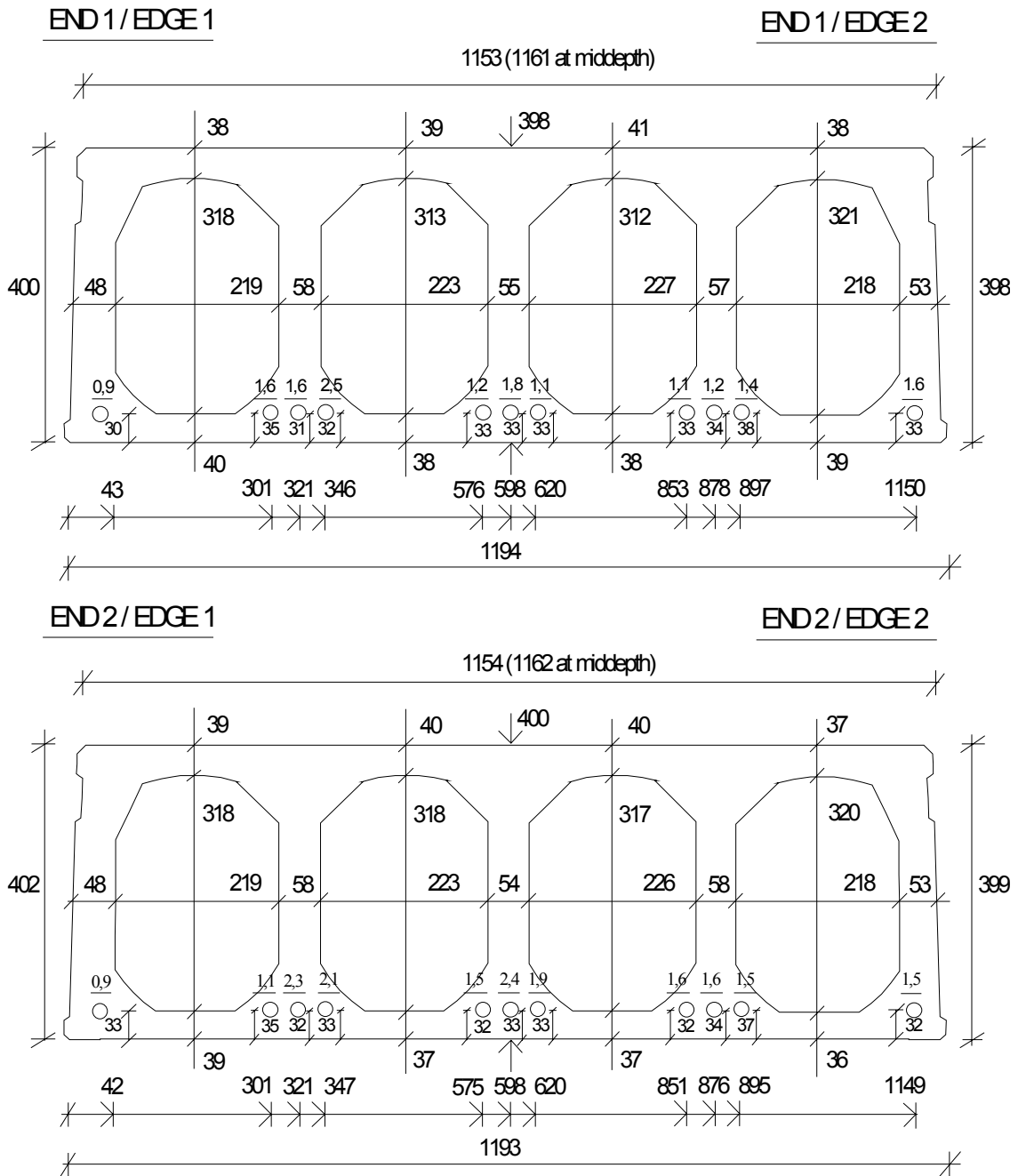


Fig. 12. ST4002E.

ST400E1M

Lower strands : 11 d 125, prestress = 1000 MPa

Length : 7077 mm

Mass : 3610 kg

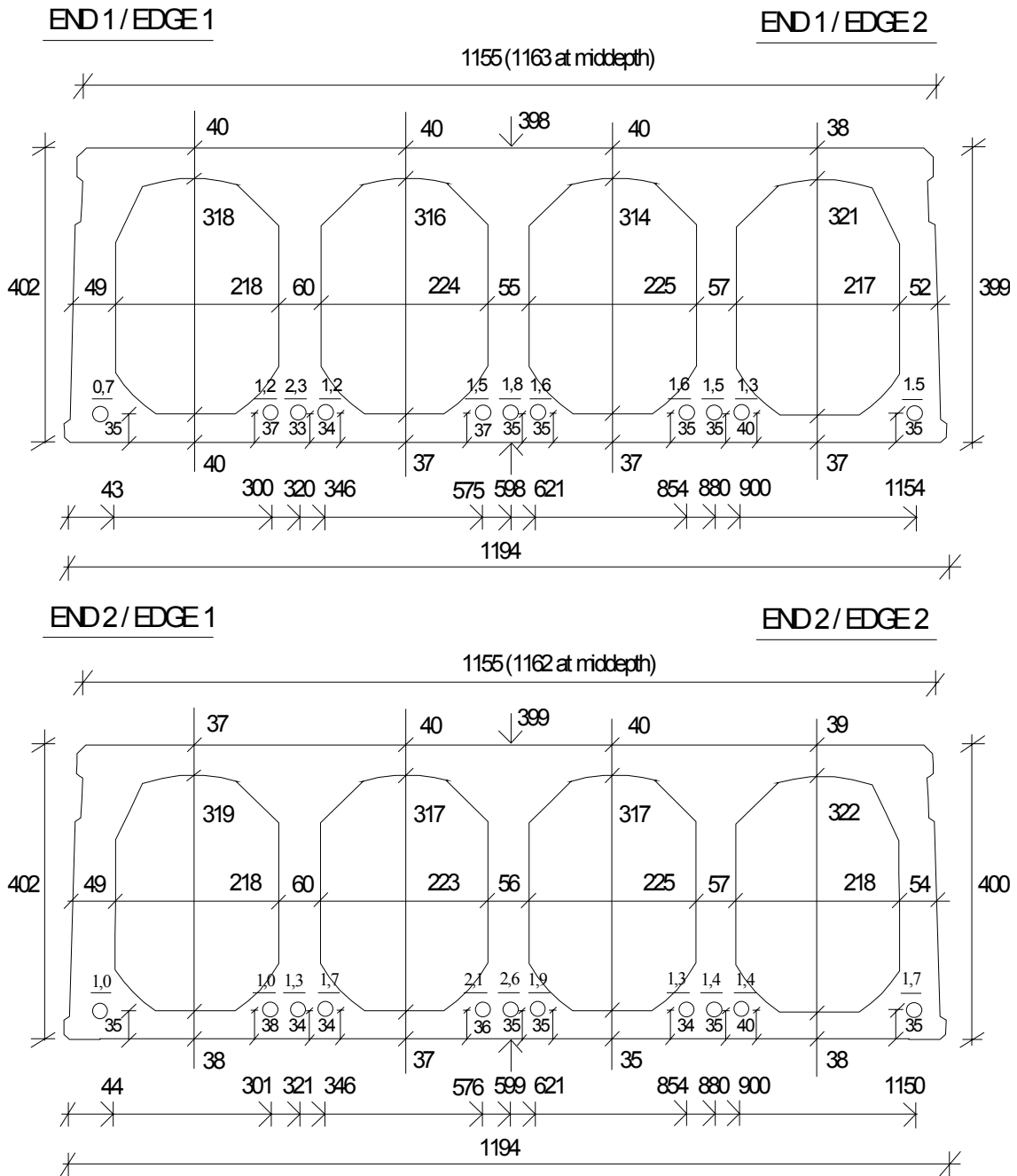


Fig. 13. ST400E1M.

SF400C

Lower strands : 11 d 12.5, prestress = 1000 MPa

Length : 7083 mm

Mass : 3600 kg

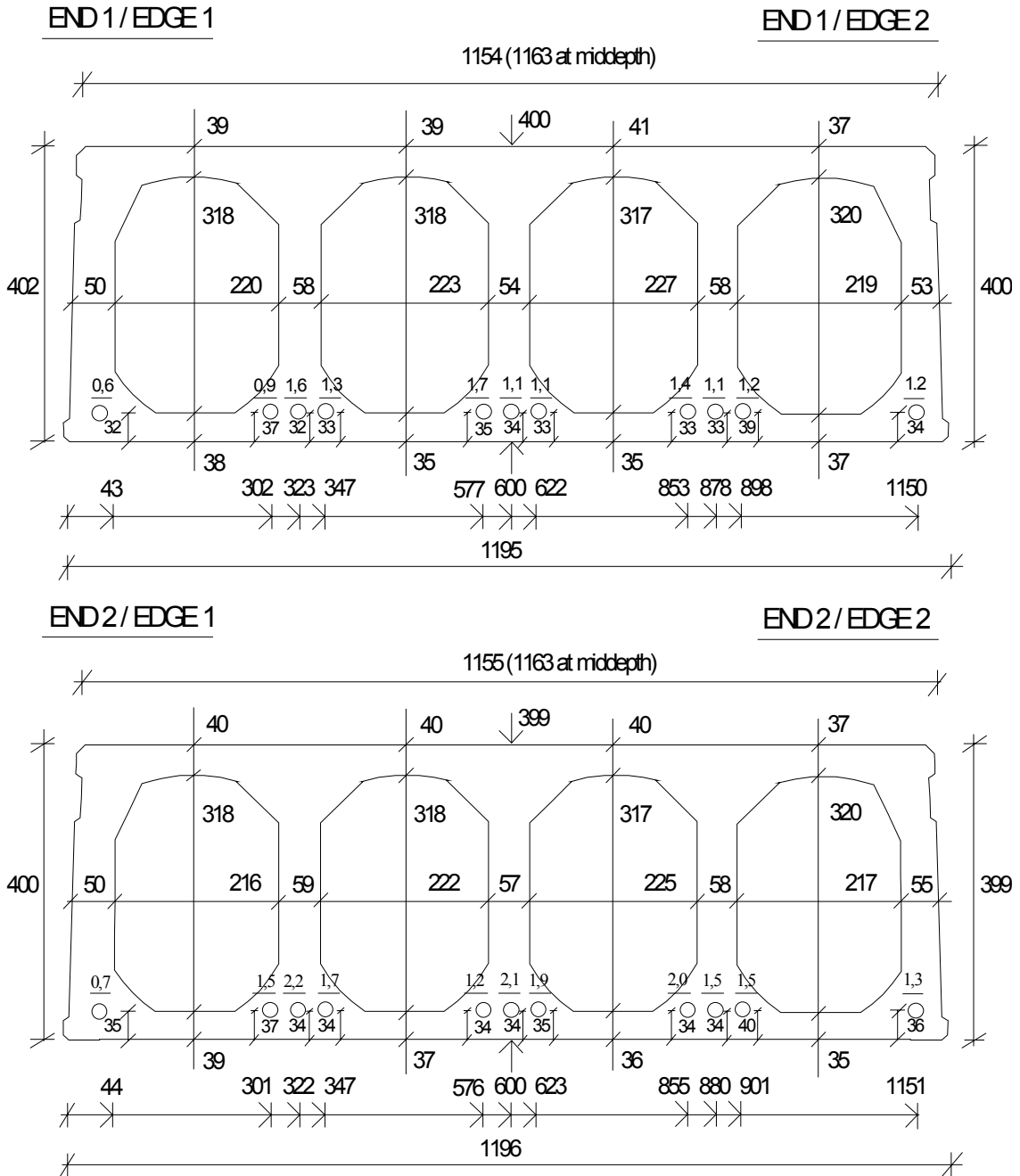


Fig. 14. SF400C.

ST400G1

Lower strands : 11 d 12.5, prestress = 1000 MPa

Length : 7075 mm

Mass : 3550 kg

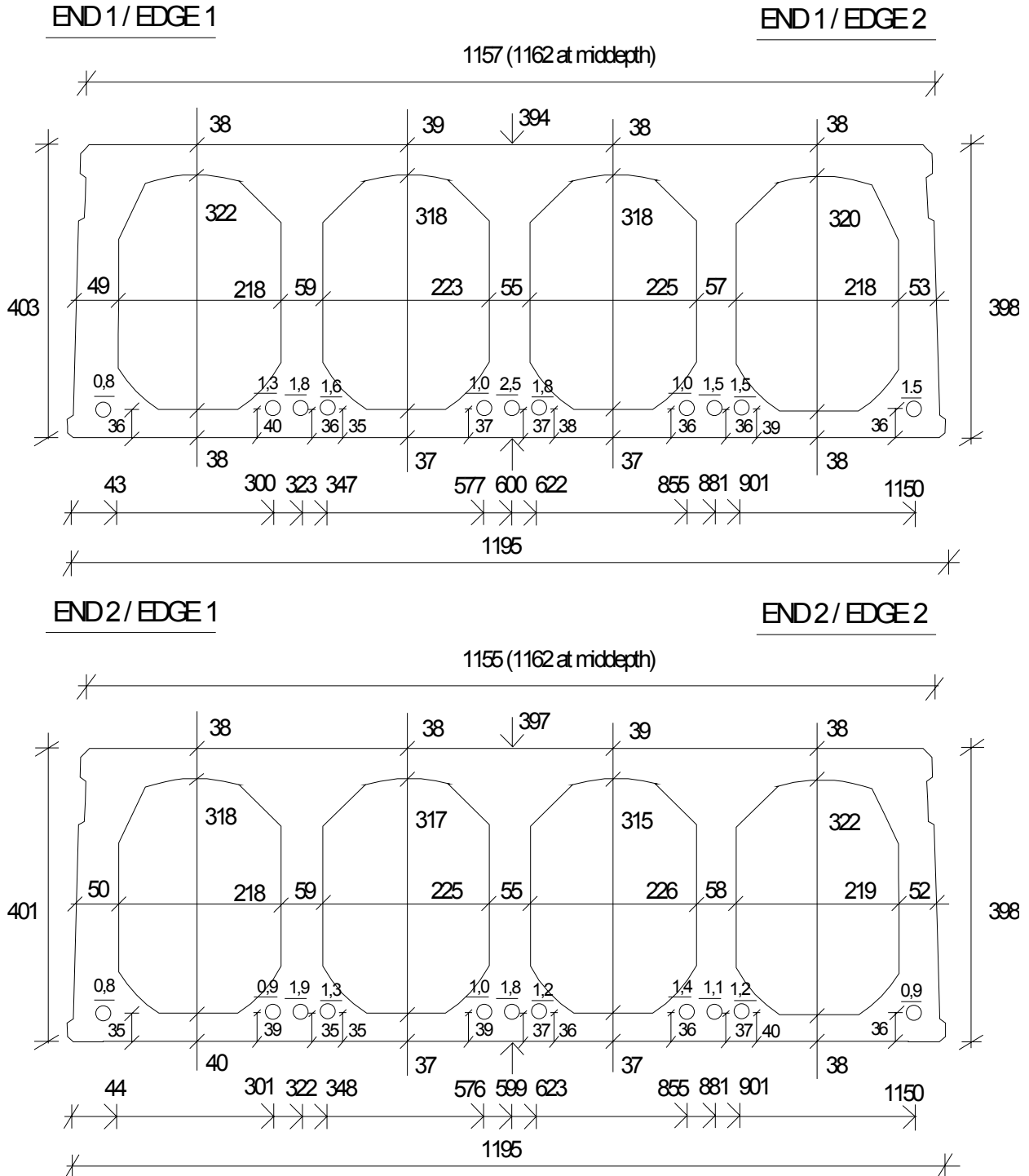


Fig. 15. ST400G1.

ST400G2

Lower strands : 11 d 12.5, prestress = 1000 MPa

Length : 7078 mm

Mass : 3560 kg

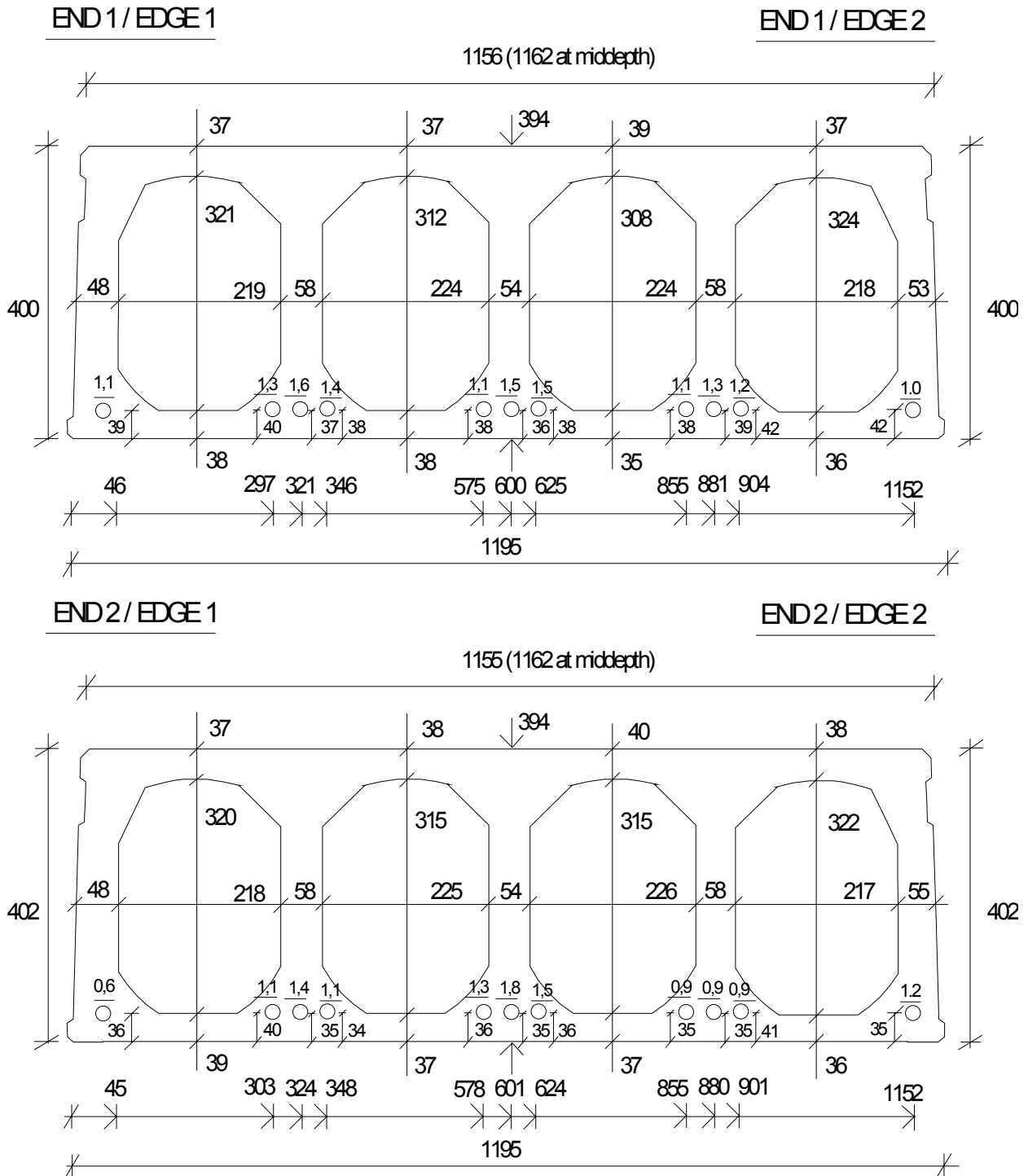


Fig. 16. ST400G2.

Appendix D: 200 mm slabs, measured displacements in shear torsion tests

The load is the actuator load without weight of loading equipment. The following terms are used for different measured displacements:

- *deflection*: vertical displacement of slab
- *transverse horizontal displacement*: horizontal displacement perpendicular to the slab
- *longitudinal horizontal displacement*: horizontal displacement of supporting beam parallel to longitudinal axis of slab
- *slippage of strand*: displacement of strand end relative to the surrounding concrete.

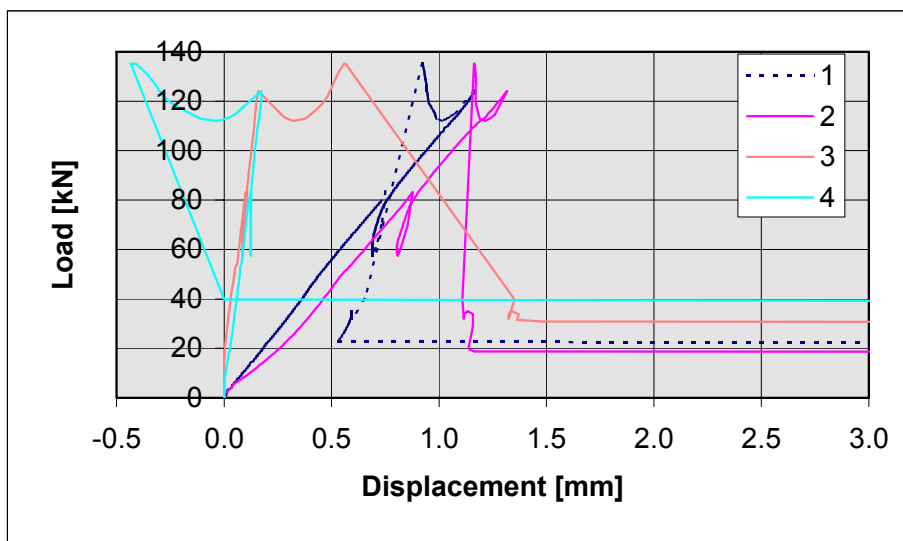


Fig. 1. ST200C. Deflections at supports. Transducers 1–4.

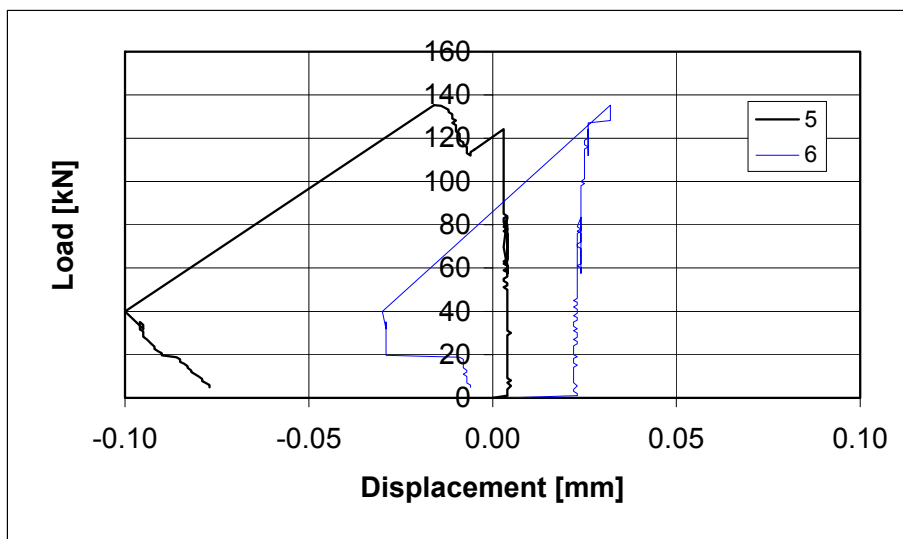


Fig. 2. ST200C. Transverse horizontal displacements. Transducers 5 and 6.

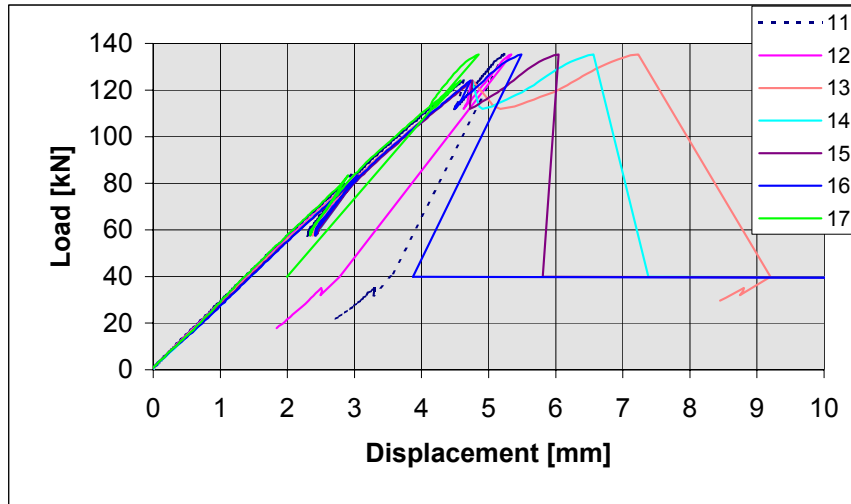


Fig. 3. ST200C. Deflections close to load. Transducers 11–17.

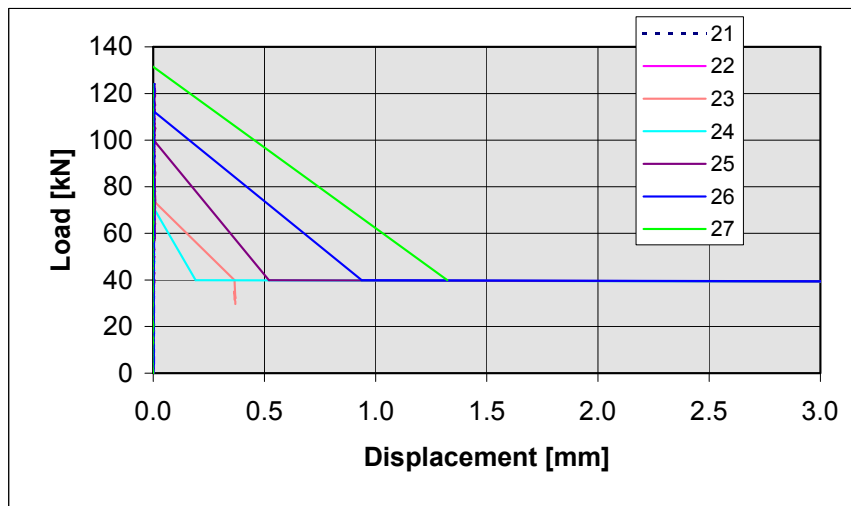


Fig. 4. ST200C. Slippage of strands. Transducers 21–27.

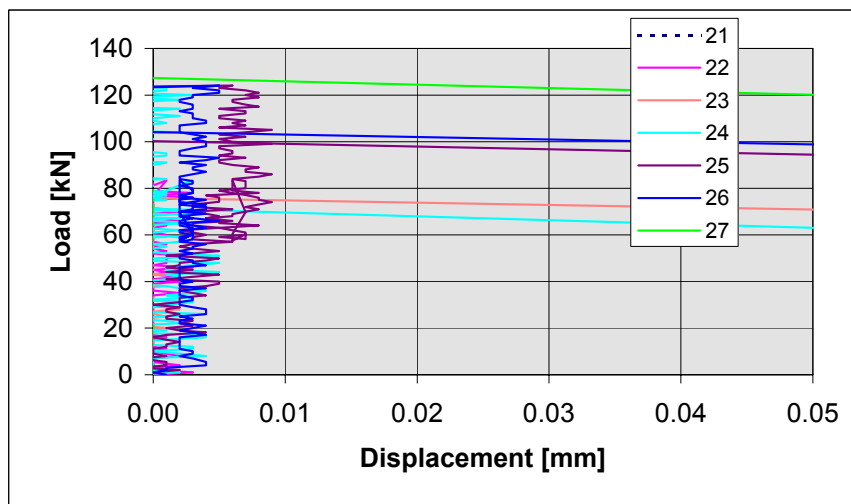


Fig. 5. ST200C. Slippage of strands. Transducers 21–27.

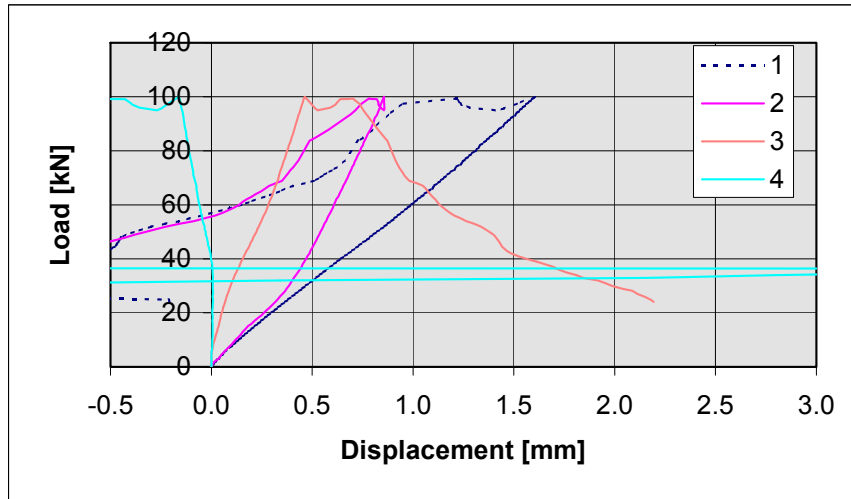


Fig. 6. ST200E1a. Deflections at supports. Transducers 1–4.

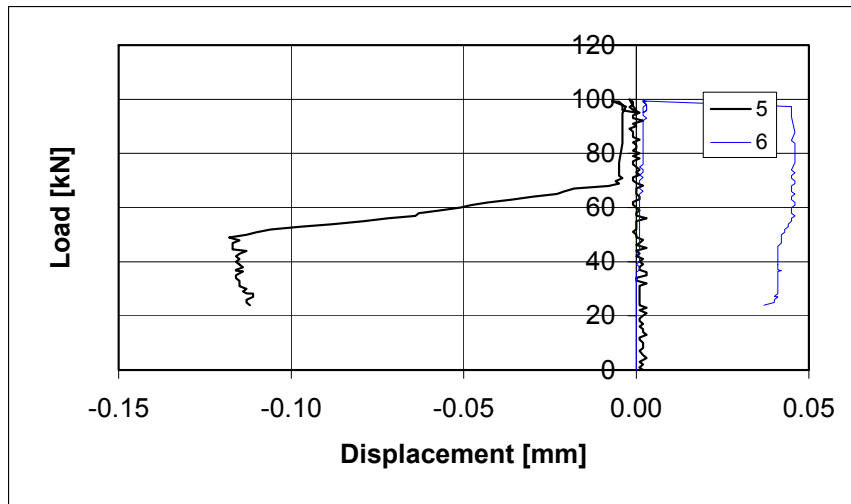


Fig. 7. ST200E1a. Transverse horizontal displacements. Transducers 5 and 6.

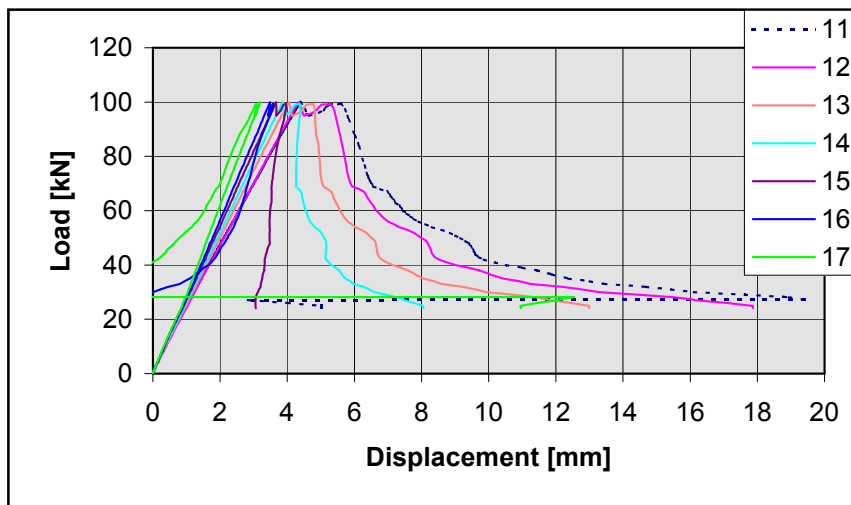


Fig. 8. ST200E1a. Deflections close to load. Transducers 11–17.

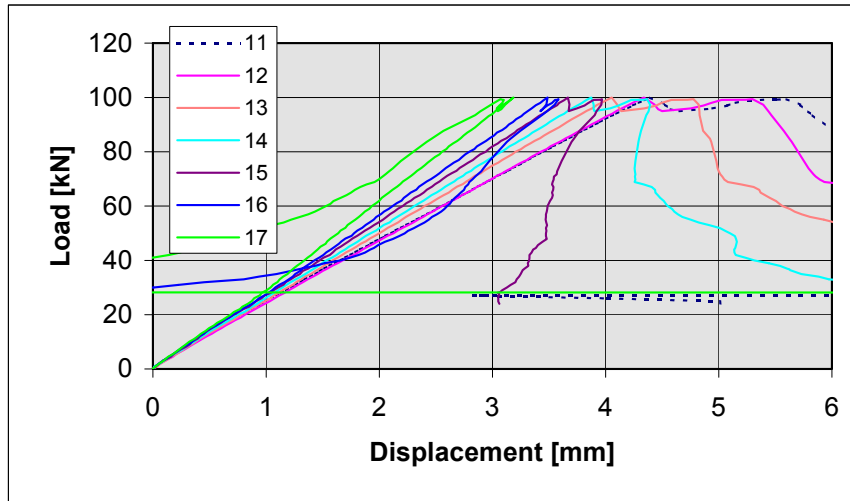


Fig. 9. ST200E1a. Deflections close to load. Transducers 11–17.

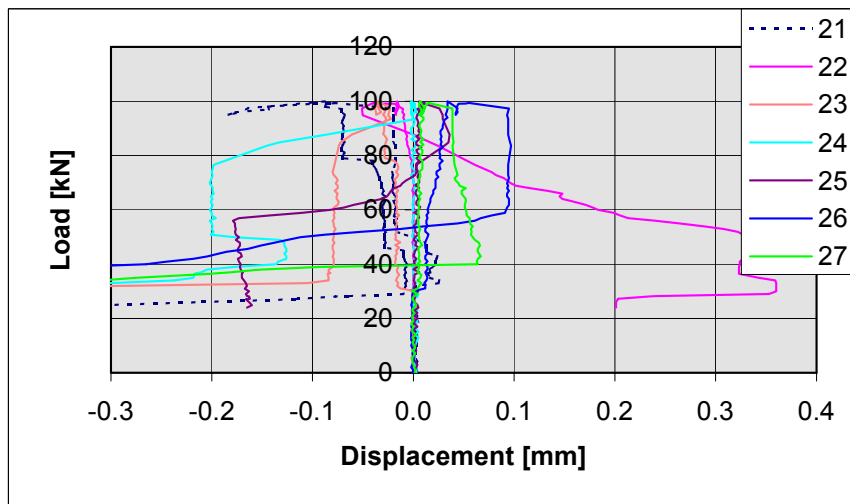


Fig. 10. ST200E1a. Slippage of strands. Transducers 21–27.

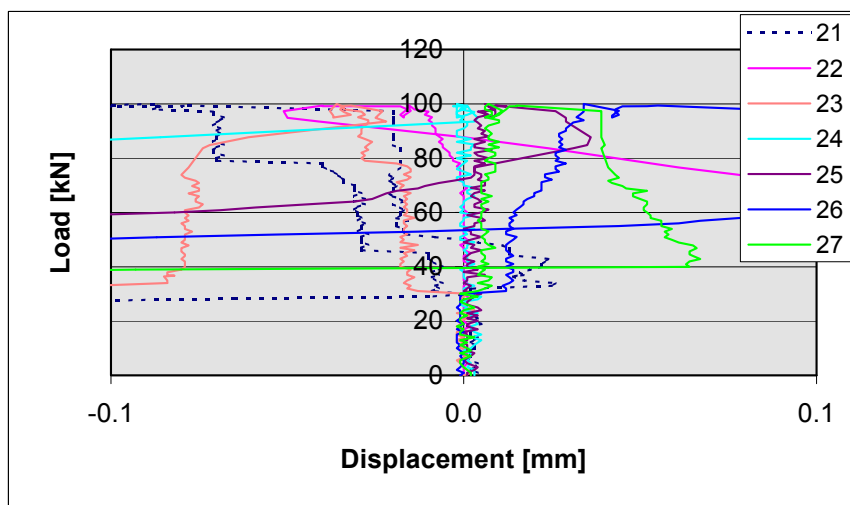


Fig. 11. ST200E1a. Slippage of strands. Transducers 21–27.

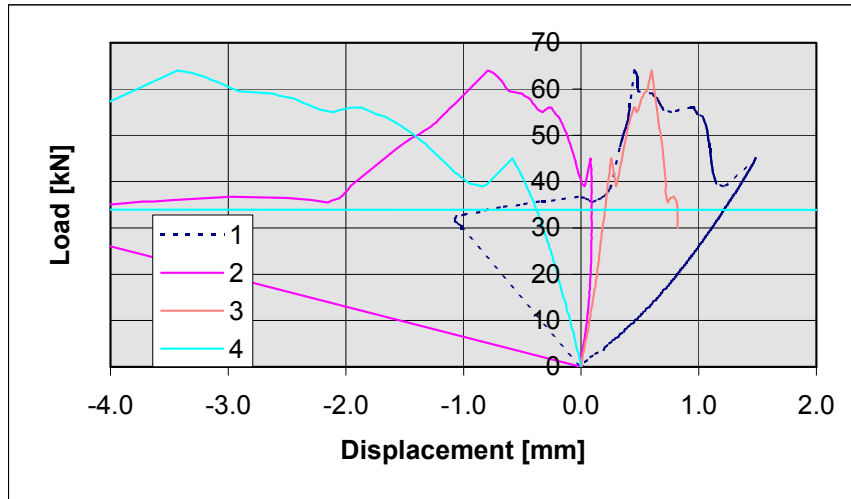


Fig. 12. ST200E2. Deflections at supports. Transducers 1–4.

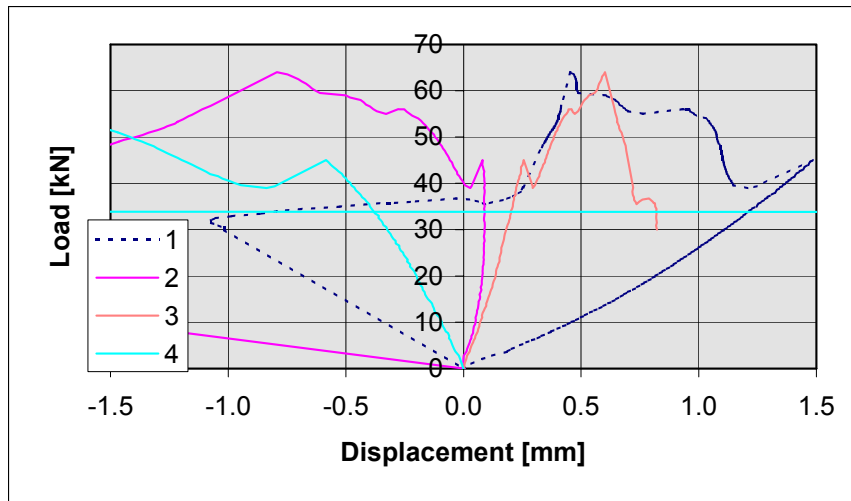


Fig. 13. ST200E2. Deflections at supports. Transducers 1–4.

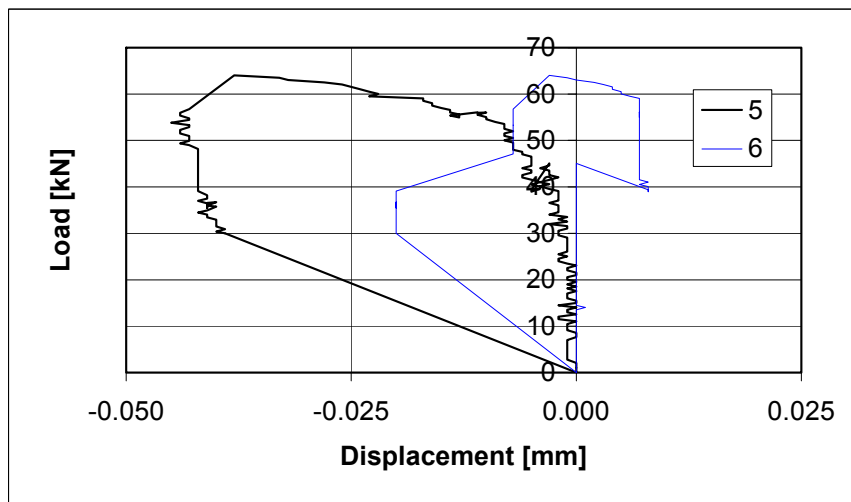


Fig. 14. ST200E2. Transverse horizontal displacements. Transducers 5 and 6.

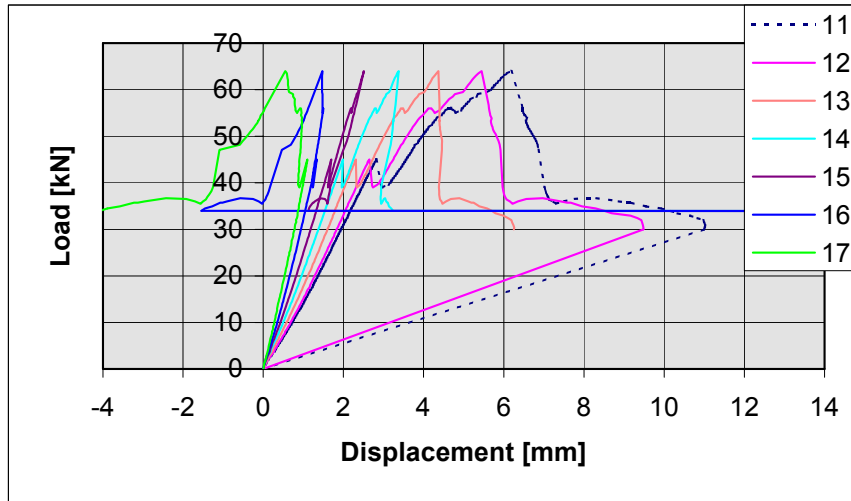


Fig. 15. ST200E2. Deflections close to load. Transducers 11–17.

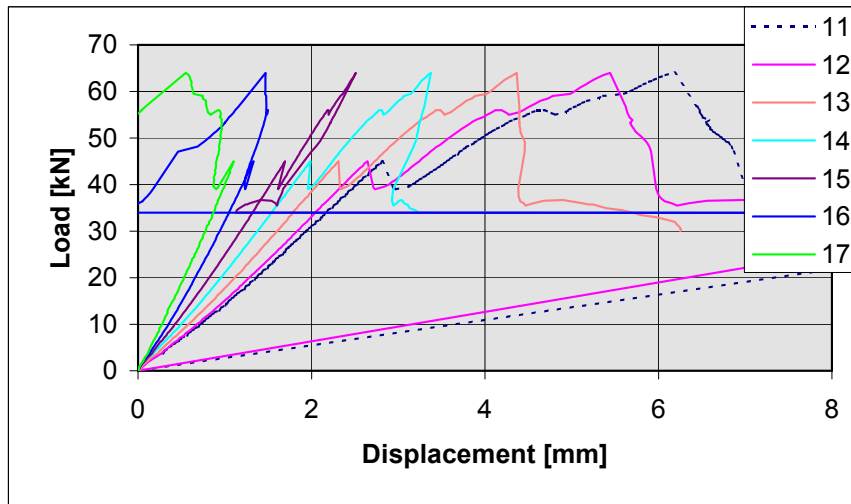


Fig. 16. ST200E2. Deflections close to load. Transducers 11–17.

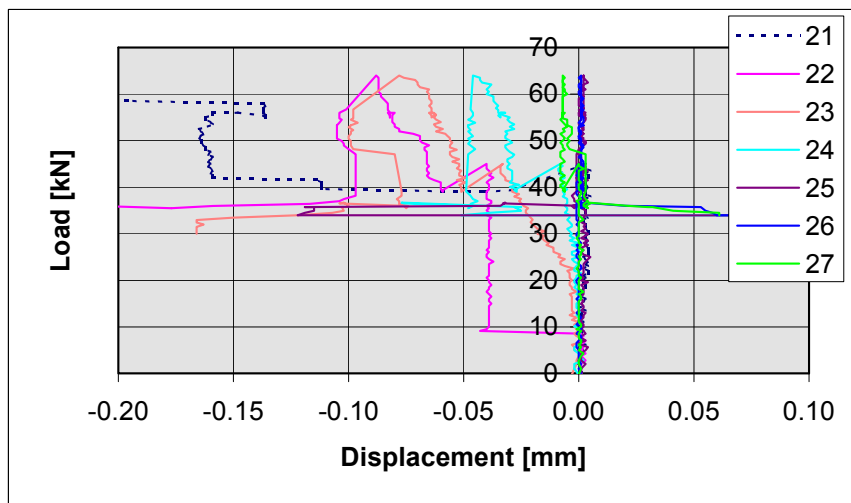


Fig. 17. ST200E2. Slippage of strands. Transducers 21–27.

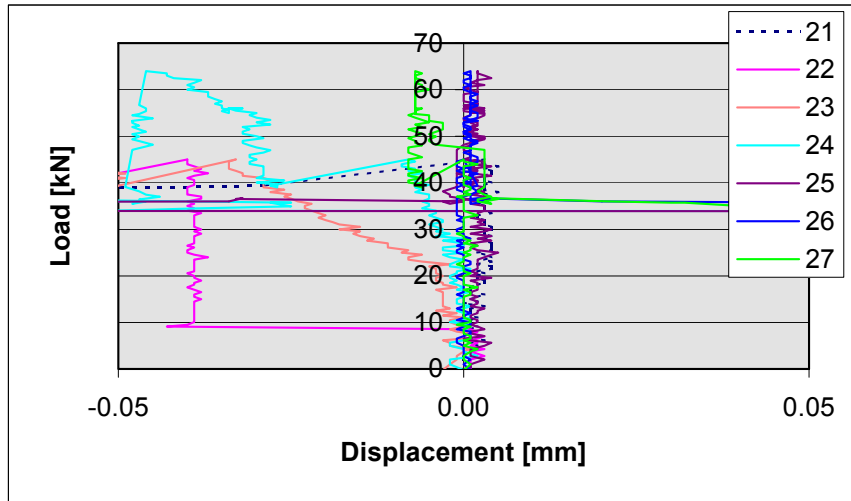


Fig. 18. ST200E2. Slippage of strands. Transducers 21–27.

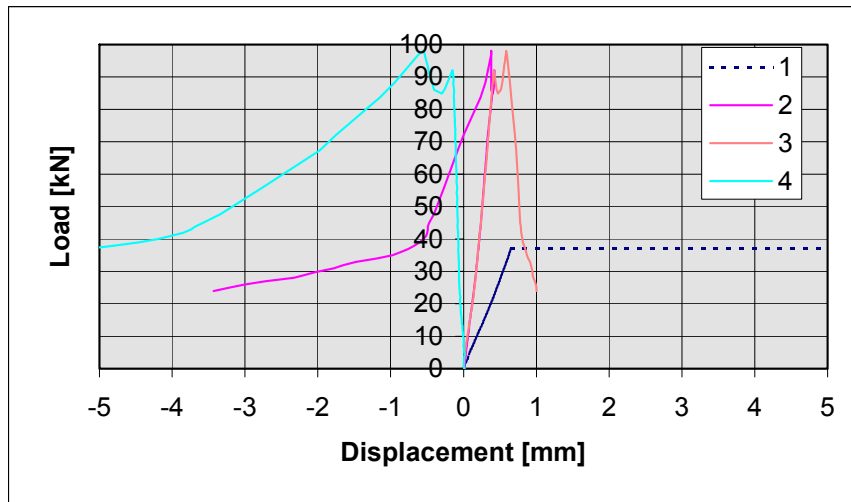


Fig. 19. ST200E1b. Deflections at supports. Transducers 1–4.

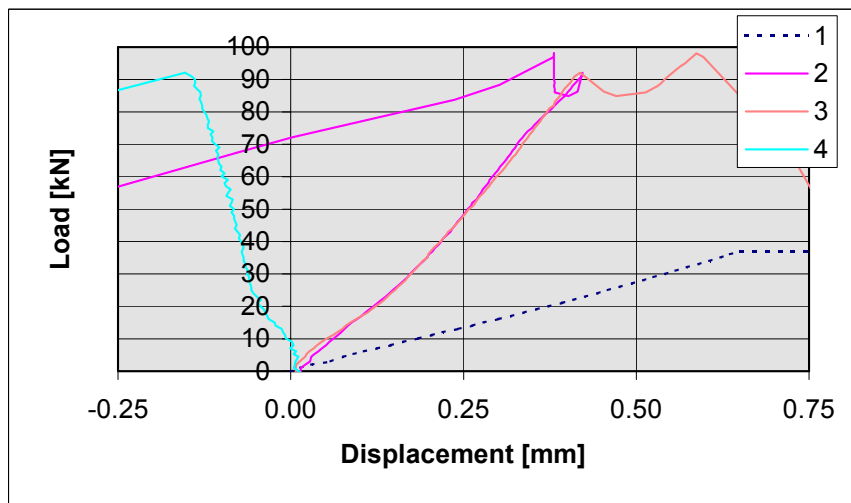


Fig. 20. ST200E1b. Deflections at supports. Transducers 1–4.

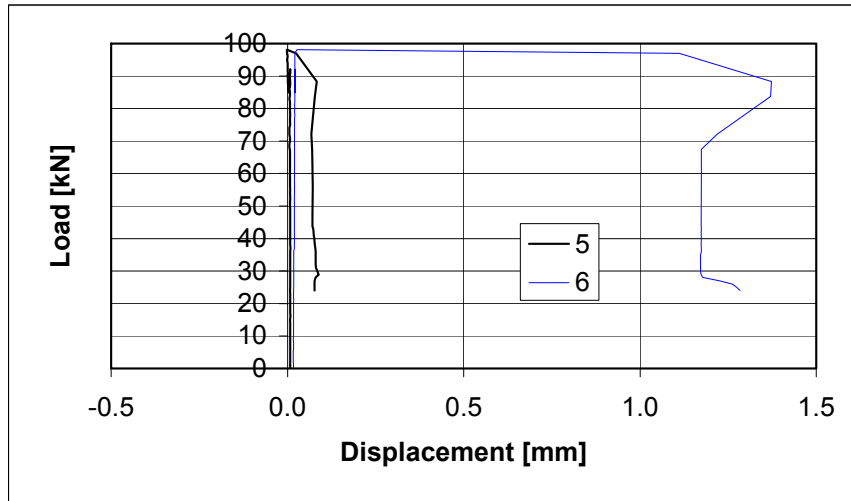


Fig. 21. ST200E1b. Transverse horizontal displacements. Transducers 5–6.

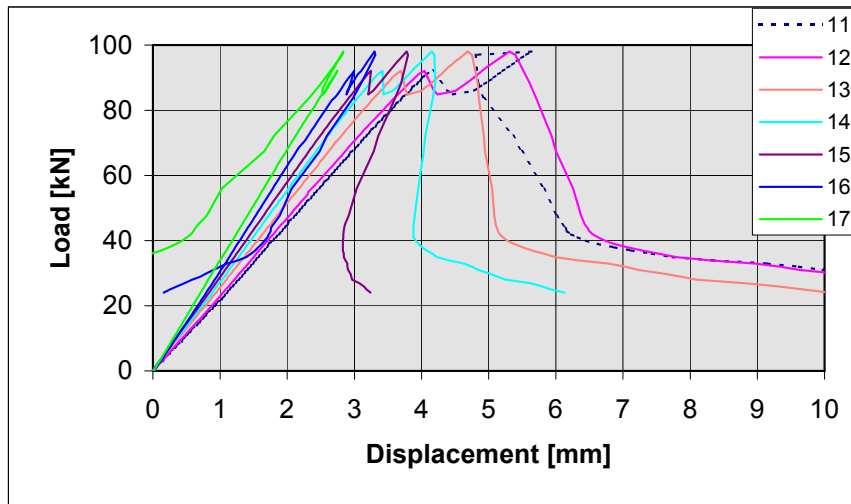


Fig. 22. ST200E1b. Deflections close to load. Transducers 11–17

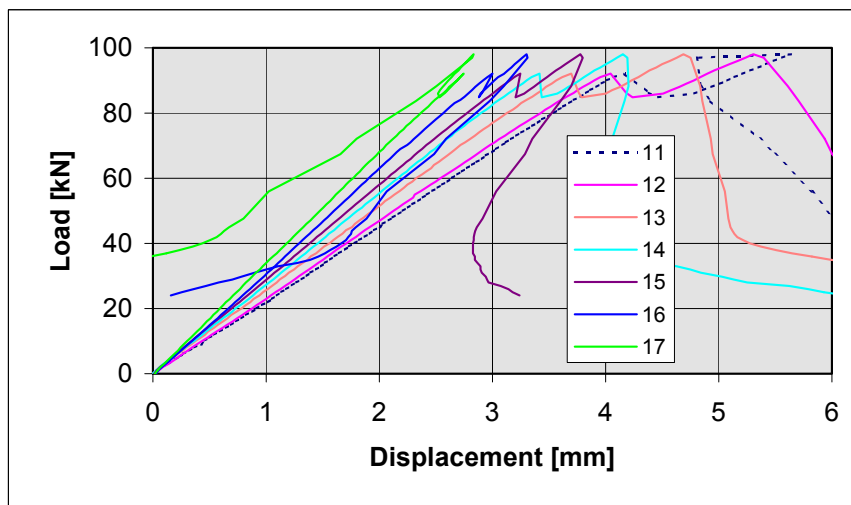


Fig. 23. ST200E1b. Deflections close to load. Transducers 11–17.

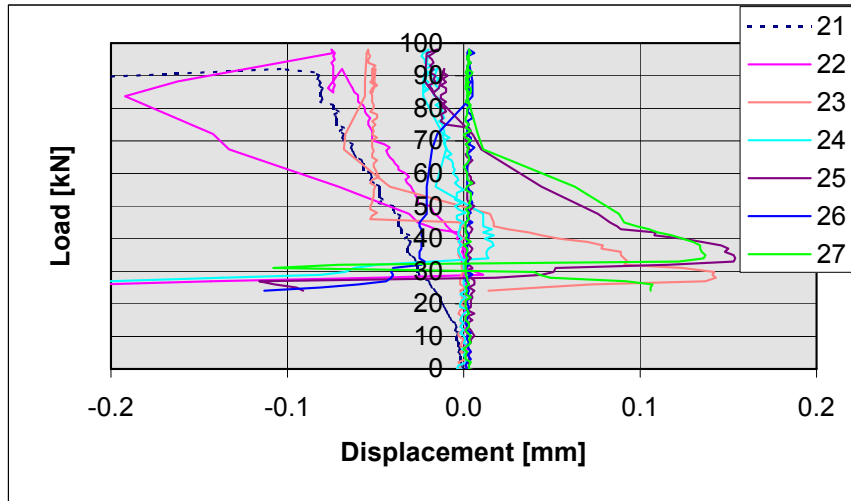


Fig. 24. ST200E1b. Slippage of strands. Transducers 21–27.

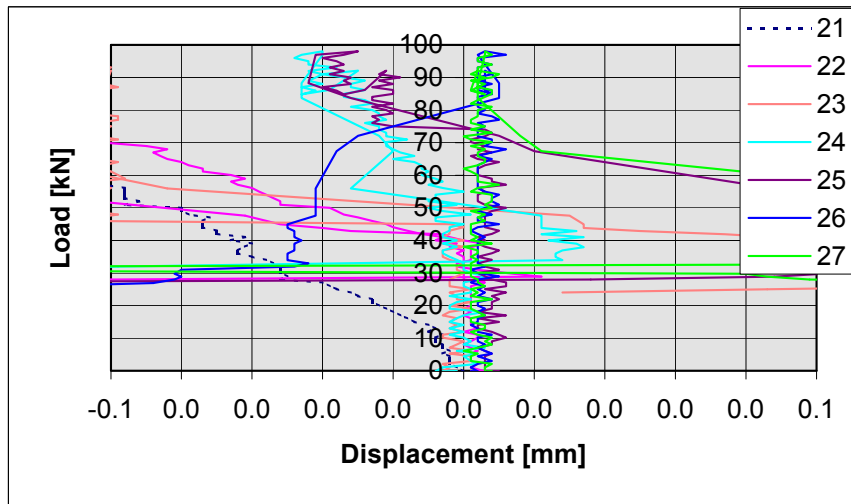


Fig. 25. ST200E1b. Slippage of strands. Transducers 21–27.

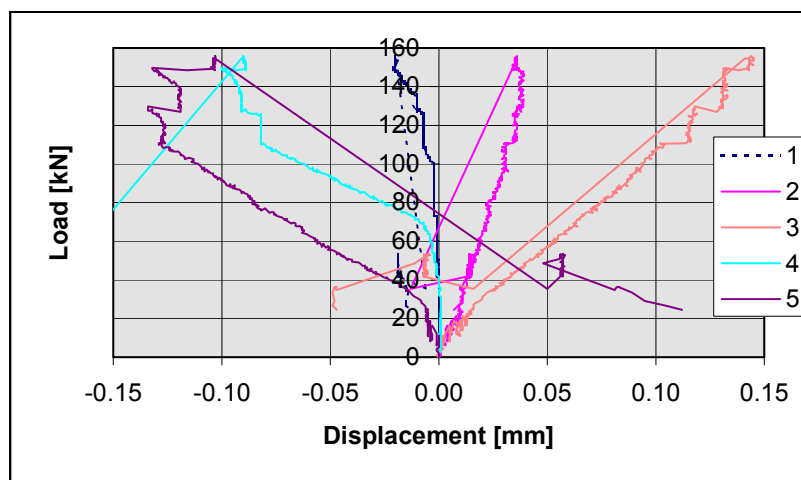


Fig. 26. ST200E1M. Deflections at supports. Transducers 1–5.

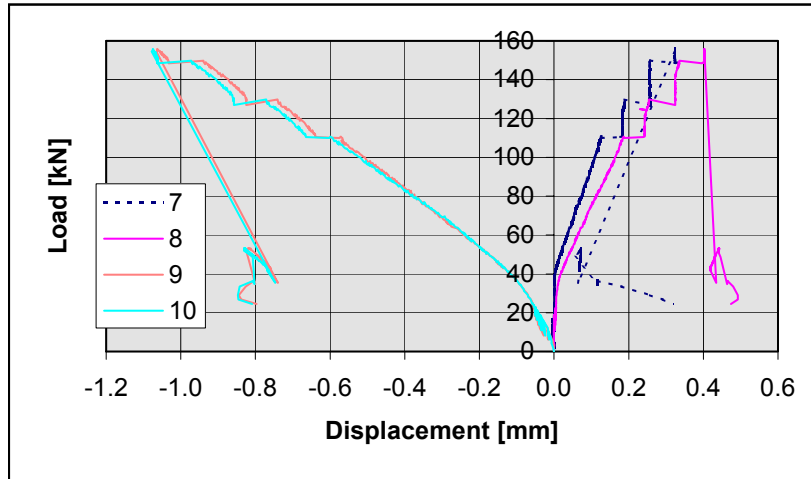


Fig. 27. ST200E1M. Horizontal displacements of beams measured by transducers 7–10.

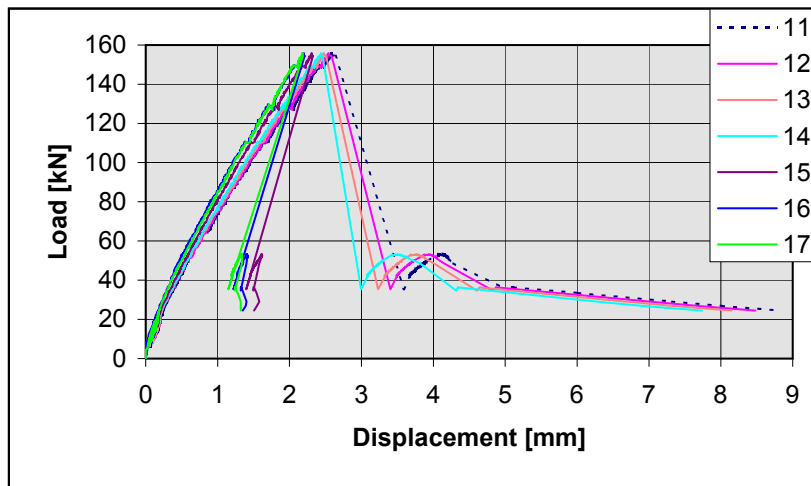


Fig. 28. ST200E1M. Deflections measured by transducers 11–17.

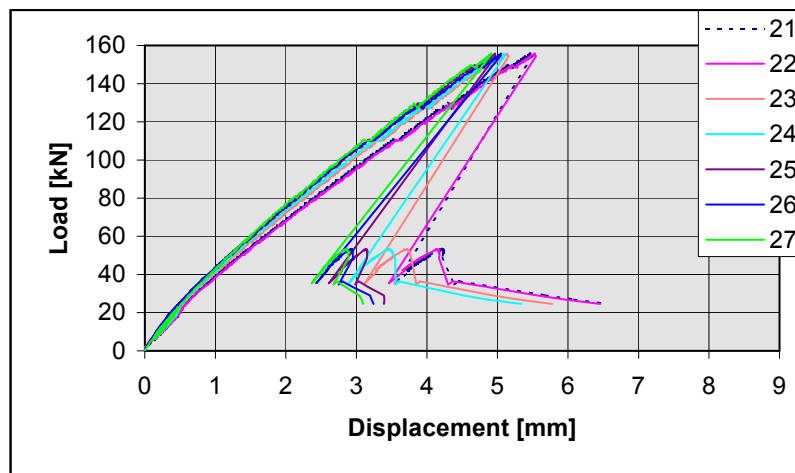


Fig. 29. ST200E1M. Deflections measured by transducers 21–27.

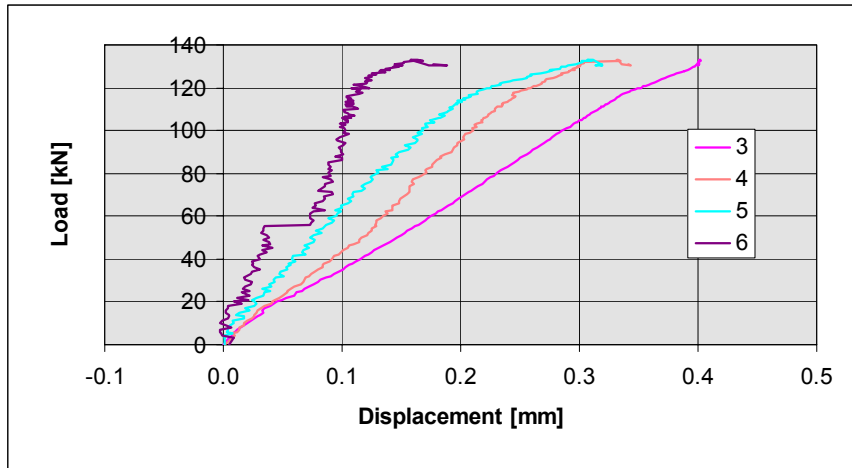


Fig. 30. ST200E2M. Deflection at support measured by transducers 1–5.

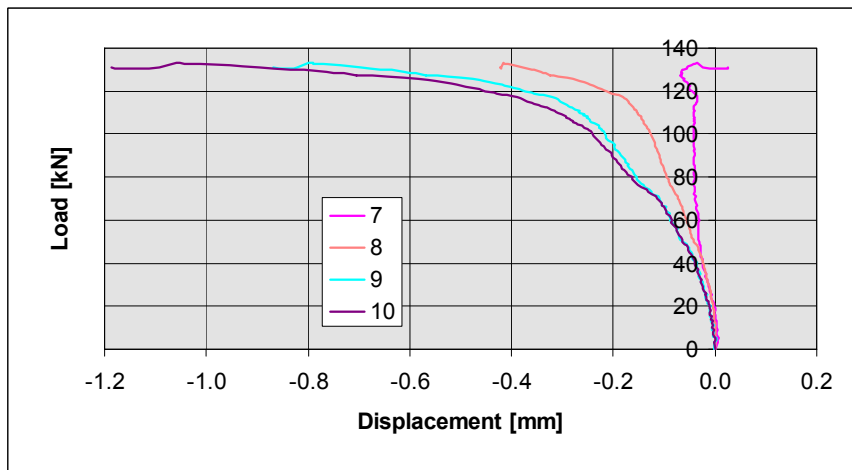


Fig. 31. ST200E2M. Deflection at support measured by transducers 7–10.

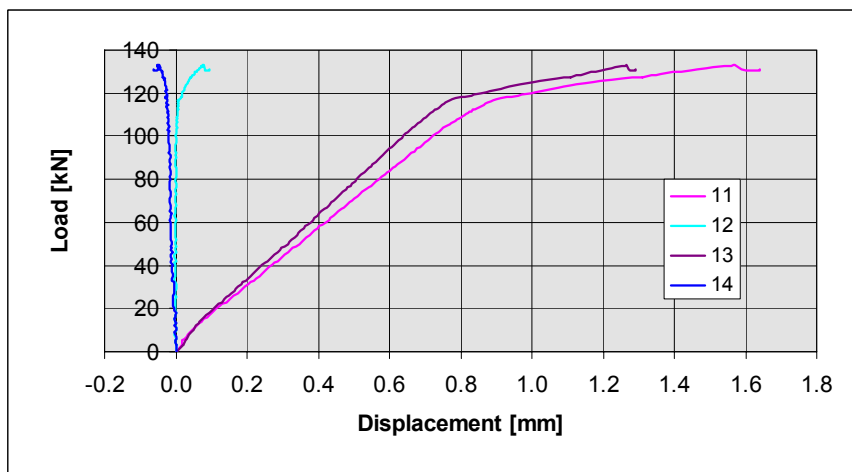


Fig. 32. ST200E2M. Horizontal displacement of beam measured by transducers 11–14.

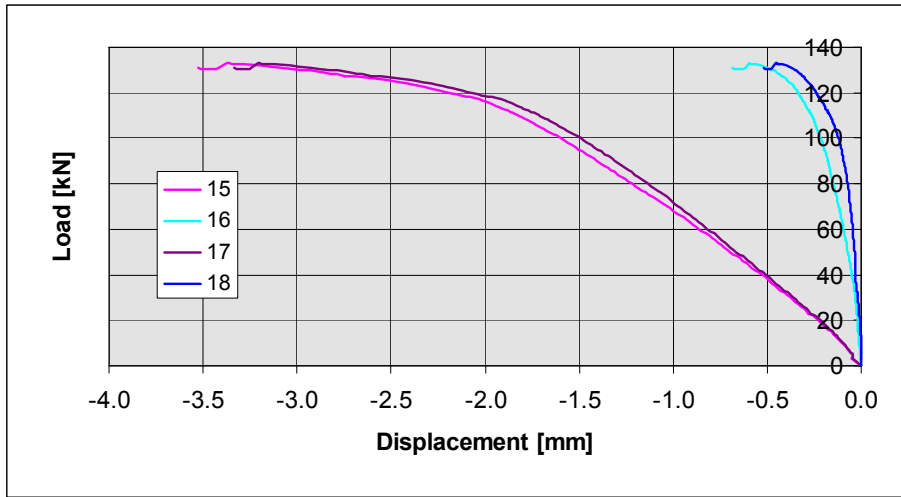


Fig. 33. ST200E2M. Horizontal displacement of beam measured by transducers 15–18.

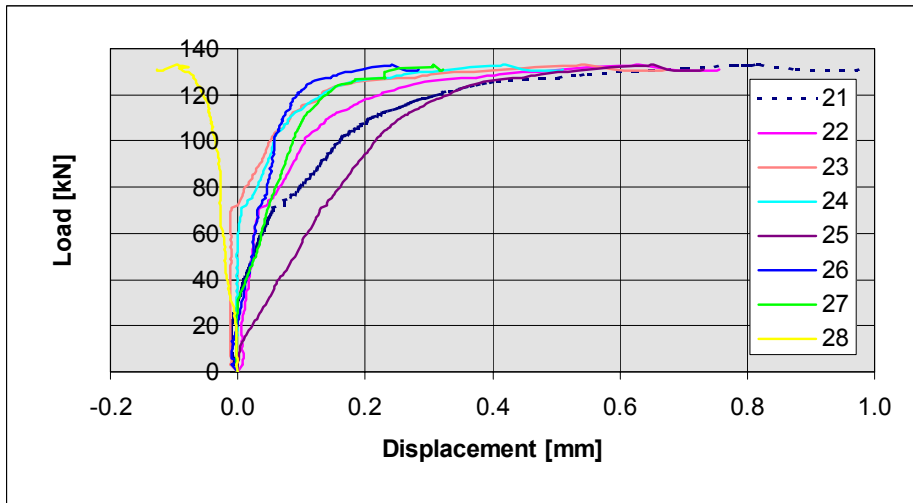


Fig. 34. ST200E2M. Horizontal displacement of slab measured by transducers 21–28.

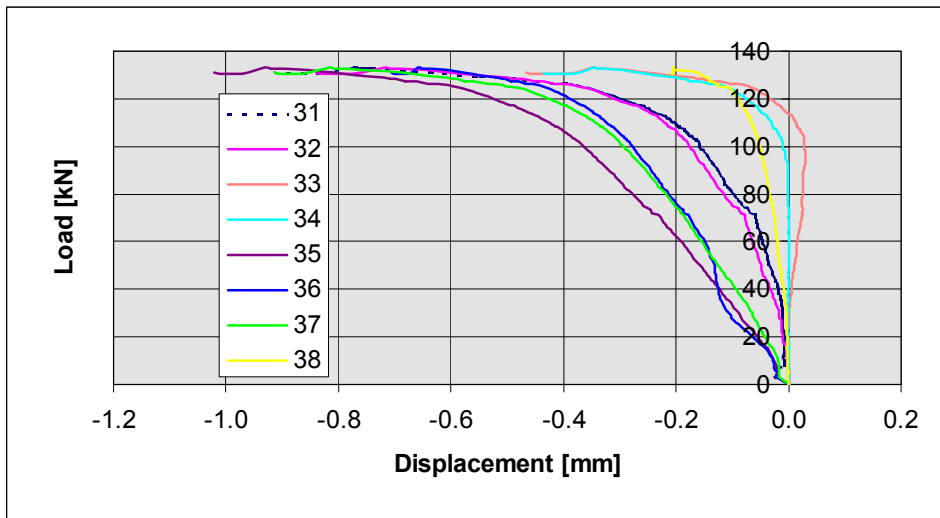


Fig. 35. ST200E2M. Horizontal displacement of slab measured by transducers 31–38.

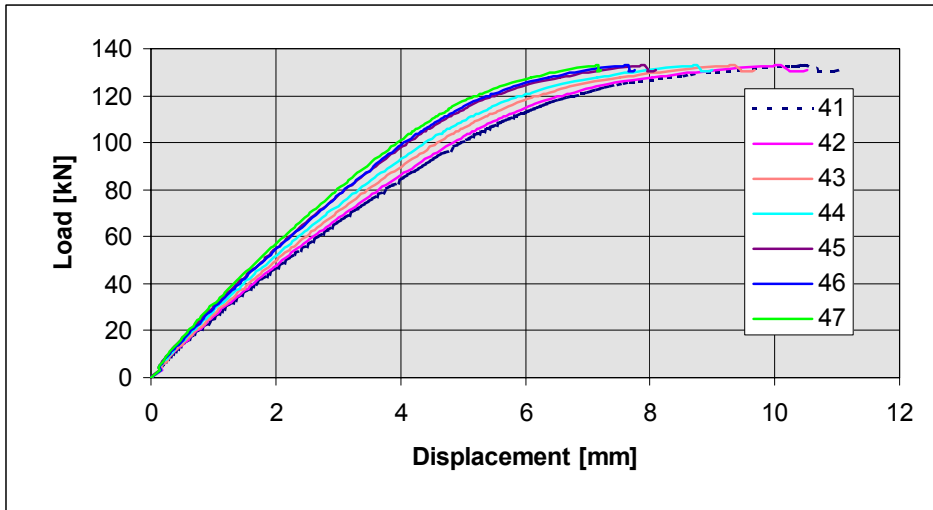


Fig. 36. ST200E2M. Deflection measured by transducers 41–47.

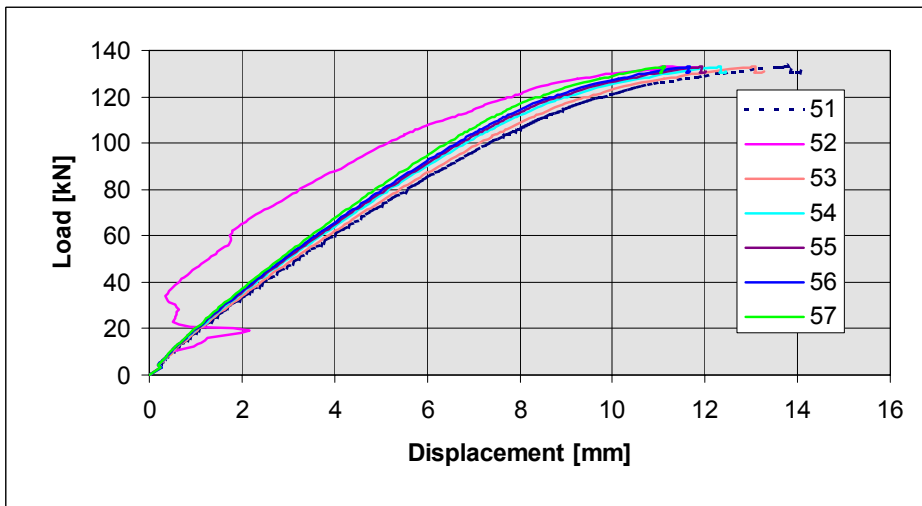


Fig. 37. ST200E2M. Deflection measured by transducers 41–47.

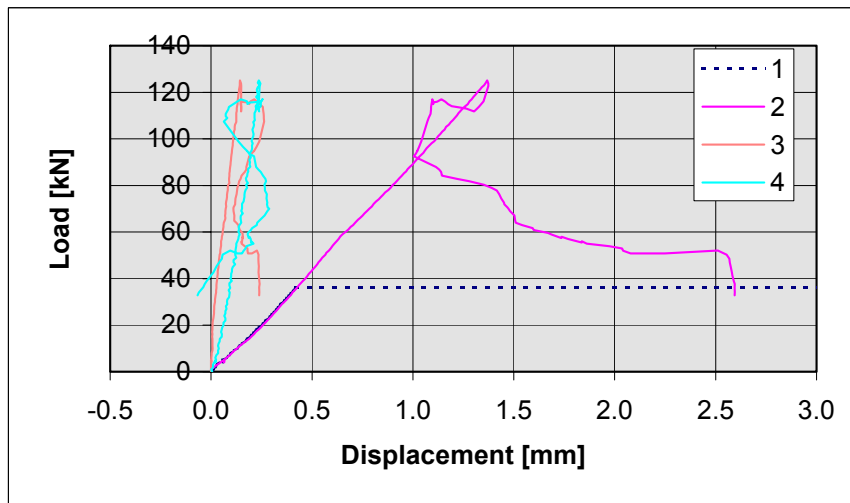


Fig. 38. STS200C. Deflections at supports. Transducers 1–4.

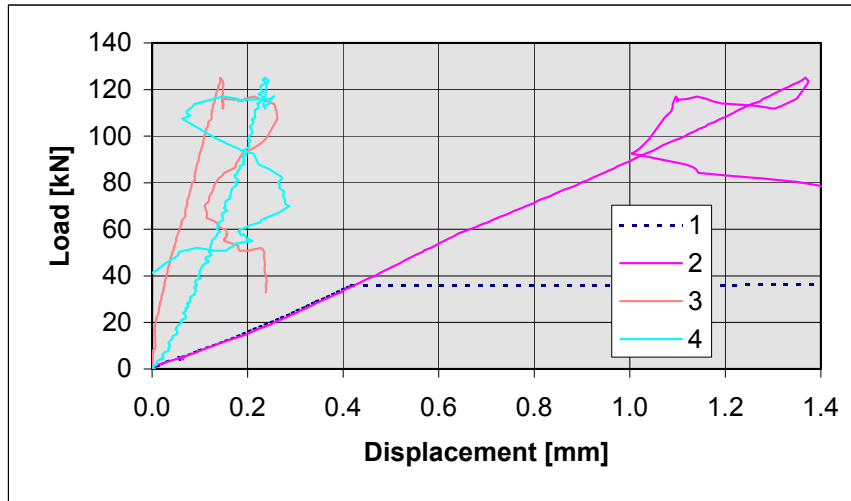


Fig. 39. STS200C. Deflections at supports. Transducers 1–4.

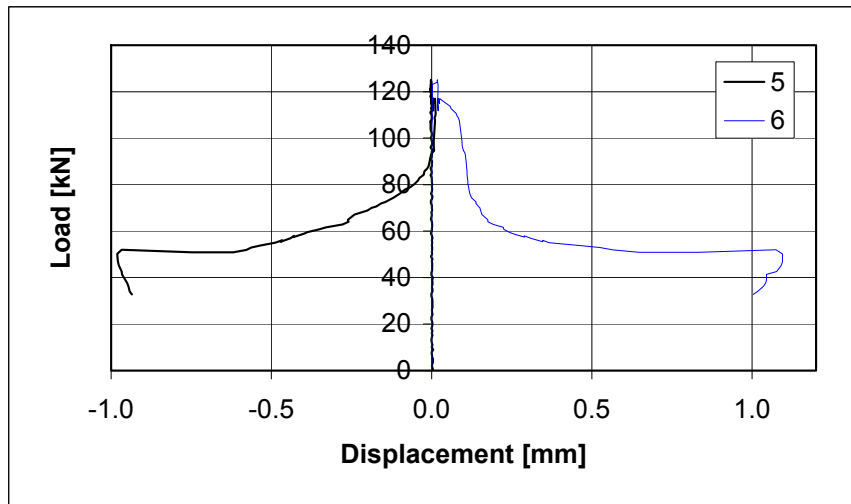


Fig. 40. STS200C. Transverse horizontal displacements. Transducers 5–6.

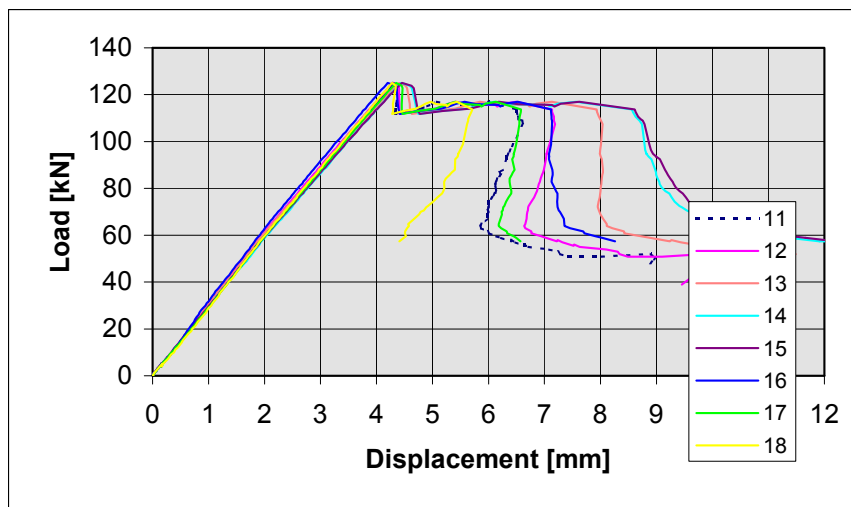


Fig. 41. STS200C. Displacements close to load. Transducers 11–18.

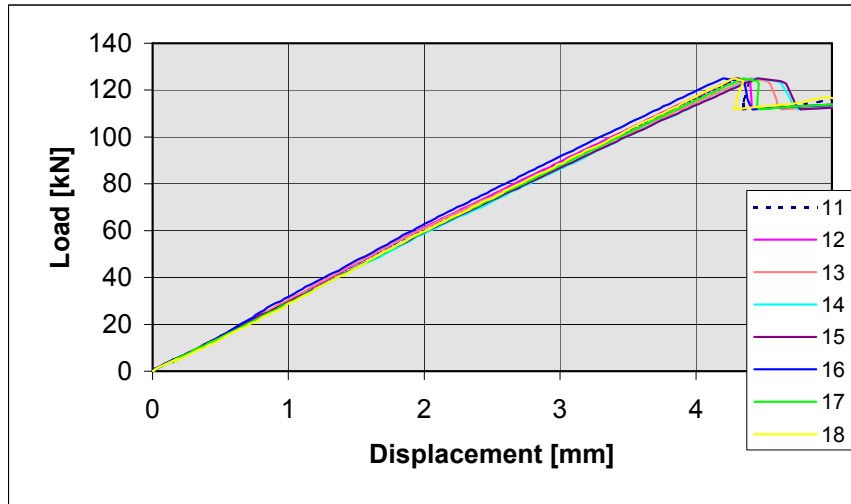


Fig. 42. STS200C. Displacements close to load. Transducers 11–18.

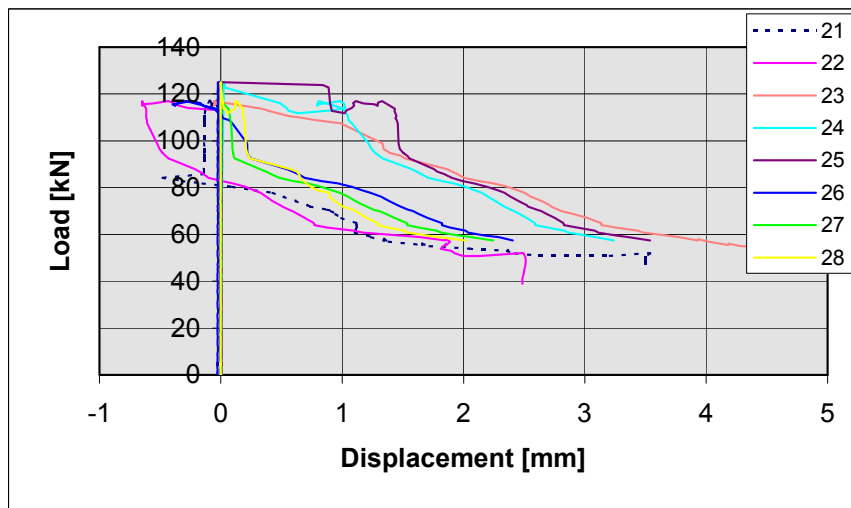


Fig. 43. STS200C. Slippage of strands. Transducers 21–28.

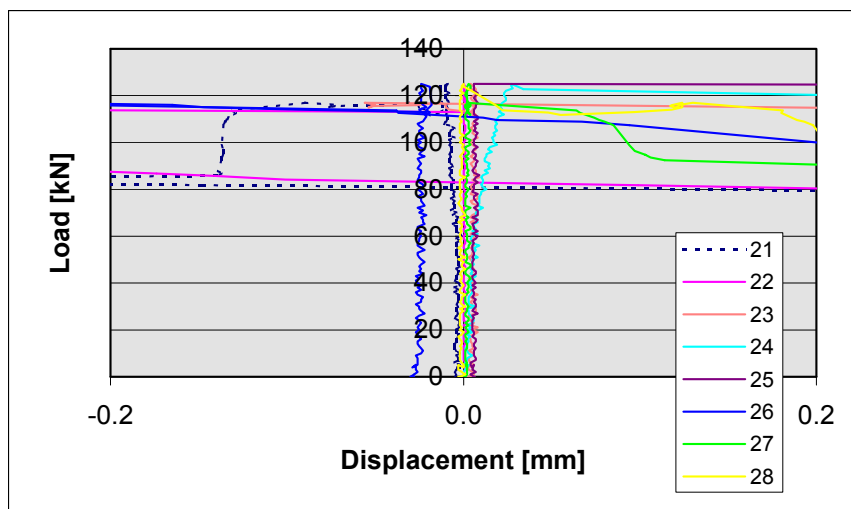


Fig. 44. STS200C. Slippage of strands. Transducers 21–28.

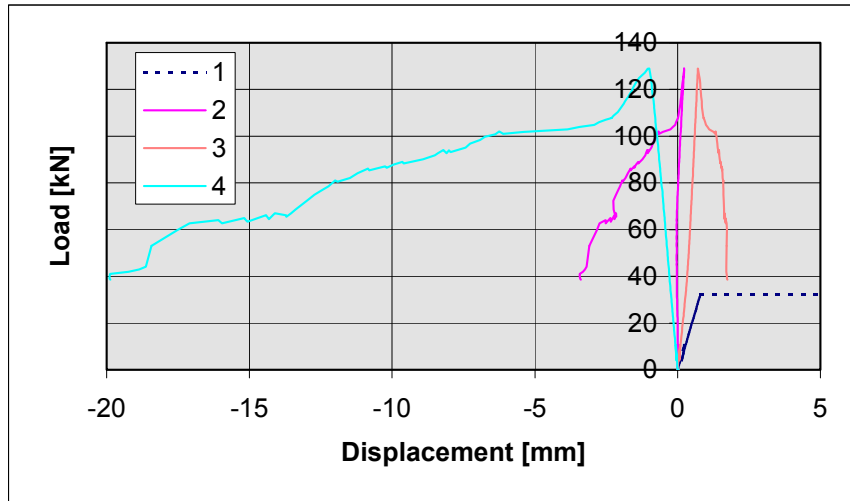


Fig. 45. STS200E1. Deflections at supports. Transducers 1–4.

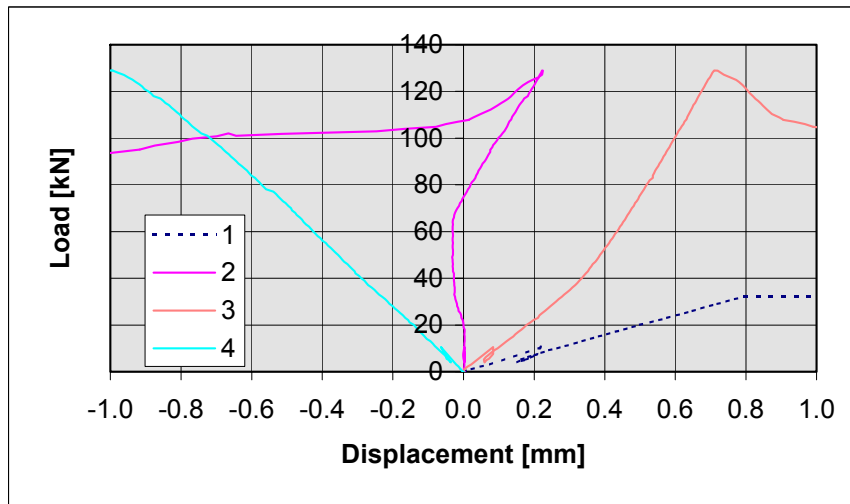


Fig. 46. STS200E1. Deflections at supports. Transducers 1–4.

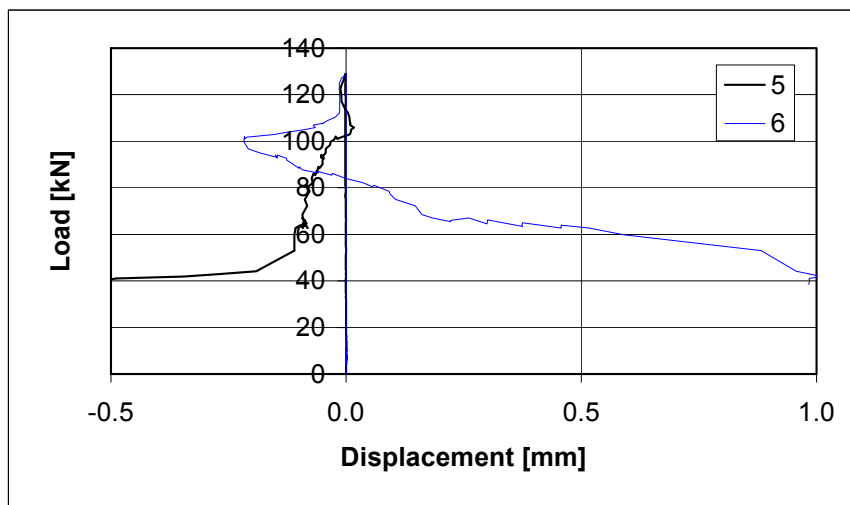


Fig. 47. STS200E1. Transverse horizontal displacements. Transducers 5–6.

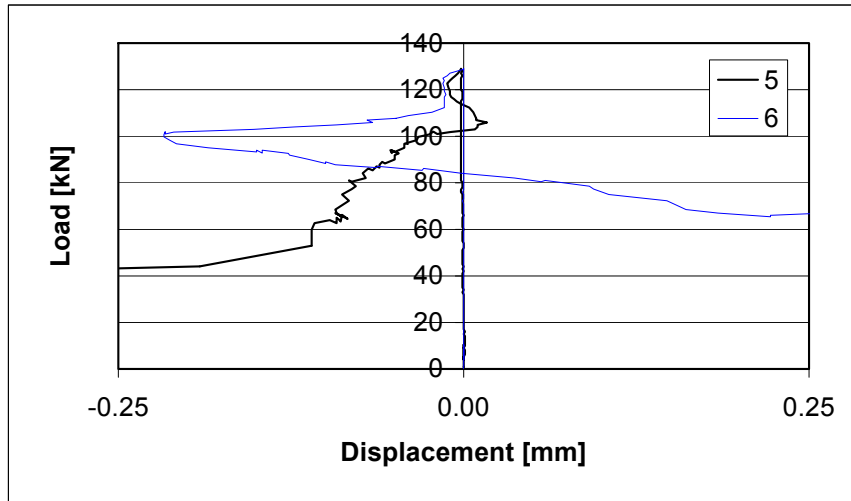


Fig. 48. STS200E1. Transverse horizontal displacements. Transducers 5–6.

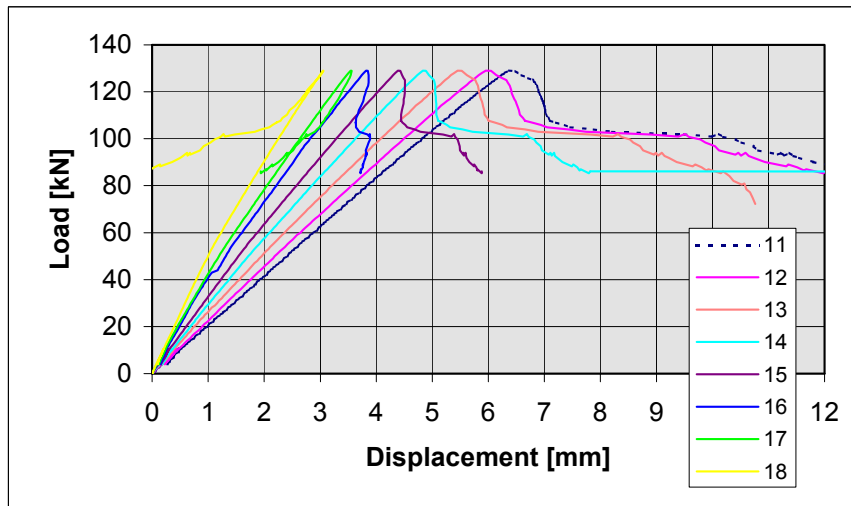


Fig. 49. STS200E1. Deflections close to load. Transducers 11–18.

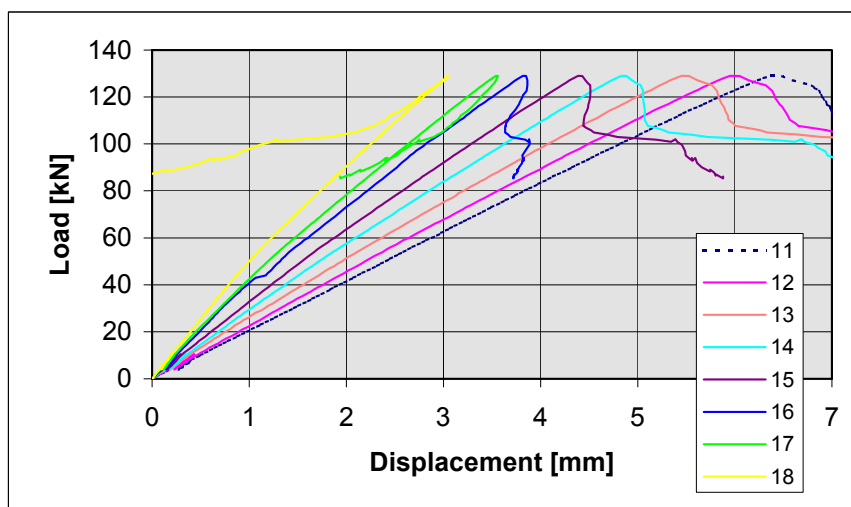


Fig. 50. STS200E1. Deflections close to load. Transducers 11–18.

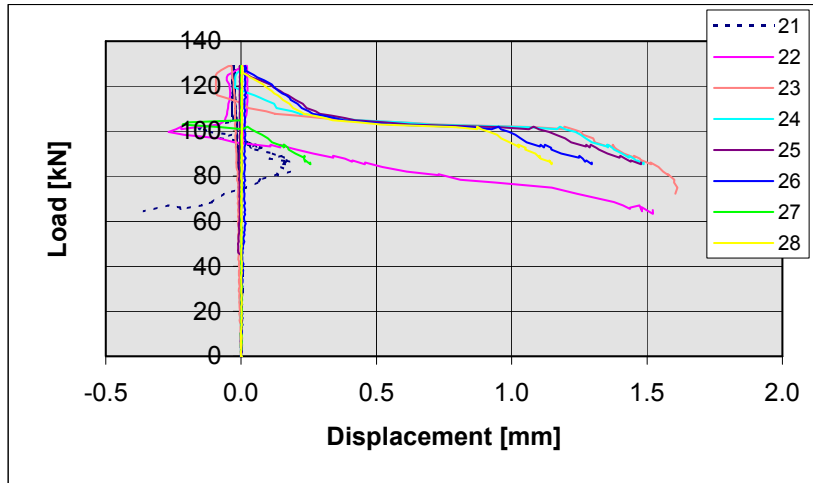


Fig. 51. STS200E1. Slippage of strands. Transducers 21–28.

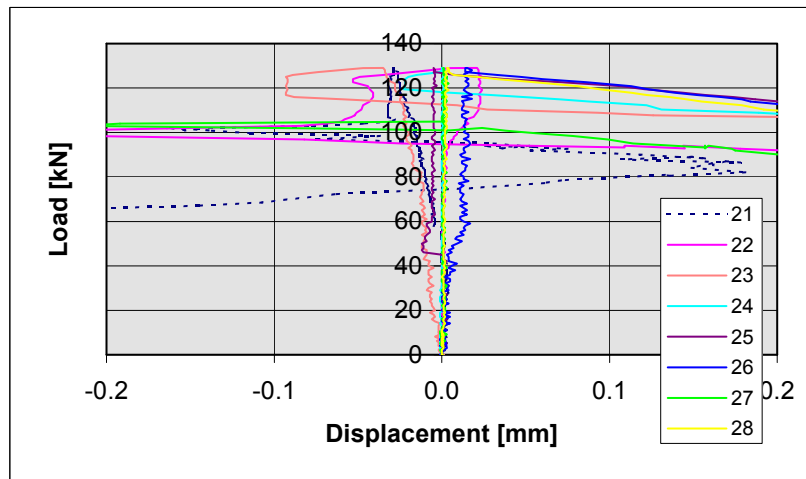


Fig. 52. STS200E1. Slippage of strands. Transducers 21–28.

Appendix E: 400 mm slabs, measured displacements in shear torsion tests

The load is the actuator load without weight of loading equipment. The following terms are used for different measured displacements:

- *deflection*: vertical displacement of slab
- *transverse horizontal displacement*: horizontal displacement perpendicular to the slab
- *longitudinal horizontal displacement*: horizontal displacement of supporting beam parallel to longitudinal axis of slab
- *slippage of strand*: displacement of strand end relative to the surrounding concrete.

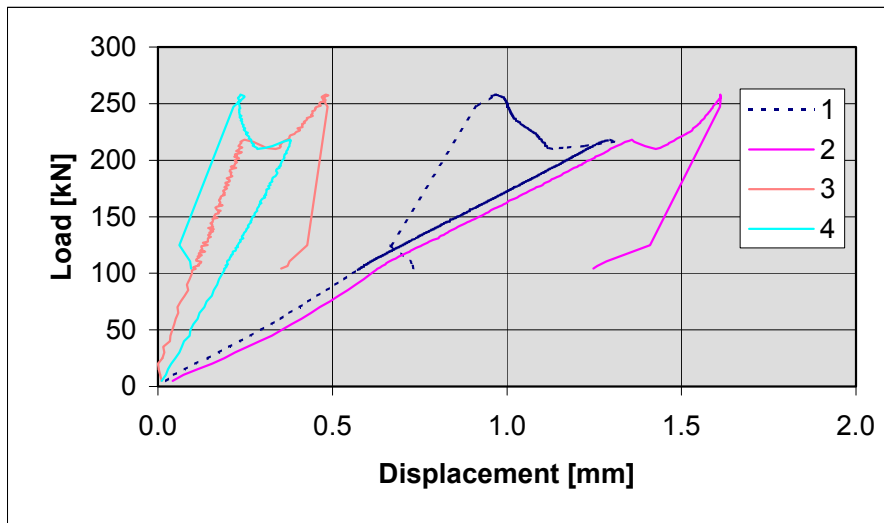


Fig. 1. ST400C1. Deflections at supports. Transducers 1–4.

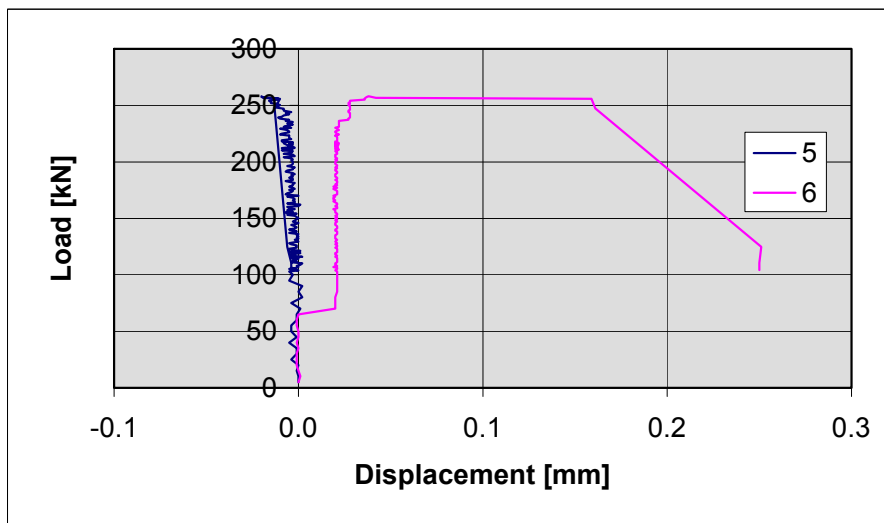


Fig. 2. ST400C1. Transverse horizontal displacements. Transducers 5 and 6.

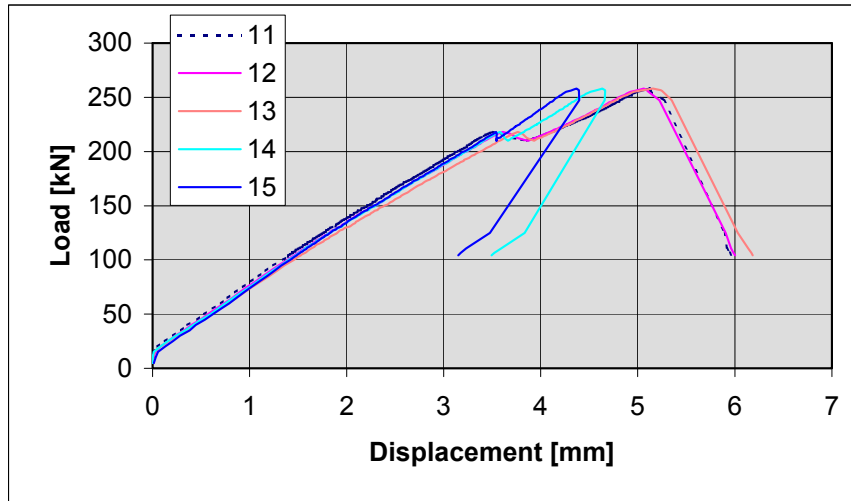


Fig. 3. ST400C1. Deflections close to load. Transducers 11–15.

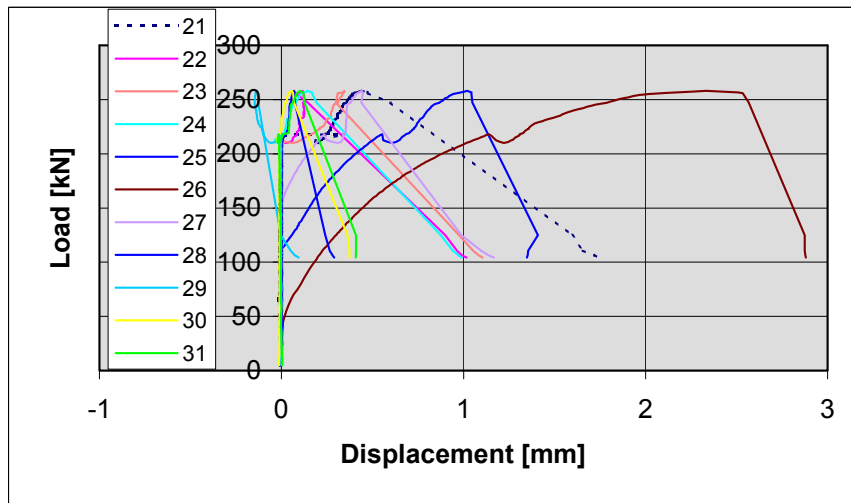


Fig. 4. ST400C1. Slippage of strands. Transducers 21–31.

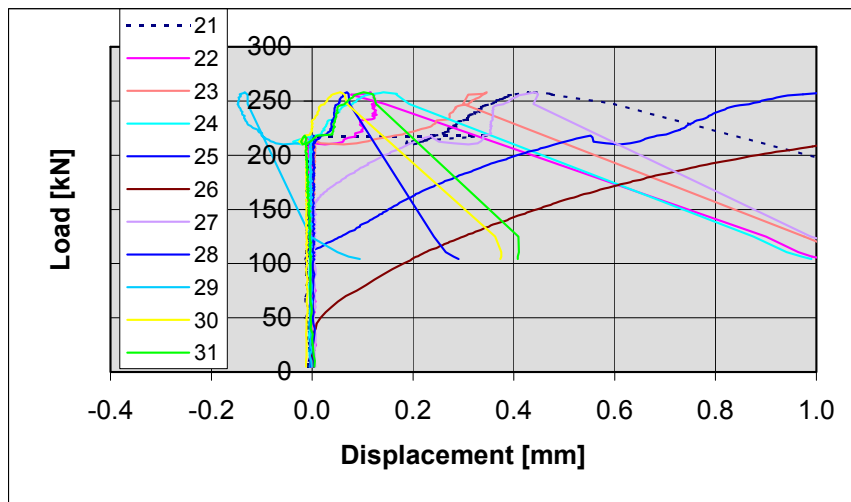


Fig. 5. ST400C1. Slippage of strands. Transducers 21–31.

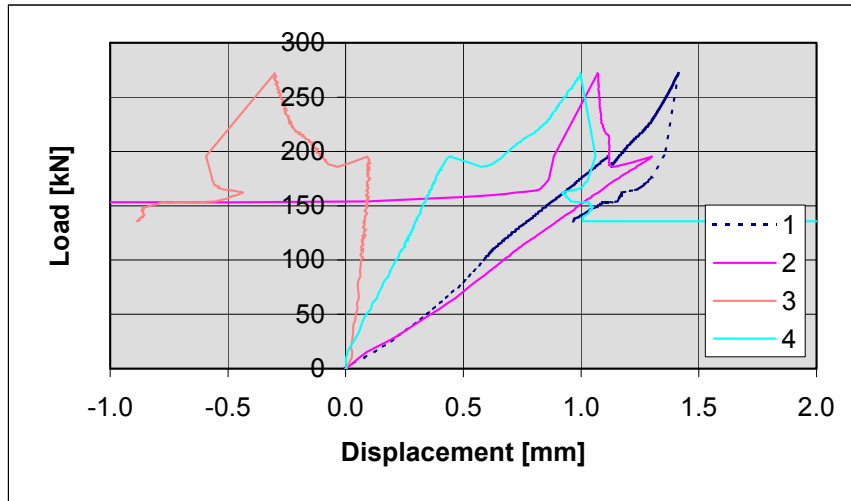


Fig. 6. ST400C2. Deflections at supports. Transducers 1–4.

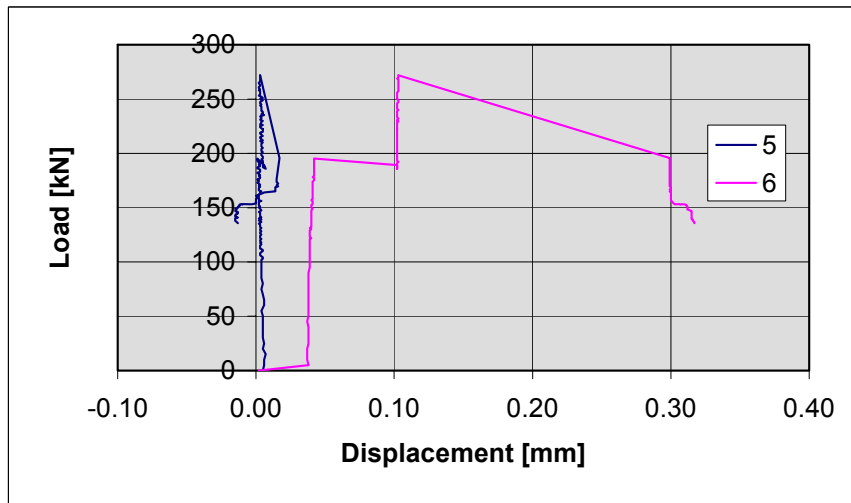


Fig. 7. ST400C2. Transverse horizontal displacements. Transducers 5 and 6.

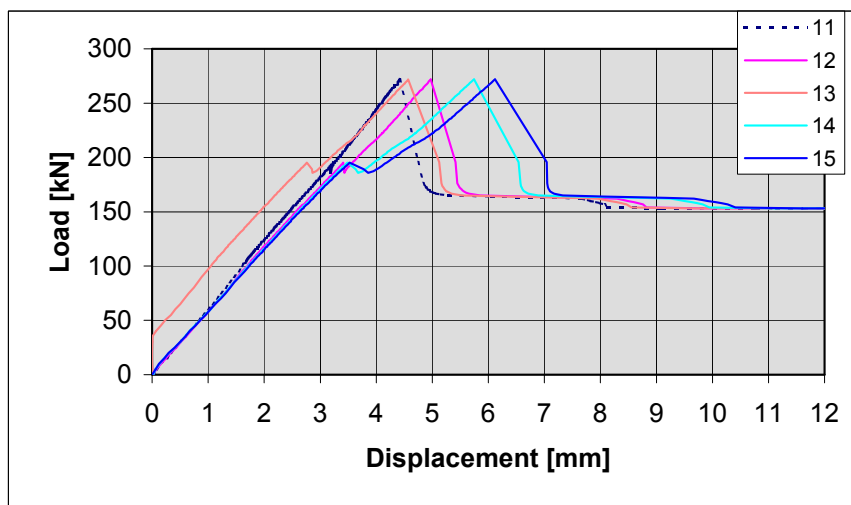


Fig. 8. ST400C2. Deflections close to load. Transducers 11–15.

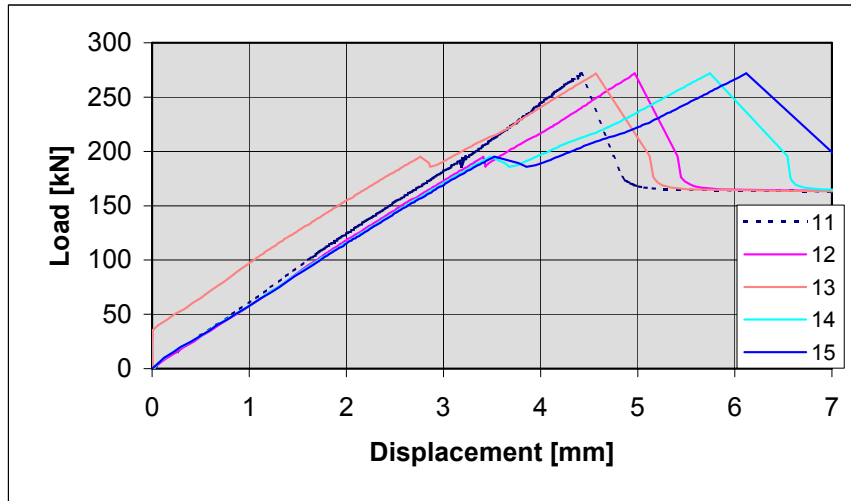


Fig. 9. ST400C2. Deflections close to load. Transducers 11–15.

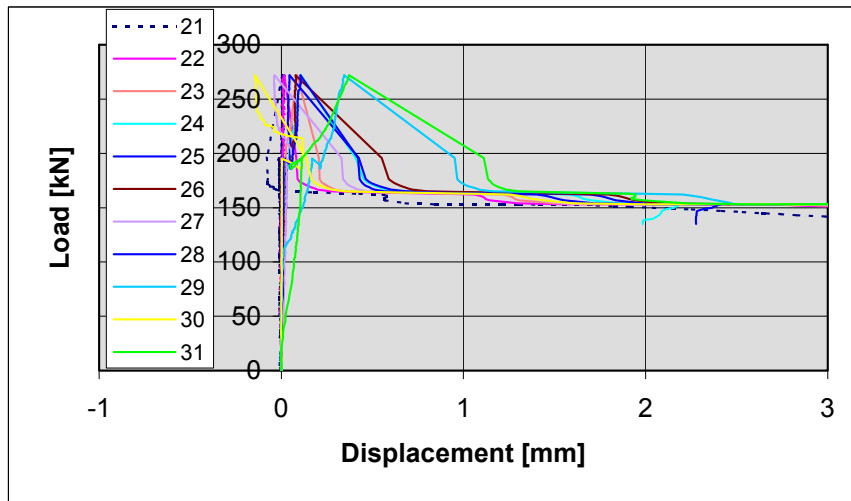


Fig. 10. ST400C2. Slippage of strands. Transducers 21–31.

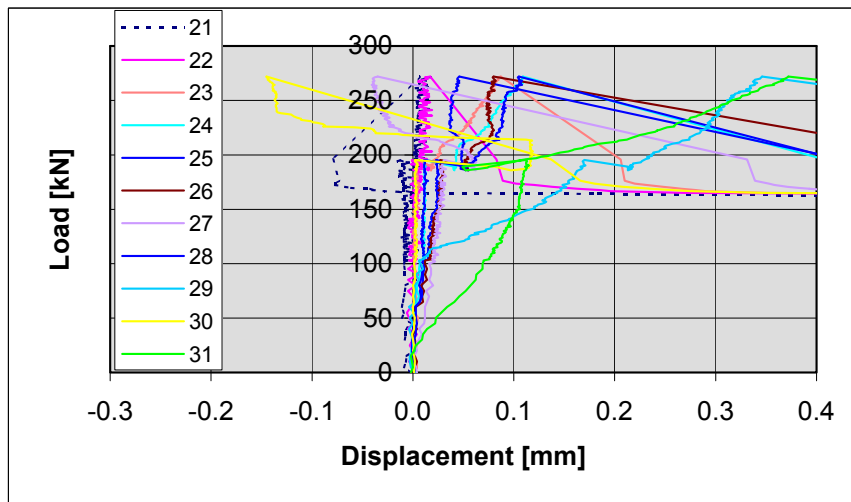


Fig. 11. ST400C2. Slippage of strands. Transducers 21–31.

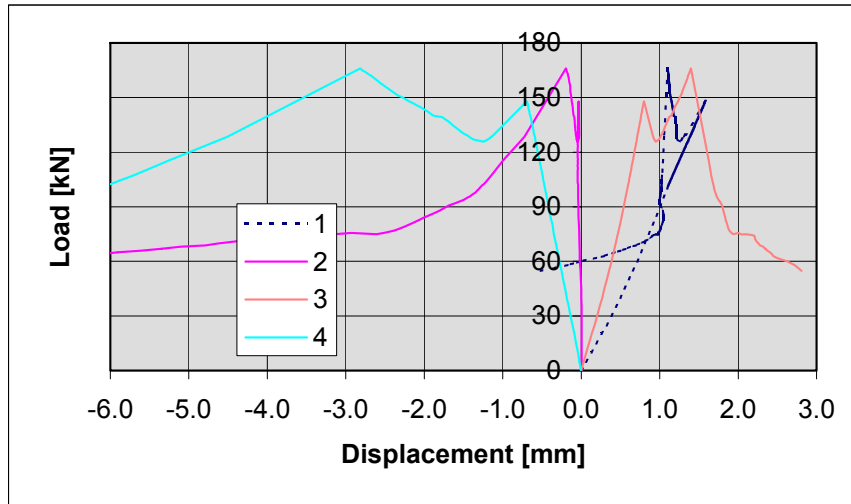


Fig. 12. ST400E1. Deflections at supports. Transducers 1–4.

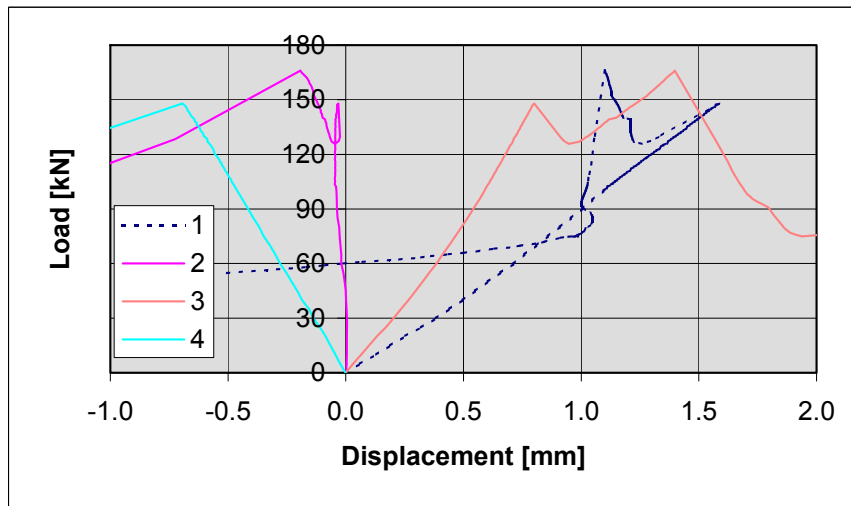


Fig. 13. ST400E1. Deflections at supports. Transducers 1–4.

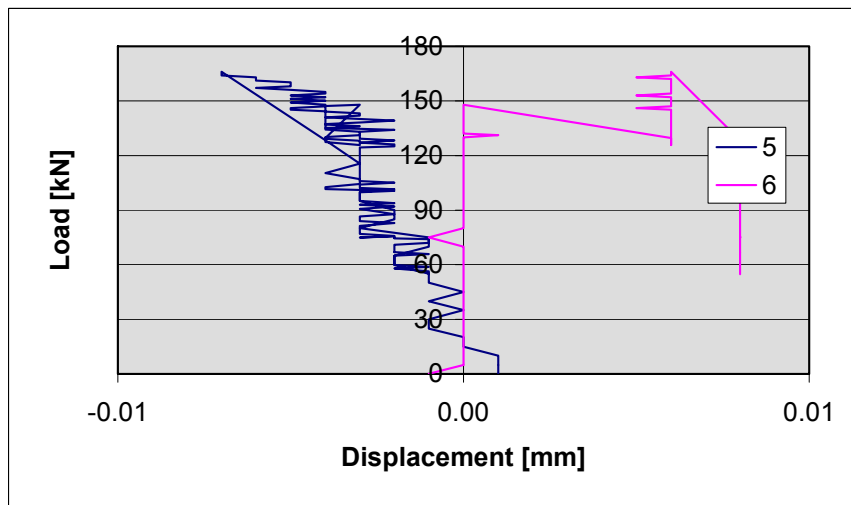


Fig. 14. ST400E1. Transverse horizontal displacements. Transducers 5 and 6.

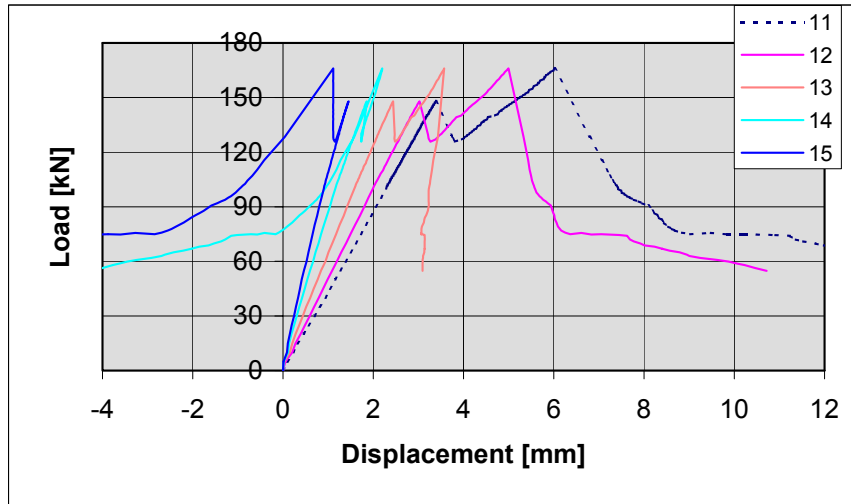


Fig. 15. ST400E1. Deflections close to load. Transducers 11–15.

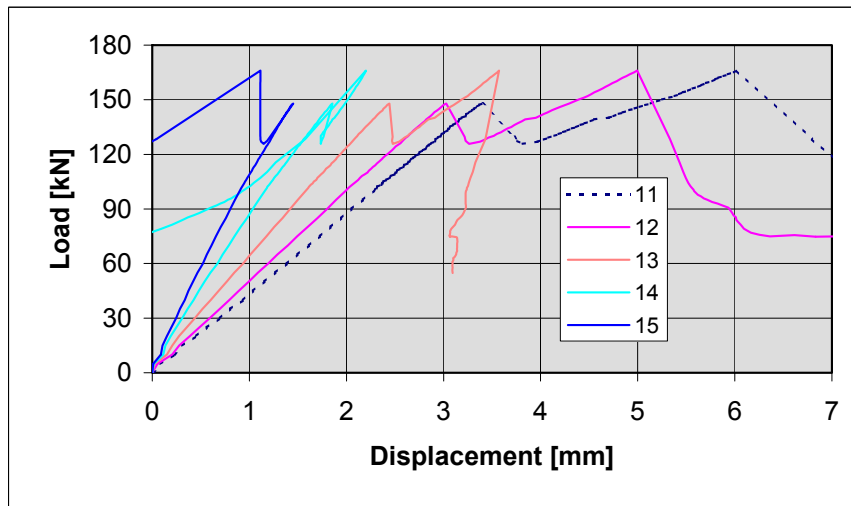


Fig. 16. ST400E1. Deflections close to load. Transducers 11–15.

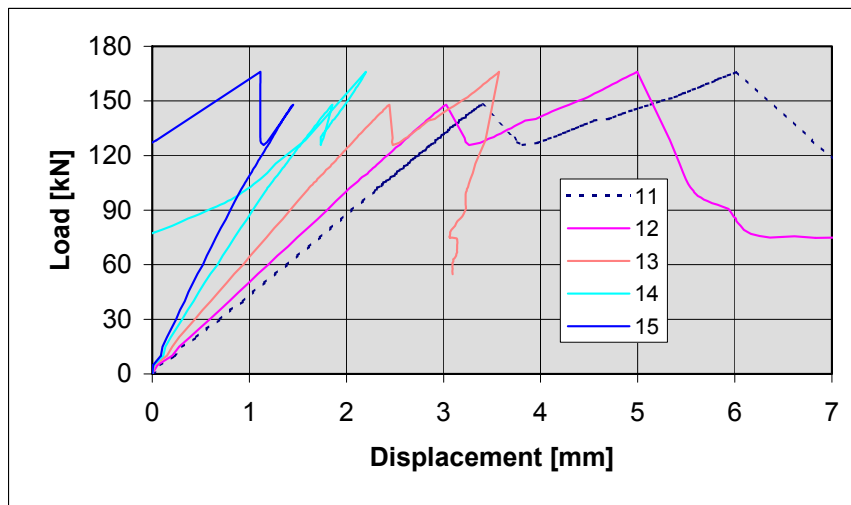


Fig. 17. ST400E1. Deflections close to load. Transducers 11–15.

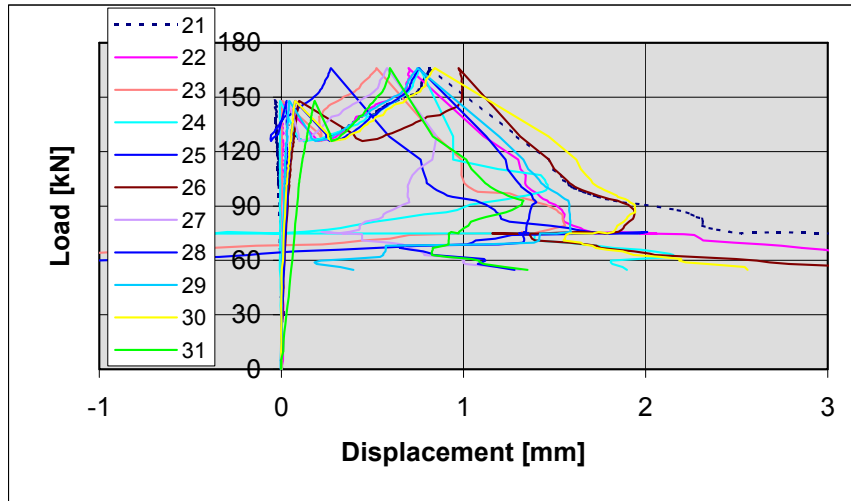


Fig. 18. ST400E1. Slippage of strands. Transducers 21–31.

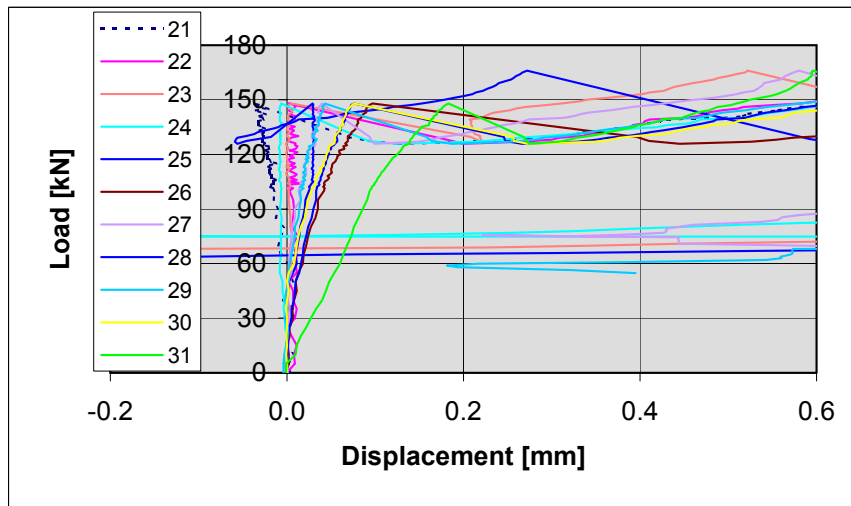


Fig. 19. ST400E1. Slippage of strands. Transducers 21–31.

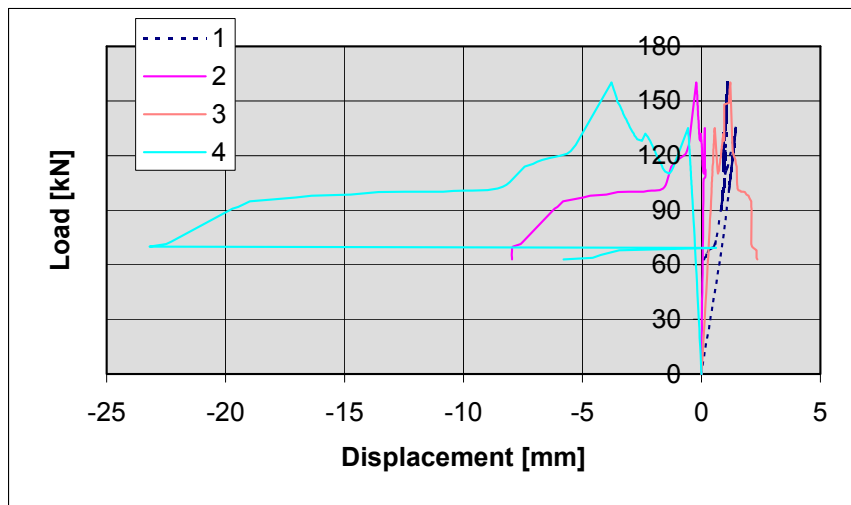


Fig. 20. ST4002E. Deflections at supports. Transducers 1–4.

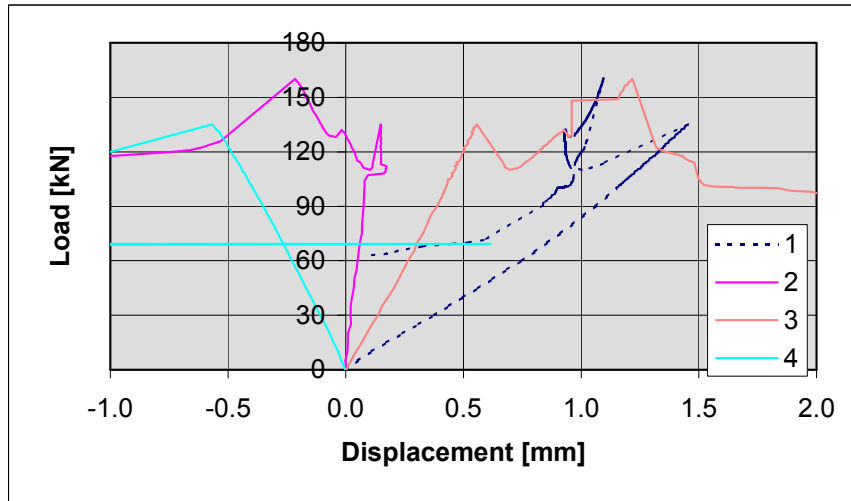


Fig. 21. ST4002E. Deflections at supports. Transducers 1–4.

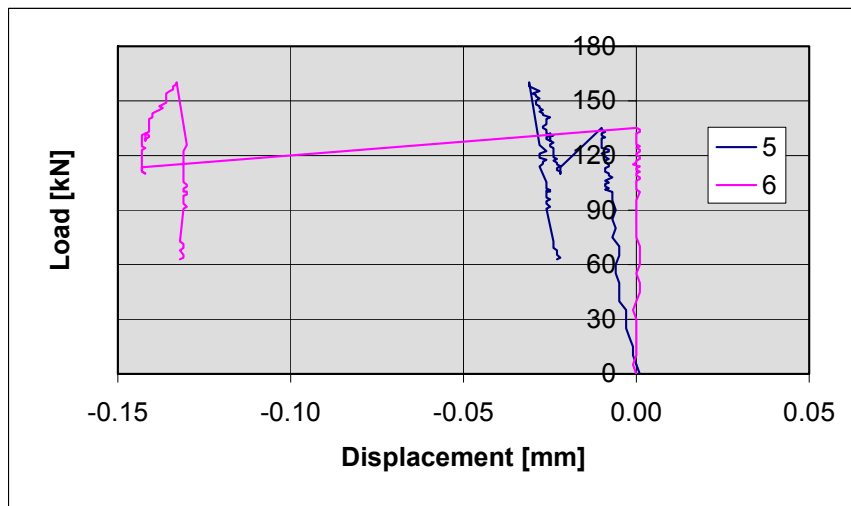


Fig. 22. ST4002E. Transverse horizontal displacements. Transducers 5–6.

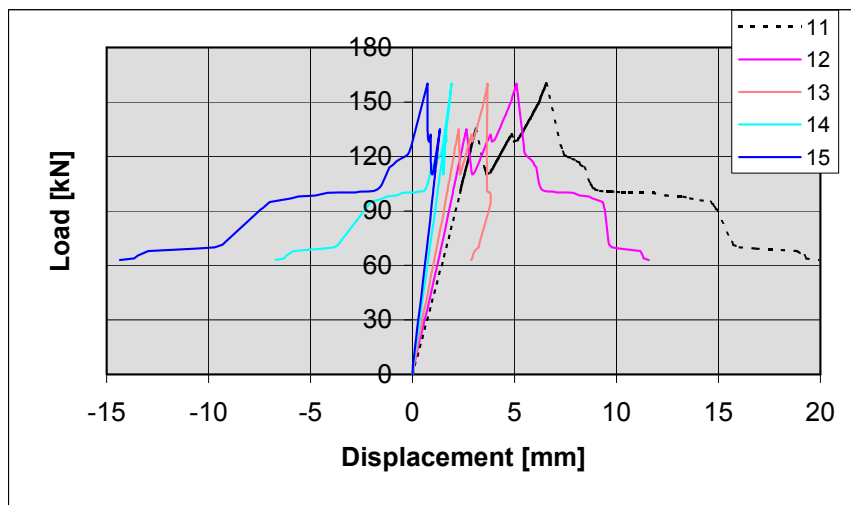


Fig. 23. ST4002E. Deflections close to load. Transducers 11–15.

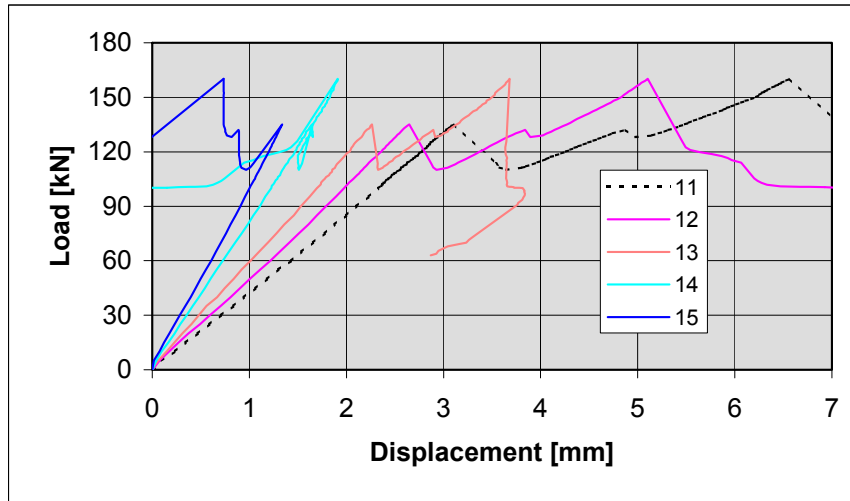


Fig. 24. ST4002E. Deflections close to load. Transducers 11–15.

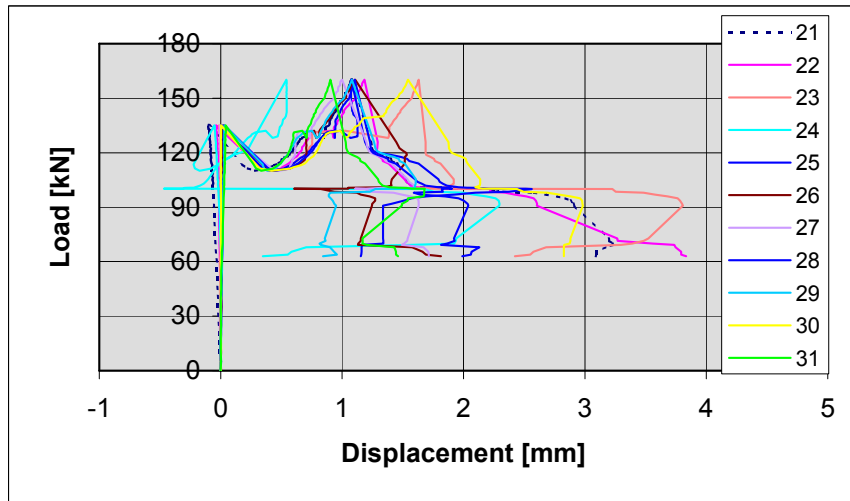


Fig. 25. ST4002E. Slippage of strands. Transducers 21–31.

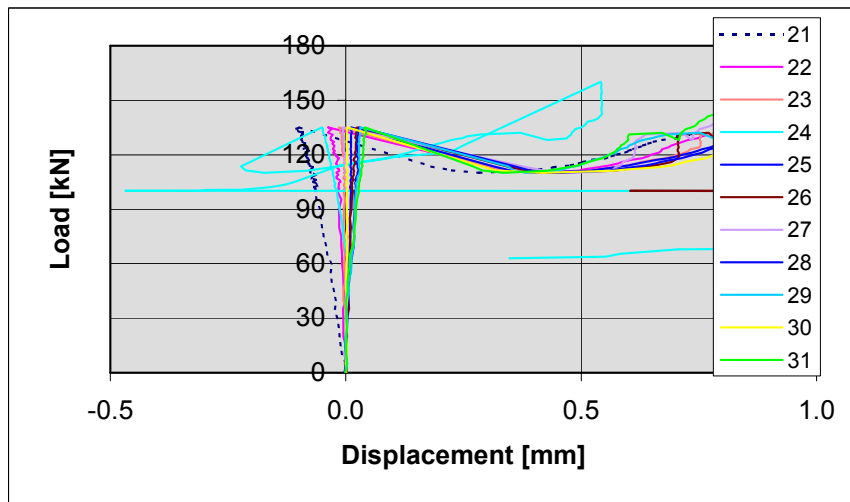


Fig. 26. ST4002E. Slippage of strands. Transducers 21–31.

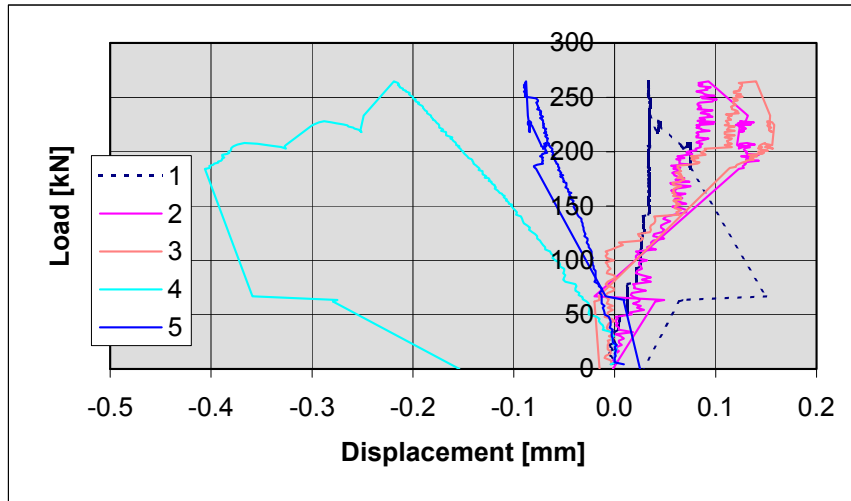


Fig. 27. ST400E1M Deflections at supports. Transducers 1–5.

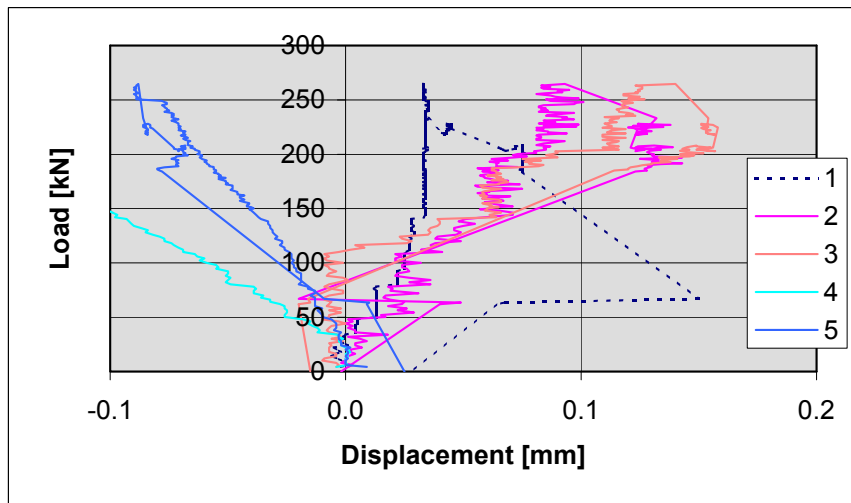


Fig. 28. ST400E1M. Deflections at supports. Transducers 1–5.

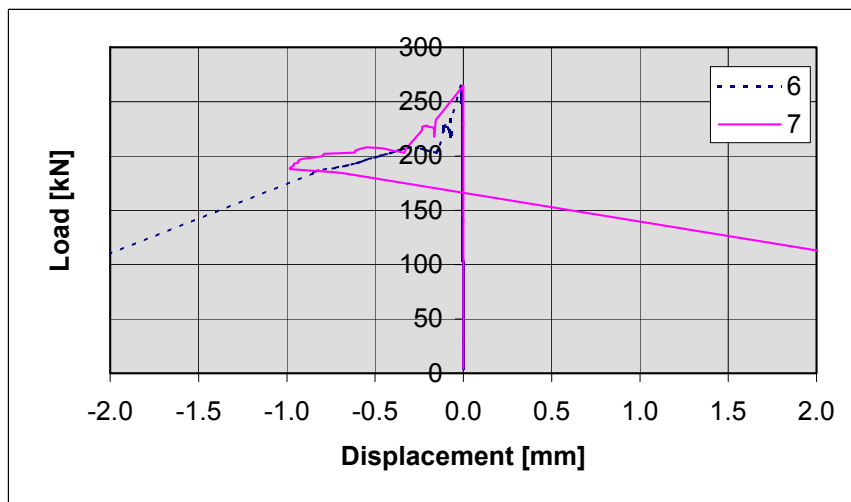


Fig. 29. ST400E1M. Transverse horizontal displacements. Transducers 6–7.

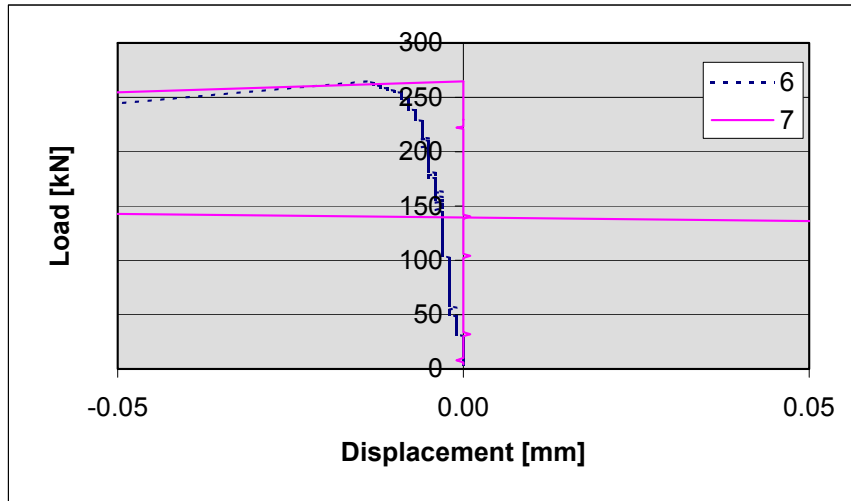


Fig. 30. ST400E1M. Transverse horizontal displacements. Transducers 6–7.

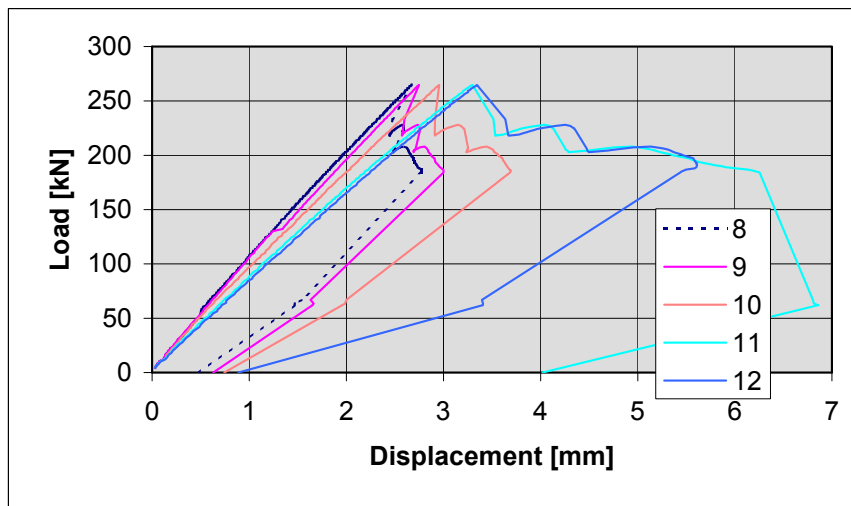


Fig. 31. ST400E1M. Deflections close to load. Transducers 8–12.

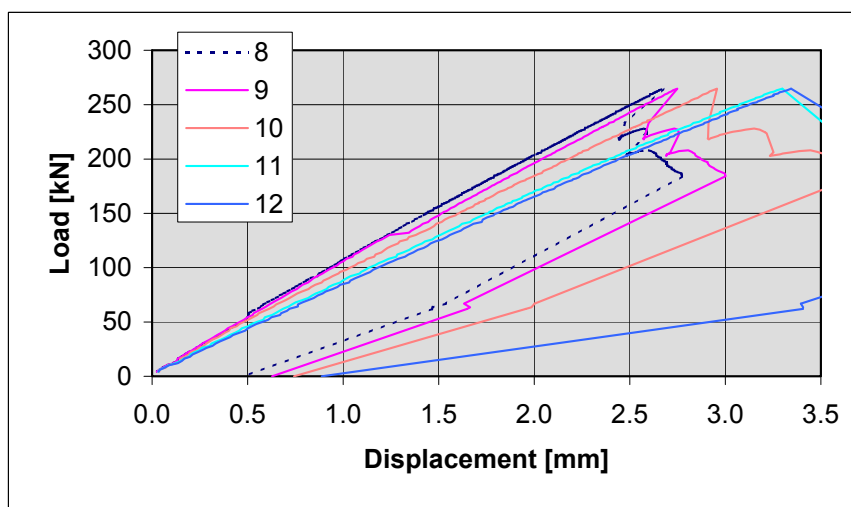


Fig. 32. ST400E1M. Deflections close to load. Transducers 8–12.

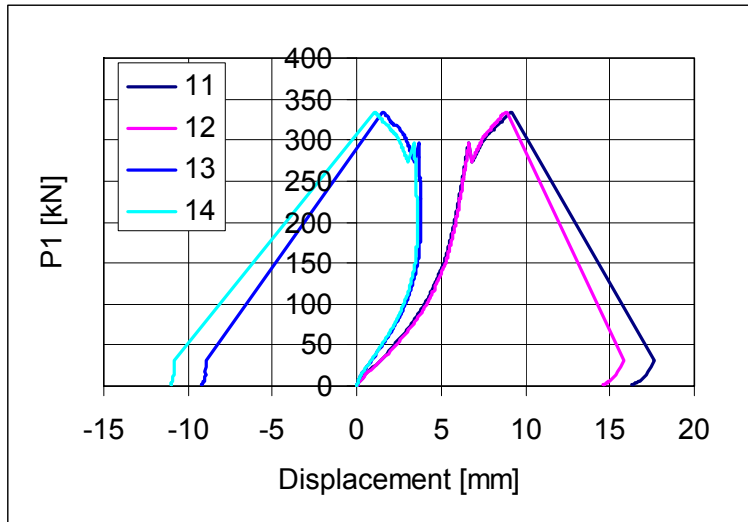


Fig. 33. ST400G1. Deflections measured by transducers 11–15.

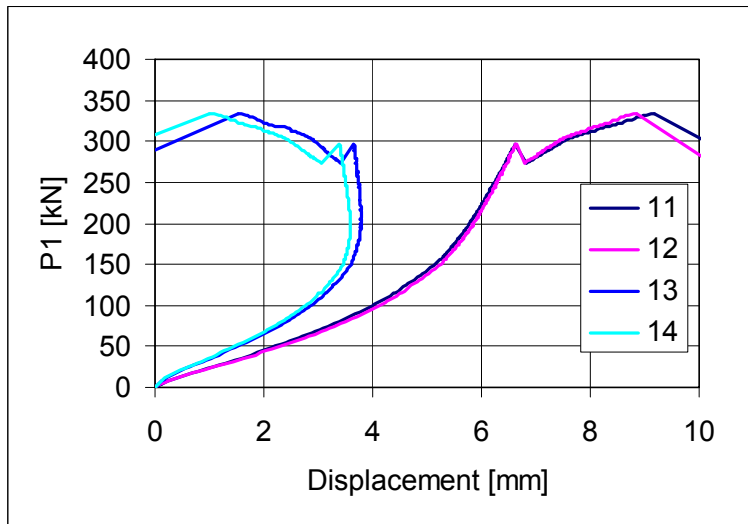


Fig. 34. ST400G1. Deflections measured by transducers 11–15.

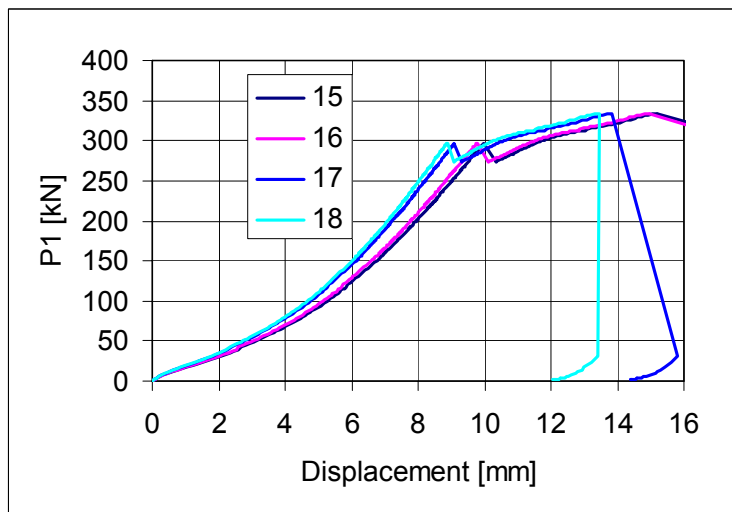


Fig. 35. ST400C1. ST400G1. Deflections measured by transducers 15–18.

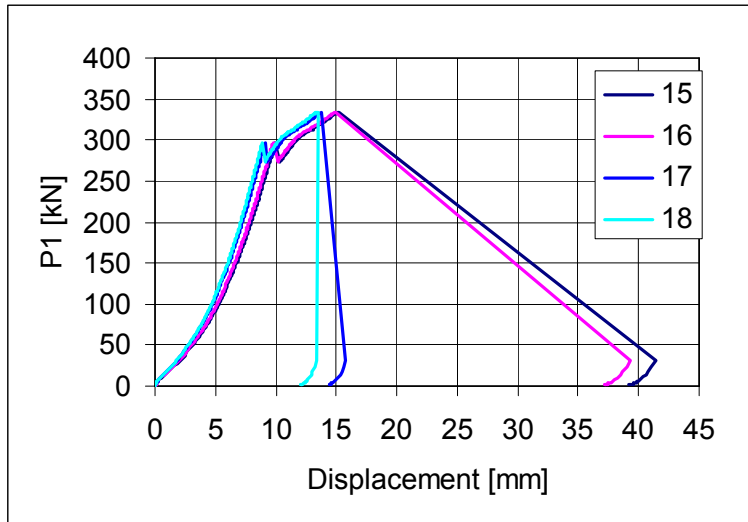


Fig. 36. ST400G1. Deflections measured by transducers 15–18.

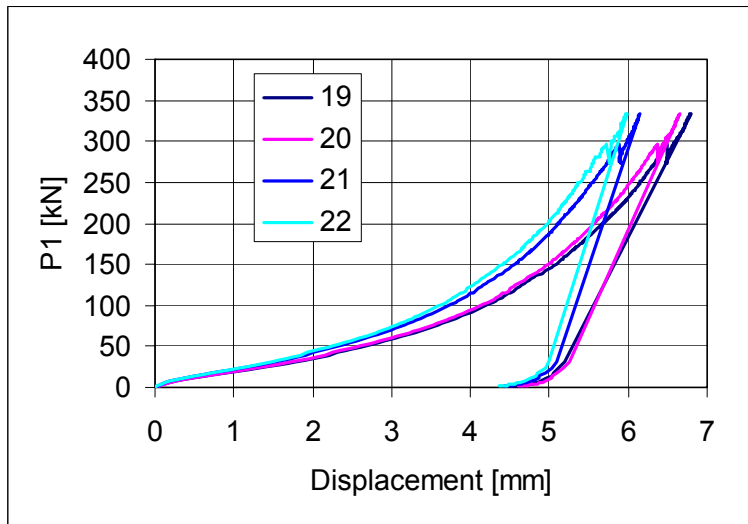


Fig. 37. ST400G1. Deflections measured by transducers 19–22.

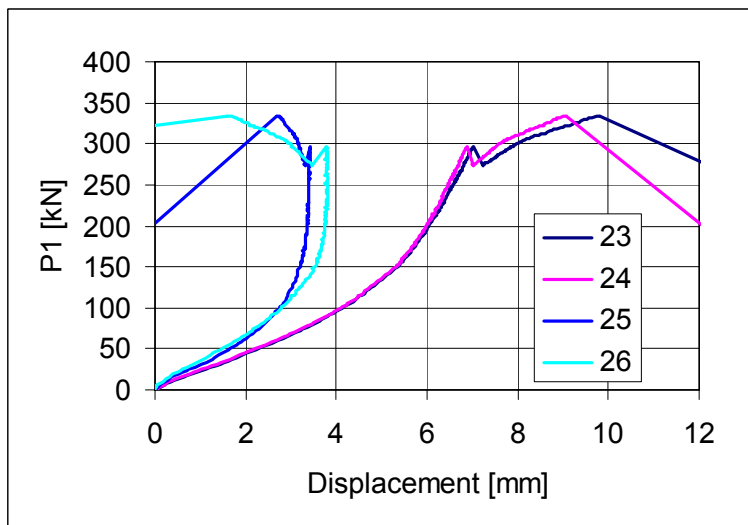


Fig. 38. ST400G1. Deflections measured by transducers 23–26.

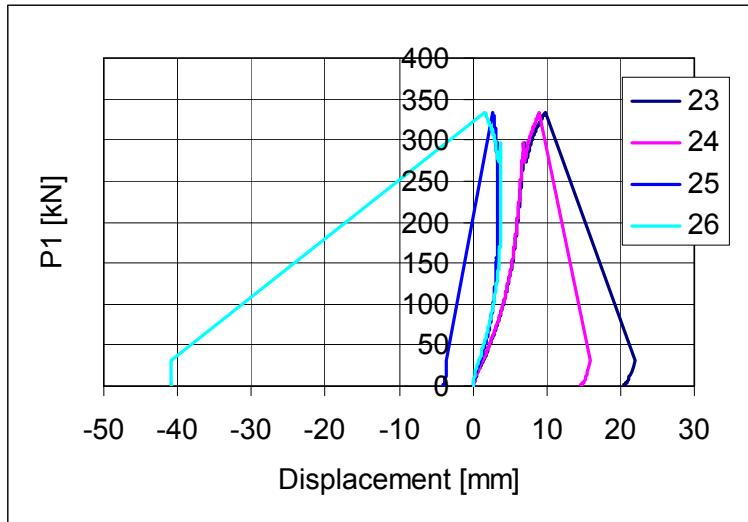


Fig. 39. ST400G1. Deflections measured by transducers 23–26.

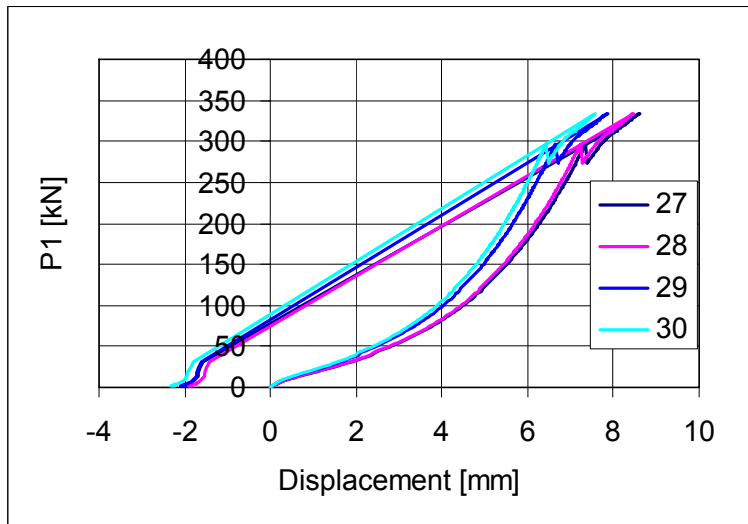


Fig. 40. ST400G1. Deflections measured by transducers 27–30.

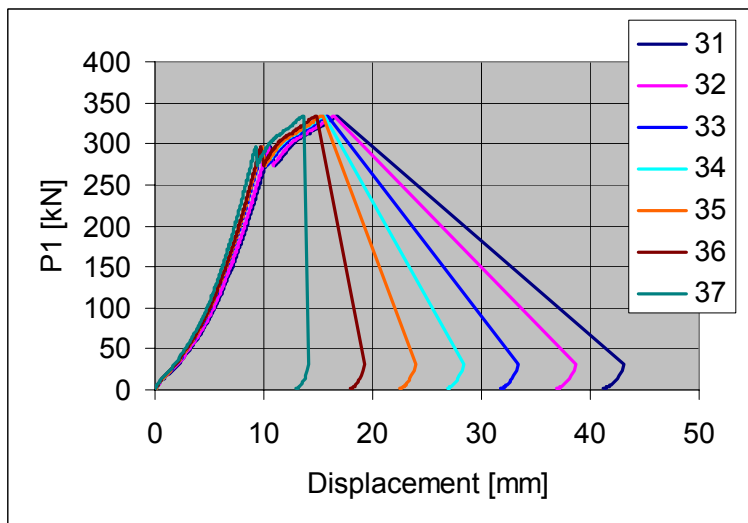


Fig. 41. ST400G1. Deflections measured by transducers 31–37.

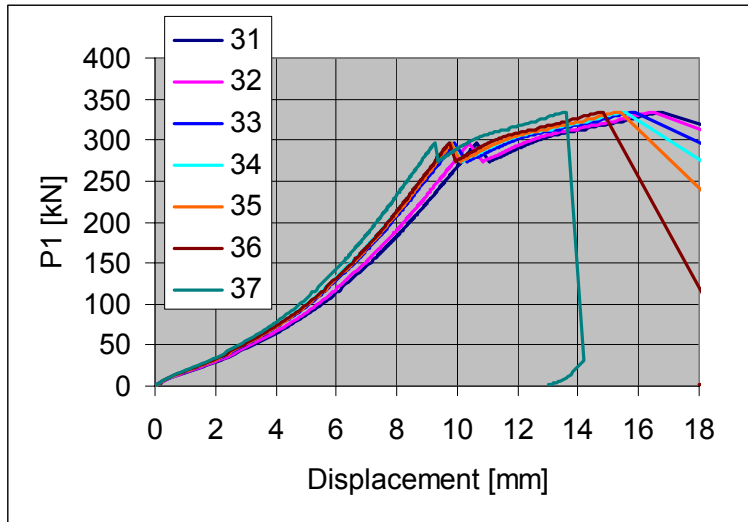


Fig. 42. ST400G1. Deflections measured by transducers 31–37.

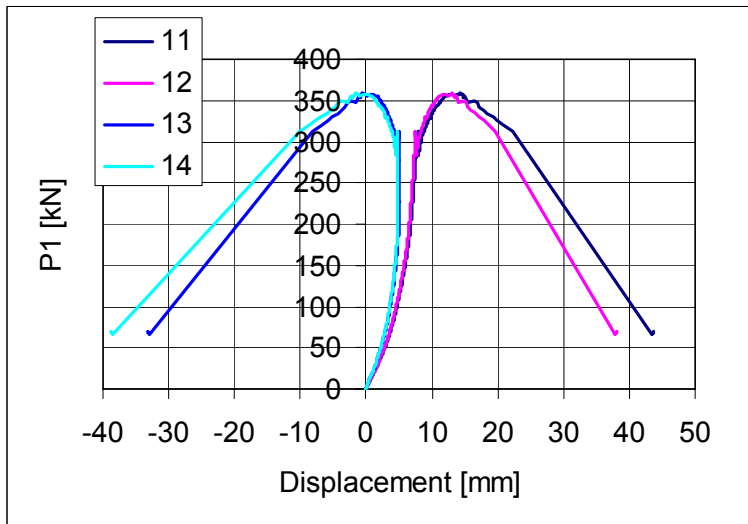


Fig. 43. ST400G2. Deflections measured by transducers 11–14.

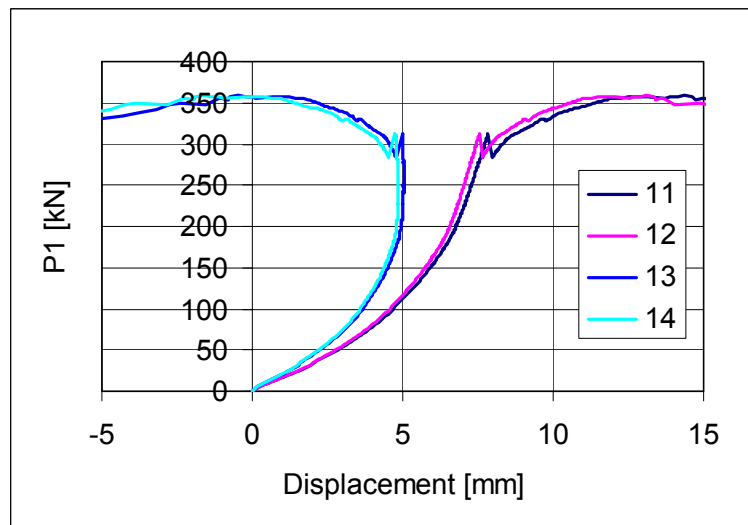


Fig. 44. ST400G2. Deflections measured by transducers 11–14.

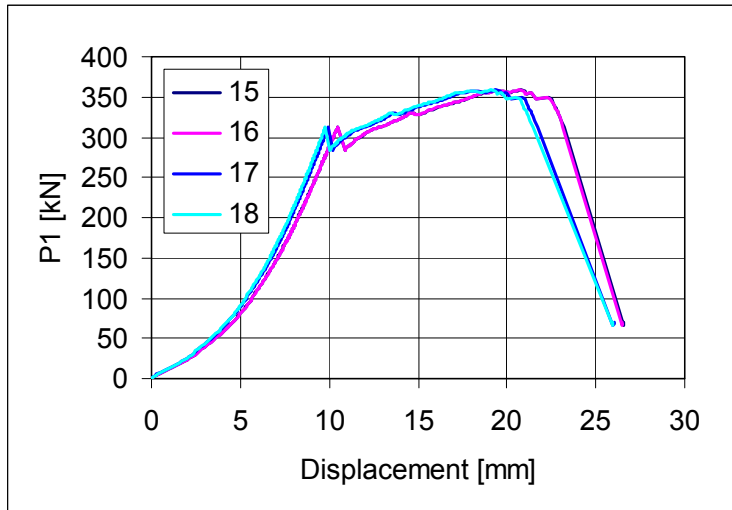


Fig. 45. ST400G2. Deflections measured by transducers 15–18.

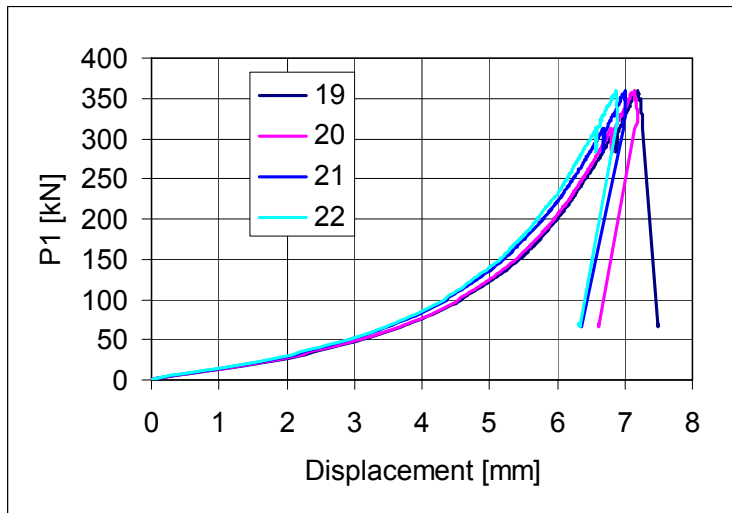


Fig. 46. ST400G2. Deflections measured by transducers 19–22.

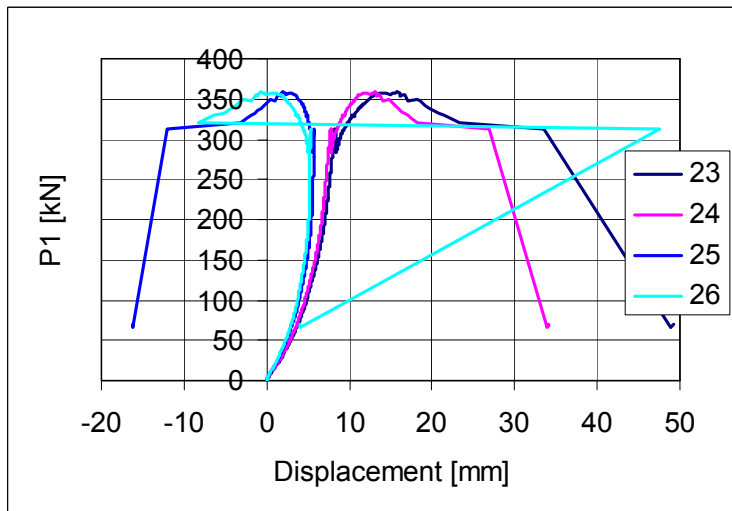


Fig. 47. ST400G2. Deflections measured by transducers 23–26.

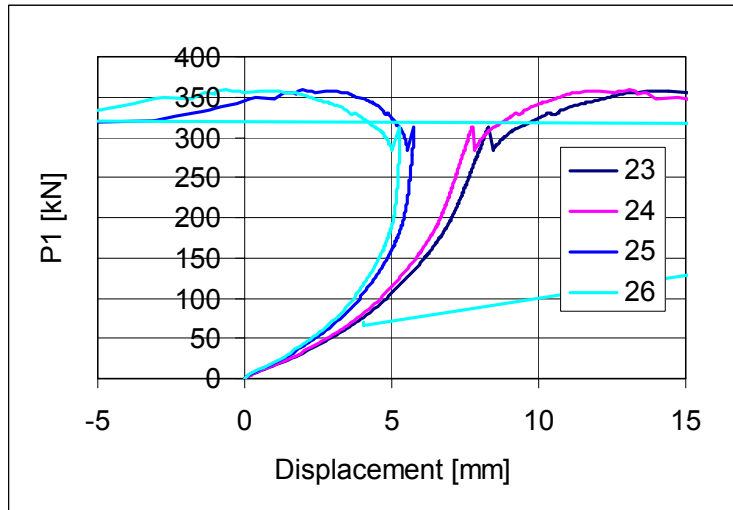


Fig. 48. ST400G2. Deflections measured by transducers 23–26.

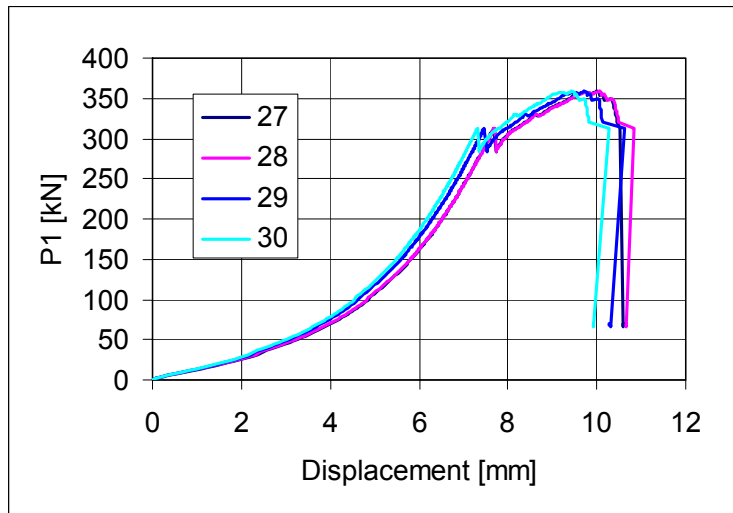


Fig. 49. ST400G2. Deflections measured by transducers 27–28.

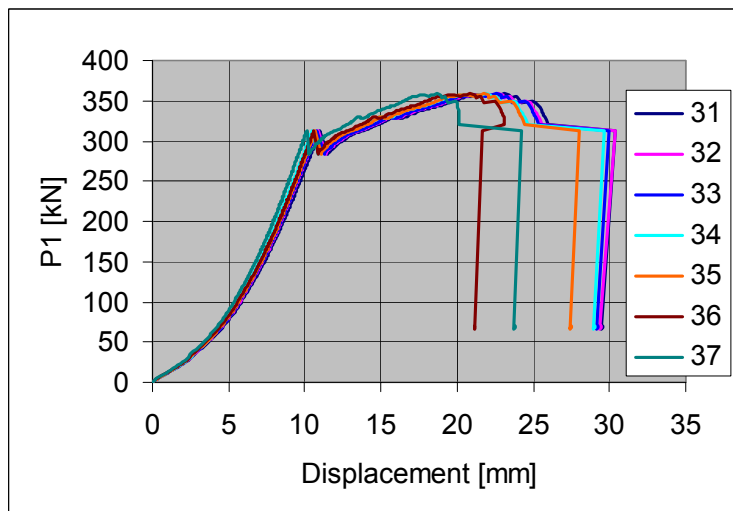


Fig. 50. ST400G2. Deflections measured by transducers 31–37.

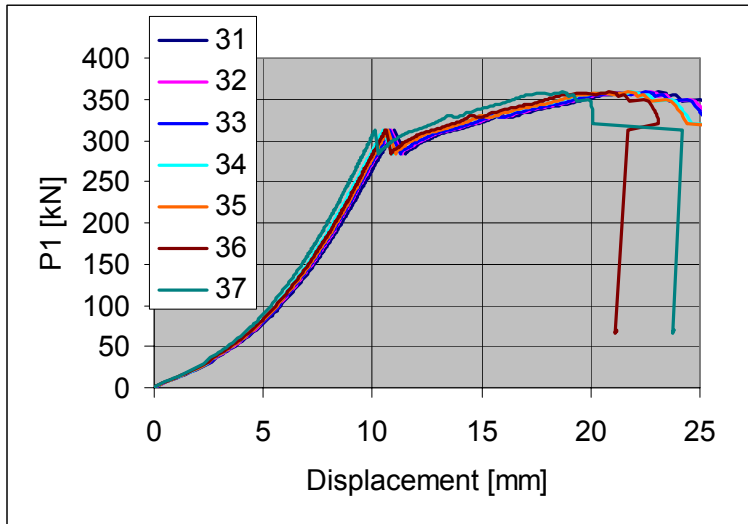


Fig. 51. ST400G2. Deflections measured by transducers 31–37.

Appendix F: Measured displacements in shear flexure test SF400C

P is the actuator load without weight of loading equipment.

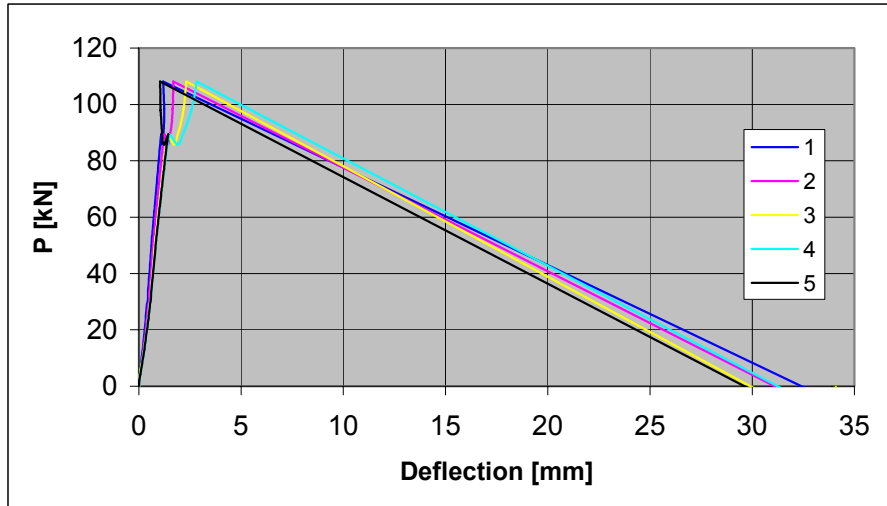


Fig. 1. SF400C. Deflections at Eastern support. Transducers 1–5.

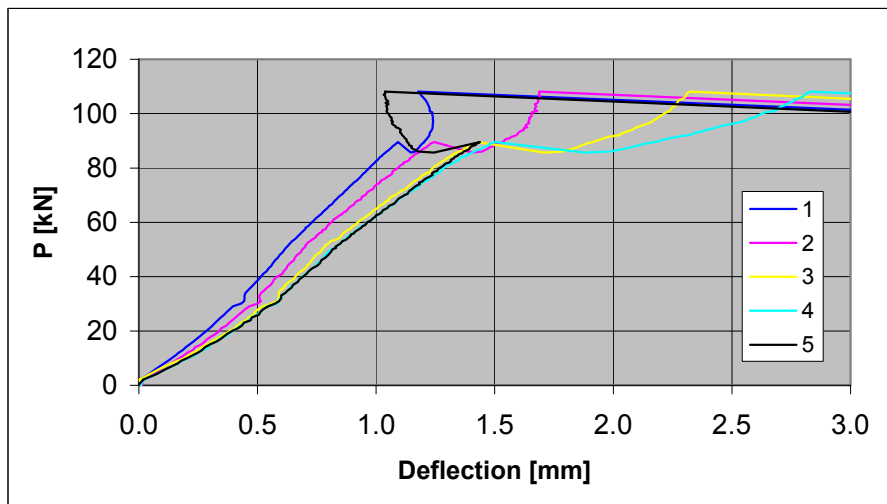


Fig. 2. SF400C. Deflections at Eastern support. Transducers 1–5.

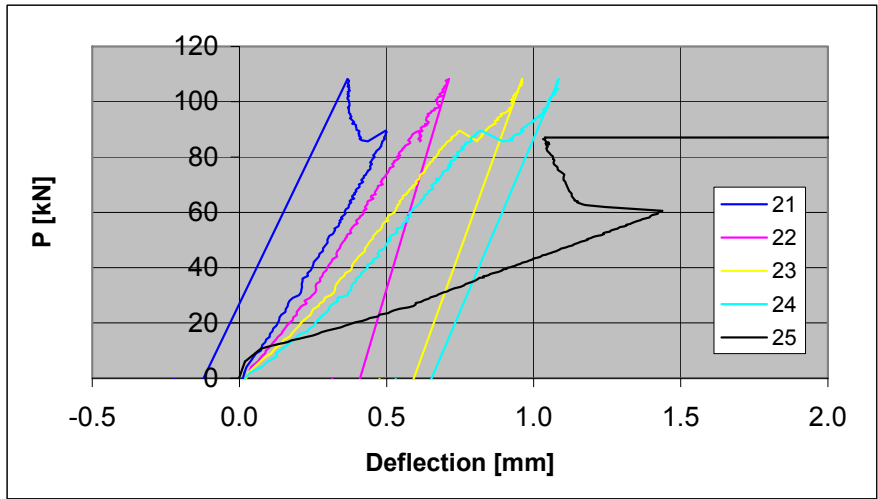


Fig. 3. SF400C. Deflections at Western support. Transducers 21–25.

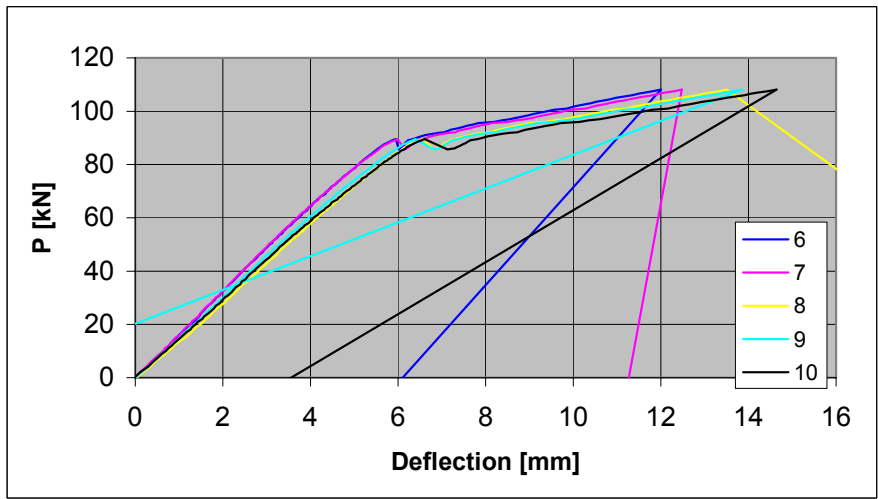


Fig. 4. SF400C. Deflections close to outermost load. Transducers 6–10.

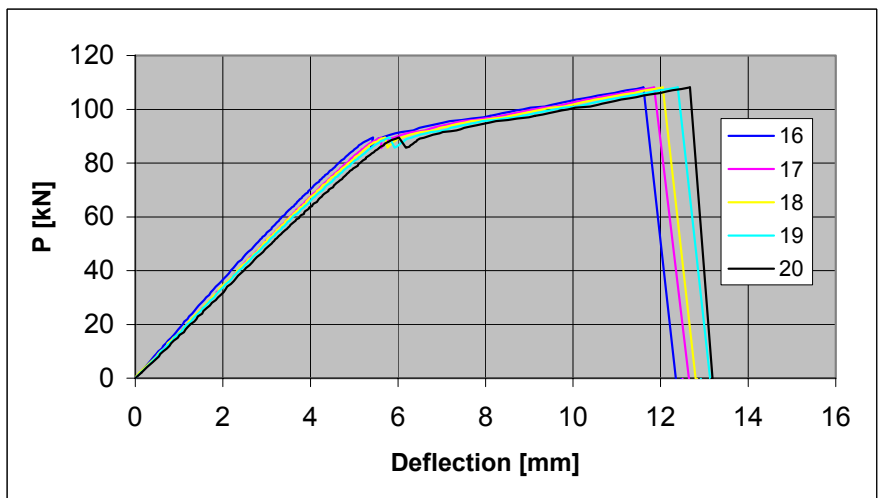


Fig. 5. SF400C. Deflections close to outermost load. Transducers 16–20.

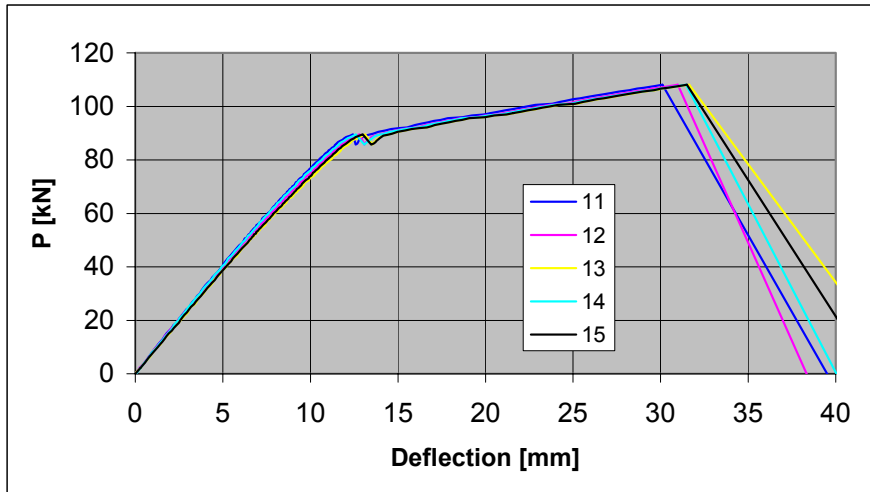


Fig. 6. SF400C. Deflections in mid-span. Transducers 11–15.

Appendix G: Determining torque from measured results

Consider a beam with length L , supported at both ends and subjected to a concentrated torque Pe at a distance of a from its one end, see Fig. 1. Assume that the supports allow some rotation around the longitudinal centroidal axis of the beam. The twisting is governed by

$$M_t = GI_t\Theta \quad (1)$$

where $G = 0.5E/(1+\nu)$ and I_t denote the shear modulus and torsion modulus, respectively, and $\nu = 0.15$ denotes Poisson's ratio. Θ is defined by

$$\Theta = \frac{d\phi}{dx} \quad (2)$$

where ϕ denotes the angle of twist and x is the coordinate measured along the axis of the twisted member.

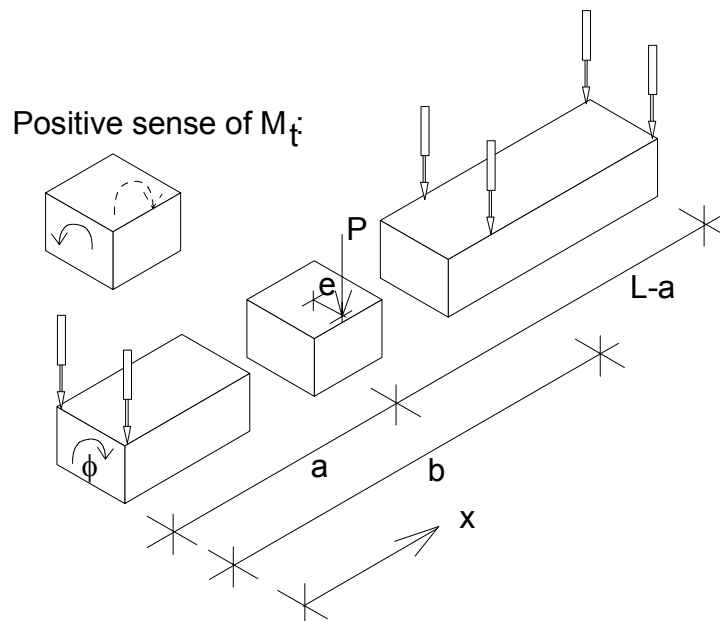


Fig. 1. Twisted member. Rotation ϕ is measured at $x = 0$, $x = b$ and $x = L$.

$$(GI_t)\phi = M_{t,a^-}x + C_1 \text{ when } 0 \leq x \leq a \quad (3)$$

$$(GI_t)\phi = M_{t,a^+}x + C_2 \text{ when } a \leq x \leq L \quad (4)$$

where C_1 and C_2 are integration constants and M_{t,a^-} and M_{t,a^+} are the torques for $x < a$ and $x > a$, respectively. If rotation ϕ is measured at $x = 0$ (ϕ_0), $x = a$ (ϕ_a) and $x = L$ (ϕ_L), the unknown parameters can be solved from the boundary conditions

$$(GI_t)\phi_0 = M_{t,a^-}0 + C_1 \quad (5)$$

$$(GI_t)\phi_a = M_{t,a^-}a + C_1 \quad (6)$$

$$(GI_t)\phi_a = M_{t,a^+}a + C_2 \quad (7)$$

$$(GI_t)\phi_L = M_{t,a^+}L + C_2 \quad (8)$$

$$M_{t,a^-} = M_{t,a^+} + Pe \quad (9)$$

For example

$$M_{t,a^+} \left(\frac{L-a}{\phi_L - \phi_a} - \frac{a}{\phi_a - \phi_0} \right) = Pe \frac{a}{\phi_a - \phi_0} \quad (10)$$

and from Eq. 1

$$(GI_t) = \frac{M_{t,a^+}}{\left(\frac{\phi_a - \phi_L}{L-a} \right)} \quad (11)$$

are obtained. In case the rotation is not measured at $x = a$ but at $x = b$ (ϕ_b) as in Fig. 1, the rotation at $x = a$ is calculated from

$$\phi_a = \phi_L + \frac{L-a}{L-b} (\phi_b - \phi_L) \quad (12)$$

If the ends of the beams cannot rotate, Eqs 10 and 9 give

$$M_{t,a^+} = Pe \frac{a}{L} \quad (13)$$

and

$$M_{t,a^-} = Pe \frac{L-a}{L} \quad (14)$$

Appendix H: Design of supporting beams in tests ST200E1M, ST200E2M and ST400E1M

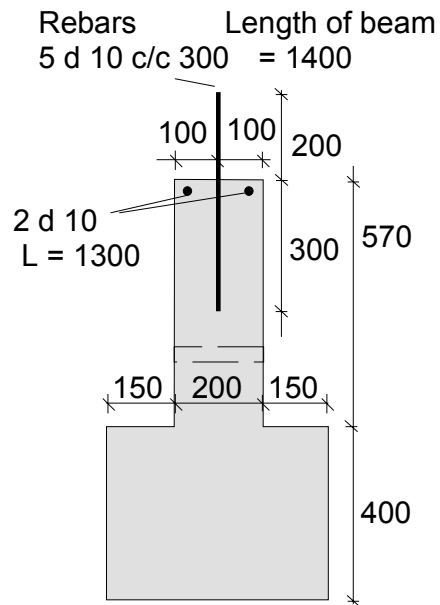


Fig. 1. Supporting beams in test ST200E1M. The target grade of concrete was K30. $d 10$ refers to reinforcing bars with diameter 10.

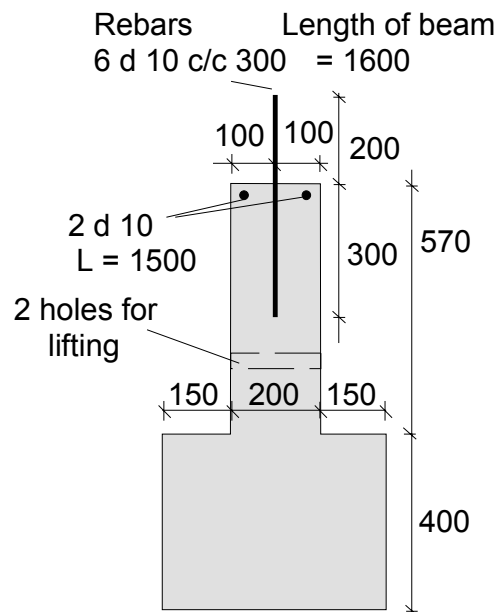


Fig. 2. Supporting beams in test ST200E2M. The target grade of concrete was K30. $d 10$ refers to reinforcing bars with diameter 10.

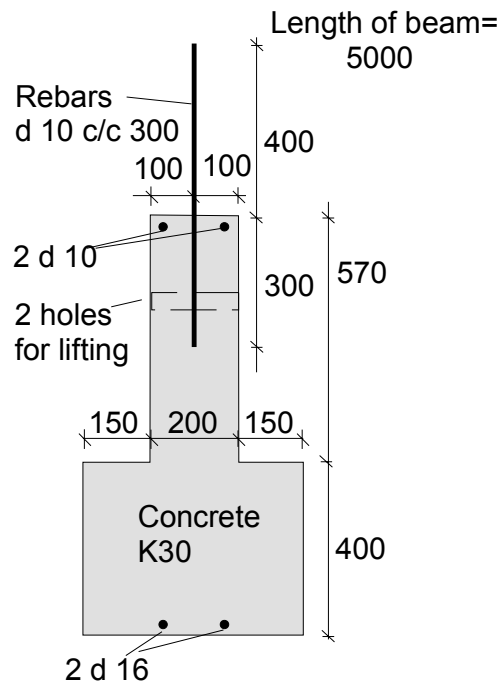


Fig. 3. Supporting beams in test ST400E1M. The target grade of concrete was K30. $d 10$ and $d 16$ refer to reinforcing bars with diameter 10 and 16 mm, respectively.

Appendix I: Elasticity of neoprene strips

To determine the elastic properties of the neoprene strips, a test specimen with thickness 10 mm and loaded area $80 \times 500 \text{ mm}^2$ was compressed with a testing machine. The strip was placed between two stiff steel plates. To measure the inner behaviour of the testing machine, the same test was carried out without neoprene. The results of both tests are shown in Fig. 1 below. The horizontal difference between the two curves represents the change in thickness of the neoprene strip.

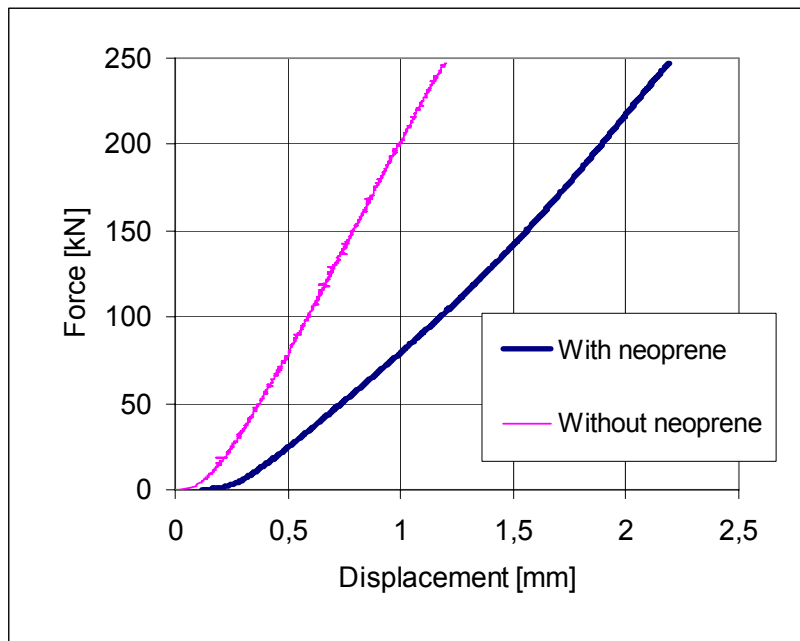


Fig. 1. Load vs. change in thickness of neoprene strip in compression test.

Author(s) Pajari, Matti			
Title Shear-torsion interaction tests on single hollow core slabs			
Abstract To clarify the interaction of shear and torsion in prestressed hollow core slabs, 15 load tests on single prestressed hollow core units were carried out. The slabs were 1.2 m in width, 7 m in length and either 200 or 400 mm in depth. The ends of the slabs were simply supported. In 13 tests the loads comprised one or two point loads close to support. In two tests there was a uniform transverse line load close to one support while the slab unit was twisted by eccentric loads at the ends. In ten tests the slabs were placed on neoprene strips with no end grouting. In these tests the transverse bending made the slab fail longitudinally first, which in most cases resulted in a lower resistance than that predicted using traditional design methods. In five tests the conditions were more realistic, i.e. the slab ends were grouted and stiffened by supporting beams or spreader beams above the slab ends. In these tests the observed resistances were of the same order or higher than those predicted using the conventional calculation methods. However, some observed stiffnesses and resistances deviated so much from the predicted results that the conventional calculation methods have to be evaluated by comparison with numerical methods.			
Keywords shear tests, torsion tests, hollow core slabs, testing, test specimens, load testing, failure loads, concrete, precast, prestressed, structure			
Activity unit VTT Building and Transport, Kemistintie 3, P.O.Box 1805, FIN-02044 VTT, Finland			
ISBN 951-38-6519-3 (URL: http://www.vtt.fi/inf/pdf/)			Project number R2SU00137
Date	Language English	Pages 76 p. + app. 122 p.	Price -
Name of project Holcotors		Commissioned by EU, Concrete industry, VTT	
Series title and ISSN VTT Tiedotteita – Research Notes 1455-0865 (URL: http://www.vtt.fi/inf/pdf/)		Published by VTT Information Service P.O.Box 2000, FIN-02044 VTT, Finland Phone internat. +358 9 456 4404 Fax +358 9 456 4374	

To clarify the interaction of shear and torsion in prestressed hollow core slabs, 15 load tests on single prestressed hollow core units were carried out. The ends of the slabs were simply supported. In 13 tests the loads comprised one or two point loads close to support. In two tests there was a uniform transverse line load close to one support while the slab unit was twisted by eccentric loads at the ends.

In ten tests the slabs were placed on neoprene strips with no end grouting. In five tests the slab ends were grouted and stiffened by supporting beams or spreader beams above the slab ends. In these five tests the observed resistances were of the same order or higher than those predicted using the conventional calculation methods. However, some observed stiffnesses and resistances deviated so much from the predicted results that the conventional calculation methods have to be reconsidered.

VTT TIETOPALVELU
PL 2000
02044 VTT
Puh. 020 722 4404
Faksi 020 722 4374

VTT INFORMATIONSTJÄNST
PB 2000
02044 VTT
Tel. 020 722 4404
Fax 020 722 4374

VTT INFORMATION SERVICE
P.O.Box 2000
FIN-02044 VTT, Finland
Phone internat. + 358 20 722 4404
Fax + 358 20 722 4374
